Modeling the Respiratory Chain and the Oxidative Phosphorylation

D I S S E R T A T I O N

zur Erlangung des akademischen Grades

d o c t o r r e r u m n a t u r a l i u m

(Dr. rer. nat.)

im Fach Biophysik

eingereicht an der
Mathematisch Naturwissenschaftlichen Fakultät I
Humboldt-Universität zu Berlin

von

Diplom-Biophysikerin Margit Heiske

Präsident der Humboldt-Universität zu Berlin:
Prof. Dr. Jan-Hendrik Olbertz

Dekan der Mathematisch Naturwissenschaftlichen Fakultät I:
Prof. Stefan Hecht PhD

Gutachter/innen:
1. Prof. Dr. David Fell
2. Prof. Dr. Barbara Bakker
3. Prof. Dr. Edda Klipp
4. Prof. Dr. Jean-Pierre Mazat

Tag der mündlichen Prüfung: 11.12.2012

Abstract

Mitochondria are cell organelles which play an essential role in the cell energy supply providing the universal high energetic molecule ATP which is used in numerous energy consuming processes. The core of the ATP production, oxidative phosphorylation (OXPHOS) consists of four enzyme complexes (respiratory chain) which establish, driven by redox reactions, a proton gradient over the inner mitochondrial membrane. The ATP-synthase uses this electrochemical gradient to phosphorylate ADP to ATP.
Dysfunctioning of an OXPHOS complex can have severe consequences for the energy metabolism and cause rare but incurable dysfunctions in particular tissues with a high energy demand such as brain, heart, kidney and skeleton muscle. Moreover mitochondria are linked to widespread diseases like diabetes, cancer, Alzheimer and Parkinson. Further, reactive oxygen species which are a by-product of the respiratory chain, are supposed to play a crucial role in aging.

The aim of this work is to provide a realistic model of OXPHOS which shall help understanding and predicting the interactions within the OXPHOS and how a local defect (enzyme deficiency or modification) is expressed globally in mitochondrial oxygen consumption and ATP synthesis. Therefore we chose a bottom-up approach.
In a first step different types of rate equations were analyzed regarding their ability to describe the steady state kinetics of the isolated respiratory chain complexes in the absence of the proton gradient. Here Michaelis-Menten like rate equations were revealed to be appropriate for describing their behavior over a wide range of substrate and product concentrations. For the validation of the equations and the parameter estimation we have performed kinetic measurements on bovine heart submitochondrial particles.
The next step consisted in the incorporation of the proton gradient into the rate equations, distributing its influence among the kinetic parameters such that reasonable rates were obtained in the range of physiological electrochemical potential differences.
In the third step, these new individual kinetic rate expressions for the OXPHOS complexes were integrated in a global model of oxidative phosphorylation. The new model could fit interrelated data of oxygen consumption, the transmembrane potential and the redox state of electron carriers. Furthermore, flux inhibitor titration curves can be well reproduced, which validates its global responses to local effects.

This model may be of great help to understand the increasingly recognized role of mitochondria in many cell processes and diseases as illustrated by some simulations proposed in this work.

This work has been realized in the framework of a cooperation ('cotutelle') between the Humboldt-Universität zu Berlin (Germany) and the Université Victor Segalen Bordeaux 2 (France) and was supervised by Prof. Edda Klipp and Prof. Jean-Pierre Mazat.

Zusammenfassung

Mitochondrien sind Zellorganellen, die für den Energiestoffwechsel von großer Bedeutung sind: Sie versorgen die Zelle mit ATP - energiereiche Moleküle, die für den Ablauf zahlreicher Prozesse benötigt werden. Das Herzstück deren Synthese ist die oxidative Phosphorylierung (OXPHOS). Hier wird, an Redoxreaktionen gekoppelt, über die vier Enzymkomplexe der Atmungskette ein Protonengradient über die innere Mitochondrienmembran aufgebaut. Dieser wird dann von der ATP-Synthase zur Phosphorylierung von ADP zu ATP genutzt.

Ziel dieser Arbeit ist die Entwicklung eines OXPHOS Modells, basierend auf relativ einfachen und thermodynamisch konformen Gleichungen, welche die Kinetiken eines jeden OXPHOS-Komplexes über weite Bereiche von Substrat- und Produktkonzentrationen, sowie unterschiedlichster Werte des elektrochemischen Gradienten, beschreiben. Dazu wurden zunächst für jeden Komplex der Atmungskette kinetische Messungen in Abwesenheit des Protonengradienten durchgeführt, die dann zur Bestimmung adäquater Gleichungen und deren Parameterwerte herangezogen wurden. Generell erwiesen sich hier Gleichungen vom Typ Michaelis-Menten als gut geeignet.

Die Berücksichtigung des Protonengradients war ein entscheidender Schritt in der Herleitung der OXPHOS Ratengleichungen. Dessen Einfluss auf die kinetischen Parameter wurde so gestaltet, dass physiologisch sinnvolle Raten in Abhängigkeit des elektrochemischen Gradients erreicht werden konnten. Die Gleichungen wurden dann in ein OXPHOS-Modell integriert, mit dem sich Literaturdaten von Sauerstoffverbrauch, $\Delta\Psi$ und ΔpH sehr gut reproduzieren ließen. Darüberhinaus konnten ohne weitere Anpassungen des Modells Inhibitor-Titrationskurven beschrieben werden, welche die Atmungsrate in Abhängigkeit der relativen Hemmung eines OXPHOS-Komplexes darstellen. Es konnte somit gezeigt werden, dass das Modell lokale Effekte auf globaler Ebene korrekt wiedergeben kann.

Das hier erarbeitete Modell ist eine solide Basis, um die Rolle von OXPHOS und generell Mitochondrien eingehend zu untersuchen. Diese werden mit zahlreichen zellulären Vorgängen in Verbindung gebracht: unter anderem mit Diabetes, Krebs und Mitochodriopathien sowie der Bildung von Sauerstoffradikalen, die im Zusamenhang mit Alterungsprozessen stehen.

Diese Arbeit wurde im Rahmen einer Kooperation ('Cotutelle') zwischen der Humboldt-Universität zu Berlin und der Université Victor Segalen Bordeaux 2 (Frankreich) erstellt, die Betreuung erfolgte duch Prof. Edda Klipp und Prof. Jean-Pierre Mazat.

Résumé

Les mitochondries sont l'usine à énergie de la cellule. Elles synthétisent l'ATP à partir d'une succession de réactions d'oxydo-réduction catalysées par quatre complexes respiratoires qui forment la chaîne respiratoire. Avec la machinerie de synthèse d'ATP l'ensemble constitue les oxydations phosphorylantes (OXPHOS). Le but de ce travail est de bâtir un modèle des OXPHOS basé sur des équations de vitesse simples mais thermodynamiquement correctes représentant l'activité des complexes de la chaîne respiratoire (équations de type Michaelis-Menten). Les paramètres cinétiques de ces équations sont identifiés en utilisant les cinétiques expérimentales de ces complexes respiratoires réalisées en absence de gradient de proton.

La phase la plus délicate de ce travail a résidé dans l'introduction du gradient de protons dans ces équations. Nous avons trouvé que la meilleure manière était de distribuer l'effet du gradient de proton sous forme d'une loi exponentielle sur l'ensemble des paramètres, V_{max} et K_m pour les substrats et les produits. De cette manière, j'ai montré qu'il était possible de représenter les variations d'oxygène, de $\Delta\Psi$ et de ΔpH trouvés dans la littérature. De plus, contrairement aux autres modèles, il fut possible de simuler les courbes de seuil observées expérimentalement lors de la titration du flux de respiration par l'inhibiteur d'un complexe respiratoire donné.

Ce modèle pourra présenter un très grand intérêt pour comprendre le rôle de mieux en mieux reconnu des mitochondries dans de nombreux processus cellulaires, tels que la production d'espèces réactives de l'oxygène, le vieillissement, le diabète, le cancer, les pathologies mitochondriales etc. comme l'illustrent un certain nombre de prédictions présentées dans ce travail.

Ce travail a été réalisé dans le cadre d'un contrat de co-tutelle entre l'université Humboldt de Berlin (Allemagne) et l'université Victor Segalen Bordeaux 2 (France) sous la co-direction des professeurs Edda Klipp et Jean-Pierre Mazat

Contents

1. General introduction **1**

1.1. Oxidative phosphorylation in the context of metabolism 1
1.2. Mitochondria - The cell's power plant 2
1.3. The respiratory chain - establishment of a proton gradient 4
1.3.1. Complex I 6
1.3.2. Complex II 9
1.3.3. Complex III 11
1.3.4. Complex IV 13
1.4. The F_1F_o-ATPsynthase - phosphorylation of ADP 15
1.5. Why modeling the respiratory chain and the oxidative phosphorylation? . 18
1.5.1. Benefits of modeling in biology 18
1.5.2. Better understanding the role and functioning of the oxidative phosphorylation in physiological and pathological situations 19
1.6. Historic and facts of modeling the respiratory chain and OXPHOS 21
1.6.1. The first models of oxidative phosphorylation are based on non-equilibrium thermodynamics 21
1.6.2. Extension of the models, including more details 22
1.6.3. More recent works 22
1.6.4. Oxidative phosphorylation in the context of large metabolic models 24
1.7. Aim of this work 24

2. Modeling the isolated OXPHOS complexes **27**

2.1. Overview of existing rate equations used for OXPHOS complexes 27
2.1.1. Enzyme kinetics and OXPHOS complexes 27
2.1.2. General OXPHOS and respiratory chain models, or more general models 29
2.1.3. Rate equations for modeling the kinetics of the OXPHOS complexes 30
2.1.4. Derivation of the extended mass action equation 35
2.2. Methods and materials 37
2.2.1. Experimental data types 38
2.2.2. Chemicals and reactants 39
2.2.3. Bovine heart mitochondria 40
2.2.4. Kinetic enzyme assays 41
2.2.5. Influence of the product concentrations on complex II activity . . . 44
2.2.6. Hydrophilic analogues to coenzyme Q 51
2.2.7. Parameter estimation 53

2.3. Rate equation for complex I . . . 53
2.3.1. Progress curves . . . 54
2.3.2. Initial velocity measurements . . . 58
2.3.3. Simulating complex I steady states kinetics using a stochastic model of complex I . . . 68
2.4. Rate equation for complex II . . . 75
2.4.1. Fitting to experimental data . . . 75
2.5. Rate equation for complex III . . . 79
2.5.1. Fitting to initial rate measurements . . . 81
2.6. Rate equation for complex IV . . . 87
2.7. Rate equation for F1Fo-ATPsynthase . . . 91
2.8. Consideration of the whole system and discussion . . . 91
2.8.1. Experimental data . . . 92
2.8.2. Fitting rate equations featuring saturation kinetics . . . 92
2.8.3. Comparing the results of the simplified Michaelis Menten like rate equations . . . 93
2.8.4. Comparison of the kinetic parameters along the respiratory chain and their relation to the quinone pool and cytochrome c pool . . . 94
2.8.5. The influence of ethanol on complex I activity . . . 99
2.9. Summary . . . 99

3. Introduction of the electrochemical gradient into the rate equations 101
3.1. Introduction . . . 101
3.2. General thermodynamical considerations . . . 101
3.2.1. Flux-force relationship . . . 101
3.3. The electrochemical gradient . . . 103
3.3.1. The electrical gradient . . . 104
3.3.2. The chemical gradient . . . 105
3.3.3. Scalar protons . . . 106
3.3.4. Energetic terms of the complexes . . . 106
3.4. Introduction of the electrochemical gradient into Michaelis-Menten-like equations . . . 108
3.4.1. A simple approach to model the influence of the proton gradient on the kinetic parameters . . . 108
3.4.2. Repartition of the proton gradient's influence among the kinetic parameters . . . 110
3.4.3. Concept of the internal energy . . . 114
3.5. Summary and Discussion . . . 118
3.5.1. Introduction of the gradient . . . 118
3.5.2. Sensitivity of the Michaelis-Menten constants to the membrane gradient . . . 121
3.5.3. Further considerations . . . 122

4. Modeling the system of oxidative phosphorylation **123**
4.1. Introduction . . . 123
4.2. The framework model . . . 123
4.3. Incorporation of the new OXPHOS rate equations . . . 127
4.4. Estimation of parameter values upon basic respiratory chain features . . . 130
4.4.1. Objective function and fitting routine . . . 132
4.4.2. Problems concerning the parameter estimation . . . 132
4.4.3. Description of the experimental data . . . 134
4.5. Analysis and Simulations . . . 139
4.5.1. Complex II as electron entry point . . . 139
4.5.2. Robustness of the model with respect to the apparent Michaelis-Menten constants of the quinones and quinols . . . 141
4.5.3. Flux-inhibition curves . . . 141
4.5.4. The proton/ATP ratio of the ATPsynthase . . . 148
4.5.5. Simulation of time courses . . . 150
4.6. Summary and discussion . . . 154

5. Conclusion **159**

Appendix A. Rate equations of the framework model **165**

Appendix B. Modeling supercomplexes **169**
B.1. Supercomplex CI + $CIII_2$ modeled with strict channeling . . . 170
B.2. Supercomplex CI + $CIII_2$ modeled with partial channeling . . . 175

Bibliography **183**

List of Figures **201**

List of Tables **203**

Acknowledgments **205**

1. General introduction

Oxidative phosphorylation (OXPHOS) plays an essential role in the cellular energy metabolism of most aerobic organisms. In this work we focus on the OXPHOS in eukaryotic cells, which takes place in mitochondria, small cellular organelles. Here, OXPHOS consists of five enzyme complexes that are located in the inner mitochondrial membrane. Four of them (complexes I-IV) compose the respiratory chain or electron transport chain whose function is to establish an electrochemical proton gradient over this membrane and the fifth complex, the F1Fo-ATPsynthase uses the force of this gradient for the phosphorylation of adenosin-diphosphate (ADP) to adenosin-triphosphate (ATP).
This chapter deals with the description of OXPHOS and its functioning. Here this enzyme system is presented in its metabolic and structural context, beginning with its role in metabolism, then a closer look to the host organelle mitochondria, followed by the description of the individual OXPHOS complexes. We show why the complexity of this biochemical system necessitates a model to understand the way of its functioning and dysfunctioning. At the end of this chapter, we shortly present already existing models and point out the need of further modeling, taking into account the kinetics and thermodynamical properties of the individual complexes.

1.1. Oxidative phosphorylation in the context of metabolism

In the early 1960's, Peter Mitchell developed the *chemiosmotic hypothesis* Mitchell [1961] which states that the phosphorylation of ADP to ATP by the ATPsynthase was coupled to the redox reactions of the electron transport chain (respiratory chain) via a electrochemical gradient of protons over a membrane without involving other intermediates. He summarized and reasoned this interrelationship in his famous review in 1966 [Mitchell, 2011]. This hypothesis was confirmed later [Jagendorf and Neumann, 1965, Neumann and Jagendorf, 1964, Mitchell, 1962, Mitchell and Moyle, 1965] and the work became a milestone in the understanding of the *oxidative phosphorylation* (OXPHOS), the term 'oxidative' steaming from the requirement of O_2 as terminal electron acceptor of the redox reactions catalyzed by the respiratory chain.
The main 'outcome' of the OXPHOS machinery is adenosine triphosphate (ATP) which has been appositely termed as 'universal energy currency in cell metabolism'. It is used to drive a huge amount of biochemical processes. An impressive illustration of this extent is that in human per day, the turnover of ATP - being used and recycled over and over - corresponds roughly to our body weight [von Ballmoos et al., 2009, Törnroth-Horsefield and Neutze, 2008].

Figure 1.1.: Oxidative phosphorylation. The respiratory chain complexes I, III and IV transfer protons over the inner mitochondrial membrane, driven by redox reactions. Thereby they establish a proton gradient which is then used by the ATPsynthase for the phosphorylation of ADP. Via NADH and succinate (suc), electrons enter in the respiratory chain at complex I and complex II, respectively. Quinone (Q) and cytochrome c (cytc) shuttle the electrons between the complexes. The final electron acceptor is oxygen. In this simplified scheme, stoichiometric constraints are not considered and neither the Q-cycle mechanism of complex III.

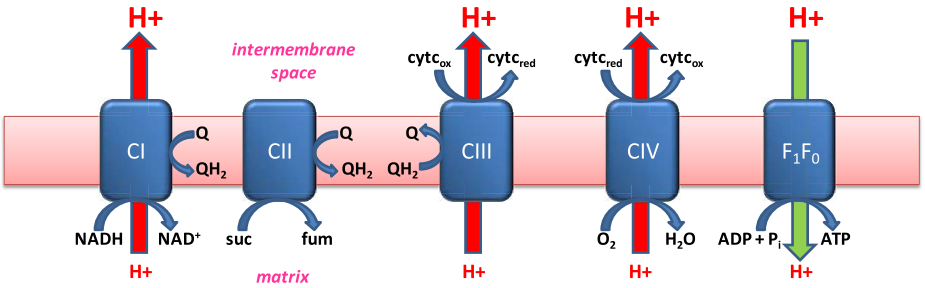

In general, cells have the ability to produce ATP in the cytosol via glycolysis by breaking down glucose. However only two molecules of ATP are gained per molecule glucose by this biochemical pathway. With help of OXPHOS aerobic organisms increase this yield substantially: In eukaryotes, the total gain can be theoretically up to 38 molecules of ATP per molecule glucose. This high yield stresses the important role of OXPHOS.
The effective gain is somewhat lower, because the proton gradient is also involved in transport processes (symport and antiport) across the membrane and because the intermediates resulting from the degradation of glucose can also be used for other metabolic pathways.

The particular structure of mitochondria is essential for the functioning of the OXPHOS within eukaryotic cells and therefore these cell organelles are presented in more details below.

1.2. Mitochondria - The cell's power plant

Mitochondria are multi tasking organelles that occur in almost all eukaryotic cells, generally in a high number (10-30% of cell volume) and in variable shape. They can build a dynamic network, see figure 1.2. The morphology, distribution and activity can be regulated by fusion and fission Chang and Reynolds [2006] and is dependent on the physiological state of the organelle. Besides the processes involved in the energy metabolism, in particular OXPHOS, mitochondria comprehend many biochemical reactions: They are involved in the synthesis of essential precursors for the biosythesis of amino acids, nucleotides, fatty acids, etc. They are also involved in apoptosis [Jeong and Seol, 2008,

Kulikov et al., 2012], calcium signaling [Nicholls, 2005] and the production of free radicals and reactive oxygen species [Cadenas and Davies, 2000].

Figure 1.2.: Mitochondria. a) An electron microscopy image of an mitochondrion from bovine heart [Gilkerson et al., 2003]. The outer membrane delimits the organelle from the cytosol. The inner membrane is folded, forming the so called 'cristae'. The OXPHOS complexes are integral to this membrane. Both membranes give rise to the inner membrane space and the matrix. This compartmentalization is essential for the functioning of OXPHOS. b) Mitochondria can form dynamical networks by fusion and fission. The shape of the network is related to the energetic state of the mitochondria. The picture is taken from Gilkerson et al. [2003].

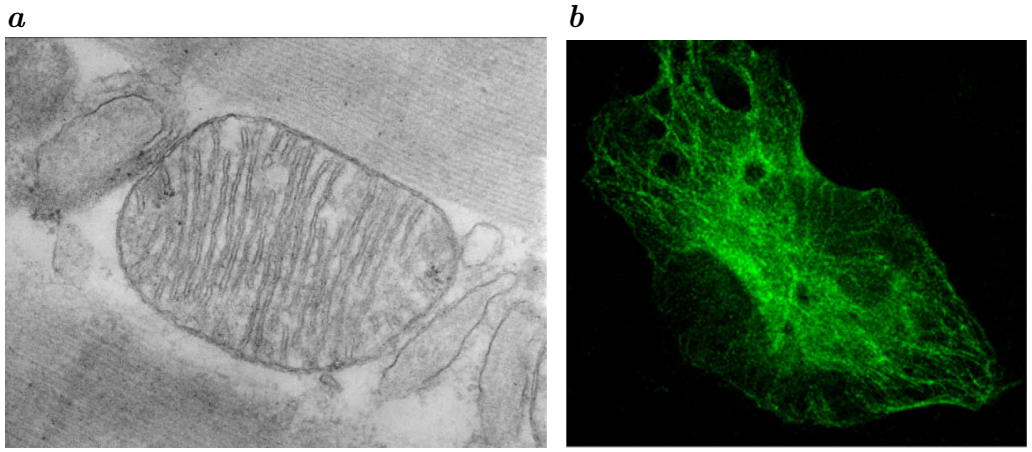

The endosymbiontic theory [Sagan, 1967] postulates that mitochondria originally steem from bacteria that were equipped with an OXPHOS system in their cell membrane: Such bacteria were 2.5 milliards years ago phagocytated by other prokariotic cells and, it occurred eventually that instead of being digested, some of them survived in the cytoplasm and became finally endosymbionts. During evolution, they have lost more and more of their autonomy and turned into cell organelles of their host cells. This theory is based on the fact that mitochondria and bacteria share many features, e.g. mitochondria contain their own DNA in form of several copies of single, circular chromosomes. Another aspect is that mitochondria have two membranes, which may have their origin in the host's phagosome surrounding the endosymbiotic bacteria.

These two membranes give rise to two compartments: the intermembrane space between the two membranes and the mitochondrial matrix, enclosed by the inner membrane, which, together with these membranes themselves, provide four distinct environments for the various biochemical and transport processes. This particular structure is essential for the functioning of OXPHOS within eukaryotic cells [Logan, 2006].
The outer membrane delimits the organelle from the cytosol. It contains porins which permit the unspecific and free diffusion of molecules up to 10kD [Voet and Voet, 1994] but hinders cytochrome c, a respiratory chain intermediate with a molecular weight of

about 12 kD, to leave the intermembrane space.
In contrast to that, the inner membrane, is very tight and allows thereby for the establishment of an electrochemical proton gradient between the matrix and the intermembrane space by the respiratory chain complexes. Only O_2, CO_2 and H_2O can freely permeate through this membrane. Besides the OXPHOS enzyme complexes, the inner membrane contains various proteins that among others control the passage of ATP, ADP, phosphate, ions and substrates like pyruvate. This membrane rich in proteins shows numerous foldings, so called cristae, which are enlarging the surface. It is alternatively speculated that rather than foldings, numerous thin membrane sacks are attached at some points to the outer membrane. The shape of the inner membrane varies among different tissues within the same organism, probably because these cells have in general different main functions an thus different energy demands.

The mitochondrial matrix accommodates the Krebs (TCA) cycle, a system of enzymes that is responsible for the degradation of certain molecules like pyruvate (which is a product of the above cited glycolysis), glutamate and others, in order to gain reduced nicotinamide adenine dinucleotide (NADH) and succinate, both substrates of the respiratory chain. The TCA-cycle is also involved in the synthesis of precursors which serve as starting points of the corresponding biochemical pathways. Further, the β-oxidation of fatty acids contributes to fuel the TCA cycle via acetyl-CoA and the respiratory chain via NADH and succinate. Depending on the physiological state, the flux through the Krebs cycle can be shifted more to energy production or more to syntheses.

Most of the mitochondrial proteins are encoded in the nuclear DNA. The existence of mitochondrial DNA (mtDNA), located in the mitochondrial matrix, is still not only an artifact of the evolution but seems to be essential for the communication between mitochondria and the nucleus in particular with respect to the regulation of the energy metabolism since all of the 13 proteins encoded in the mtDNA are part of the OXPHOS system: This concerns 7 subunits of complex I, 1 subunit of complex III, 3 subunits of complex IV and 2 subunits of the F1Fo-ATPSynthase. In addition there are 2 genes encoding mitochondrial rRNA and further 22 genes encoding tRNA.
In the following, we will have a closer look on the energetic core, the OXPHOS complexes, and present first the respiratory chain as a whole and then each of its components followed by the F1Fo-ATPsynthase.

1.3. The respiratory chain - establishment of a proton gradient

The respiratory chain is composed of four enzyme complexes which are integral proteins of the inner mitochondrial membrane. By translocating protons from the matrix (also negative side, n-side) into the intermembrane space (also positiv side, p-side), complexes I, III and IV establish an electrochemical proton gradient, with the inner membrane serving as isolation between the two oppositional charged compartments. This highly endergonic process is fueled by the redox energy freed from the stepwise transfer of elec-

trons from NADH and succinate onto oxygen. The corresponding overall reactions are presented below, on the right side the total Gibbs standard energy that is freed during the transfer is given:

$$\mathrm{NADH} + \mathrm{H^+} + \frac{1}{2}\mathrm{O_2} \rightleftharpoons \mathrm{NAD^+} + \mathrm{H_2O} \text{ where } \Delta \mathrm{G}'_0 = -220\,\mathrm{kJ} \tag{1.1}$$

$$\text{succinate} + \frac{1}{2}\mathrm{O_2} \rightleftharpoons \text{fumarate} + \mathrm{H_2O} \text{ where } \Delta \mathrm{G}'_0 = -152\,\mathrm{kJ} \tag{1.2}$$

Each of these molecules feed 2 electrons into the respiratory chain. While the reduction of oxygen via the oxidation of NADH leads to the translocation of 10 $\mathrm{H^+/2e^-}$ from the matrix into the intermembrane space, the yield via the oxidation of succinate is lower with 6 $H^+/2e^-$. This difference is due to the the two 'entry points' of the respiratory chain: Complex I oxidizes NADH to reduce ubiquinone and uses this redox energy to pump 4 H^+. Complex II catalyzes the transfer of two electrons from succinate to ubiquinone, but this reaction is not coupled to proton translocation. The subsequent way for the common product ubiquinol (2 fold reduced ubiquinone) is the same, and thereby the differences in yield is due to the first step. In the next step ubiquinol becomes reoxidized at complex III. Here the electrons are relayed on cytochrome c, which shuttles them to complex IV, where they are eventually employed for the reduction of oxygen, the final electron acceptor in the chain. Both, complex III and IV use the redox energy for proton translocation. This stepwise organisation permits a controlled usage of the redox energy and makes thereby possible the endergonic translocation of protons from the matrix to the intermembrane space.
Due to the two distinct electron entry points into the respiratory chain, the system can be divided into two subsystems: CI+CIII+CIV and CII+CIII+CIV, which can be experimentally and theoretically analyzed independently.

Ubiquinone, the first electron shuttle can transport two electrons as do the electron donors NADH and succinate. However, cytochrome c, the second electron shuttle can transport only one electron and moreover complex IV needs even four electrons (and thus four reduced cytochrome c) to reduce one molecule of oxygen. This curious relationships are reflected in the mechanisms of the enzymes and will be detailed in the sections below.
Both electron shuttles are spatially separated from each other which avoids a direct transfer of electrons between them and thus a short circuit that would omit complex III: since ubiquinone is highly lipophilic it is restricted to the inner mitochondrial membrane and cannot be in contact with the hydrophilic cytochrome c which is dissolved in the water partition of the intermembrane space.
The spacial separation of the electron shuttles, the inner membrane functioning as an isolator, the outer as barrier for cytochrome c, and last but not least the location of the TCA cycle in the matrix, providing NADH for complex I at the n-side of the membrane where it is needed, shows the impressive link of the functioning of the respiratory chain

(and the whole OXPHOS) with the mitochondrial architecture.

1.3.1. Complex I

Complex I, also called NADH dehydrogenase, is an electron entry point of the respiratory chain. It catalyzes the oxidation of NADH and the reduction of ubiquinone. The free energy of the reaction makes possible proton pumping from the matrix into the inner membrane space against an electrochemical gradient. For mitochondrial complex I, the number of the translocated protons has been found to be 4 with ubiquinone as electron acceptor [Wikström, 1984, Galkin et al., 1999, 2006].

$$NADH + Q + 5\,H_x^+ \rightleftharpoons NAD^+ + QH_2 + 4\,H_{is}^+ \tag{1.3}$$

The Gibbs energy of this reaction is $\Delta G_0' = -69.4\,\mathrm{kJ}$ [Beard, 2005]. The reaction can be reversed in presence of a high membrane gradient [Chance and Hollunger, 1960, Löw and Vallin, 1963, Rottenberg and Gutman, 1977].

Mitochondrial Complex I is with about 1000 MDa the largest complex within the respiratory chain [Morgner et al., 2008], and even one of the largest membrane integral protein in general. It is composed of 45 subunits [Carroll et al., 2006]. In contrast to that, the minimal set for functional complex I consists of 14 subunits and is found in bacteria [Friedrich et al., 1995]. These core subunits appear all in mitochondrial complex I, seven of them being encoded in mtDNA (MT-ND1, MT-ND2, MT-ND3, MT-ND4, MT-ND4L, MT-ND5, and MT-ND6).
Although combined comparison of protein sequences and structures suggest that mitochondrial complex I is highly conserved among eukaryotes with more than 40 subunits being essentially the same [Cardol, 2011], the role of most of the 'accessory' (non-core) subunits remain unclear. They may have functions in regulation of activity, protection of the core against reactive oxygen species and could be important for stability and especially the assembly, since here nuclear and mtDNA coded proteins have to interact, as summarized and discussed in [Hirst, 2011].

Complex I has an L-shaped form, see figure 1.3 c): Its hydrophobic domain is embedded in the inner mitochondrial membrane and perpendicular to it, the hydrophilic part is protruding into the matrix [Zickermann et al., 2009]. Four sub-complexes can be distinguished: Iα comprises the lipophilic arm and some of the membrane standing hydrophobic subunits while Iβ and Iγ are made up of the remaining membrane integral subunits. The lipophilic arm alone represents also a sub-complex, called Iλ. It comprises 15 subunits and can dissociate from the rest [Lazarou et al., 2009].
At the peripheral side of the hydrophilic arm a flavin mononucleotide (FMN) is non-covalently bound. Here, NADH binds, becomes oxidized and reduces the FMN. In eukaryotes , eight iron sulfur clusters, of which two are binuclear ([2Fe-2S]) and six tetranuclear ([4Fe-4S]) arrange for the subsequent electron transfer along the peripheral

Figure 1.3.: Structur of complex I, a) show the hydrophilic domain of complex I of *T. thermophilus*, and b) illustrates the corresponding locations of the redox centers, which allow for the electron transfer, the main pathway is indicated by the blue arrows. The numbers are the distances between the centers in angstroms. Both pictures are taken from Sazanov and Hinchliffe [2006]. In c) the whole architecture of the L-shaped complex I is presented (*T. thermophilus*). d) indicates the sites where protons are pumped. The horizontal spanned helices are likely to be involved in linking the reduction of quinone to the proton pumping. The images are taken from Efremov et al. [2010]. Note that the matrix side is at the top.

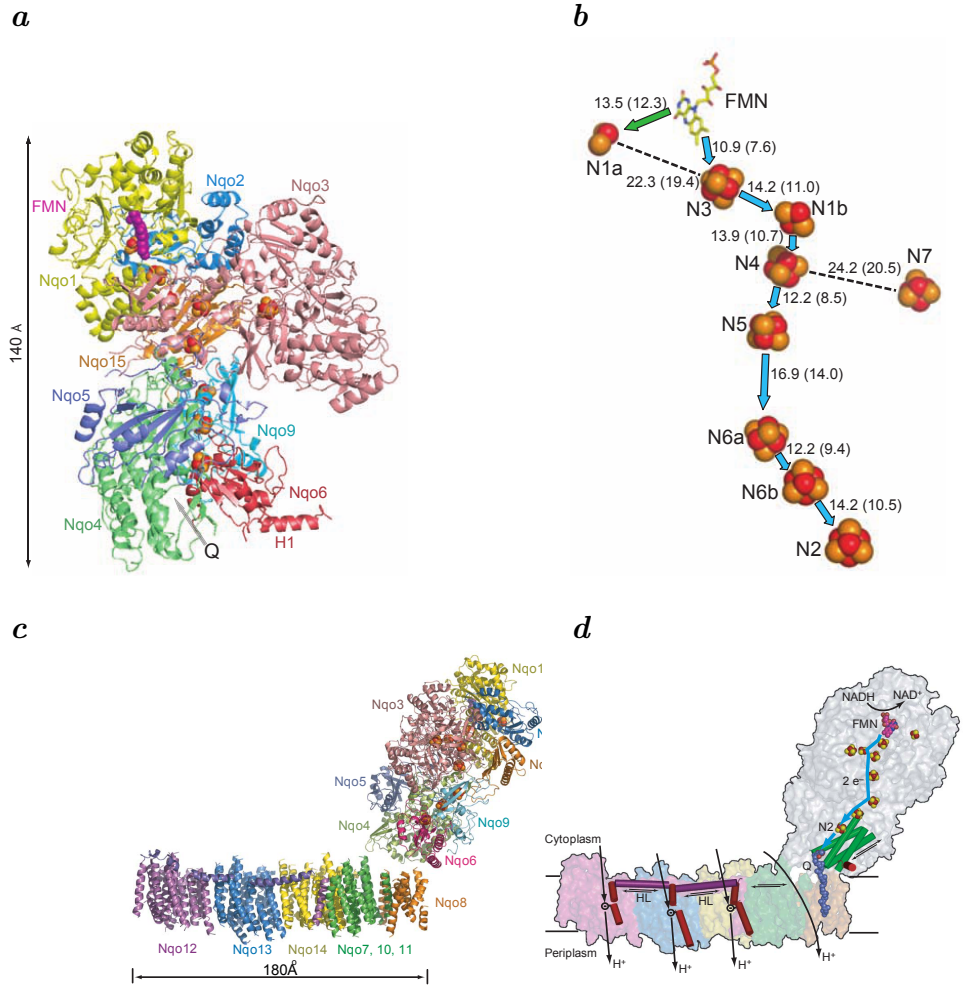

arm to the Q-binding pocket, where Q becomes reduced [Lazarou et al., 2009]. This binding pocket is assumed to consist of several overlapping Q binding sites and is situated close to the membrane but still in the hydrophilic part. The heads of the quinones are thought to be guided from the membrane to this location, the hydrohobic tail or a part of it still anchored in the membrane. It has been suspected that the reduced quinone does not leave at the exactly same site where the binding of oxidized quinone takes place Angerer et al. [2012].

The first seven iron sulfur clusters (N1a, N3, N1b, N4, N5, N6a, N6b) do not seem not to be involved in the proton pumping step(s) because they have similar energy levels around -250 mV and thus the electron transfer between them cannot free a significant amount of energy. They might rather serve as an electron reservoir, which is able to provide rapidly electrons for the Q reduction Brandt [2011]. Only the last iron sulfur cluster has a significant lower energy level of about - 150 mV and may thus be coupled to the proton pumping process, however the crucial step seems to be the reduction of quinone. The role of N1a is still discussed. It possibly makes more efficient the electron transport [Roessler et al., 2010]. The location of the electron centers are illustrated in figure 1.3 b).

The enormous size and the large hydrophobic part of complex I made it for a long time difficult to get precise insight in its structure and therefore it was not clear how electron transfer is coupled to proton pumping. Only recently Efremov et al. [2010], Efremov and Sazanov [2012] could shed light thereon, having attained a more detailed insight in the structure of the hydrophobic domain of E. Coli via X-ray crystallographic analyses. The authors could reveal three subunits in the membrane integral part (NuoL, NuoM and NuoN in E. Coli nomenclature) that have a very similar structure, each containing 14 aligned transmembrane helices(NuoL contains 2 additional helices) whereof two are interrupted in the middle of the membrane. Such patterns are assumed to be important for the functioning of various transporters and channels and thus they strongly indicate that in case of complex I they are responsible for the proton translocation. The conformational change of these three subunits is due to the movement of two helices HL and β H, both parallel to the membrane plane, whereof the first is linked to the distant Q binding site [Efremov and Sazanov, 2011], see figure 1.3 c) and d).

A forth putative proton channel was discovered between the quinone binding site and the three subunits. Proton pumping within this channel could thus additionally be coupled to the movement of HL. These findings were achieved upon E. Coli, however, due to highly conserved principal structures it is very likely that this 'steam engine' like mechanism is also found in mitochondrial complex I [Efremov and Sazanov, 2011].

Complex I can occur in two catalytic and structurally distinct conformations, the active form and the deactivated form. The transition is dependent on the pH and divalent Both substrates, NADH and quinone need to be present for the activation of the enzyme [Oyedotun and Lemire, 2004, Vinogradov, 1993].

1.3.2. Complex II

Complex II, also known as succinate dehydrogenase or succinate quinone oxidoreductase, is an alternative electron entry point into the respiratory chain and catalyzes the reversible reaction

$$suc + Q \rightleftharpoons fum + QH_2 \tag{1.4}$$

Unlike the other respiratory chain complexes, complex II is not involved in proton translocation over the inner membrane, the low standard energy of the catalyzed reaction, $\Delta G0' \approx -2.9kJ$ [Voet and Voet, 1994] would simply not permit for it [Schultz and Chan, 2001]. Still, this enzyme complex has a particular role because, besides channeling electrons into the respiratory chain, it is also a member of the TCA cycle and thus directly connects these two central pathways of energy metabolism. This implies that it has key function in regulation [Hägerhäll, 1997].

Complex II is the smallest respiratory chain complex. In mitochondria, it has no accessory subunits as have complexes I, III, IV and the ATP-synthase compared to their bacterial analogues. It consists only of four subunits: The lipophilic subunits SdhC and SdhD are anchored in the membrane and SdhA (flavin protein) and SdhB form a hydrophilic dimer that protrudes into the mitochondrial matrix. The succinate binding site is located on SdhA and a flavin adenin dinucleotid (FAD) is covalently bound to this subunit. SdhB is the smaller of the hydrophobic subunits and is attached to SdhC. It contains three iron sulfur clusters, [2Fe-2S], [4Fe-4S], [3Fe-4S]. SdhC and SdhD enclose a heme (heme b) and contain two spatially separated and non-equivalent Q-binding sites, Q_P at the matrix side of the membrane and Q_D at the intermembrane space side, the indexes denoting 'proximal' and 'distal' [Sun et al., 2005]. The overall structure is given in figure 1.4.
All subunits of mitochondrial complex II are encoded by nuclear DNA [Rutter et al., 2010] [1]. The sequence and structure of SdhA and SdhB are well conserved across the species, whereas the membrane integral part can be classified into four distinct groups depending on the heme and subunit composition [Hägerhäll and Hederstedt, 1996].

Electrons coming from succinate first reduce FAD to $FADH_2$. Then they are transferred to SdhB where they pass via the three iron sulfur clusters to the membrane integral subunits. The subsequent electron transfer within these subunits, however, remains subject of discussion, and several possibilities have been proposed, as detailed in the following. Sun et al. [2005] assumed that electrons would first go on heme b, pass subsequently onto Q_P and when quinone at this site becomes completely reduced, further electrons would attain the quinone at the Q_D site. The exchange of quinones and quinols

[1] There are rare exceptions: Burger et al. [1996] showed that in the evolutionary distant eukaryotes *Porphyra purpurea*, a multicellular red algae, and *Reclinomonas americana* an unicellular bacteriovore, the genes corresponding to SdhB, SdhC and SdhD are mtDNA encoded.

Figure 1.4.: Structure of complex II. On the right, the corresponding locations of the redox centers are illustrated and the distances between them are given in angstroms and the midpoint potentials are given in mV. The pathway taken by the the electrons is indicated by arrows. Note that the order of steps in the second part of the path are controversy discussed. The image corresponds to mitochondrial complex II and is taken from Sun et al. [2005]. The matrix side is at the top.

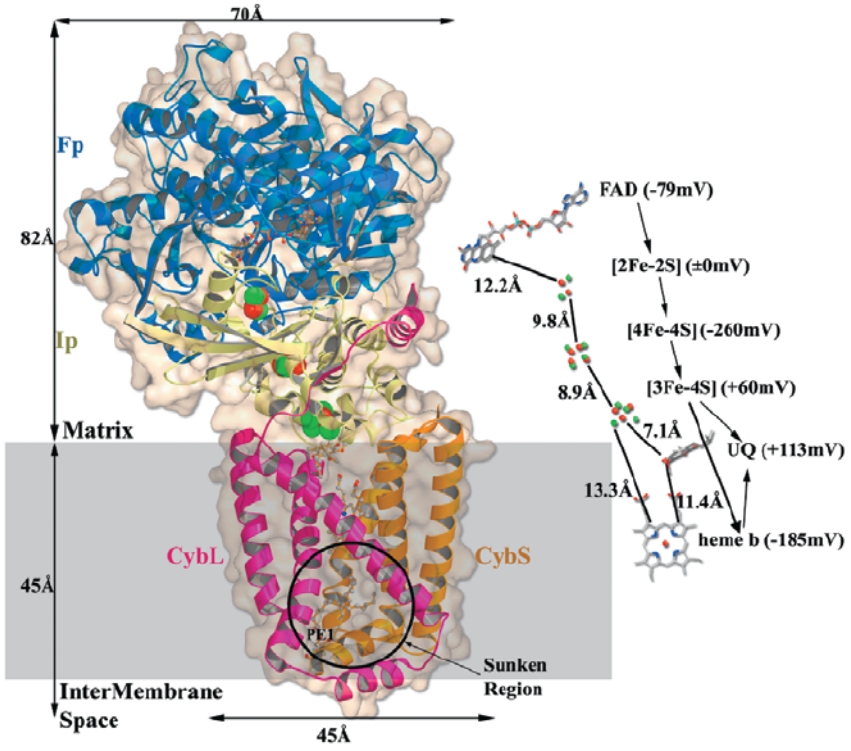

with the Q pool is assumed to be possible for both sites. In contrast Oyedotun and Lemire [2004] suggested for complex II in *S. cerevisiae* that electrons would first channel to a quinone bound at Q_p and then via heme b to Q_D to finally reduce another quinone . The latter would then be released into the Q-pool.
In both scenarios, the authors suppose that the existence of the 2 Q-sites plays a role in stabilizing the semiquinone intermediates [Sun et al., 2005, Oyedotun and Lemire, 2004], which generally occur in the context of quinone reduction and which can, if little stabilized, cause the formation of reactive oxygen species. A very different possibility was described by Cecchini [2003] who assumes that heme b in mammals is only involved in the reduction of fumarate (reverse reaction), but not in the reduction of quinone, the latter would take place at Q_D (because the distance of the two Q sites is too long for direct interactions i.e. without passing by heme b). Further it has been discussed whether heme b would have a exclusively a role in the assembly of this complex II but would not be involved in electron transport.
Hence, although being the smallest respiratory complex, the electron transfer within mitochondrial complex II is not fully understood. This complex has seen renewed interest due to the discovery of its role in human diseases [Rutter et al., 2010].

1.3.3. Complex III

The ubiquinol-cytochrome c reductase, also called bc1 complex, oxidizes ubiquinols to reduce cytochrome c. The net reaction is

$$QH_2 + 2\,cytc_{ox} + 2\,H_x \rightleftharpoons Q + 2\,cytc_{red} + 4\,H_{is}^{+} \tag{1.5}$$

The Gibbs energy of this reaction is $\Delta G'_0 = -32.5\,\mathrm{kJ}$ [Beard, 2005]. The reaction is further coupled to the transfer of two net charges. The respiratory complex is a dimer, consisting of two complex III monomers, each composed of 11 subunits having a total mass of around 240 kDa [Iwata, 1998]. Four prosthetic groups are located in the three subunits essential for the transfer of electrons during the catalysis: the cytochrome b subunit contains the two hemes b_L and b_H, another heme is located in the cytochrome c1 subunit, and eventually the Rieske Iron Sulfur Protein (ISP) holds an iron-sulfur cluster ([Fe-S]). The head of the ISP is mobile and moves between different positions [Iwata, 1998]. Only the cytochrome b is encoded by the mitochondrial DNA. Bacterial complex III contains only these three subunits, the role of the additional ten subunits in mammalian probably play a role in assembly and stability of the enzyme complex and regulation of its activity. The sequences of the core subunits 1 and 2 might indicate a proteinase activity [Iwata, 1998]. The overall structure of complex III is shown in figure 1.5 a).

The underlying mechanism of the reaction catalyzed by complex III is the so called Q-cycle. The hypothesis that in order to transfer protons from the matrix into the intermembrane space, complex III involves alternating oxidation of quinol and reduction of quinone at two spatially separated Q sites was originally formulated by Mitchell [1975]

Figure 1.5.: Structure of complex III and Q-cycle mechanism. a) Architecture of the dimeric complex III, taken from Zhang et al. [1998]. b) The Q-cycle mechanism. For each QH_2 becoming oxidized at the Q_o site, one electron is passed to a cytochrome c and another is transfered to the Q_o site, where it reduces a Q to semiquinone (SQ) in the first reaction cycle or a SQ to QH_2 in the second reaction cycle. Hence Q and QH_2 are both substrates and products of complex III. The scheme is taken from Berry et al. [2000].

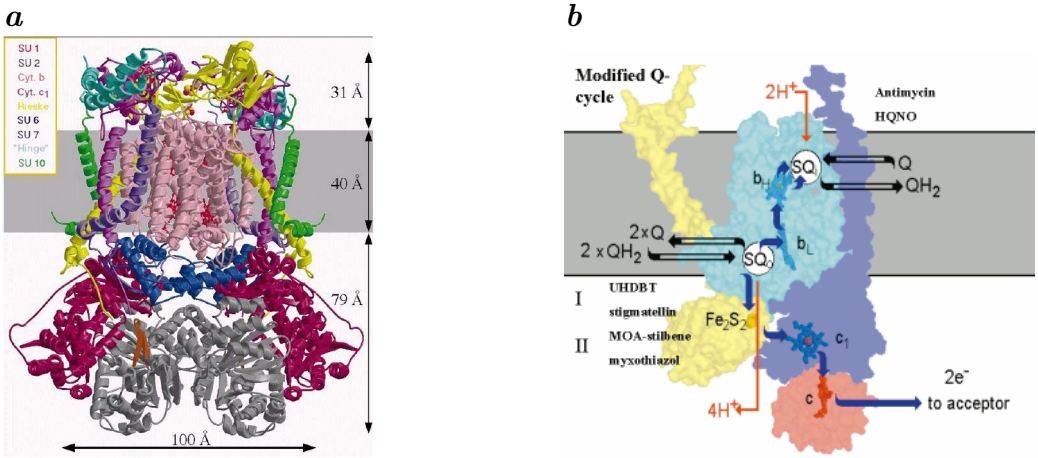

and modified later [Hunte et al., 2003, Berry et al., 2000]. It is illustrated in figure 1.5 b) and described below.
There are two binding sites for the redox pair Q/QH2 called Q_o and Q_i. The Q_o site is situated next to the intermembrane space. Binding to this site, ubiquinol releases two protons into the intermembrane space and donates consecutively two electrons to complex III. The first electron is transferred directly to the [Fe-S] of the ISP and is the passed to the heme of subunit cytochrome c1 and reduces finally a cytochrome c. The movement of the ISP head is suspected to approach the electron to the cytochrome c1 Zhang et al. [1998]. The second electron is transferred to the low potential b_L, from there against the electrical membrane gradient to the high potential b_H and then to the Q_i site. Here it reduces a quinone to a semiquinone (SQ) Hunte et al. [2003], Berry et al. [2000]. Since the activation energy is high for the oxidation of QH_2 at the Q_i-site, it is a rate limiting step, and hence the two bifurcated electron transfers appear as concerted Crofts and Wang [1989], Berry et al. [2000]. For the complete reduction of this molecule, the whole process is repeated: again a QH_2 becomes oxidized at the Q_o-site, the first electron being transferred to another cytochrome c and the second to reduce the SQ to QH_2, [Hunte et al., 2003, Berry et al., 2000]. The catalysis consist thus of two consecutive sub-reactions, constituting the Q cycle:

1. $Q^oH_2 + cytc_{ox} + Q^i \rightleftharpoons Q^o + cytc_{red} + SQ^i + 2H^+_{is}$
2. $Q^oH_2 + cytc_{ox} + SQ^i + 2H^+_x \rightleftharpoons Q^o + cytc_{red} + Q^iH_2 + 2H^+_{is}$

The indexes 'i' and 'o' denote the site where Q, QH_2 and SQ act. This makes possible the uptake of two protons from the matrix and the release of four protons into the intermembrane space for one complete turnover, i.e. the oxidation of two molecules QH_2, without a direct pumping of protons. The charge transfer is realized by the electrons passing from b_H to b_L.

1.3.4. Complex IV

Complex IV, also known as cytochrome c oxidase, is the last complex in the respiratory chain. By oxidizing cytochrome c it catalyzes the reduction of molecular oxygen to water. During one turnover four electrons are pumped from the matrix space into the intermembrane space. The reaction scheme is as follows:

$$4\,cytc_{red} + 8\,H_x^+ + O_2 \rightleftharpoons 4\,cytc_{ox} + 2\,H_2O + 4\,H_{is}. \tag{1.6}$$

In total, eight net charges are transfered against the electrochemical gradient. Gibbs energy of this reaction is $\Delta G_0' = 122.9\text{kJ/m}$. Bovine heart complex IV consists of 13 subunits whereof the 3 largest, subunits I - III, are mitochondrial encoded. The respiratory complex contains in total four metal sites, three of them are found in subunit I: heme a, heme a_3 and the copper Cu_B. The forth, copper Cu_A is included in subunit II. Subunit III does not contain a metal site but provides the O_2 pathway [Tsukihara et al., 1995, 1996].
These three subunits are the minimal requirement for the catalysis: Cu_A receives electrons from the cytochrome c, which are then transferred via heme a to heme a_3 and Cu_B. The two latter enable the binding of oxygen and its stepwise reduction to water via a fixed sequence of charge transfers [Brändén et al., 2006, Siletsky and Konstantinov, 2012].
The ten nuclear encoded subunits have probably functions in stabilization and assembly of complex IV and in particular they play a role in regulation of this enzyme complex Capaldi [1990], Stiburek and Zeman [2010]. Bacterial cytochrome c oxidase is also composed of the well conserved subunits I-III but contains in contrast only one additional subunit, while yeast has 9 additional subunits [Srinivasan and Avadhani, 2012]. The bacterial structure is shown in figure 1.6 a).

The protons that are used for the reduction of oxygen (scalar protons) and for the proton pumping (vectorial protons) need to be transferred from the matrix to the active site and to the intermembrane space, respectively. In bovine cytochrome c oxidase there are three different proton conducting pathways consisting of water molecules and polar residues: the K- and the D-pathway beginning at the matrix side and ending near the ensemble of heme a_3 and Cu_B. The D-path transfers both scalar and vectorial protons. The H-pathway overlaps partially with the D-pathway then continues until the intermembrane space side of the enzyme, see figure 1.6 b). It is supposed to transfer the vectorial protons [Brändén et al., 2006].
The oxygen reduction must be tightly coupled to the transfer of scalar and vectorial

Figure 1.6.: Structure of complex IV. a) Shows the 4 subunits constituting the cytochrome c oxidase of *R. sphaeroides*, whereof 3 are essential for the catalysis. Mammalian complex IV contains additional subunits. b) The red arrows indicate the positions of the K- and D-pathway for proton transfer up to the catalytic site where the reduction of oxygen takes place. The H-pathway partially overlaps the D-pathway and leads the vectorial protons to the intermembrane space (in top of the scheme), indicated by the dashed red arrow. Both figures are taken from Brändén et al. [2006].

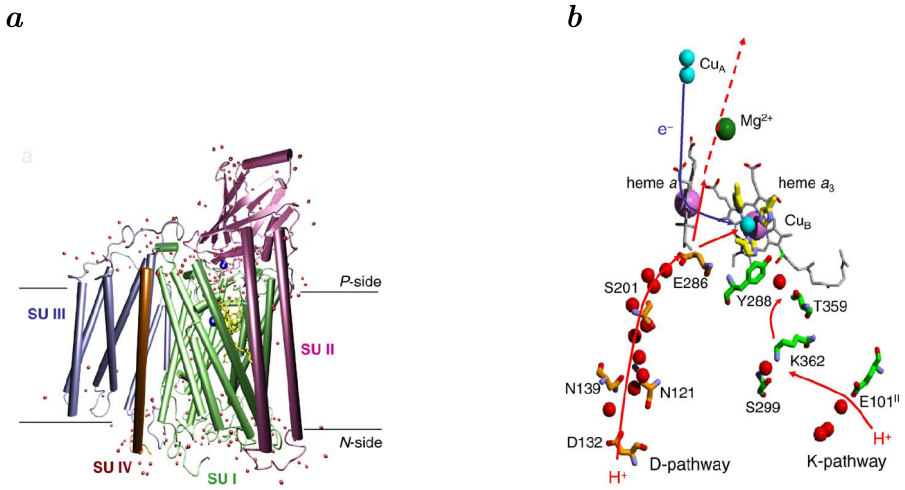

protons for an energy efficient functioning [Brändén et al., 2006]. Each reduction step of O_2 induces the transfer of 2 protons to the transmembrane space and/or the active site, depending on the reduction step [Siletsky and Konstantinov, 2012]. In *R. sphaeroides* a conformational change is supposed to alternately open either the K-path or the D-path for proton transfer [Qin et al., 2009]. The change might be triggered by the reduction of Cu_B [Ferguson-Miller et al., 2012]. A similar gating mechanisms can be expected for bovine complex IV. However the mechanism of coupling of oxygen reduction to proton translocation remains still unclear Ferguson-Miller et al. [2012].

Shinzawa-Itoh et al. [2007] found that Complex IV incorporates 13 different phospholipids. Their positions were revealed to be equal for bovine and *paracoccus* complex IV [Qin et al., 2007], which indicates that they have an important role. It has been proposed that they may insulate the internal proton pathways from the surroundings, adapting flexibly to conformation changes [Ferguson-Miller et al., 2012].
Complex IV is highly regulated: There are the direct effects on the enzyme's activity by reduced and oxidized cytochrome c and the electrochemical membrane gradient. But further the enzyme is inhibited by ATP Arnold and Kadenbach [1997] and is very sensitive to the ATP/ADP ratio: 7 binding sites for ADP and ATP have been determined and additionally 3 being specific for ADP. Further it could be demonstrated that besides the matrix ATP/ADP ratio also the cytosolic ATP/ADP ratio is regulating the cytochrome c oxidase [Napiwotzki and Kadenbach, 1998].
Further phosphorylation plays an important role in regulation: at least 10 subunits of complex IV contain phosphorylation sites. [Helling et al., 2008]
Another regulator is nitric oxygen (NO). Brown and Cooper [1994] showed that it inhibits reversibly complex IV competing with oxygen for the oxygen binding site. The author hypothesized that NO may have a role in sensing the concentration of oxygen and regulating correspondingly the affinity of respiration for oxygen Brown [1995], it may be of importance for the distribution of oxygen parts of tissues with a low oxygen concentration Brookes et al. [2003].
Complex IV is moreover regulated on the expression level: There are nuclear encoded subunits which have several isoforms in different tissues or they can be induced specifically for a given condition [Srinivasan and Avadhani, 2012].

1.4. The F_1F_o-ATPsynthase - phosphorylation of ADP

Like the respiratory chain complexes, the F_1F_o-ATPsynthase is localized inner mitochondrial membrane. It uses the proton gradient that is established by the respiratory chain in order to drive the phosphorylation of ADP [Mitchell, 2011], catalyzing the following reaction

$$ADP + P_i + n_A\, H_{is} \rightleftharpoons ATP + H_2O + n_A\, H_x \tag{1.7}$$

The reaction is reversible, i.e. by hydrolyzing ATP the F_1F_o-ATPsynthase pumps protons from the matrix into the inner membrane space [Sone et al., 1977, Van Der Drift

et al., 1978]. The stoichiometric factor n_A is for bacteria and mitochondria in general between 2 and 4, with some exceptions, as summarized by Tomashek and Brusilow [2000]. The value of n_A is probably related to the particular structure of this enzyme complex which is shortly described below and then related to its engine-like catalytic mechanism.

The F_1F_o-ATP-synthase can be divided into the two subcomplexes F_1 and F_o. F_o contains all hydrophobic membrane integral subunits, i.e. an oligomer of 8-15 alike subunits c that are symmetrically arranged in the form of a cylinder whose axis is perpendicular to the membrane plane [Pogoryelov et al., 2005, Watt et al., 2010], and one subunit a that is laterally attached at it [Jiang and Fillingame, 1998]. F_o comprises further a stator composed of 2 (E. coli : b dimer [Rodgers et al., 1997]) to 4 (bovine: OSCE, b, d, F6 [Collinson et al., 1994]) subunits. It is linked to the c-ring and subunit a [Ono et al., 2004] and protrudes into the matrix space, where it is laterally attached to the globular structure of F1 [Rees et al., 2009] This flattened sphere is made up of six circular arranged and alternating α and β subunits that enclose subunit γ [Abrahams et al., 1994, Rees et al., 2009]. The latter constitutes an axle which emerges out up to the c-ring where it is attached at its membrane side . ϵ stabilizes the interaction between δ and γ subunits. The structure of the F_1F_o-ATP-synthase is shown in figure 1.7.
The subunits a and A6L (beef nomenclature) are encoded by mtDNA, all the remaining subunits are nuclear encoded.

The special structure of ATP-synthase is strongly related to the mechanism of the F_1F_o-ATP synthesis, that is comparable to a miniature engine or a mill:
Sambongi [1999] demonstrated that the c-ring is a rotor along with the axle composed of theγ and adjacent subunit(s). In case of a sufficiently high proton motive force, it is driven by a channeled influx of protons from the intermembrane space into the matrix. This channeling is realized by the a subunit, which mediates the binding of a proton coming from the intermembrane space on the c-subunit next to it. Hereby, a conformational change of the latter is induced, provoking a rotation of the c-ring such that the (unoccupied) adjacent c subunit is moved under the cover of a [Vik and Antonio, 1994]. Again a proton will be bound to the 'actual' c-subunit and the same process is repeated and hence keeps turning the c-ring. After an almost complete revolution, an occupied c-subunit releases its proton into the matrix space, which is also mediated by a. This subunit is hence responsible for the parallel influx and efflux of the protons to and from the c-ring.
The rotation of the c ring implies also a rotation of the attached axle, the γ subunit, whose asymmetric head is located in the center of the ring structure of F_1. Here, its movement provokes conformational changes of the β subunits. Each β subunit contains a binding site for ADP or ATP, respectively, as well as for Pi, with an α subunit being faced to it. The conformational changes result in approaching bound ADP and Pi and eventually their transformation into ATP. Each β subunits undergo the same series of stages, i.e. Pi-binding, ADP-binding, ATP formation, ATP release, each time with a 120 $\circ$ rotation, with respect to the orientation of the head of γ [von Ballmoos et al., 2009]. During a complete revolution, 3 molecules of ATP are formed. Because the revolution of

Figure 1.7.: Structure of ATPsynthase. a) The overall architecture, composed of subunit structures steaming from different organisms, mostly bacteria. For the mitochondrial enzyme complex, the F_1 subcomplex is located in the matrix, while the protons are pumped in the intermembrane space. The figure is taken from von Ballmoos et al. [2009]. The Scheme in b), taken from Fillingame et al. [2003], illustrates the mechanism of the ATPsynthase: Protons coming from the outside will bind to the c-ring and force it to turn. This movement causes conformational change in the global structure of the F_1 subcomplex which allow the phosphorylation of ADP.

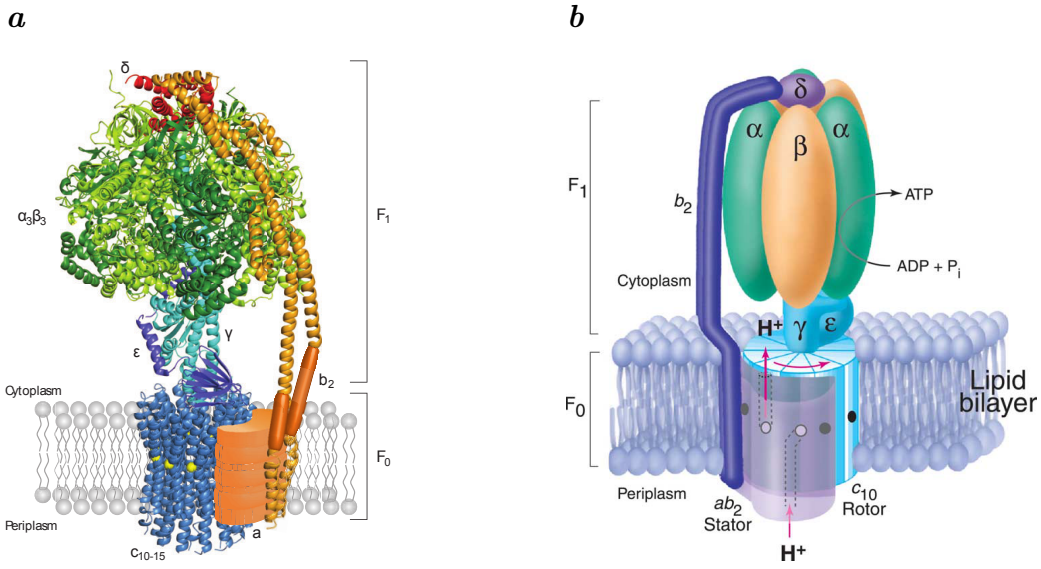

the $\alpha_3\beta_3$-ring is coupled to the rotation of the c-ring, in bovine, where the c-ring contains 8 subunits, ideally 8 H^+ of the intermembrane space are required in order to produce 3 ATP, which explains the above cited stoichiometric factor n = 8/3 [Watt et al., 2010]. However, the c-ring of yeast contains 10 subunits c and thus n = 10/3. Depending on the organisms (plants, bacteria) the number of subunits in the c-ring can vary, e.g. plants, microbacteria. Within one species, however, n is constant [Watt et al., 2010].
The $\alpha_3\beta_3$-ring is fixed permanently via a stator, the b dimer, to subunit a, in order to avoid that the torque entails a rotation of this ring structure, which would amount to the loss of power transmission for the (mechanical) ATP production.
ATP hydrolysis corresponds to the inversion of the above described process.

1.5. Why modeling the respiratory chain and the oxidative phosphorylation?

The oxidative phosphorylation is a complex system and not all properties and dependencies can (easily) be regarded with a pure experimental approach.

1.5.1. Benefits of modeling in biology

In general, modeling helps understanding complex systems which are often not interpretable by intuition, and further intuition may lead to wrong conclusions. In many biological disciplines one is often confronted with large systems and/or a high complexity: transcriptomics, proteomics, metabolomics, ecology , etc. Further the considered problem can comprise several levels, e.g. the regulations and interactions in tissues may encompass gene expression until the single cell's metabolism and the functioning of the whole tissue.
Here, models can help testing hypothesis by predicting the behavior of a system. Analyses of the model can help to identify important components or components which play only a minor role. For instance, drug targets can be tested, and in particular the simultaneous application of several drugs affecting different components in a given system may reveal unexpected interactions. This is in particular interesting for medical research, e.g. for finding an optimal treatment for different types of cancer, or in agriculture, where the application of fungicides and pesticides should be optimized and not harm other organism.
Models can also be used for planning experiments, e.g. by identifying conditions which are important to assay. Further models permit to analyze situations which are difficult to access experimentally.

Hence modeling is a powerful tool to address actual questions with a theoretical approach. But a model has to be built very carefully: First, the nature of approach, e.g. stochastic or deterministic, is to adapt to the problem. For instance a single enzyme's functioning may be very precisely described with a stochastic approach, but for a system

composed of several enzymes a stochastic model can be computationally much too time consuming. Here, the enzymes behavior may be sufficiently well represented using rate equations in a deterministic approach.
Then, the choice of model components and the way they are described is essential for the reliability of the model: too many unknown parameters make predictions too uncertain, too less details cannot reproduce the behavior of the system of interest. In this regard it is also important whether the parameters values have a biological meaning and can be directly determined by experiments, like the maximal catalytic rate of an enzyme, or whether they have to be fitted to more general results, which increases the uncertainty. A theoretical approach is thus always a kind of compromise and does not reproduce reality completely. However, knowing the limits of a model is also knowing the framework in which results are reliable and thus where simulations can contribute much to the understanding of systems.

1.5.2. Better understanding the role and functioning of the oxidative phosphorylation in physiological and pathological situations

Why is it worth to investigate the respiratory chain and oxidative phosphorylation with a theoretical approach? First of all, the system itself is complex: The OXPHOS complexes have all intricate mechanisms and their turnover rates are influenced by the proton gradient which they they establish or use during catalysis. Even though OXPHOS is composed of only five complexes, the simulation of this ensemble requires the implication of further components such that a flux through the system is possible. The mitochondrial compartmentalization has to be considered in order to account for the proton pumping over the inner membrane.
Then, OXPHOS plays a central role in metabolism. It is linked to many processes which are of high importance and of high interest in many research field, for both under physiological and pathological conditions.

Oxidative phosphorylation under physiological conditions

- The relative composition of OXPHOS complexes differs within different tissue; also the specific activities have been found to be different [Benard et al., 2006]. This is certainly in relation with the workload on the cell and the thereof resulting energy demands. It is obvious that for instance cardiac myocytes have energy demands other than do have liver cells.

- The respiratory chain complexes assemble to super complexes, in different stoichiometries CI_{0-1} + $CIII_2$ + CIV_{0-2} [Dudkina et al., 2010, Genova et al., 2008]. It is supposed that the assembly renders more efficient the system, possibly by substrate channeling. Schäfer et al. [2006] found a higher activity for supercomplex CI+$CIII_2$+CIV than for the assembly CI+$CIII_2$.

- Complex I and complex III are the main sites of production of reactive oxygen species (ROS) [Cadenas and Boveris, 1977, Hirst et al., 2008, Selivanov et al.,

2011]. The extend of ROS production is dependent on the electrochemical gradient [Rottenberg et al., 2009, Tahara et al., 2009]. ROS can cause damage to proteins, lipids and nucleotides. It is hypothesized that ROS is a major player in aging processes. The mitochondrial theory of aging says that ROS damage mitochondrial DNA, which would thus respectively increase the rate of mutations and thereby increase dysfunctioning of respiratory chain complexes and finally enhance ROS production [Kowald, 2001, Cadenas and Davies, 2000, Lenaz et al., 2006]. Moreover the mtDNA reparation system is less efficient than the nuclear one. But on the other side superoxide dismutase activity removes ROS. Besides their damaging role, ROS have also be linked to signaling and regulation [Camello-Almaraz et al., 2006, Echtay et al., 2002, Klimova and Chandel, 2008].

- Mitochondria can exist in large dynamic networks, the state of the networks being ascribed to different energy states. Fusion and fission are suspected, amongst other factors, to be dependent on the electrochemical proton gradient.

- The availability of substrates an other conditions will shift the system more to aerobic or anerobic metabolism, also very dependent on the organism. The respiratory chain and especially complex IV is suspected to sense the oxygen concentration. This may allow to adapt to low oxygen concentration, an may also assure that cells distant to blood vessels will be supplied with oxygen, preventing the upstream cells from consume to much.

Oxidative phosphorylation in the context of pathologies

- Mutation causing dysfunctioning within the OXPHOS system can have severe consequences. Concerned are in particular tissues with a high energy demand, like heart and skeleton muscle, brain, kidney and retina [Koene and Smeitink, 2011].

- Mitochondrial diseases are rare genetic disorders causing dysfunctioning of a respiratory chain complex. They are often lethal.

  The 'milder' disorders are mostly multisystemic, i.e. several organs are affected in the diseases, but also only one isolated organ can be concerned. The phenotypes of a dysfunctioning can be various, and various different dysfunctions can lead to the same or similar phenotype. Depending on the degree of heteroplasmy of mitochondrial DNA, the phenotype may be more or less expressed, and mutations may be compensated until a certain degree.

  Some disorders shall be shortly noted here: The Leigh-Syndrom, early onset (3-12 months) includes psychomotoric retardation, fatigue and brain system dysfunction; the Leber-Hereditary Optic Neuropathy (LHON) starts at the age of 15-30 years leading to a loss of vision due to degeneration of optic nerves and retina. Maternally Inherited Diabetes and Deafness (MIDD) has its onset for deafness at 30 years, 40 years diabetes. Mitochondrial Encephalomyopathy, Lactic Acidosis, Stroke-like Epsisodes (MELAS) symptoms are epilepsy and dementia, often accompanied

by migraine and psychological problems and stroke-like episodes. Other clinical syndromes often accompany these 'core symptoms' [Koene and Smeitink, 2011].

Until today, there is no possibility to cure these disorders, and often the progress of the diseases can hardly be retained. One of the rare exception is Coenzyme Q deficiency, which causes cerebellar ataxia and atrophy, mental retardation, muscle weakness, nephropathy etc. In some cases the symptoms can be improved by administration of excess of CoQ [Koene and Smeitink, 2011].

- OXPHOS is also implicated in very wide spread diseases: Dysfunctionings in the mitochondrial energy metabolism can promote Parkinsons disease [Exner et al., 2012], and abnormalities in the mitochondrial metabolism have been found related to Alzheimer [Atamna and Frey, 2007], Huntington and other neurodegenerative diseases [Schapira, 2012]. Mitochondrial disorders are often accompanied by type-2 diabetes.

- Recently a new interest is put on complex II, it has been suspected to play a significant role in cancer [King et al., 2006]. being member of the respiratory chain *and* the Krebs cycle. In many types of cancer, the cells often produce their ATP by glycolyses (Warburg effect), thus the mitochondrial metabolism has changed significantly.

- In the extreme case of anoxia, the respiratory chain will be blocked, the ATP-synthase will reverse, hydrolyzing ATP will help maintaining a membrane proton gradient.

  In transplantations of organs, but also in other situations where ischemia appears, like circular shock and stroke, the reoxygenation causes cellular injury in which ROS are involved [Li and Jackson, 2002]: The respiratory chain intermediates are suspected to be largely reduced, since the terminal complex IV is blocked, lacking oxygen. A sudden supply with oxygen enhances the ROS production because the substrate pressure on the complexes is high (reduced substrates).

1.6. Historic and facts of modeling the respiratory chain and OXPHOS

The modeling of oxidative phosphorylation has a long history, and reaches from basic considerations up to large models. The summary below is taken from Mazat et al. [2006] and has been modified and extended.

1.6.1. The first models of oxidative phosphorylation are based on non-equilibrium thermodynamics

Rottenberg [1979] developed one of the first significant model in the framework of Non-Equilibrium Thermodynamic model (NET-Model) involving a linear dependence of the flux on the thermodynamic forces . Also based on NET Stucki [1980b,a] describes all

the states of oxidative phosphorylation dynamics (state 4, state 3, uncoupled state, etc.) in terms of energy conversion with the use of phenomenological coefficients; the author looked for the optimal efficiency of the system and for the maximal net rate of ATP synthesis, and calculated further the degree of coupling in these conditions. Even if one can argue that oxidative phosphorylation could be out of the linear domain around equilibrium, Stucki's description is simple and indicates the fundamental parameters involved: degree of coupling, thermodynamic forces, rates, optimal efficiency, phenomenological stoichiometry, etc.
A similar model was derived by Pietrobon et al. [1982]. Pietrobon and Caplan [1985] described redox-driven proton pumps and ATP synthesis in mitochondria with the NET approach. Both models were combined for the simulation of inhibitor and uncoupler titrations [Pietrobon, 1986].

1.6.2. Extension of the models, including more details

Bohnensack [1981] was probably the first to derive a quantitative model involving nearly all the components of oxidative phosphorylation in an algebraic model, and further using kinetic expressions. With the help of this model Bohnensack et al. [1982], Gellerich et al. [1983] as well as Groen et al. [1982] were able to demonstrate that the control of oxidative phosphorylation was shared by several steps as predicted by metabolic control analysis (MCA) [Kacser and Burns, 1973, Heinrich and Rapoport, 1974, Reder, 1988].
Holzhütter et al. [1985] also considered all components of oxidative phosphorylation, the respiratory chain however described by one simple equation. The modeling approach is now dynamic, based on ordinary differential equations applied to isolated rat liver mitochondria.
Korzeniewski [1991] then developed a more comprehensive model also based on ordinary differential equations, which was applied to isolated mitochondria or to intact tissues (muscle, heart and liver). The model was used to calculate the control coefficient in oxidative phosphorylation [Korzeniewski and Froncisz, 1992], to fit threshold curves in muscle and to predict the shape of threshold curves at low oxygen pressure Korzeniewski and Mazat [1996]. Further the model served to study the transition from rest to intensive work in muscle [Korzeniewski and Zoladz, 2001], leading to the concept of parallel activation of the respiratory complexes Korzeniewski [2001, 2007]. For this large field of application, it was necessary to develop, adapt and extend the model. The simple rate equations for the respiratory chain complexes and the ATPsynthase remained the same except for some applications, notably extreme conditions like threshold effects and strong ATP decrease [Korzeniewski and Mazat, 1996, Korzeniewski, 1998].

1.6.3. More recent works

All the previous models, based on ordinary differential equations, necessarily assume that the mitochondrial compartments (matrix, inner membrane and inter-membrane space) are homogeneous.

Aliev and Saks [1997] developed a model to describe the energetics in heart myocytes, including the phosphorylation of ADP and consumption of ATP, including the diffusion and transport of the adenosine nucleotides between the different compartments. This model was refined by Vendelin et al. [2000, 2004], the equations constituting the respiratory chain of Korzeniewskis model were included. It takes into account the presence of creatine kinase and adenylate kinase, both in the inter-membrane space and in the cytosol, to ensure first the conversion of ATP in phosphocreatine, which diffuses in cytosol and then the conversion of phosphocreatin back to ATP where it is used; a backward diffusion of creatine closes the functional cycle.

Ramakrishna et al. (2001) studied the constraints imposed by the stoichiometry of biochemical reactions, especially the maintenance of an NADH steady-state. Flux balance analysis (FBA) was used to characterize the optimal flux distributions for maximal ATP production. The model includes glycolysis, TCA cycle, lactate production and β-oxidation of fatty acids. Using FBA, they also characterized the metabolic behavior due to genetic diseases, particularly the overproduction of metabolites from TCA cycle as sometimes observed in clinical studies of mitochondrial pathologies. However, this study is performed under the assumption that ATP synthesis has to be maximal, which is not necessarily the case. Further it does not take into account the rate laws of the different steps of the mitochondrial network, nor does it respect thermodynamical constraints.

Cortassa et al. [2003] developed an integrated model of cardiac mitochondrial energy metabolism and calcium dynamics. The model includes a representation of the TCA cycle, the transport of Ca^{2+} across the mitochondrial inner membrane and the regulation of dehydrogenases by Ca^{2+}. One aim of this model is to describe the supply of mitochondrial energy to the cellular demand, through the variations of intracellular and intramitochondrial Ca^{2+}. The model was then extended further and used for different application. For instance, the excitation and contraction of cardiac myocytes has been linked to the mitochondrial ATP generation Cortassa et al. [2006], and the model has been extended to incorporate pH, Na^{+} and phosphate dynamics [Wei et al., 2011].

Beard [2005] proposed a biophysical model of the mitochondrial respiratory system and oxidative phosphorylation mainly applied to cardiac mitochondria. It describes mainly the same components as the model of Korzeniewski, however used less constraints and more state variables, increasing the dynamics of the model. The complexes of the oxidative phosphorylation are represented by modified mass action law, allowing for a more important role of the substrates and product concentrations on the rates. Wu et al. [2007] combines this model with an extensive model of the TCA-cycle and includes several transporters over the inner membrane. The model reproduced in vitro data from isolated cardiac mitochondria and in vivo data from human skeleton muscle and was used to analyze the regulative roles of NAD and ADP with respect to the TCA cycle and could show that consequently to a decrease of cytosolic pH the potential over the inner mitochondrial membrane decreased as well as the ATP production. The context of this model is further enlarged in the model of Bazil et al. [2010]. It includes Ca^{2+} dynamics and takes into account mitochondrial volume dynamics.

1.6.4. Oxidative phosphorylation in the context of large metabolic models

With a Systems Biology approach and within the framework of the e-cell project, Yugi and Tomita [2004] built a model of 58 reaction linking 117 metabolites. They found 286 out of 471 kinetic parameters in 45 articles. The model involves the respiratory chain, the TCA cycle, the β-oxidation of fatty acids, and the carriers of the inner mitochondrial membrane. Users can observe the time-course of enzyme activities and of metabolite concentrations. One can criticize this model for integrating a too vast set of parameters from different species (human, bovine, pig, rabbit and rat) and different tissues (heart, liver, etc.).
Vo et al. [2004] reconstructs the mitochondrial metabolism of human cardiomyocytes based on proteomic and biochemical data and includes thereby the above cite model of Ramakrishna et al. [2001]. The metabolic network involves 189 reactions and 230 metabolites. FBA was applied to calculate optimal flux according to three separate objective functions : ATP production, heme biosynthesis and phospholipids biosynthesis.

1.7. Aim of this work

The general aim of this work is to build a model of OXPHOS in order to better understand how local defects (enzyme deficiencies) are expressed globally in mitochondrial ATP synthesis and oxygen consumption. The model shall be a reliable and well suited representation of the OXPHOS which allows then, combined with other models to simulate and analyze the role of OXPHOS with respect to the aspects listed in section 1.5.2.
For this purpose, we need to have a good description of the kinetic properties of each of the OXPHOS complexes, since a deficiency of one complex may cause abnormal situations for the other complexes, i.e. extremely high or low substrates and products concentrations, which may compensate the given deficiency up to a certain extent . Further it is to be expected that such a perturbation will also affect the electrochemical gradient, which will in turn affect the kinetics of the complexes and other activities linked to the gradient.

None of the above presented models (section 1.6) used suitable equations for this task. Usually very simple rate equations have been employed for the OXPHOS complexes. An exception is the model of Yugi and Tomita [2004], where classical saturation kinetics describe these enzyme complexes. However, with exception of the F1Fo-ATPsynthase, all employed kinetics are independent of the membrane gradient, hence denying its influence on the enzyme's activities.

We have thus chosen the bottom up approach to build an OXPHOS model. Our approach follows the philosophy to build a model upon well described components, then assemble them to a system and finally compare the outcome with experimental data. In consequence of discrepancies, the basis has to be readapted, which can be a refinement of the equations or even a change of an equation type, as well as the integration of

additional components in the model. Also effectors (activators and inhibitors) may be taken into account.
The main modeling steps are reflected in the chapters of this work:

Chapter 2 We search for a good representation of the kinetics of each OXPHOS complexes in the absence of the membrane proton gradient. In order to have a consistent data set, we decided to perform kinetic measurements. They served to evaluate different types of rate equations upon a large ranges of substrate and product concentrations. Being based on the same tissue (bovine heart) and equal experimental conditions, the therefrom obtained parameter values are compatible for the different complexes.

Chapter 3 The effect of the membrane proton gradient is integrated into the rate equations, respecting thermodynamic constraints. The aim is to modify the equations such that they can describe the complexes kinetics over a wide range of the proton gradient.

Chapter 4 The new rate equations were now put together in a system. The system has to contain further components in order to take account of the mitochondrial structure and basic reactions linked to OXPHOS. Then the functioning of the ensemble of the new OXPHOS rate equations is evaluated and compared to experimental data.

2. Modeling the isolated OXPHOS complexes

The first step in the project of modeling the oxidative phosphorylation is to find relatively simple rate equations for each of the respiratory chain complexes and for the ATP synthase, which describe well their kinetics over a wide range of substrate and product concentrations firstly in the absence of the membrane proton gradient.
In this chapter, we first give an overview of the features that play a role in the kinetics of the OXPHOS complexes and discuss then equations that have been used in other respiratory chain or OXPHOS models or which are resulting directly from a supposed kinetic mechanisms at steady state.
We list typical rate equations for enzyme kinetics and analyze them afterwards with respect to their capability to describe the respiratory chain complexes upon experimental data obtained from kinetic measurements that we have performed on submitochondrial particles in absence of the membrane gradient.

2.1. Overview of existing rate equations used for OXPHOS complexes

2.1.1. Enzyme kinetics and OXPHOS complexes

The kinetics of an enzyme describes the behavior of its catalytic activity dependent on substrate and product concentrations. Typically their activity is low for small substrate concentrations and increases until a saturating substrate concentration is reached, at this point, the binding of substrates to the enzyme is faster than the maximal turnover of the enzyme. In an enzyme assay this maximal rate is termed V_{max}. It can be related to the enzyme concentrations E and the specific activity k_{cat}:

$$V_{max} = E \cdot k_{cat} \tag{2.1}$$

A very simple example for the mathematical description of enzyme kinetics is the Michaelis-Menten equation [Michaelis et al., 2011], which describes an irreversible catalyzes:

$$v = \frac{V_{max} \cdot [S]}{K_m + [S]} \tag{2.2}$$

according to the reaction scheme

$$E + S \rightleftharpoons ES \rightarrow E + P \tag{2.3}$$

Here [S] is the concentration of the substrate S and the Michaelis-Menten constant K_m denotes the substrate concentration at which the catalytic rate is half of its maximal activity. P denotes the product.
The equation is restricted to the particular reaction scheme 2.3, but catalytic processes are often reversible For this case, we use the terms V^+_{max} and k^+_{cat} for the forward rate and V^-_{max} and k^-_{cat} for the reverse rate. With increasing number of substrates and products, the enzyme rate laws become more complicated. To every substrate and product, a K_m can be assigned. Both, K_m and V_{max} are apparent and do not necessarily correspond to a Michaelis-Menten scheme of reactions.

The negative effect of an inhibitor on the enzyme activity is described by its inhibition constant, K_i. In case of a non-competitive inhibition, i.e. the inhibitor does not compete with a substrate or product for a binding site, but docks on a regulative site of the enzyme. The value of K_i corresponds to the inhibitor concentration, where the activity is half of its rate measured in absence of the inhibitor. For competitive inhibition, this statement is not valid, since the degree of inhibition is dependent on both, the inhibitor concentration and the concentration of the substrate with which it competes for the same binding site. Also for a product, a K_i can be determined, since it can be considered as competitive inhibitor with respect to its corresponding substrate.
There are also activators which exert a positive effect on enzyme activity. The simplest form of activation would be an activator that acts similar to a substrate, thus in its absence one would have zero activity and an activation constant K_a would denote the activator concentration at which half of the maximal activation is achieved.

Enzymes catalyze their reactions according to different mechanisms, which define generally the binding and release order of substrates and products. This is also constitutive for the observed activities, e.g. if two substrates share the same binding site and therefor must access it subsequently, they act not only as substrates but also as reciprocal inhibitors. The proper description of steady state kinetics can therefore involve additional parameters.
Further enzyme activities are influenced by temperature: increasing temperature within a certain range often accelerate catalysis. Enzymes feature also a pH optimum, even if protons do not take part in the catalyzed reaction. The activity dependence on pH can vary significantly among different enzymes.

All these considerations are in general valid for enzyme kinetics. Although this chapter focuses on the determination of an appropriate description of the kinetics of the OXPHOS complexes, at this point we will also mention the following issues for a complete consideration of these particular enzymes: since the respiratory chain complexes I, III and IV and the ATPsynthase are involved in proton translocation over the inner mitochondrial membrane the following two components also influence essentially their kinetic behavior. That is on one hand the electrical gradient over this membrane and on the other hand the pH difference between both sides of the membrane.
Figure 2.1 summarizes what influences the kinetics of the isolated OXPHOS complexes

and lists additionally features that are important for the modeling of the whole OXPHOS system.

Figure 2.1.: Aspects of modeling the oxidative phosphorylation

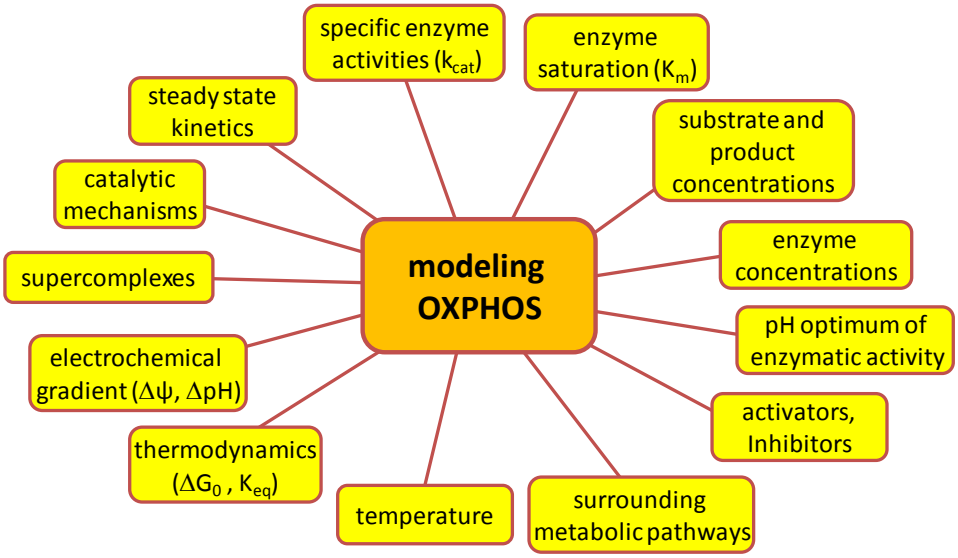

2.1.2. General OXPHOS and respiratory chain models, or more general models

In the general introduction we gave insight into the long history of modeling OXPHOS and mentioned various approaches to describe the OXPHOS system. We will have a closer look at two of them, the prominent models of Beard [2005] and Korzeniewski [2001]. Both authors modeled the OXPHOS complexes individually, however, they used very simple rate laws for the description of their kinetics and did not take into account the afore mentioned general aspects of enzyme kinetics.

Korzeniewski models complexes I and III with near equilibrium thermodynamics, where the enzyme activities are proportional to the free reaction energy ΔG_R.

$$v = k \cdot (-\Delta G_R) \tag{2.4}$$

where

$$\Delta G_R = \Delta G_0 + \Delta \mu_H + RT \cdot \left(\ln \frac{\prod_j P_j^{\eta_j}}{\prod_i S_i^{\nu_i}} \right)$$

with S_i the substrates and P_j the products and their corresponding stoichiometric factor ν_i and η_j, respectively. ΔG_0 is the Gibbs standard energy of the reaction and $\Delta\mu_H$ is the proton motive force.

Complex IV is modeled with mass action and independently of the membrane gradient, complex II is not part of the model.

Beard uses basically mass action law for the description of the individual complexes:

$$v = k \cdot \left(\prod_i S_i^{\nu_i} \cdot e^{\Delta G_0 + \Delta\mu_H} - \prod_i P_i^{\nu_i} \right) \tag{2.5}$$

The author has extended the rate equations for complex III and IV by some multiplicative factors in order to improve the data description. They do not change the general nature of mass action. Also this model does not include complex II.
Mass action is often well suitable for the description of chemical reactions but does not allow to reproduce the typical enzyme saturation behavior. The rate goes up linearly with increasing substrate concentrations. But at least a limit is set by the total concentrations of the OXPHOS relevant components being fixed.

Indeed both models reproduce the general features of the whole OXPHOS-system in the presence of a physiological membrane potential difference, when put together in a differential equation system. However, when these equations are applied for the description of the kinetics of the isolated OXPHOS complexes in absence of the membrane gradient, they are far from describing a typical enzyme behavior. This is clearly shown in figure 2.2 where the initial rate measurements performed on complex IV cannot be reproduced, neither by the Korzeniewski model nor by the Beard model. In contrast, the curves simulated with Michaelis-Menten like kinetics are very close to the experimental data points.
The models of Beard and Korzeniewski are thus very limited with respect to the analysis of the individual role of the OXPHOS complexes and the effects of deficiencies in the context of the whole system. Besides such simple approaches there are models which are too detailed for our purpose focusing on the precise description of the internal catalytic steps of an isolated complex. We want to find a good compromise between these two very different levels of modeling for a good but still relatively simple representation of the complexes kinetics.

2.1.3. Rate equations for modeling the kinetics of the OXPHOS complexes

We think that it is very important to consider the basic enzyme features, i.e. to account for saturation as well as the interaction of components with their binding sites and the competition of a substrate with its corresponding product. These aspects are quite important in the background of mitochondrial diseases or when regarding the influence of drugs on the OXPHOS complexes: binding sites may be altered, changing substrate enzyme interactions, as well as mutations may concern the inner catalytic processes or lead to a lower level of an OXPHOS complexes.

Figure 2.2.: Comparison of rate equations for the description of OXPHOS complexes upon initial rate measurements performed on complex IV, where the total amount of cytochrome c has been varied. a) In the model of Korzeniewski [2001] the rate of complex I and III is assumed to be proportional to the Gibbs energy of reaction (see equation 2.4). b) The author uses further mass action law (MAL; equation 2.5) for complex IV. This type of rate equation is further used in the model of Beard [2005]. Both equations, especially NET, are not suitable for a satisfactory description of the typical enzyme saturation behavior. c) For comparison:a Michaelis-Menten like equation (simplified random binding, equation 2.47) can describe the data points with good accuracy. The parameters of all equations have been estimated mimimizing the root mean square deviation of the simulated and experimental data points: NET: k = 0.0562 nmol/min/mg; MAL: $k_f = 0.515$ nmol/min/mg; RBs: $k_{catf} = 14361$ nmol/min/mg, $K_{cred} = 70.2\mu M$, $K_{cox} = 62.5\mu M$, $[O_2]/K_{O2} = 200/1$ (fixed). The reverse velocities are quasi zero du to the high Gibbs energy of reaction and have thus been neglected. Experimental series: + 94% 51%◇ 24% reduced cytochrome c.

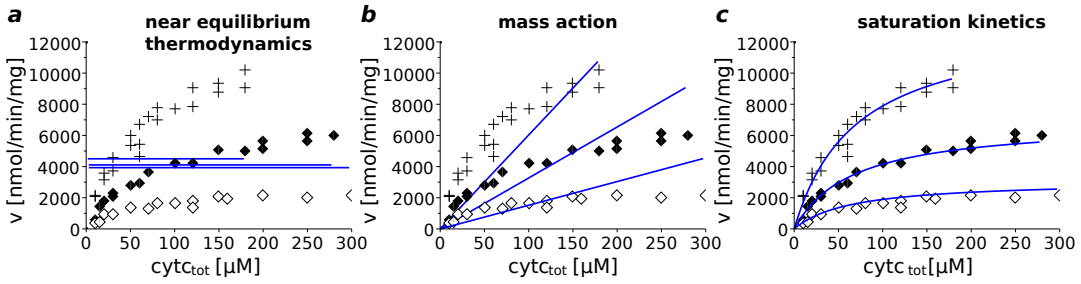

Obviously, Michaelis-Menten like equations are good candidates because they account for these issues whilst still having simple structures and a limited number of parameters: The binding affinity can be assigned to Michaelis-Menten constants K_m, the rate is limited by the V_{max}, representing the inner catalytic steps and also the concentration of intact enzymes. It is advantageous that the parameters have a concrete biological interpretation, this helps manipulating their values for concrete questions to the model. In the following we shortly describe how other components influencing the kinetics are treated in this work.

Proton concentration The equations are analyzed upon experimental data that have been obtained at a constant pH (7.5) on fragmented membrane particles, thus the proton concentration is not considered in the first instance. The implication of pH for the kinetics of the OXPHOS complexes is treated later in this work (see chapter 3).

$\Delta\Psi$ and Δ pH . Accordingly both components of the electrochemical gradient are not yet considered, the fragmented membranes in the experiments would not allow for this. Their influence on the OXPHOS complexes' kinetics is the subject of chapter 3.

Temperature Modeling the mammalian OXPHOS, we deal with a constant temperature, thus changes in temperature and subsequent effects will not be treated in this work.

Activators, inhibitors. Only inhibitions by products or substrates are considered. External activators and inhibitors are not treated in this work, with exception of a phosphate dependent activation of complex III [Beard, 2005, French Mitochondrial Diseases Network] which is not yet considered until the modeling of the whole OXPHOS system, because in the experiments that we have performed, the employed phosphate concentration was constant, high and saturating.

Equilibrium constant. The equilibrium constant K_{eq} does not play a role in the absence of the membrane gradient, because the OXPHOS complexes favor so extremely the products, that a reverse reaction cannot be detected. The only exception is complex II, which is reversible under these conditions. K_{eq} becomes important for the integration of effect of the proton gradient into the rate equations.

Michaelis-Menten-like rate equations

The Michaelis-Menten like equations which we considered for the respiratory chain complexes are presented below. They are based on the description of the following global reaction scheme:

$$\sum_{i=1}^{m} \nu_i S_i \rightleftharpoons \sum_{j=1}^{n} \eta_j P_j$$

where S_i is the i^{th} substrate of the reaction and P_j the j^{th} product with the stoichiometric factors ν_i and η_j, respectively. The concentrations of the reaction components are classically noted by square brackets. In order to clearly represent the equations, we make the following assignments for the concentrations which occur in the equations mostly normalized by their Michaelis-Menten constant, denoted by a K with the component as index: $s_i = \frac{[S_i]}{K_{S_i}}$ and $p_j = \frac{[P_i]}{K_{P_i}}$. The maximal forward and reverse velocities are denoted by V^+_{max} and V^-_{max}. If not specified, the equations are taken from Segel [1993b,c].

Ping pong BiBi mechanism (PPM) The equation describes a two substrate-two product reaction, where the first substrate S_1 binds, and in the next step the corresponding product P_1 is released, then S_2 binds and P_2 is released:

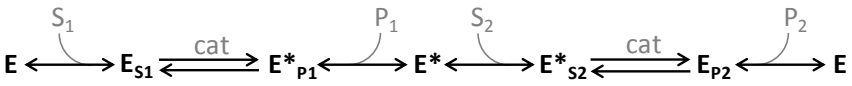

The corresponding equation reads

$$v = \frac{V^+_{max} \cdot s_1 \cdot s_2 - V^-_{max} \cdot p_1 \cdot p_2}{s_1 + s_2 + p_1 + p_2 + s_1 \cdot s_2 + p_1 \cdot p_2 + \frac{S_1}{Ki_{S_1}} \cdot p_1 + s_2 \cdot \frac{P_2}{Ki_{P2}}} \tag{2.6}$$

There are two different possibilities to assign the substrate and product couples, depending on which of both substrate binds first.

In the simplified form (PPMs), it is assumed that the K_i values equal their corresponding K_m values so that:

$$v = \frac{V^+_{max} \cdot s_1 \cdot s_2 - V^-_{max} \cdot p_1 \cdot p_2}{s_1 + s_2 + p_1 + p_2 + s_1 \cdot s_2 + p_1 \cdot p_2 + s_1 \cdot p_1 + s_2 \cdot p_2} \tag{2.7}$$

The simplified equation is symmetric with respect to which substrate binds first.

Ordered Bi Bi mechanism (OM) Like PPM, this equation is designed for two substrates - two products reactions, following a special binding and releasing sequence: S_1 binds followed by S_2, then P_1 is released followed by P_2

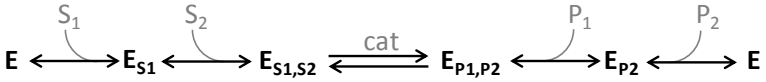

Hence there are four possibilities to assign the substrates and products to S_1 and S_2, and to P_1 and P_2, respectively, covering all possible binding orders. The rate equation is as follows

$$v = \frac{V^+_{max} \cdot s_1 \cdot s_2 - V^-_{max} \cdot p_1 \cdot p_2}{\left[\begin{array}{c} \frac{[S_1]}{Ki_{S_1}} + s_2 + p_1 + p_2 + s_1 \cdot s_2 + p_1 \cdot p_2 \\ + \frac{[S_1]}{Ki_{S_1}} \cdot p_1 + s_2 \cdot \frac{[P_2]}{Ki_{P_2}} + s_1 \cdot s_2 \cdot \frac{[P_1]}{Ki_{P_1}} + \frac{[S_2]}{Ki_{S_2}} \cdot p_1 \cdot p_2 \end{array}\right]} \tag{2.8}$$

The special order results in a non symmetric equation: the indexes 1 and 2 cannot be changed.
To simplify this equation (OMs), it is assumed that the K_i values are equal to their corresponding K_m values:

$$v = \frac{V^+_{max} \cdot s_1 \cdot s_2 - V^-_{max} \cdot p_1 \cdot p_2}{\left[\begin{array}{c} 1 + s_1 + s_2 + p_1 + p_2 + s_1 \cdot s_2 + p_1 \cdot p_2 + s_1 \cdot p_2 \\ + s_2 \cdot p_1 + s_1 \cdot s_2 \cdot p_1 + s_2 \cdot p_1 \cdot p_2 \end{array}\right]} \tag{2.9}$$

Also in the simplified form of the ordered mechanism four possibilities arise to assign the substrate and products.

Random Binding Order (RB) Here the binding order is random, however as for OM both substrates have to be bound to make possible the catalytic step:

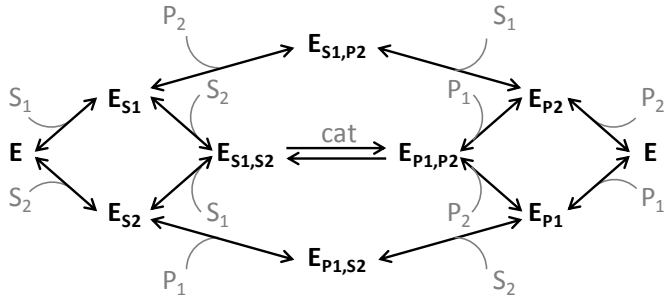

The corresponding equation is

$$v = \frac{V^+_{max} \cdot \alpha \cdot s_1 \cdot s_2 - V^-_{max} \cdot \beta \cdot p_1 \cdot p_2}{\left[\ 1 + s_1 + s_2 + p_1 + p_2 + \alpha \cdot s_1 \cdot s_2 + \beta \cdot p_1 \cdot p_2 + \gamma \cdot s_1 \cdot p_2 + \delta \cdot s_2 \cdot p_1\ \right]} \tag{2.10}$$

α, β, γ and δ describe a possible difference in binding when the enzyme is free to the situation where another component is already bound. There is only one possibility to assign the substrate and products: one substrate and product couple has the index '1', the other '2'. The equation is symmetric with respect to the indexes.

In order to simplify the equation, α, β, γ and δ were set to 1. We can thereby rewrite the equation as follows:

$$v = \frac{V^+_{max} \cdot s_1 \cdot s_2 - V^-_{max} \cdot p_1 \cdot p_2}{(1 + s_1 + p_1) \cdot (1 + s_2 + p_2)} \tag{2.11}$$

For the respiratory chain complexes with a different stoichiometry and number of substrates and products the equations was extended to a *general rate equation*:

$$v = \frac{V^+_{max} \prod_i s_i^{\nu_i} - V^-_{max} \cdot \prod_i p_i^{\nu_i}}{\prod_i (1 + s_i + pi)^{\nu_i}} \tag{2.12}$$

The stoichiometric factors ν_i may be non integers, however they must be equal for a substrate and its respective product or have to be included in an arbitrary way. If a substrate has no corresponding product or vice versa, the equation is simply written without the missing component.

Convenience kinetics (CK) is a generic rate equation which can account for any number of substrates and products, the only limitation is that stoichiometric factors must be integers. It has been proposed by Liebermeister and Klipp [2006], and is based on the reaction scheme

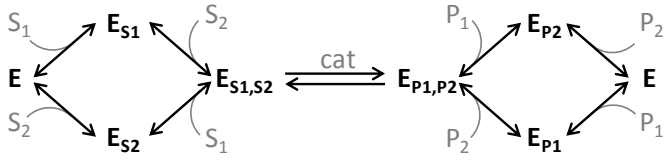

The equation reads

$$v = \frac{V^+_{max} \cdot \prod_i s_i^{\nu_i} - V^-_{max} \cdot \prod_j p_j^{\eta_j}}{\prod_i \left(1 + s_i + s_i^2 + \cdots + s_i^{\nu_i}\right) + \prod_j \left(1 + p_i + p_i^2 + \cdots + p_i^{\eta_j}\right) - 1} \tag{2.13}$$

Extended mass action equation (EMA) This rate law is in between mass action kinetics and Michaelis-Menten like kinetics. It shows saturation behavior, but there is only one global Michalis-Menten constant for all substrates (C_S) and one for all products (C_P). The equation can account for any substrates and product numbers and can also have non integer stoichiometric constants, which makes it very flexible. We have derived it as a compromise between the Michaelis-Menten like equations and mass action law, due to to the underestimation of parameters when fitting to time course experiments of complex I. The derivation is shown in subsequent section 2.1.4.

$$v = \frac{V^+_{max}\frac{\prod_{i=1}^{m}[S_i]^{\nu_i}}{C_s} - V^-_{max}\frac{\prod_{j=1}^{n}[P_j]^{\eta_j}}{C_p}}{1 + \frac{\prod_{i=1}^{m}[S_i]^{\nu_i}}{C_s} + \frac{\prod_{j=1}^{n}[P_j]^{\eta_j}}{C_p}} \tag{2.14}$$

All of the presented rate equations are reversible and hence their K_m and V_{max} can be related to the equilibrium constant via the Haldane equation:

$$K_{eq} = \frac{V^+_{max}}{V^-_{max}} \cdot \frac{\prod_{j=1}^{n} K_{P_j}^{\eta_j}}{\prod_{i=1}^{m} K_{S_i}^{\nu_i}} \tag{2.15}$$

for the non simplified random binding equation, the expression has to be multiplied with the factor α/β. and in case of the EMA equation, the Haldane equation reads

$$K_{eq} = \frac{V^+_{max}}{V^-_{max}} \cdot \frac{C_P}{C_S} \tag{2.16}$$

2.1.4. Derivation of the extended mass action equation

We consider the following general reaction catalyzed by the enzyme E:

$$E + \sum_{i=1}^{m} \nu_i \cdot S_i \rightleftharpoons E + \sum_{j=1}^{n} \eta_j \cdot P_j \tag{2.17}$$

The EMA equation 2.14 can be based on two different reaction mechanisms, both consisting of two steps. Each of these steps is expressed in terms of mass action and the two resulting equations are then linked by the assumption of a rapid equilibrium. The first way is closer to the usual way to derive enzyme rate laws. The second is based on the assumptions that the enzyme can switch between two conformations.

EMA equation - complex formation as rate limiting step

By comparison with the early derivations of the Michaelis-Menten equation [Briggs and Haldane, 1925, Michaelis et al., 2011], we should introduce in the reaction mechanism

the substrates-products-enzymes complexes species. We will sybolize these species by only one intermediate state of the enzyme E* which leads to the mechanism:

$$E + \sum_{i=1}^{m} \nu_i S_i \underset{\mathrm{k_{-1}}}{\overset{\mathrm{k_1}}{\rightleftharpoons}} E^* \underset{\mathrm{k_{-2}}}{\overset{\mathrm{k_2}}{\rightleftharpoons}} E + \sum_{k=1}^{n} \eta_j P_j \tag{2.18}$$

where k_1, k_{-1}, k_2 and k_{-2} are forward and backward rate constants of these two reactions. describing the two successive reactions in terms of mass action law leads to

$$v_1 = k_1 \cdot [E] \cdot \prod_i [S_i]^{\nu_i} - k_{-1} \cdot [E^*] \tag{2.19}$$

$$v_2 = k_2 \cdot [E^*] - k_{-2} \cdot [E] \cdot \prod_j [P_j]^{\eta_j} \tag{2.20}$$

Taking into account the conservation of enzyme molecules: $[E_t] = [E] + [E^*]$ and with the classical assumption of steady-state, $\frac{d[E^*]}{dt} = 0$, we derive the rate equation:

$$v = [E_t] \cdot \frac{k_2 \cdot \frac{k_1}{k_2+k_{-1}} \cdot \prod_i [S_i]^{\nu_i} - k_{-1} \cdot \frac{k_{-2}}{k_2+k_{-1}} \prod_j [P_j]^{\eta_j}}{1 + \frac{k_1}{k_2+k_{-1}} \cdot \prod_i [S_i]^{\nu_i} + \frac{k_{-2}}{k_2+k_{-1}} \prod_j [P_j]^{\eta_j}} \tag{2.21}$$

We set $\mathrm{V}^+_{\max} = k_2$, $\mathrm{V}^-_{\max} = k_{-1}$, $\mathrm{C_S} = \frac{k_2+k_{-1}}{k_1}$ and $\mathrm{C_P} = \frac{k_2+k_{-1}}{k_{-2}}$. Thereby we obtain equation 2.14.

With these constraints it is obvious, that the enzyme complex dissociation steps are rate limiting, as $[E^*] \leq [E_t]$ and thus $-k_{-1} \cdot [E_t] \leq v_1 = v_2 \leq k_2 \cdot [E_t]$

Rate limiting step: enzyme relaxation

It has often been supposed that enzymes undergo conformational changes between different conformations with different activities [Frieden, 1979]. We assume here that the enzyme shows two conformations $\mathrm{E_A}$ and $\mathrm{E_B}$ in equilibrium with the total enzyme concentration $\mathrm{E} = \mathrm{E_A} + \mathrm{E_B}$. In addition we suppose that the substrates can only bind to the conformation E_A and the products only to E_B. This implies that during the catalysis E_A is converted to E_B or vice versa. This is summarized by both reactions below.

$$E_A + \sum_i \alpha_i S_i \underset{\mathrm{k_{-1}}}{\overset{\mathrm{k_1}}{\rightleftharpoons}} E_B + \sum_j \beta_j P_j \tag{2.22}$$

$$E_B \underset{\mathrm{k_{-2}}}{\overset{\mathrm{k_2}}{\rightleftharpoons}} E_A \tag{2.23}$$

k_1, k_{-1} are the forward and backward rate constants for the enzymatic step and k_2 and k_{-2} are the corresponding constants for the enzyme transconformational step. Describing

the two steps in terms of mass action leads to

$$v_1 = k_1 \cdot [E_A] \prod_i [S_i]^{\alpha_i} - k_{-1} \cdot [E_B] \cdot \prod_j [p_j]^{\beta_j} \tag{2.24}$$

and

$$v_2 = k_2 \cdot [E_B] - k_{-2} \cdot [E_A] \tag{2.25}$$

Assuming steady state, $v_1 = v_2$ we derive the following equation:

$$v = [E_t] \cdot \frac{k_2 \cdot \frac{k_1}{k_2+k_{-2}} \cdot \prod_i [S_i]^{\alpha_i} - k_{-2} \cdot \frac{k_{-1}}{k_2+k_{-2}} \cdot \prod_j [P_j]^{\beta_j}}{1 + \frac{k_1}{k_2+k_{-2}} \cdot \prod_i [S_i]^{\alpha_i} + \frac{k_{-1}}{k_2+k_{-2}} \cdot \prod_j [P_j]^{\beta_j}} \tag{2.26}$$

Thereby it is obvious that v_2 limits the rate of the system in forward and backward direction, as $[E_A] \leq [E_t]$ and $E_B \leq [E_t]$B and thus $k_{-2} \cdot [E_t] \leq v_2 = v_1 \leq k_2 \cdot [E_t]$
Setting $V^+_{max} = k_2$, $V^-_{max} = k_{-2}$, $C_S = \frac{k_2+k_{-2}}{k_1}$ and $C_P = \frac{k_2+k_{-2}}{k_{-1}}$ we obtain equation 2.14.
It must be pointed out that the same equation is obtained with two very different underlying mechanisms. In all cases, the EMA equation as well as the other equations cited above (except for mass action law), amount to the reversible Michaelis-Menten equation when only one substrate and one product is present.

2.2. Methods and materials

We have performed experiments for the determination of the kinetics of the respiratory chain complexes instead of using literature data. For the consistency of the data among the respiratory chain complexes it is a high advantage to have data coming from the same tissue and being performed under similar conditions. Furthermore literature values of the products K_m or K_i are rather rare although product concentrations can have an important influence on the enzymes activities. Moreover, if the enzymes mechanism is not clear or not completely described by the above listed equations, the respective K_m or K_i-values can be quite different for the different for the description of the same data set. Thus it is advantageous to estimate the parameter values directly upon experimental data than employing values from literature.

Bovine heart mitochondria have been chosen as experimental model. The French Mitochondrial Diseases Network used this model as reference for the establishment of consensus protocols of enzyme assays for evaluating the integrity of the respiratory chain complexes of muscle biopsies from human patients. And still they serve as reference for these activity measurements. We have used these protocols in a slightly modified form for the performance of our kinetic measurements. Since a main part of the present thesis has been worked out on in the background of research in mitochondrial diseases in the INSERM lab *U688 Bordeaux, physiopathologie mitochondriale*, which was part of this

Network, it was obvious to chose bovine heart mitochondria as model.

Working on submitochondrial particles, we refer the complexes activities on the mitochondrial protein content, hence for the data description we will use generally the relationship

$$V_{max}^{+} = p_{mt} \cdot k_{cat}^{+} \text{ and } V_{max}^{-} = p_{mt} \cdot k_{cat}^{-} \tag{2.27}$$

where p_{mt} is the mitochondrial protein concentration and k_{cat}^{+} and k_{cat}^{-} are the enzymes activities for the forward and reverse reactions.

2.2.1. Experimental data types

For gathering information on enzyme activity as a function of product and substrate concentrations principally two types of experimental data can be considered:

Initial rate measurements (quasi steady state measurements) During a short time interval right after the initiation of the reaction the ideally linear and small concentration change of a substrate or product is used to calculate the initial velocity. Within an experimental series usually only one substrate or product concentration is varied while the others remain constant. The outcome is a quasi steady state rate as a function of different initial concentrations, which are assumed to be constant during the measurement.

Progress curves (time course experiments) After having started an enzymatic reaction the consequent changes in substrate or product concentrations are recorded, and followed for a relatively long time interval, e.g. until the equilibrium of the catalyzed reaction has been reached. The direct information given by this measurement is the concentration of the recorded substrate or product concentration as a function of time. The remaining concentrations can be calculated since their initial concentrations as well as their stoichiometric factors are known. These data can also be represented as catalytic activity at a given set of substrate and product concentrations.
During the evolution of a reaction from a high to a low substrate concentration, one can thus obtain a huge set of data points. But since the concentrations are interdependent, several curves with different sets of initial concentrations need still to be performed.

Time course measurements are in the first view very efficient compared to initial rate measurements: a progress curve consists of many data points while with the same material, for the latter method only one data point is obtained, albeit faster, however the time for preparation is equal for both methods. But errors in the initial concentrations run through the whole progress curve, which abates the advantage and during the measurements also other complications could occur like a loss of enzyme activity and parasite reactions influencing the substrate and product levels besides the catalyzes of interest.
The prerequisites for the acquisition of experimental data are described in the following.

2.2.2. Chemicals and reactants

All chemicals used for mitochondrial preparations and enzymological studies were purchased from Sigma-Aldrich, except potassium cyanide (KCN) which was purchased from Merck, and potassium ferricyanide, purchased from Rhône-Poulenc.
Decylubiquinone and antimycine A were diluted in ethanol, rotenone in equal parts in ethanol and dimethyl sulfoxide. The solutions were stored at $-80°$ C (DQ) and $-4°$ C, respectively. Potassium cyanide (KCN) was diluted in H_2O. Equine heart cytochrome c (oxidized), nicotinamide adenine dinucleotide (NADH), and 2,6-dichlorophenolindophenol (DCIP) were always freshly prepared in 75 mM phosphate buffer (pH 7.5).
In the following the procedures for the reduction of quinone and cytochrome c are described.

Decylubiquinol Two different procedures have been applied for the reduction of the quinones (Q):

Neutralisation of the reducing agent. Sodium borohydride was added to the yellow colored Q solution (50 mM in ethanol) until the solution became just colorless. Then 7 μL 3 mM HCl per 200 μL have been added for neutralisation of the slight excess of sodium borohydrid, followed by a centrifugation at 12000g (5 min, $4°$ C). The supernatant has been stored at $-80°$ C.

Neutralisation and extraction of the reducing agent by hexanol. 10 mL of a $16mM$ quinone solution was reduced by adding an excess of sodium borohydride until the solution became colorless. Then 5 mL of a buffer containing 0.1 M KH_2PO_4 and 0.25 M sorbitol (pH 7.4) have been added, followed by 3 mL of cyclohexane. The mix was agitated intensely and then centrifuged for 2 min at 10000 g. The organic phase (supernatant) was extracted. The remaining phase was again mixed with 5 mL buffer and 3 mL cyclohexane, followed by strong agitation, centrifugation and again extraction of the organic phase. The addition and extraction of cyclohexane was in total repeated 5 times. The accumulated organic phase is then evaporated under nitrogen. The residue was then dissolved in 10 mL ethanol and then distributed tubes and from where the ethanol was evaporated under nitrogen. The dried DQH_2-containing tubes were then stocked in liquid nitrogen and have been redissolved in ethanol just before using it in the kinetic assays.

The method we chose for quinone reduction was the first, both proving equal, because it was simpler to realize. The second and more sophisticated method has been used as control to exclude a possible remainder of active borohydride in the quinone solution which was suspected to reduce directly cytochrome c in the complex III assays; however no difference was found for these methods.

Final concentration and reduction state of the decylubiquinone solution The absorption spectrum of a decylubiquinone or decylubiquinol solution was recorded in ethanol in the interval between 230 nm and 320 nm (using quartz-cells). Concentration and reduction state were then estimated by minimizing the root mean

Figure 2.3.: Spectrum of decylubiquinone at different reduction states, represented as extinction coefficient ϵ in dependence of the wavelength. The curves at 25, 50 and 75 % reduction were calculated from the spectrometrically determined ones at 0 and 100 % reduction. The spectra were used for a precise determination of the concentration and reduction state of quinone solutions used in the experiments.

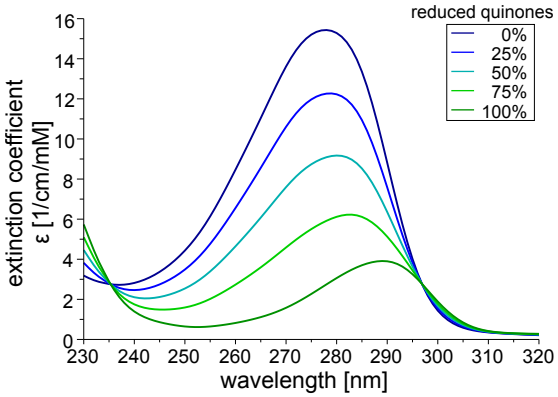

square deviation to a theoretical spectrum resulting from the superposition of the basic spectra of fully oxidized and fully reduced decylubiquinones, see figure 2.3. The spectrum of the completely reduced decylubiquinol solution was obtained by adding an excess of sodium borohydride. These spectra were corrected with respect to their concentration such that they correspond to the average of literature values taken from $\epsilon_{278}(0\%\text{red.}) \approx 15.4$ and $\epsilon_{290}(100\%\text{red.}) \approx 4.0$[Sherwood and Hirst, 2006, Fato et al., 1996, Esposti et al., 1996, Ouchane et al., 2002].

Reduction of cytochrome c A small volume of the oxidized horse heart cytochrome c solution was completely reduced by adding an excess of sodium dithionite. Small parts of this solution were then used to reduce stepwise the main volume until its desired reduction level was achieved. The reduction states were determined by photo-spectrometry at 550 nm using the extinction coefficient $9.1 mM^{-1} cm^{-1}$ for the oxidize cytochrome c and 27.6 $\text{mM}^{-1}\text{cm}^{-1}$ for its reduced form [Margoliash and Frohwirt, 1959]. For the enzymatic assays, the reduction state of the cytochrome c solution was never 100 % in order to avoid traces of dithionite in the reaction mix which would reduce directly the oxidized cytochrome c in the enzyme assays for complexes III and IV.

2.2.3. Bovine heart mitochondria

We are grateful to the group of Dr. Joel Lunardi (Grenoble) for providing shock frozen bovine heart mitochondria which have been stored at $-80°$. Submitochondrial particles (SMP) with fragmented membranes have been obtained by freezing and thawing and

further the osmotic conditions in the reaction mix. This permits to analyze the kinetics of the respiratory chain complexes in the absence of a proton gradient and permits NADH and succinate to have free access to their binding sites on complex I and II, respectively. The fragmentation should also be beneficial for the integration of external added quinones into the membranes.

Protein assay. The protein content of the homogenate has been determined according to a modified Lowry method Lowry et al. [1951] using bovine serum albumin (BSA) as standard: BSA, 2 mg/mL H_2O has been used in 5 different concentrations for a basic regression line and 3 different concentrations of homogenate for the determination of its protein content: BSA (0, 5, 10, 15, 20 μL) and homogenate (5, 7.5, 10 μL) have been diluted in a in a total volume of 200 μL H_2O. To each probe 200 μL NaOH (1 mM) and 2 mL of solution A (containing 10 g Na_2CO_3, 100 mg tartrate and 50 mg $CuSO_4$ in 500 mL H_2O) have been added; probes have been left 10 min in room temperature before an addition of 100 μL Folin; then the probes have been kept in obscurity for 20 minutes. The absorption measurement was performed at 700 nm.

2.2.4. Kinetic enzyme assays

Since complex I, III and IV are quasi irreversible in the absence of the electrochemical gradient, only the forward reactions were measurable and thus for the products only the strength of inhibition of the enzymes' activities could be obtained for the kinetic analyses. Complex II activity is generally reversible. However due to problems in the activity measurements, which will be detailed later, also here only the forward reaction was analyzed.

The experimental conditions for the kinetic assays of the respiratory chain complexes have been derived from the protocols of the *French Mitochondrial Diseases Network* and have been slightly modified such that all complexes activities have been measured in the same basal reaction mix: 67 mM phosphate buffer at pH 7.5 in presence of 0.2 mM EDTA and 2 mg/mL BSA). All assays were carried out at 37° C in a reaction volume of 1 mL wherein the SMP have been incubated for 4 minutes.
The absorptions of the respiratory chain intermediates have been recorded employing a UV-vis photo-spectrometer (SAFAS UVmc1), and converted into concentrations using the Lambert-Beer law:

$$A_\lambda = -log\left(\frac{I_1}{I_0}\right) = \epsilon_\lambda \cdot c \cdot d \tag{2.28}$$

where A is the absorption I_0 and I_1 the intensity of the incident light and transmitted light respectively, ϵ is the absorption coefficient, c the concentration in mM and d the distance in cm that the light travels through the probe; the index λ indicates the wavelength used for the measurement. For the experiments, cells with a light path of 1 cm

Figure 2.4.: Complex I: Dependence of the activity on the ethanol concentration (a) and of the incubation time at 37°C (b). In both cases, a significant decrease of activity was observed. The assays have been performed with 100 μM NADH and 100 μM quinone. The relative activities are referred to the value at 10 ‰ethanol and 4 min incubation time, respectively.

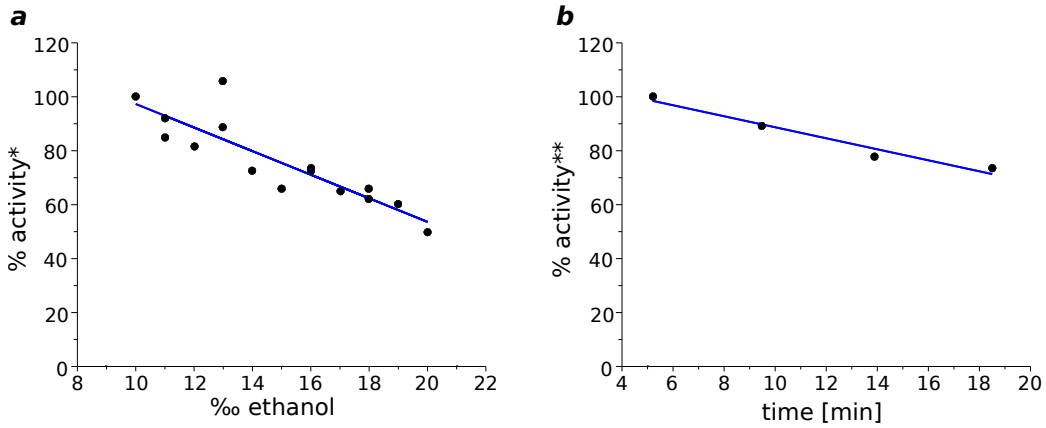

have been employed, except for complex IV measurements and some of CIII we chose cells with a light way of 0.4 cm, because of the high absorption by reduced cytochrome c.

Complex I (NADH-ubiquinone dehydrogenase). The assay was performed by following the decrease in absorption at 340 nm resulting from the reduction of NADH in the presence of 0.046 mM Antimycin A. For the *initial rate measurements* the amount of mitochondrial protein was $4.4\mu g/ml$. The control assays contained additionally 0.013 mM rotenone. The net activity was calculated by subtracting the control activity from the total activity. For the *progress curves*, higher protein concentrations have been chosen, i.e. 21.9 and 43.9 μg/mL, that allows for a faster reduction of Q and avoids a significant loss of complex I activity, see figure 2.4. The disadvantage is that here the progress curves cannot be combined with initial rate measurements since for the latter the small time gap between the initiation of the reaction and the onset of the recording is no longer negligible and hence the steady state assumption would be no longer valid.

Depending on the experimental series, the concentrations of NADH and Q have been varied, and, for the initial velocity measurements, also those of NAD^+ and QH_2. The reaction was initiated by the addition of NADH. The extinction coefficient used for the NADH determination was 6.22 $mM^{-1}cm^{-1}$ [Benard et al., 2006]. The ethanol concentration was kept constant at 8 μL/mL, because complex I was revealed to be sensitive to ethanol, see figure 2.4. However, it was not possible to omit ethanol completely, because it served as carrier substance for Q, QH_2 and antimycine. The total ethanol concentration has thus been fixed to 6 ‰.

When adding Q and/or QH_2 to the reaction mix, one can observe an absorption

peak with subsequent decrease with time. Probably this is a change in light refraction caused by a reorganization of these amphiphilic molecules, i.e. integration into the membrane fragments and reaching an equilibrium between monomeric existence and formation of micelles [Fato et al., 1996]. For low Q and QH2 concentrations, this effect is small then increased significantly with a pointed optimum at approximately 75 μM and a fast decline afterwards.

Given that complex I is not stable at 37° in the reaction mix during a long time period, see figure 2.4, waiting until the quinones have completely equilibrated seems not to be reasonable. Hence the reactions were initiated by adding NADH after 2 minutes of incubation with the quinone species (3 min for both, Q and QH_2), which already allowed to reach a relatively low value in the exponential decline of the pseudo kinetic curve and thus to diminish the experimental error.

In retrospect it seems to be more convenient to measure the activity of complex I at 340-380 nm to correct for the refraction of quinones, since at 380 NADH does not absorb any more. However with the given spectrometer (SAFAS UVmc1) it was not possible to switch rapidly enough between these wavelengths.

Complex II (succinate-ubiquinone dehydrogenase). Succinate and fumarate do not absorb such that their interconversion could be followed by photo-spectrometry, neither do Q and QH_2 since their absorption overlaps with proteins and further a clear signal is here only possible in ethanol.

As neither succinate, fumarate, decylubiqionol nor decylubiquinol can be followed directly by photospectrometry, complex II activity was measured via DCIP, which becomes rapidly reduced by QH_2 and thus serves as final electron acceptor. The absorption was recorded at 600 nm using an extinction coefficient of 19.2 $mM^{-1}cm^{-1}$ [French Mitochondrial Diseases Network].

The reaction was carried out in presence of 1 mM potassium cyanide (KCN) with 8.8 μg/ml mitochondrial protein. It was initiated by addition of succinate after incubation with Q (and QH_2).

For the variation of either succinate or Q in absence of products, 60 μ M DCIP was present in the reaction mix. The influence of the products concentrations on the enzymes activity could not be analyzed this way, since QH_2 is immediately oxidized by DCIP and fumarate is converted into malate by fumarase. A new method was conceived to estimate K_{QH_2} under very similar conditions, which is described more precisely in section 2.2.5. The measurement of the product inhibition by fumarate was not possible with this experimental setup, see also in the indicated section.

Complex III (ubiquinol-cytochrome c reductase). The oxidation of decylubiquinol by complex III was determined by following the absorption change of the electron acceptor cytochrome c (cytc) at 550 nm in presence of 1 mM KCN, employing the extinction coefficient $\epsilon = 18.5 mM^{-1}cm^{-1}$ [Margoliash and Frohwirt, 1959]. The assay was performed using 4.4 μg/ml mitochondrial protein and the reaction was

initiated by the addition of oxidized cytc, after incubation with Q and QH_2. Depending on the experimental series, the initial concentrations of Q, QH_2, oxidized and reduced cytc have been varied.

The activity was corrected for the important direct transfer of electrons from QH_2 to oxidized cytc, which has been measured in absence of mitochondrial protein. This parasite reaction has a clear linear relationship with respect to cytochrome c concentration, therefore the background could be better determined and the resulting net activities were less noisy for the curves where cytc was varied. In contrary, varying the ubiquinol concentration, saturation of this direct reaction was observed.

We regard as less useful the subtraction of the antimycin insensitive reaction, i.e. in presence of mitochondrial protein but with the complex III inhibitor antimycin, as proposed in the protocol since this inhibitor does not completely inhibit complex III and further it makes electrons shunt the Q-cycle and go directly on cytc, which would happen in a much lesser extent in the absence of this inhibitor. Anyway, the antimycin independent activity is very low compared to the direct electron transfer from QH_2 to cytc.

Borohydride has been used to reduce quinone. To exclude that the side reaction was caused by a residual activity of borohydride, reducing directly cytochrome c, a more sophisticated procedure for the quinone reduction was tested to avoid any remainder of borohydride (see above), but no difference was observed between the experiments. Moreover, with a quinone solution which was not fully reduced and thereby a remaining reduction potential of borohydride could be excluded, we could also observe this side reaction.

The extinction coefficient used to calculate the actual concentration and reduction state of cytc upon the absorption difference between the oxidized and reduced cytc is 18.5 $mM^{-1}cm^{-1}$ Benard et al. [2006], Margoliash and Frohwirt [1959].

Complex IV (cytochrome c oxidase). Cytochrome c oxidase activity was determined spectrometrically monitoring the absorption of cytochrome at 550 nm using the extinction coefficient $\epsilon = 18.5\,mM^{-1}cm^{-1}$ [Margoliash and Frohwirt, 1959] for conversion into concentration. The mitochondrial protein amount in the assays was 2.2 μg protein /mL. The reaction was initiated by the addition of (partially) reduced cytochrome c. The total concentration of cytochrome c or the reduction level, respectively, was varied corresponding to the experimental series. The control assays were performed in presence of 1 mM KCN.

2.2.5. Influence of the product concentrations on complex II activity

For complex II, the conversion of substrates into products cannot be directly observed and hence an additional electron acceptor, DCIP is used, see also section 2.3.1. This allows for the determination of the enzyme activity as a function of substrate concentrations, however it is not reasonable to measure the influence of the product concentrations

in this way, since both products QH_2 and fumarate are further consumed in this environment:

$$\begin{aligned}&\text{complexII} : : suc + Q \rightleftharpoons fum + QH_2\\&\text{chem.reaction} : DCIP + QH_2 \rightleftharpoons DCIPH_2 + Q\\&\text{fumarase} : fum \rightleftharpoons mal\end{aligned}$$

The fumarase is the next enzyme downstream of complex II within the Krebs cycle and converts fumarate into malate. The reaction system shows that estimating the strength of product inhibition by proceeding like for the other respiratory chain complexes, i.e. measuring the forward activity as a function of the product concentration, is not possible since fumarate is consumed by the fumarase and QH_2 would be immediately oxidized by DCIP.

Complex II is generally reversible in absence of a membrane gradient because the catalyzed reaction has a relatively low standard Gibbs energy of $\Delta G_0 \approx -2.9$kJ. It is thus tempting to measure directly the activity of the reverse reaction, i.e. the reduction of fumarate by QH_2, in order to determine K_{QH_2} and K_{fum}. But here also fumarate would simultaneously be consumed by fumarase, the equilibrium constant of the catalyzed reaction is $K_{eq} \approx 5$ (pH 7.3, 25 C; $\Delta G_0 \approx 4$kJ [Bock and Alberty, 1953]) and its activity is relevant for the system e.g for rat liver mitochondria 890 nmol/min/mg was found [Kobayashi et al., 1981], which is in the same range as the complex II activity that we have measured for the forward reaction, see table 2.9. Since no other substrate is involved herein, the reaction cannot be suppressed just by the absence of a second substrate.

Some Krebs cycle intermediates have been reported as competitive inhibitors, but naturally not with a sufficiently high inhibitive effect, having $K_i s > 10^{-4}$M, [Massey, 1953]. S-2,3-Dicarboxyaziridin is a strong inhibitor with $K_i = 0.08\mu$M [Greenhut et al., 1985] but was commercially not available.

Working with a concentration of fumarate high enough for saturating both enzymes, complex II and fumarase, could allow us to measure at least the influence of QH_2 under quasi steady state conditions. However, fumarate turned out to have a non sufficient solubility: Literature values suggest that the K_m of fumarate should have approximately the same value as the K_m of succinate Grivennikova1993, Tushurashvili1985. However, it was not possible to achieve concentrations in the order of $K_{suc} \approx 20$ mM that we have measured for complex II in our assays, neither in the buffer solution nor in pure water, despite heating it. This approach was hence abandoned.

In order to evade these problems one might carry out the activity measurements on isolated complex II that has been extracted and reincooperated into an artificial membrane structure. A disadvantage may here be that the extraction might lead to a loss of activity or more generally to a change in kinetic properties, due to the extraction routine and to the non physiological environment. Such a method to measure the forward and reverse reaction on isolated complex II has been established by [Grivennikova et al., 1993], where the forward reaction was tracked by DCIP and the reverse reaction

had been monitored using a QH_2 recycling system by NAD(P)H-quinone reductase (E 1.6.99.2) and following the decrease of NAD(P)H.

A Method to estimate the product inhibition by quinol

A new approach to estimate QH_2 is presented in this section. It makes use of time course measurements that are carried out under the same experimental conditions except that the reaction is now started in absence of DCIP. At distinct time points, a small volume is extracted from the reaction mix and is added in a separate reaction cell containing 25 μ M DCIP. The subsequent decrease of DCIP absorption in this analytic solution is then used to calculate the concentrations of QH_2 in the reaction mix. Further the concentrations of Q, succinate and fumarate at the distinct time points could be calculated from the QH_2 concentrations via the initial concentrations and the stoichiometric constraints of the reaction.

Three different ways to determine the QH_2 concentration at the distinct time points came into consideration, the first two are based on the assumption that mass action kinetics should be well suited to describe the reduction of DCIP via QH_2 because this is a purely chemical reaction.

1. Measurement of the initial rate of the decrease in DCIP and calculation of the QH_2 concentration with
$$\frac{d[DCIP]}{dt} = k_f \cdot [QH_2] \cdot [DCIP] \tag{2.29}$$
The reverse reaction can be neglected, since the initial concentrations are considered as quasi constant and thus the product concentrations are quasi zero. Further the reaction favors highly the products, thus that presence of small product concentrations is negligible.

2. Determination of the QH_2 concentration using the entire time course curves resulting from the analytic DCIP-QH_2 reaction. This can be done by integrating
$$\frac{d[DCIP]}{dt} = k_f \cdot \left([QH_2] \cdot [DCIP] - \frac{1}{K_{eq}} \cdot [Q] \cdot [DCIPH_2] \right) \tag{2.30}$$
.

3. From the entire time courses one can further calculate the velocity as a function of concentrations from the experimental curves , $\mathrm{v(t) = f(QH2(t), Q(t), suc(t), fum(t))}$ an then fit directly equation 2.30.

4. Recording the analytic reaction until completion and using the difference in absorption at t_0 and t_{end} for the calculation of the QH_2 concentration.

During the DCIP reduction in the analytic mix, a residual catalytic reduction of Q is still present, because the extracted volume from the reaction mix contains also submitochondrial particles and thus complex II. However this activity should be relatively low

Table 2.1.: Reduction of DCIP by QH_2. The rate constant k_f has been determined with different methods upon the same experimental data set see also figures 2.5) and 2.6). The equilibrium constant K_{eq} was initially set to $1 \cdot 10^7$ and remained at this value during the parameter estimation, indicating that the reaction highly favors the products and the reverse reaction has no significant weight.

method	**data**	$\boldsymbol{k_f}$ $\left[\frac{1}{\mu M \cdot sec}\right]$	**equation**
1	initial rate (non corrected)	$0.71 \cdot 10^{-3}$	2.29
1	initial rate (extrapolated)	$1.17 \cdot 10^{-3}$	2.29
2	concentration time course	$1.53 \cdot 10^{-3}$	2.30
3	rate time course	$1.20 \cdot 10^{-3}$	2.30

since the reaction mix was diluted 20 times within the analytic mix.

Determining the concentration of QH_2 via initial velocity measurement seems most suitable, because it is quasi independent of the ongoing residual complex II activity. For this method and for fitting to progress curves, it is necessary to determine the rate constant k_f of the DCIP reduction by QH_2, see equations 2.29 and 2.30. We could confirm that these kinetics can be sufficiently well described with mass action kinetics, as shown in figure 2.5 where time courses are described by integrating equation 2.30.
The values for the forward rate constant k_f obtained by the different approaches are listed in table 2.1, the equilibrium constant K_{eq} was initialized with 10^{-7} and did not change during the local fitting procedure, indicating that the equilibrium is highly favoring the products. For the estimation via the initial velocities, it has been additionally considered that between initiation of the reaction and the onset of the data recording there is a small time gap of approximately 4 seconds: to each experimental curve we assigned an exponentially decaying curve $(a + b \cdot \exp c \cdot t)$ which matched quasi perfectly and which was then extrapolated to correct for this initial time gap.

To check the coherence of the different approaches we controlled whether in the complex II assays, the time dependent concentrations that were determined with the given methods are consistent with the known initial concentration of QH_2. This is illustrated in figure 2.7.
The data obtained from the initial rate measurement were too noisy but when corrected for the initial time gap, the QH_2 concentrations at the distinct time points were underestimated. This could either be an indication for an untypical substrate saturation of the chemical reaction or the way of extrapolating is not suitable. Such a saturation behavior was already observed for the kinetics of the DCIP reduction, when varying DCIP at low QH_2 concentrations, see figure 2.6 c). The saturation could be due to the micelles formation of QH_2: Above a certain ratio of the concentrations of DCIP to QH_2, the micelles-monomer transition of QH_2 could become rate limiting.

In contrast to the approach via the initial rate, the analyzes of the actual QH_2 contents via the time course data showed a good agreement with the initial QH_2 concentrations,

Figure 2.5.: Time courses of the non-enzymatic reduction of DCIP by ubiquinol. The black curves are the measured data, the blue curves results from fitting theoretical time courses assuming mass action kinetics, see equation 2.30

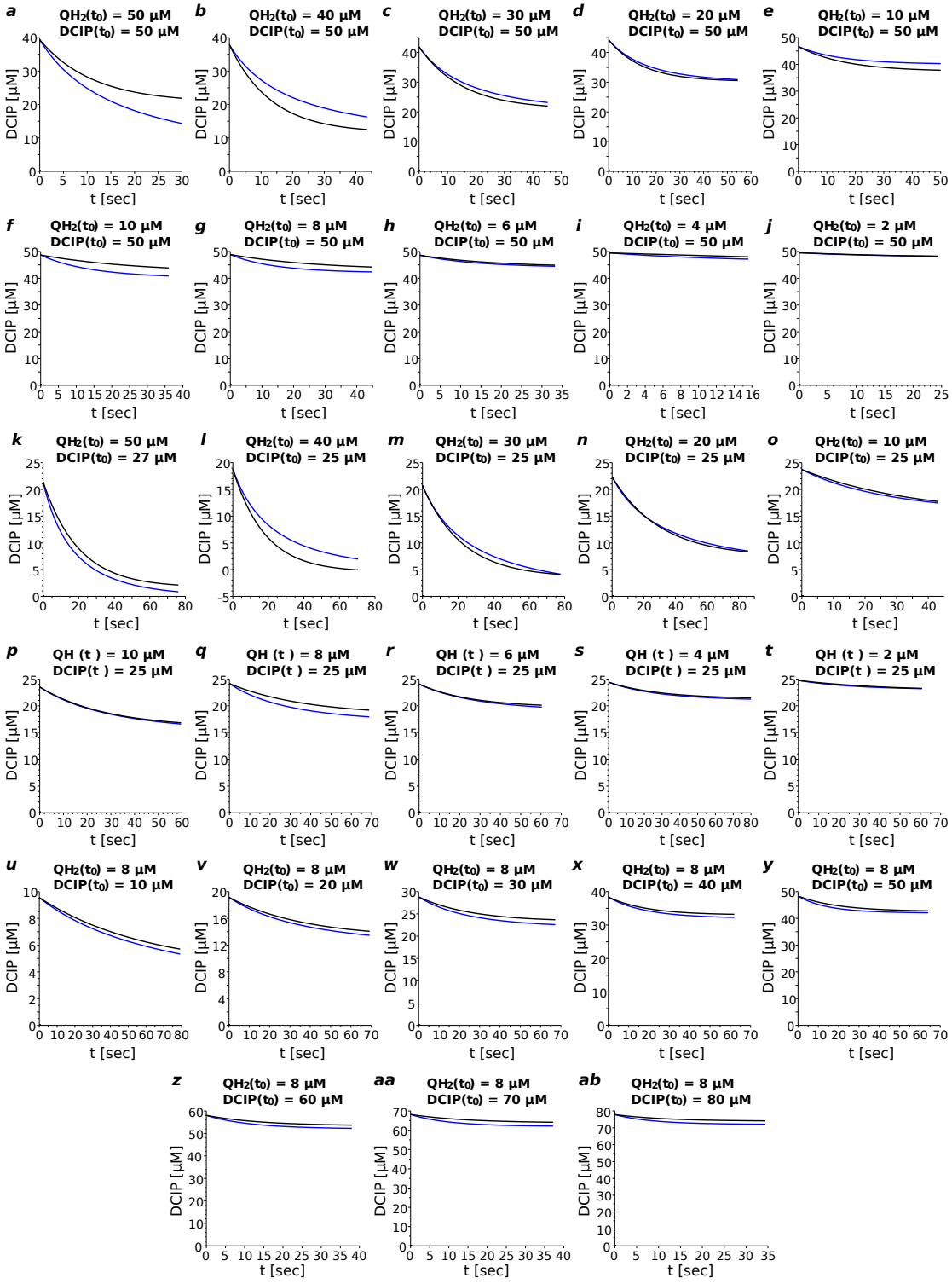

Figure 2.6.: Initial rate measurements of the chemical reduction of DCIP by ubiquinol. The black points are the measured initial velocities, the blue lines are the result of the estimation of the kinetic forward constant k_f, assuming mass action and absence of products, see equation 2.29. a)-c) Initial rates determined directly from the experimental data. The data in c) show that with increasing concentration of DCIP the velocity seems to follow a saturation behavior. To exclude that this effect does not result from an underestimation of the velocity due to a time discrepancy between initiating the reaction and starting the measurement, we have extrapolated each of the experimental curves by exponentially decaying curves and eventually we have determined their initial velocities which are plotted in d)-f). The data corresponds to the initial velocities of figure 2.5.

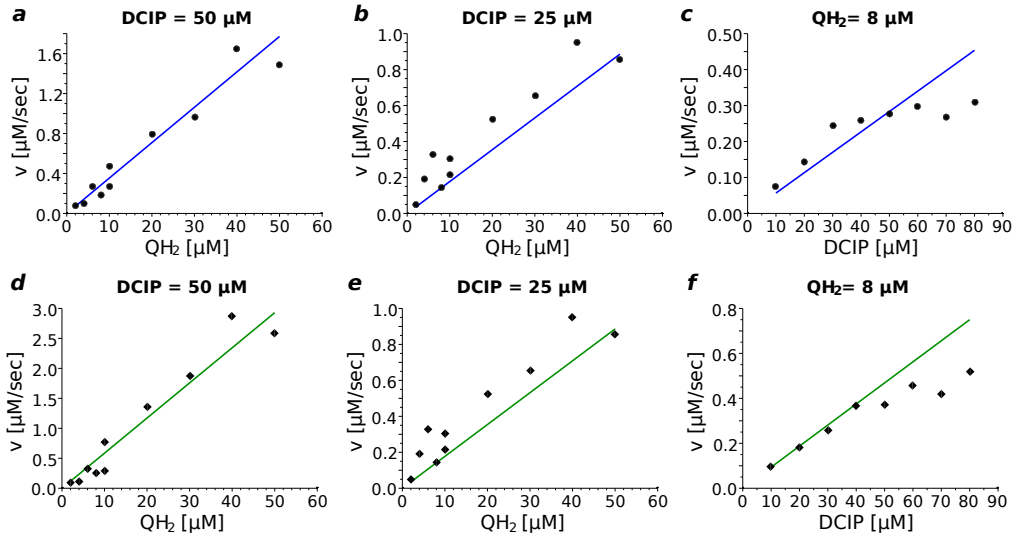

especially when the velocities as a function of the concentrations were fitted. The effects of the residual complex II activity turned out to be negligible in this approach. Hence we chose the results of this method for the determination of K_{QH_2}.

The approach to determine the actual QH_2 concentration via the total absorption difference of DCIP led to somewhat overestimated concentrations for the experimental series with lower initial QH_2, but showed good results for higher initial concentrations. This is consistent with a residual activity of complex II in the reaction mix being stronger for low initial QH_2 concentrations, since here the product inhibition of complex II is weak. The error resulting from this residual catalytic activity is higher for the approach via the total absorption difference because only the difference between the start and end of the analytical reaction counts. In comparison, for the progress curves the whole time interval is considered and hence the error given by the production of QH_2 due to the residual complex II activity is shared by many data points.
Still, the approach of absorption difference should not be desisted per se, since it is a very simple approach not needing much calculations, and can thereby be helpful for a quick and rough estimation of K_{QH_2}. But it should be kept in mind that here the value is probably somewhat overestimated. And in particular, if a strong inhibitor of complex II is available, the problem of ongoing Q reduction would be resolved.

Figure 2.7.: Comparison of the different approaches for the determination of quinols. The most reliable results were obtained using the rate time course data. Gray line: initial rate measurement, non corrected (method 1); black line: initial rate measurements on extrapolated curves (method 1); light blue: concentrations time course (method 3), blue: rate time course (method 3); green: absorption difference (method 4). The black triangles indicate the initial QH_2 concentrations which serve as reference to estimate whether the time dependent QH_2 concentrations determined by the given approaches are reasonable.

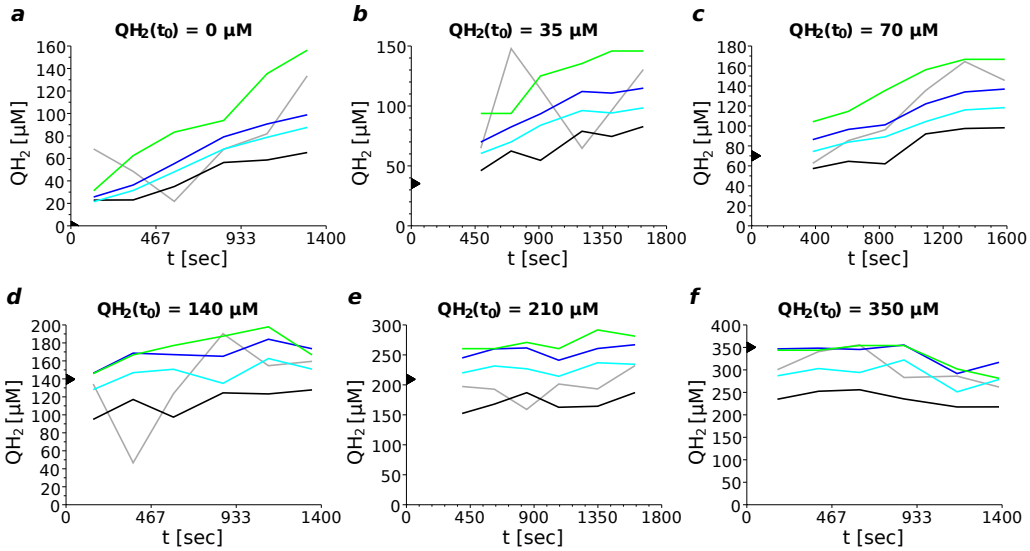

Little is known about the values for K_{QH_2} in the literature. This is certainly due to the fact that for the measurement of complex I activity, in general artificial electron acceptors are used, that take rapidly the electrons from QH_2, like DCIP, or take the electrons directly from complex II, like ferrycyanide and PMS (phenazine methosulfate). Hence with these classical methods, the K_m of QH_2 cannot be determined.
The here presented method makes it possible to assess the inhibitory effect of QH_2 on the forward activity of complex II on SMP, without the necessity to purify complex II and to use an additional enzyme to track the catalysis.
This method is experimentally simple to realize, the calculation of the K_QH2 is however somewhat more complicated, when using the fits to progress curves. With an appropriate inhibitor for fumarase, the method can also be used to determine the inhibitory strength of fumarate.

2.2.6. Hydrophilic analogues to coenzyme Q

The physiological type of quinone in beef heart mitochondria is the coenzyme Q_{10}. Here Q stands for the quinone head of the molecule and '10' refers to the number of isoprenoid subunits composing its tail. Among different organisms, Q_6 - Q_{10} have been observed [Lester and Crane, 1959]. The head is hydrophilic while the longer the isoprenoid side chain, the more lipophilic it is. Q_{10} has a very long side chain and is thus extremely lipophilic. Hence when adding these molecules into an aquatic solution (which is the case for the reaction mix) they form structures in order to minimize the surface exposed to water, which may hamper these molecules to reach the corresponding binding sites.
For this reason, it is common to use more hydrophilic and water soluble short chain ubiquinones, like Q_1, Q_2 and decylubiquinone (DQ) in the kinetic assays for the respiratory chain complexes [Fato et al., 1996, Hano et al., 2003a,b, Nakashima et al., 2002a, de Wit et al., 2007]. Their side chains are much shorter and thus the properties are shifted to amphiphilic behavior, which facilitates their distribution in the reaction mix and thus their integration into the mitochondrial membrane fragments. The structure of these ubiquinones are shown in figure 2.8.

Fato et al. [1996] calculated the critical micelle concentrations for different quinone species; according to this Q_2 already forms micelles in the low μM range, and DQ, which we have used in our experiments, even below. The authors suppose that the monomerization for DQ micelles would be slower than the complex I activity, thus they estimate this process as rate limiting. They did not considered that the micelles might directly fuse with the membrane fragments. The authors stated further that among the analyzed ubiquinones Q_1 and pentylubiquinone, an analogue to decylubiquinone, with shorter side chain, were the best substrates for complex I, upon them the highest rates were observed. In contrast, Esposti et al. [1996] found decylubiquinone to be a better substrate as the short chain Q_{10} analogues Q_1 and Q_2 and showed that complex I activity was increasing with the length of the side chain from order propenyl-, nonyl-, decyl- to undecyl-ubiquinone, according to this tendency decylubiquinone should have a significantly higher activity than pentylubiquinone. Finally, Fato et al. [1996] assumes

Figure 2.8.: Structural formula of coenzyme Q (a) and decylubiquinone (b). The number of isoprenoid subunits of CoQ varies from n = 6 - 10 among different species, for most mammalian organisms it is n = 10 [Lester and Crane, 1959]. Its isoprenoid side chain is lipophilic, its head is hydrophilic. Therefor short chain analogues with n = 1 or n = 2 as well as decylubiquinone are commonly used in kinetics assays because they are amphiphile and can thus disperse better in the assay volume, however they have still tendency to form micelles. Propenyl-, nonyl, and undecylubiquinone are analogies of decylubiquinone having respectively a shorter or longer side chain.

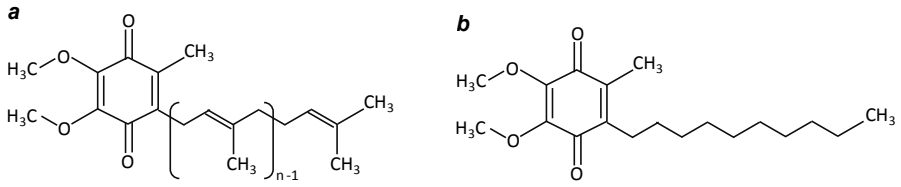

that decylubiquinone and Q_1 have similar complex I activities as the natural Q_9 or Q_{10}. Confronted with different statements, we finally decided to use DQ, as given in the protocol of the French mitochondrial diseases network and incubated the SMP with DQ (and DQH_2) before initiating the reaction, in order to minimize the effect of micelles formation on the effective concentration in the membrane.

It is difficult to estimate the concentration of ubiquinones in the membrane of the SMP, therefore the K_m of Q and QH_2 are usually referred to the amount of quinones normalized by the total volume of the reaction mix. Fato et al. [1996] approached for DQ that the real concentration in the membrane is about 80 times higher than the concentration with respect to the total assay volume. This number should be regarded with caution since it has been estimated based on the partition coefficient of DQ with respect to hexanol and water phase. Moreover, as mentioned above, micelles could also fuse with other membrane fragments, and hence the effect on the integration of the quinones into the membrane fragments is difficult to assess.

Different hydrophobicities of the ubiquinones may be reflected in the interaction with their binding sites on complexes CI, CII, CIII. More hydrophilic ubiquinones could have an advantage to access the binding site of complex I, since it is located somewhat external to the membrane plane and thus in an aqueous surrounding. In contrast, the quinone binding sites of complex II and III are located in the membrane, thus more lipophilic molecules may be advantageous.

In summary the real Michaelis-Menten constants of the ubiquinones in their oxidized and their reduced form can only be roughly estimated, but in any case, the ratios of K_{QH_2} to K_Q should be less concerned by these problems and give a good estimation on their general influence on the enzymes' kinetics.

2.2.7. Parameter estimation

Upon initial rate measurements and progress curves, parameter values have been estimated minimizing the root mean square deviation (RMSD) between the experimental and theoretical data points.

$$RMSD = \sqrt{\frac{\sum_i \left(x_i^{exp} - x_i^{theo}\right)^2}{n}} \tag{2.31}$$

where x_i^{exp} and x_i^{theo} are i^{th} experimental and theoretical data point, n is the total number of data points.
Therefore a basic genetic algorithm was implemented in Scilab. The initial generation consisted of 2000 randomly created 'individuals' (parameter sets). The following generations with 200 'individuals' were created by cross over of the best 50 'parents', a mutant rate per gene was set to 0.1. After 60 generations, the ten best 'individuals' that occurred during the whole fitting routine were refined with a newton based local search routine, and therefrom the best result was taken. If the parameters were not found to be clearly defined after several runs, this process was repeated altogether 125 times in case of initial rate measurements and 25 times for the progress curves. For each respiratory chain complex all experimental series were fitted simultaneously unless otherwise noted. The fits have been realized using Scilab 5.3.0, [Scilab Enterprises, 2012]. We have implemented the genetic algorithm, the local search routine was a built in function ('leastsq', quasi Newton method).

The reactions catalyzed by the respiratory chain complexes I, III and IV are highly exergonic. Further, for the initial rate measurements there was mostly only none or one product present, so that in this case the reverse reaction can be neglected. Hence we did not fit the backward constants k_{cat}^- with the data of the initial rate measurements but calculated them via the Haldane relationship 2.15 (and equation 2.16 for EMA) with the equilibrium constant

$$K_{eq} = \exp\left(-\frac{\Delta G_0}{RT}\right) \tag{2.32}$$

where R = 8.314 J/mol/K. The temperature in the experiments was T = 310 K. ΔG_0s for the complexes at pH 7.5 are taken from table 4.6.

2.3. Rate equation for complex I

We compare now the rate equations presented in section 2.1.3 for their ability to describe experimental data of the respiratory chain complex I, and therefore estimate their parameter values.

The reaction catalyzed by complex I in absence of the proton gradient is

$$NADH + Q + H^+ \rightleftharpoons NAD^+ + QH_2 \tag{2.33}$$

It is a 2-substrates-2-products reaction thus being generally compatible with all above listed equations. We start with estimating parameter values using time course measurements and focus then on initial rate measurements. Complex I has been reported to be inhibited by Q [Lenaz et al., 1975] and by QH_2 Bénit et al. [2008], which we considered in the analyses. Further we used a stochastic model for having a closer look on its functioning and reproducing steady state kinetics.

2.3.1. Progress curves

Initially we estimated the parameters of the different rate equations via a couple of time course measurement that have been obtained by following the oxidation of NADH catalyzed by complex I until completion, see also section 2.2.
Due to the high equilibrium constant the products are favored strongly and either the NADH concentration should approximate zero for $t \to \infty$ if its initial concentration is lower than that of Q or it should reach NADH $\approx$ NADH(t =0) - Q(t=0) if the initial concentration of NADH is higher than that of Q. Figure 2.9

We have only fitted the simplified rate equations to these data because already here, the parameters were underdetermined, i.e. very different parameter sets led to similar fits. For the non simplified rate equations that involve more parameters determination would be worse. The results are summarized in table 2.2.

This problem was the reason to derive a rate equation exhibiting saturation kinetics, but having less parameters in order to avoid such an underdetermination. The outcome was the extended mass action law (EMA), the derivation of which is shown in section 2.1.4. Here the K_m of the substrates are summarized within one global constant C_S and correspondingly for the K_m of the products C_P. However, it turned out that here the parameters were also underdetermined, albeit the relative deviations were lower, in particular for the rate constant k_{catf}. Despite this better definition, the accuracy of data description achieved by EMA was lower than that of all other tested rate equations. Nevertheless, the precision was still acceptable, at least for a rough data description, see figure 2.9.

At this place we just give a rough idea whether the average parameter are in an acceptable range; literature data for comparison are given below in the section 2.3.2. Globally for the simplified rate equations and convenience kinetics one can say that the determined averaged values for K_{NADH} are in a good range, those for K_{NAD} are also acceptable, however for k_{cat}^+ they are rather elevated, compensating the also elevated K_Q. Both parameters correlate strongly which is one origin of the high deviations, see figure 2.10. For the other parameters values however only low correlation coefficients were found.

Figure 2.9.: Complex I: Fit to progress curves. The curves resulting from the simplified random binding equation (blue lines) and the extended mass action equation (dashed gray lines) are plotted for comparison with the experimental curves (black lines) and show a good agreement. Here, the initial concentrations of NADH and Quinone have been varied, and since NADH was not fully reduced, for most experiments 82%, there was always an initial concentration of NAD^+, thus the concentrations of both products were never equal. In e)-f) the initial concentrations of Quinones were 17.5, 37, 52.5 and 70 μM, respectively. The theoretical progress curves were obtained by integrating the rate equations using as initial concentrations those that can be derived from the first data point of the recorded progress curves, the initially added concentrations and the stoichiometric constraints. This was necessary because there is a small time gap between initiation of the catalyzes and the start of the measurement, and since a high enzyme concentration has been used in the experiments, to avoid effects of enzyme activity loss during the experiment (see also section 2.3.1. The protein quantity in the assays was 21.9 μg/mL, except for d) where it was 43.9 μg/mL.

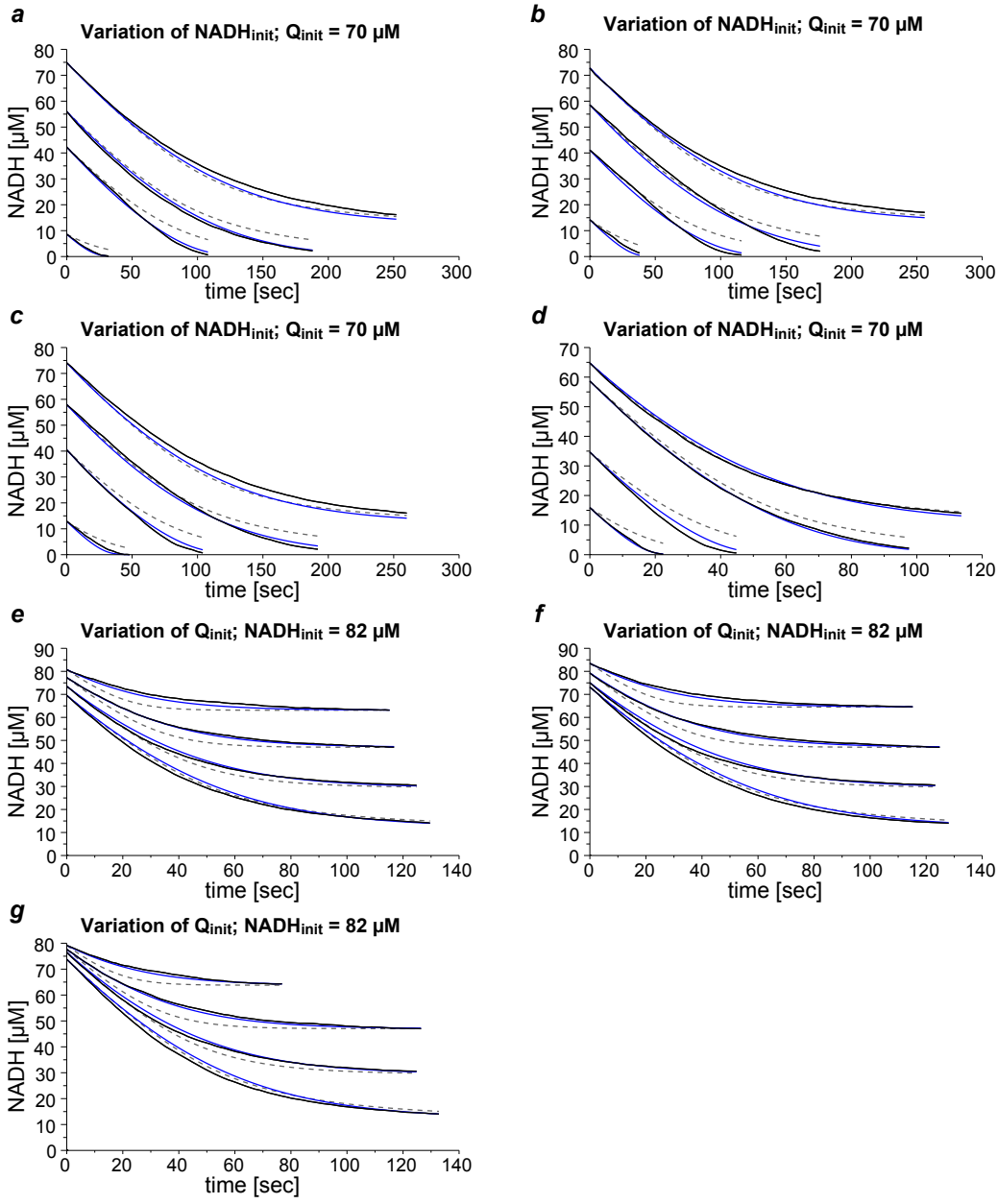

Table 2.2.: Complex I: Fit to time course measurements. In general, for the simplified rate equations as well as the rate equations CK and EMA good accuracies have been observed, however their parameters were underdetermined, i.e. very different sets of parameter values resulted in similar accuracies, which is reflected in the large deviations from the average parameter values. In case of complex I, EMA has two parameters less than the simplified Michaelis-Menten like equations, however also here parameters remained underdetermined. The given values are the averages of the ten best results out of 25 from the parameter estimation using a genetic algorithm and a subsequent refinement with a local algorithm. *The $kcat^-$ were calculated from the average values using the Haldane relationship 2.15 (and 2.15 for EMA), see also section 2.2.7.

Equation	**RMSD**	$\mathbf{k^+_{cat}}$	$\mathbf{k^-_{cat}}$*	$\mathbf{K_{NADH}}$	$\mathbf{K_Q}$	$\mathbf{K_{NAD+}}$	$\mathbf{K_{QH_2}}$
	[μM]	[nmol min^{-1}mg^{-1}]		[μM]	[μM]	[μM]	[μM]
PPMs	1.4 - 1.5	5790 ± 1410	$0.41 \cdot 10^{-3}$	26.2 ± 12.8	127 ± 36	5862 ± 3199	6137 ± 3580
OMs (NQNQ)	1.2 - 1.5	3058 ± 554	$1.60 \cdot 10^{-3}$	2.3 ± 2.7	55.4 ± 14.0	2533 ± 2207	4075 ± 161
OMs (NQQN)	1.3 - 1.6	3472 ± 1366	$2.17 \cdot 10^{-3}$	2.1 ± 2.1	70.8 ± 37.7	3680 ± 4534	3897 ± 3682
OMs (QNNQ)	1.2 - 1.4	2789 ± 703	$2.30 \cdot 10^{-3}$	2.4 ± 1.6	48.3 ± 19.2	5572 ± 3292	2649 ± 3142
OMs (QNQN)	1.3 - 1.5	3494 ± 687	$1.73 \cdot 10^{-3}$	2.2 ± 1.8	68.0 ± 19.0	6324 ± 4432	1811 ± 3215
RBs	1.2 - 1.5	3168 ± 859	$1.59 \cdot 10^{-3}$	3.2 ± 2.0	56.8 ± 21.0	4282 ± 3870	3300 ± 3270
CK	1.2 - 1.4	2930 ± 711	$0.33 \cdot 10^{-3}$	2.1 ± 2.3	53.9 ± 18.0	1343 ± 2526	1469 ± 2286
EMA	2.4	1695 ± 57	$4.68 \cdot 10^{-7}$	$C_S = 744 \pm 90\mu M^2$		$C_P = 31714 \pm 13823\mu M^2$	

The values for K_{QH_2} turned out to be much too high, QH_2 is even suspected to have an additional inhibitory effect Bénit et al. [2008] besides a strong affinity for the binding site. The high standard deviations for the results permitted generally small and high values for the product K_ms, not being significantly correlated. In general, the influence of the products seemed not to play an important role during the fitting routine.

Figure 2.10.: Correlation between the specific activity and the Michaelis-Menten constant of quinone. The values for k_{catf} and K_Q were estimated on fits to progress curves. They correlated strongly with $R^2 = 0.95$. The other parameters were only slightly correlated ($R^2 < 0.41$).

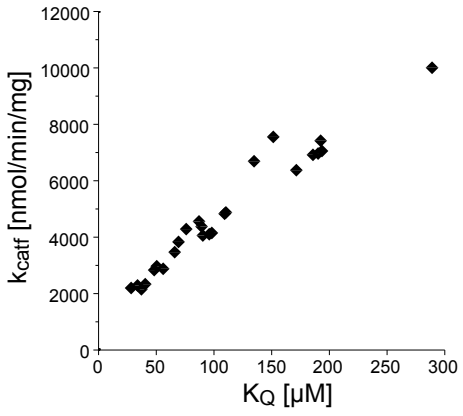

An underdetermination in particular of the products K_m could partially be due to the fact that mainly only the initial concentrations of the substrates have been varied. But since NADH was not completely reduced (for most experiments 82 %) there was always a corresponding concentration of NAD^+ present, while Q was completely oxidized, so that the concentrations of the products NAD^+ and QH_2 were always different. But maybe this difference in product concentrations was not sufficient for a precise determination of the product K_m-values. But this is not the reason for the high variations found for the substrate K_m values and for the k_{cat}^+. Neither does it explain the low affinity of QH_2 (high K_{QH_2}), since for the fits it made no difference whether a high value was attributed to both or only one product K_m.

A closer look on the experimental data themselves reveals that they might be the origin of the problem. Theoretically, the observed change in NADH concentration should be as follows: as long as both substrate concentrations are saturating, the decrease in NADH is linear and turns then into an exponential shaped decrease until completion of the reaction. This was generally observed for the progress curves where the initial concentration of Q was higher than the initial NADH concentration. However for the progress curves where this relation was inversed it was not possible to clearly define when the reaction was completed. These curves faded finally into a slight but still significant linear decrease of NADH, as illustrated in figure 2.11. This leads to errors with respect to the assignment of the NADH concentration to the experimental data points, i.e. a precise definition of the y-offset of the curve is not possible. NADH alone was quite stable in the reaction mix, and a direct reduction of quinone has not been observed. Hence the effect has probably its origin in a autooxidation of QH_2 which would allow for an ongoing oxidation of NADH. The recycling of Q being present during the whole measurement, the experimental error for the actual Q and QH_2 concentrations would become greater with time.
A contribution of the complexes II and III is rather improbable, because there is no succinate and cytochrome c in the reaction mix and further complex III was inhibited with antimycin. The 'pseudo kinetics' resulting from the addition of Q to the reaction mix, see section , can be excluded to be the reason for the slight linear decrease, since first the effect should be equally observed for whether the initial concentration of NADH is greater than Q or the inverse. Further one can assume that these 'pseudo-kinetics' are already completed at such late time points.

It is difficult to correct the progress curves for such background activities that influence a substrate or a product concentration during the measurement. The side reaction would have to be identified and its kinetics to be expressed in a function in order to integrate the latter in an ODE system with the rate equation for complex I, a complicated and error prone approach. Background activities that have a time dependent influence on the measured signal but not on the concentrations themselves can be corrected when subtracting a time course in absence of complex I activity, i.e. in presence of an inhibitor. But at least for rotenone there remains a residual activity, which again affects substrate and product concentrations.

Figure 2.11.: Complex I: Shapes of experimental progress curves. a) When the initial concentration of Q is lower than the initial concentration of NADH, the experimental time courses show no clear end of the reaction, but continue with a linear decrease (red and blue curve). This is probably due to an autooxidation of QH_2, such that Q becomes available again and the reaction catalyzed by complex I can continue. Such a linear behavior is not observed when integrating the rate equations (grey dashed line). b) Here, the initial concentration of Q is higher than that of NADH. The very slight decrease in absorption can be neglected. The simulated curve has been obtained by integrating the simplified random binding equation and employing the average parameter values given in table 2.2.

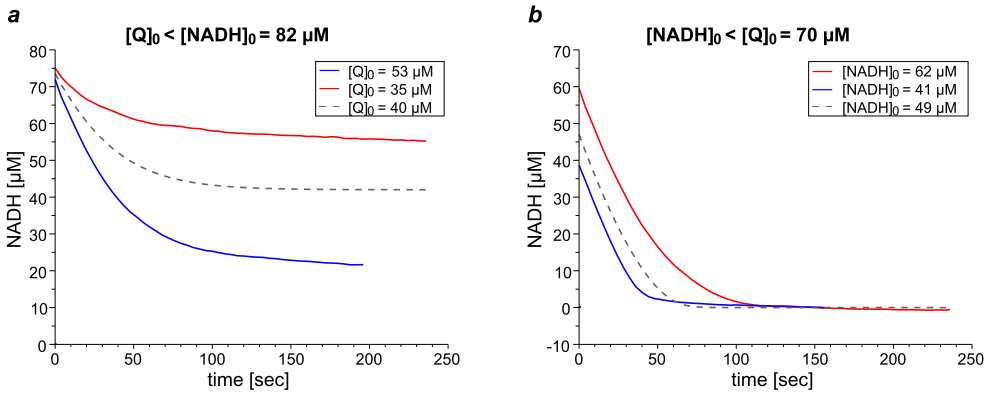

At least with respect to complex I, one can state about the use of progress curves that the advantage which they feature, i.e. saving time and material costs, is diminished by the uncertainties resulting in a high deviation of parameter values, and also by rather complicated error handling. This could be improved by accumulating more curves, but finally the advantage of saving time and material would vanish with respect to initial velocity measurements.
Consequently we have decided to perform the classical initial rate measurements for all respiratory chain complexes, also because each complex would have its special challenge with respect to the progress curves: For tracking the complex II activity spectrometrically, an additional electron acceptor is needed, thus a second reaction has to be handled. The complex III catalysis is accompanied by a strong direct reaction of the components, making this measurement difficult. Finally, for complex IV the experimental set-up does not allow for following the oxygen concentration nor to calculate it from the decrease in reduced cytochrome c, nor to fix it since the reaction cell is open to air.

2.3.2. Initial velocity measurements

Albeit the material and time costs are higher for initial rate measurements when compared to progress curves, a clear advantage is that the data can be corrected for the background simply by subtracting the control activity from the total measured activity. Moreover, observing the experimental series, wherein usually one component is varied

while the others are kept fixed, one can already get a first good guess of the substrate and product affinities as well as the maximal velocities. In the following, we present first the results obtained with the mechanisms based rate equations, then those of their simplified forms and of the general rate equations.

Rate equations based on a steady state mechanism

For all above listed rate equations based on a steady state mechanism, the accuracies of data description were satisfactory. Since the accuracies were similar for all equations (see table 2.3), the ping pong equations for both, with NADH or Q as first substrate, are revealed as advantageous because of their good parameter definition. For the rest, there are partly very large variations for some parameters values. This can be ascribed to PPM having two parameters fewer, but it may also indicate that more experiments could be necessary for a more precise parameter determination. For all OM binding sequences, except for that where NADH binds first and NAD^+ is the last substrate to leave, some K_i or K_m tend to extreme values which were restricted in the fitting routine by maximal and minimal values.
Enlarging the limits for the parameter estimation led to higher uncertainties in the parameter values and moreover the accuracies were lower, indicating on one hand that the investment in the fitting must be increased in order to increase the accuracy and on the other hand that the equations are too complex and contain more parameters than necessary for a good data description. Therefore, we turn towards the simplified and general rate equations, which are more compact and feature fewer parameters.

Simplified forms of the mechanistic rate laws and general rate equations

The accuracies that were achieved with the simplified rate equations were about the same as for their non simplified analogues, and now the parameters were always well defined. For the generic rate equations, the results of convenience kinetics (CK) were comparable, while with the extended mass equation (EMA), the accuracies were less good. The results are listed in table 2.4, and the random binding mechanism (RB) and EMA are plotted versus the experimental data points in figures 2.12 and 2.13.
In some cases the accuracies of the simplified ordered equations were even slightly better than those of their non simplified counterparts. This implies that for the latter the global optimum has not been found yet repeating 125 times the global fitting procedure with subsequent local refinement, see also 2.2.7, the parameter space interspersed with parameter sets resulting in optima with similar accuracies. One could intensify the fitting procedure, but this expense is not of interest for our modeling, because our aim is to have robust rate equations that can well describe the kinetics of the respiratory chain complexes, but which are only as complex as necessary and easy to handle and this also with respect to the parameter estimation.

The simplified Michaelis-Menten like rate equations and CK are thus good candidates. However their similar accuracies permit not to point out a mechanism that is followed

Table 2.3.: Complex I: Parameters values for the enzyme mechanism based rate equations. The accuracies for the description of the experimental data are in most cases very similar, with the ordered mechanisms (OM) slightly better than the ping pong mechanism (PPM), with exception of OM 'QNQN', the abbreviation coding the binding order: first letter of the first substrate to bind, then of the second substrate, followed by the first letter of the first product to leave and finally of the last product to leave. RMSD is the root mean square deviation of at least the ten best results out of 125, having very similar accuracies. If no standard deviation is given, the value is well defined. 'll' and 'ul' are the lower and upper limits, respectively, that were restricting the parameter search. Enlarging the intervals lead to higher deviations of the parameter values the accuracy was further not improved. *The kcat$^-$ were calculated from the average values using the Haldane relationship 2.15, see also section 2.2.7.

Equation	**RMSD**	$\mathbf{k^+_{cat}}$ $\mathbf{k^-_{cat}}$*	$\mathbf{K_{NADH}}$ $\mathbf{Ki_{NADH}}$	$\mathbf{K_Q}$ $\mathbf{Ki_Q}$	$\mathbf{K_{NAD+}}$ $\mathbf{Ki_{NAD+}}$	$\mathbf{K_{QH_2}}$ $\mathbf{Ki_{QH_2}}$
		[nmol min^{-1}mg^{-1}]	[μM]	[μM]	[μM]	[μM]
PPM	161	1903	6.1	13.0	401	2.4
(NNQQ)		$1.50 \cdot 10^{-7}$	46.6	x	x	5.3
PPM	161	1903	6.1	13.0	401	2.4
(QQNN)		$1.50 \cdot 10^{-7}$	x	28.4	3085	x
OM	157	1941 ± 3	6.3 ± 0	13.4 ± 0.1	100000 (ul)	2.6 ± 0.3
(NQNQ)		$4.00 \cdot 10^{-5}$	26.4 ± 7.9	0.1 (ll)	10000 (ul)	5.3 ± 0.6
OM	157	1883 ± 5	5.7 ± 0.2	12.3 ± 0.1	2956 ± 7047	1.9 ± 0.5
(NQQN)		$9.77 \cdot 10^{-7}$	96.4 ± 21.6	0.1 (ll)	1012 ± 130	3718 ± 3672
OM	158	1944 ± 3	6.2 ± 0	13.3 ± 0.1	6319 ± 2041	1.1 ± 0
(QNNQ)		$1.06 \cdot 10^{-6}$	0.1 (ll)	45.9 ± 13.2	10000 (ul)	4706 ± 2896
OM	176	1754 ± 0	3.6 ± 0	6.8 ± 0	100000 (ul)	115 ± 0
(QNQN)		$5.34 \cdot 10^{-3}$	4681 ± 3599	0.1 (ll)	896	7931 ± 2696
RB	160	1847 ± 43	1.3 ± 1.1	2.8 ± 2.4	62195 ± 28770	455 ± 191
	-163		α =	β =	γ =	δ =
			455 ± 191	0.26 ± 0.25	93.8 ± 11.6	73.8 ± 33.8

Table 2.4.: Complex I: Simplified equations. The table shows that the root mean square deviations (RMSD) between simulated and experimental data are very close among the different types of the simplified rate equations, the convenience kinetics equation and the extended mass action equation. *The kcat$^-$ were calculated using the Haldane relationship 2.15 (and 2.16 for EMA), see also section 2.1.3.

Equation	**RMSD**	$\mathbf{k^+_{cat}}$	$\mathbf{k^-_{cat}}$*	$\mathbf{K_{NADH}}$	$\mathbf{K_Q}$	$\mathbf{K_{NAD+}}$	$\mathbf{K_{QH_2}}$
	[nmol(NADH) $\cdot$ min^{-1}mg^{-1}]			[μM]	[μM]	[μM]	[μM]
PPMs	162	1910	$1.3 \cdot 10^{-6}$	6.1	13.1	2064	4.0
OMs (NQNQ)	161	1802	$1.0 \cdot 10^{-5}$	4.4	9.9	13931	2.7
OMs (QNQN)	162	1797	$5.0 \cdot 10^{-6}$	4.3	9.8	774	23.6
OMs (QNNQ)	164	1801	$1.9 \cdot 10^{-5}$	4.4	9.7	13087	5.3
OMs (NQQN)	168	1793	$9.1 \cdot 10^{-6}$	4.3	9.8	1666	20.1
RBs	164	1791	$1.1 \cdot 10^{-6}$	4.3	9.7	780	5.3
CK	167	1773	$1.4 \cdot 10^{-8}$	4.2	9.5	88	0.6
EMA	244	1333	$1.8 \cdot 10^{-10}$	$C_S = 166\mu M^2$		$C_P = 3.4\mu M^2$	

in steady state. Rather it reflects the diverging findings of several authors with respect to the enzymes' steady state mechanism: Fato et al. [1996] showed that complex I exhibits ping pong behavior using Q_1 and pentylubiquinone. However, other authors found complex I to behave like an ordered mechanism, with Q_1 as first substrate to bind and Q_1H_2 as last product to go off [Nakashima et al., 2002a] and NADH as first substrate to bind and NAD^+ as last product to go off Hano et al. [2003a], respectively. For the latter Q_2 and decylubiquinone was used.
It is unlikely that the type of ubiquinones would change the binding order of the enzyme. Rather it is possible that none of the binding orders exactly describes the mechanism of complex I. Different quinones having different properties with respect to binding and release can simply be the reason of favoring one or the other apparent mechanism in the fitting procedure. This issue of the steady state mechanism will later be discussed upon a stochastic model of complex I.

When comparing the K_m values that have been found for the simplified equations, one can generally observe that the K_m of the substrates are very similar, but the K_m for the products can differ within an order of magnitude. The similarity of the first is due to the equations being identical in absence of the products (except for PPMs). In order to describe well the experimental data in absence of products, K_{NADH} and K_Q can only be in a very small range. Note that for PPMs which has not '+ 1' in the denominator the values are somewhat different. If it was possible to reverse the reaction and determine K_{QH_2} and K_{NAD} in the absence of NADH and Q, their values would also be equal among the equations. However, the reaction is quasi irreversible without the impact of the membrane gradient, the only way to determine K_{QH_2} and K_{NAD} is via the forward reaction. Under this situation the equations are no longer identical, an hence their different structures must mainly be compensated by the values of the product K_m in order to obtain similar fits. This is a good example to emphasize that the apparent product K_m presented here are not equal to the real K_m. Therefore simply taking literature values can lead to a strong over or underestimation of these parameter values.

Featuring two parameters fewer, the EMA equation is significantly less precise for the description of the given data. However, for most data curves EMA is still comparable to the other rate equations, as one can see in figures 2.12 and 2.13. But since the product inhibition by QH_2 and NAD^+ are approximately three orders of magnitude apart, it is obvious that EMA cannot describe accurately the influence of both. Here the fits lead to a good description of the influence of QH_2, but in contrast, in the series where NAD^+ was varied the data description is not satisfactory at all: since no QH_2 was present the global product expression in the equation becomes zero and the calculated rate is thus not affected by NAD^+.

Comparison with literature data

For all equations that we have fitted, original or simplified forms and the CK equation, the Michaelis-Menten constants of the substrates as well as the maximal velocities are

Figure 2.12.: Complex I: rate equations versus experimental data points. The accuracy of description of the data points is exemplified for the simplified random binding rate law (red line) and extended mass action equation (dashed gray line). Figure to be continued in figure 2.13

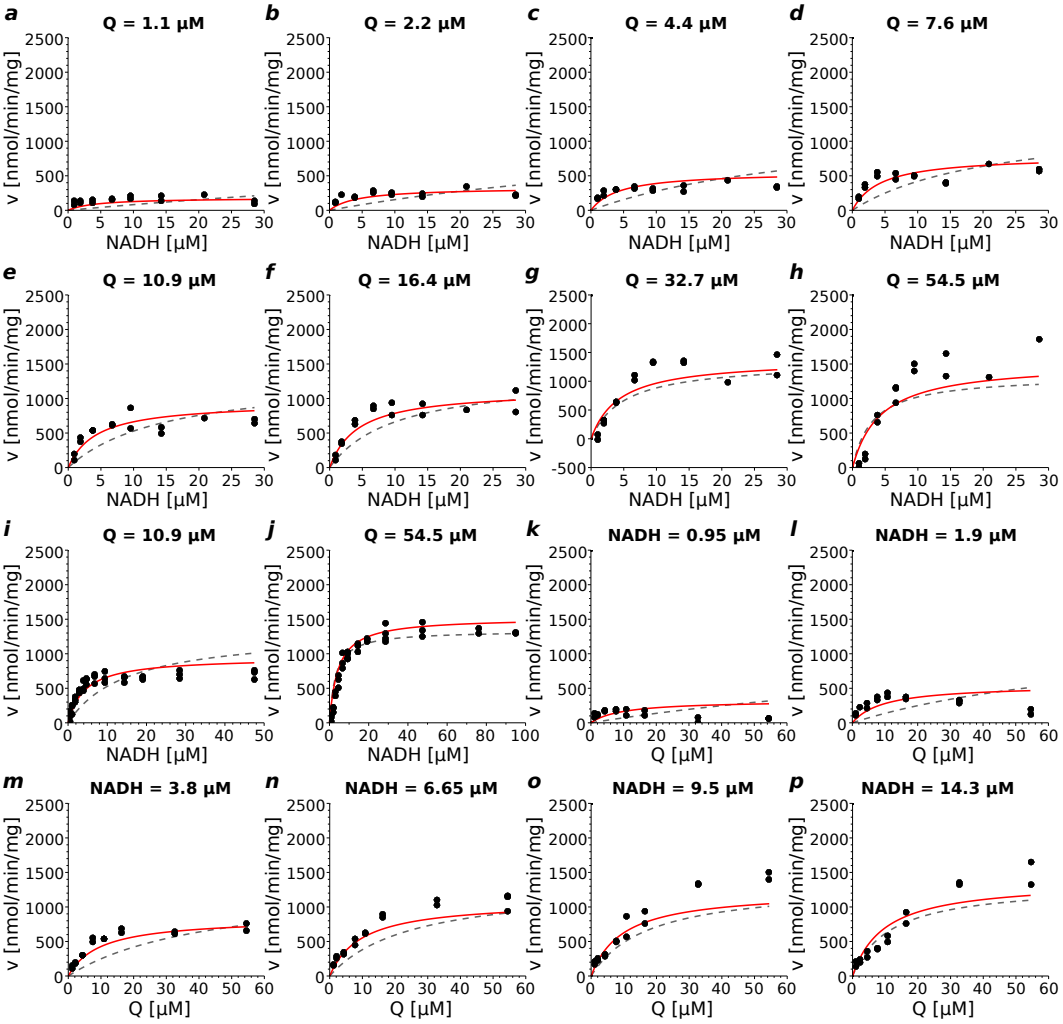

Figure 2.13.: Complex I: rate equations versus experimental data points. Continuation of figure 2.12. Simplified random binding rate law (red line) and extended mass action equation (dashed gray line)

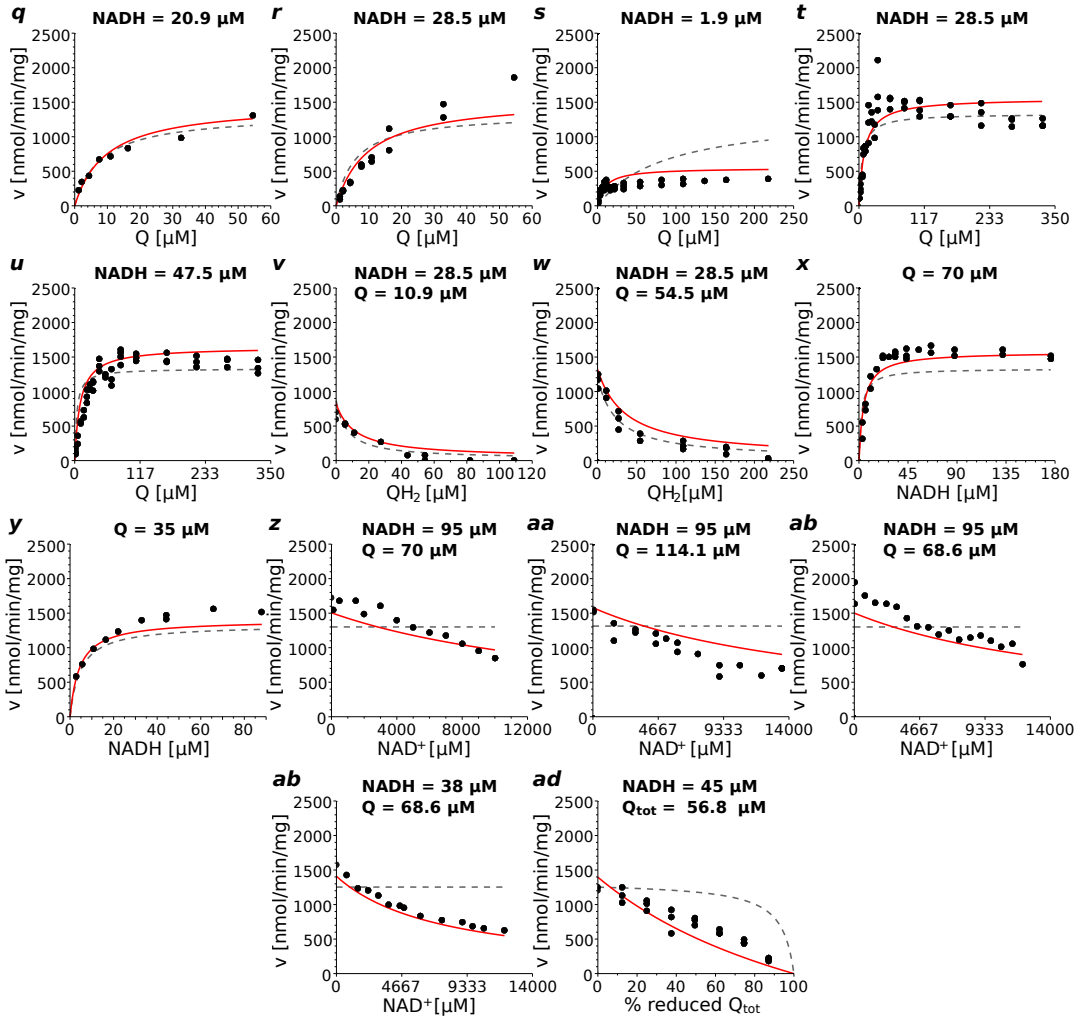

consistent with literature data. Unless otherwise noted, the data refer to bovine heart mitochondria.

The k^+_{cat} that Fato et al. [1996] determined on submitochondrial particles for different types of quinone ranged from 170 to 1560 nmol/min/mg. Here, the value for decylubiquinone was 580 nmol/min/mg. Also on SMP, Sherwood and Hirst [2006] reported a much higher rate with 3100 nmol/min/mg.

K_{NADH} was found to be in the range of 0.6 - 2.7 μM on isolated complex I in the presence of different quinone types, among them also decylubiquinone [Hano et al., 2003a,b, Nakashima et al., 2002a,b]. For SMP a value of 9.2 μM has been found [Fato et al., 1996]. Vinogradov [1993] reported for K_{NADH} 7.6 μM and 7.2 μ M for coupled and uncoupled SMP, respectively. And for the reverse reaction on coupled SMP $K_{NADH} = 40\mu$M.
The values found for K_Q are more variable, also due to the different type of quinone that has been used. Fato et al. [1996] determined the K_Q for 7 different types of quinones on bovine submitochondrial particles, their values being spread within an interval of 0.8 to 65 μM. Here the K_m for decylubiquinone (DQ) was found to be approximately 1.8 μM but has also been reported to be much higher with 24 μM [Sherwood and Hirst, 2006]. For isolated complex I values of 4.4 - 12.9 for Q_1 and Q_2 [Nakashima et al., 2002a,b, Hano et al., 2003b]and 51 μM [Hano et al., 2003a] for DQ.

Less data are available with respect to the K_m values of the products and they are more difficult to compare because of their dependence on the rate equations structures.
Vinogradov [1993] found a K_i value for NAD^+ of 1250 μM on uncoupled SMP, which lies among the K-values we found for the different equations. However, for the reverse reaction under coupled conditions the author reported a K_m of 7.2 μM for NAD^+. To explain the difference of about three orders of magnitude it was suggested that NAD^+ binds to a different site for the reverse sense. But this large difference may also be due to the equation that has been used for the determination of these values: as we could show such a differences among the K-values can be quite possible for different equation types, see table 2.4.
The values for the product K_i were not given in the other above mentioned publications [Hano et al., 2003a,b, Nakashima et al., 2002a,b], but by means of the given k^+_{cat} values under different fixed product concentrations one can appraise whether our experimental data are in the range of their findings, considering that the fixed substrate concentrations, were quite different to that used in our work and that substrate and products compete for their respective binding sites: Nakashima et al. [2002a,b] found upon Q_1 as electron acceptor an approximately 20 times stronger inhibition by NAD^+, while the data of Hano et al. [2003a,b], using DQH_2 and Q_2H_2 are in agreement with ours. Generally, the influence of the ubiquinols that one can derive from all of these publications were compatible with our findings.

We can conclude that our experimental data of complex I and the therefrom determined parameter values are consistent with literature data.

Inhibition by quinone and quinols

In our experimental data one can observe an inhibition of complex I at high concentrations of decylubiquinone. Indeed oxidized quinones have been suspected to exert a negative effect on complex I activity at higher concentrations. Lenaz et al. [1975] showed an inhibitory effect by the short chain CoQ analogue Q_3 and assumed that there is need for long chain ubiquinone for a proper functioning of complex I. Grivennikova et al. [2001] reported even a very strong inhibition by the short chain ubiquinone Q_1. However we see these results of the latter very critically: upon our experiments we could see that if we did not respect the incubation time for the quinones and if we further we did not subtract the residual pseudo kinetics provoked by refraction effects of these molecules (see also section 2.3.1) we would observe a strong apparent inhibition effect of quinones. This effect is very similar to the apparent extreme inhibition observed by this author. Bénit et al. [2008] found that decylubiquinone is a strong inhibitor and assigned this inhibition to a mechanism more complex than a simple product inhibition.

Albeit the reported facts are ambiguous, the location of the Q-binding site gives reason not to exclude per se an inhibition by ubiquinones at high concentrations: this binding site was found to be situated external to the membrane plane so that in order to reach it quinones have to move out of the membrane to a significant extent Clason et al. [2007]. It is not evident how these lipophilic molecules access the binding site that is located in a hydrophilic environment. It is plausible, that they are guided by a path. We assume, that when a high amount of Q and/or QH_2 molecules are present, the path to enter the Q-site could be obstructed by both oxidized and reduced forms and hinder thereby ubiquinones to enter the site or ubiquinols to leave, both slowing down the catalysis. Alternatively Q and QH_2 could wrongly bind in the large binding pocket forming the reducing site and thereby hinder other molecules to bind correctly for catalysis.

On the example of the simplified random binding equation several inhibition terms have been tested in order to account for a possible inhibition. The equation reads then

$$v = \frac{V^+_{max} \cdot n_r \cdot q_o - V^-_{max} \cdot n_o \cdot q_r}{(1 + n_r + n_o) \cdot (1 + q_r \cdot I_s + q_o \cdot I_s)} \cdot I_{nc} \tag{2.34}$$

With the inhibition terms I_s, I_c and I_{nc} as described in the following

Substrate or steric inhibition I_s is the first choice, corresponding to a possible obstruction of the access to the Q-binding site, as mentioned above. We use the same inhibition term for Q and QH_2, assuming that a possible obstruction has an equal effect on both molecules.

$$I_s = 1 + \frac{[Q]}{Ki_1} + \frac{[QH_2]}{Ki_2} \tag{2.35}$$

Where the Ki_1 and Ki_2 are the inhibition constants. It may be argued that only QH_2 should have an obstructive effect on Q, since Q is the substrate and cannot

block itself on the way to the binding site, whereas both Q and QH_2 can hinder QH_2 to leave from the binding site and for the reverse reaction it would be vice versa. Distinguishing between these cases would render the rate equation much more complex while the benefit is expected to be rather low. But we consider this possible inhibition in more detail using a stochastic model in section 2.3.3.

Non competitive inhibition I_{nc} Another possibility is the Q and or QH_2 binding to a second Q site which is modifying the activity of complex I. This binding would be non competitive with the binding on the catalytic site. The existence of a second site has been suggested by Nakashima et al. [2002a]. The generic expression for the description of non competitive inhibition is

$$I_{nc} = \left(\frac{1}{1 + \frac{[Q]}{Ki_1} + \frac{[QH_2]}{Ki_2}} \right)^n \tag{2.36}$$

Here n has been fixed to 1 or 2; additionally n has also been fitted.

For the steric and-non competitive inhibition, we tried different possibilities, e.g. for the non-competitive inhibition we tested as inhibitor Q or Q_{tot}, but not QH_2 alone, because the latter alone cannot reproduce an inhibition of the enzyme's activity for high ubiquinone concentrations. In the case of steric inhibition, both forms, oxidized and reduced should be involved. Therefore the inhibition term contained either Q_{tot} or Q combined with QH_2.
In most cases similar accuracies have been obtained; steric inhibition by Q_{tot} is among the best results. The most relevant expressions and their respective parameter values are summarized in table 2.16. Taking either Q or Q_{tot} as a non-competitive inhibitor made no difference in accuracy, it could be compensated by the K_{QH_2}. Interestingly, the values for K_Q remain approximately the same for all different inhibition types and among the Michaelis-Menten constants it is only K_{QH_2} that changes significantly.
In figure 2.14, as an example the RBs equation with steric inhibition by Q_{tot} and without inhibition are plotted versus the initial rate measurements. For nearly all experimental curves not so much difference could be revealed, but expectedly for the series where Q has been varied until high concentrations, the data were better reproduced.

Compared to the results without inhibition the improvement in accuracy is less than 10% of the RMSD, however the use of inhibition factors has an important effect at higher Q and QH_2 concentrations. The ubiquinone concentration in the inner mitochondrial membrane is assumed to be in the mM range. However this is to be regarded with great caution since, as for the K_m, also for the K_i the determined values are apparent because the real concentration of ubiquinones in the SMP in the experiments is unknown (for more details see also in materials and methods 2.2.6). Further it has been supposed that within the inner membrane, 2 or 3 Q-pools exist which could be separated structurally or by gradient, and thereby only a part of the ubiquinones would be used as electron shuttles within the respiratory chain. Moreover the physiological quinones have different

Figure 2.14.: Complex I: Fit to initial rate measurements with quinone inhibition. Different types of inhibition have been tested. Below, the results of the random binding equation with steric inhibition is shown (blue line) and compared to the same equation type without inhibition (red dashed line). a) and b) At high concentrations of Q, the inhibition term is advantageous for data description. c) When the concentration of Q is rather low, the results for with and without inhibition are quite similar. The fits to the remaining curves of complex I are not shown, because the curves are very similar.

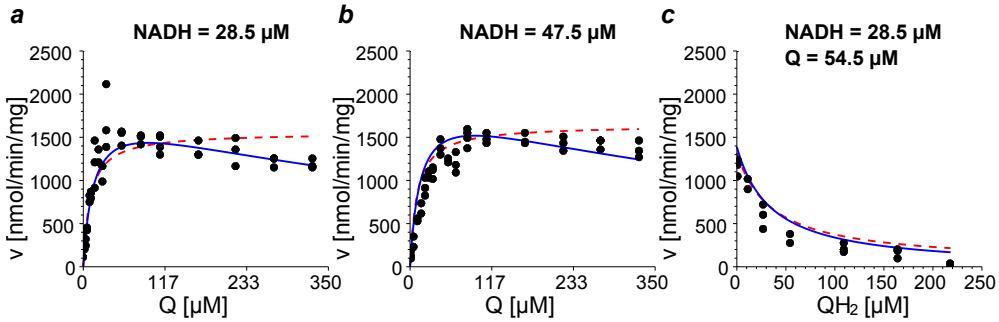

Table 2.5.: Complex I: Inhibition by quinones. The table list the results of the simplified random binding rate equation where a term for substrate (steric) inhibition (I_s) or non-competitive inhibition (I_{nc}), respectively, has been included in order to take into account a negative effect on the enzyme's activity by Q or the total Q concentration (Q_{tot}). RMSD is the root mean square deviation between simulated and experimental data. When there is only one inhibitory constant it is called Ki in the equation and listed in the Ki_1 column. *The $kcat^-$ were calculated using the Haldane relationship 2.15, see also section 2.2.7.

Inhibition	**RMSD**	$\mathbf{k_{cat}^+}$	$\mathbf{k_{cat}^-}$*	$\mathbf{K_{NADH}}$	$\mathbf{K_Q}$	$\mathbf{K_{NAD}}$	$\mathbf{K_{QH_2}}$	$\mathbf{Ki_1}$	$\mathbf{Ki_2}$
		[nmol min^{-1}mg^{-1}]		[μM]	[μM]	[μM]	[μM]	[μM]	[μM]
$I_s = 1 + \frac{[Q]}{Ki_1} + \frac{[QH_2]}{Ki_2}$	151	2185	$7.42 \cdot 10^{-6}$	4.5	14.7	740	46.9	598	25.4
$I_s = 1 + \frac{[Q_{tot}]}{Ki}$	153	2194	$1.20 \cdot 10^{-6}$	4.5	14.7	743	7.5	576	
$I_{nc} = \frac{1}{1+\frac{[Q_{tot}]}{Ki}}$	153	2254	$1.21 \cdot 10^{-6}$	4.5	15.1	743	7.6	561	
$I_{nc} = \frac{1}{1+\frac{[Q]}{Ki}}$	154	2244	$1.07 \cdot 10^{-6}$	4.5	15.0	744	6.7	575	
$I_{nc} = \left(\frac{1}{1+\frac{[Q_{tot}]}{Ki}}\right)^2$	153	2209	$1.18 \cdot 10^{-6}$	4.5	14.7	740	7.4	1319	
$I_{nc} = \left(\frac{1}{1+\frac{[Q]}{Ki}}\right)^2$	154	2200	$1.07 \cdot 10^{-6}$	4.5	14.5	741	6.6	1351	
$I_{nc} = \frac{1}{1+\frac{[Q]}{Ki_1}+\frac{[QH_2]}{Ki_2}}$	152	2236	$1.04 \cdot 10^{-5}$	4.5	15.0	741	65.6	589	29.8
$I_{nc} = \left(\frac{1}{1+\frac{[Q]}{Ki_1}+\frac{[QH_2]}{Ki_2}}\right)^2$	151	2198	$2.83 \cdot 10^{-5}$	4.5	14.6	737	177	1367	56.8

properties compared to the artificial ones that are used in the experiments. For instance, being amphiphilic, decylubiquinone is suspected to access more easily the Q-binding site that is surrounded by an aqueous environment.

With respect to all these uncertainties inhibition by Q or Q_{tot} should not be overestimated. It could however have a regulatory aspect.

2.3.3. Simulating complex I steady states kinetics using a stochastic model of complex I

In the previous section, we could not point out a steady state mechanism being in particular suitable for our experimental data. The literature information on the binding order is also controversial. This is possibly due to the series of electron transferring iron-sulfur clusters in this large respiratory complex that constitute probably an electron buffer serving for an efficient reduction of quinone Brandt [2011]. This is a particular feature which may influence the steady state kinetics.
This issue is examined in the following, using the stochastic model of complex I developed by Ransac et al. [2010]. This model is briefly presented below and the results relevant for the discussion of the steady state kinetics are summarized afterwards. More details can be found in the publication [Ransac et al., 2012].

Stochastic model of complex I

The model is designed to simulate the processes occurring in a single complex I in absence of the membrane gradient. It takes into account all redox steps from the oxidation of NADH up to the reduction of quinone, i.e. the transfer of electrons along the chain of redox centers. The transfer from one center to another is strongly dependent on the distance between them and the potential difference. The empirical Marcus-type equation [Crofts and Rose, 2007, Moser et al., 2006] was used to calculate from this information the corresponding electron transfer rate constants:

$$log(k_{et}) = 13 - (1.2 - 0.8\rho) \cdot (D - 3.6) - \frac{F}{4 \cdot RT \ln 10} \cdot \frac{(\Delta G^0 + \lambda)^2}{\lambda} \tag{2.37}$$

Here D is the distance between the redox centers, ΔG^0 is the standard Gibbs free energy of the electron transfer, $\rho = 0.76$ is the packing density and $\lambda = 0.7$ represents the reorganization energy. The distances have been taken from the complex I structure of *Thermus thermophilus*. As mentioned in the introduction, the core units of complex I are well conserved among the species, thus a good general validity should be given. Electron transfers over a relatively high distance between two redox centers are very unlikely, hence electrons transfers above a distance of 23 Å were excluded. The subsequent 19 considered reactions with their kinetic parameters, the distances and the thermodynamic properties are summarized in table 2.6. The ensemble of reactions is simulated using a Gillespie-algorithm, with one exception: since NADH and FMN are very close (3.2 Å) most of the simulation time would be needed to calculated the rapid exchange of

electrons between them, therefore an equilibrium replaces this reaction. More details on the model can be found in Ransac et al. [2010] with slight modifications in Ransac et al. [2012].

Table 2.6.: Parameters used in the stochastic model of complex I. Below the distances between the redox centers are listed, as well as the Gibbs energies of reaction and the forward and backward rate constants of the electron tunneling. The latter are calculated via equation 2.37 and distances were obtained from the structure of *Thermus thermophiles*. The scheme on the right side illustrates the locations of the redox centers. The table and the figure are taken from Ransac et al. [2012].

Reactions	Distance (in Å)	ΔG^0 (in eV)	$k_{forward}$ (in s^{-1})	$k_{backward}$ (in s^{-1})
2 e^- transfer from NADH to FMN	1.0	0.042	$2.21\ 10^{11}$	$1.06\ 10^{12}$
e^- transfer from FMNH2 to N1a	11.3	0.087	$7.03\ 10^{4}$	$1.82\ 10^{6}$
e^- transfer from FMNH• to N1a	11.3	− 0.009	$4.68\ 10^{5}$	$3.34\ 10^{5}$
e^- transfer from FMNH2 to N3	7.6	− 0.043	$1.34\ 10^{8}$	$2.68\ 10^{7}$
e^- transfer from FMNH• to N3	7.6	− 0.139	$6.39\ 10^{8}$	$3.52\ 10^{6}$
e^- transfer from N3 to N1b	11.0	− 0.05	$1.47\ 10^{6}$	$2.26\ 10^{5}$
e^- transfer from N3 to N4	13.8	0.05	$4.98\ 10^{3}$	$3.23\ 10^{4}$
e^- transfer from N1b to N4	10.7	0.10	$1.21\ 10^{5}$	$5.10\ 10^{6}$
e^- transfer from N1b to N5	16.8	0	220	220
e^- transfer from N4 to N5	8.5	− 0.10	$1.02\ 10^{8}$	$2.43\ 10^{6}$
e^- transfer from N5 to N6a	14.0	0.10	$1.35\ 10^{3}$	$5.68\ 10^{4}$
e^- transfer from N6a to N6b	9.4	− 0.10	$3.00\ 10^{7}$	$7.12\ 10^{5}$
e^- transfer from N6b to N2	10.4	− 0.10	$7.68\ 10^{6}$	$1.82\ 10^{5}$
e^- transfer from N1a to N3	19.4	− 0.13	577	0.45
e^- transfer from N4 to N7	20.4	− 0.05	4.00	0.62
e^- transfer from N3 to N5	21.1	− 0.05	1.54	0.24
e^- transfer from N5 to N6b	22.3	0	0.12	0.12
e^- transfer from N2 to Q	12	0.02	$1.04\ 10^{5}$	$2.21\ 10^{5}$
e^- transfer from N2 to SQ•	12	− 0.10	$8.67\ 10^{5}$	$2.06\ 10^{4}$

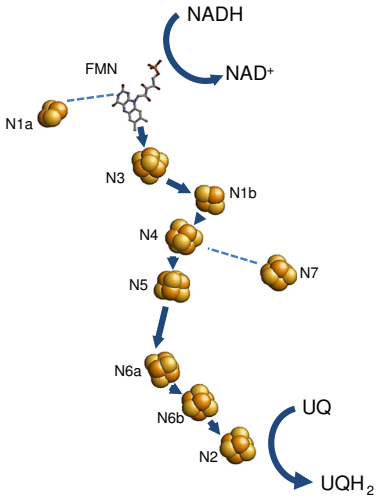

Simulation of steady state kinetics

We used this model to reproduce the initial rate measurements of complex I, mimicking *in silico* the *in vitro* experiments.
In order to have the same conditions the substrate and product concentrations were converted into number of molecules per volume available for a single complex I molecule. A volume of $1.4 \cdot 10^{-4}$ L of membrane/molecule CI and $2.8 \cdot 10^{-4}$ L of matrix/molecule CI was estimated [Ransac et al., 2010]. A rough guess is sufficient, since the ratio of molecules per volume unit is assumed to be constant.
The activity of a single complex I for a given set of substrate and product concentrations was estimated by running the simulation for a short time interval yet sufficiently long enough to be able to calculate a kind of steady state activity, i.e $v = \Delta QH_2/\Delta t$. A time interval of 3 seconds appeared to be sufficient and for each concentration set 10 simulations have been performed and averaged.

It should be emphasized that k_{on} and k_{off} of the substrates and products were the only parameters in the model that have been adjusted; the other parameters were fixed,

Table 2.7.: Rate constants of substrate and product binding and release used in the stochastic model of complex I.

	k_{ON} [$M^{-1} s^{-1}$]	k_{OFF} [s^{-1}]	K_d [M]	E [V]
NADH	29,000,000	285	$9.8\ 10^{-6}$	− 0.308
NAD	2,200,000	1500	$682\ 10^{-6}$	− 0.195
Q	15,000,000	580	$38.7\ 10^{-6}$	− 0.272
QH_2	37,500,000	320	$8.5\ 10^{-6}$	− 0.312

calculated with the distances between the redox centers and the corresponding redox potentials. The adjustment of the k_{on} and k_{off} values was performed manually, because the calculation took much time and hence running a global search algorithm would have been extremely time expensive. For the comparison of the simulated activities in molecules/sec/complex I with the experimental data given in nmol/min/mg, we employed the conversion factor 6.6 nmol/min/mg $\cdot$ sec, which corresponds to a maximal turnover rate of $292s^{-1}$ compared to a specific activity of 1920 nmol/min/mg.

Results

The model can well reproduce the initial rate measurements for Q and QH_2 concentrations below the onset of an inhibition effect by Q_{tot} using the k_{on} and k_{off} values given in table 2.7. The dissociation constant K_d of all substrates and products calculated from these rate constants are in the range of literature K_m values. The stochastic model describes the experimental curves better than the common steady state kinetic rate laws: The latter shows a hyperbolic shaped curve for the activity as a function of substrate concentration as it is typically found for enzyme kinetics. However, the curves of the stochastic model feature a different behavior, which agrees better with the experimental data: When NADH was varied at fixed concentration of Q (and in absence of products) a plateau was reached, already at low concentrations of NADH, the onset of the plateau being shifted to higher concentrations with increasing (fixed) Q concentration. When Q was varied, for small concentrations of NADH we observed also a plateau effect (NADH $< 4\mu$M), but the effect vanished with higher (fixed) concentrations of NADH, and the shapes showed finally a hyperbolic behavior, see figure 2.15.

A plausible explanation for the plateau occurring when varying NADH is that the reduction of Q is under most conditions the rate limiting step and since the oxidation of NADH happens much faster, the redox centers between the two binding sites are more and more reduced with increasing NADH concentration. Hence a higher concentration of NADH can thus not accelerate the reaction, leading to this plateau effect .
At low NADH concentrations ($< 4\mu$M i.e $< K_{NADH}$), a plateau can also be observed when increasing the concentration of Q. Here, due to relatively low NADH concentrations, the oxidation of NADH is slow and rate limiting. At higher fixed NADH concentrations, the variation of Q results in a hyperbolic rate substrate dependency.
Thus not only the non-hyperbolic shapes of the experimental curves, but also this plausible hypothesis for this behavior strongly suggest that both reactions, i.e. oxidation of

Figure 2.15.: Stochastic model: Description of initial rate measurements. When varying the concentration of NADH at fixed concentration of Q the activity of complex I increases and a plateau is reached, not showing the hyperbolic dependency which is typical for enzyme kinetics. When varying the concentration of Q, the behavior is different: For small concentrations of NADH $< 4\ \mu M$ a plateau is exhibited, but for higher NADH concentrations the shape becomes hyperbolic. This can be ascribed to the electron buffer effect of the seven redox centers, which makes spatially independent from each other the oxidation of NADH and the reduction of Q. In the case where the oxidation of NADH is faster than the reduction of Q, the redox centers are reduced to a high degree and thereby the reduction of Q is not directly dependent on the timing of NADH oxidation: an increase of the NADH concentration cannot accelerate the reaction and a plateau is consequently observed. The reduction of Q is revealed to be in general rate limiting at high concentration of NADH, because here a plateau can always be observed. For the variation of Q it is different: the electron buffer effect is visible only for low concentrations of NADH, where a plateau occurs for high concentrations of Q. With increasing NADH concentrations, the plateau transforms into a hyperbolic shape. The curves are extracted from Ransac et al. [2012], where more curves can be found.

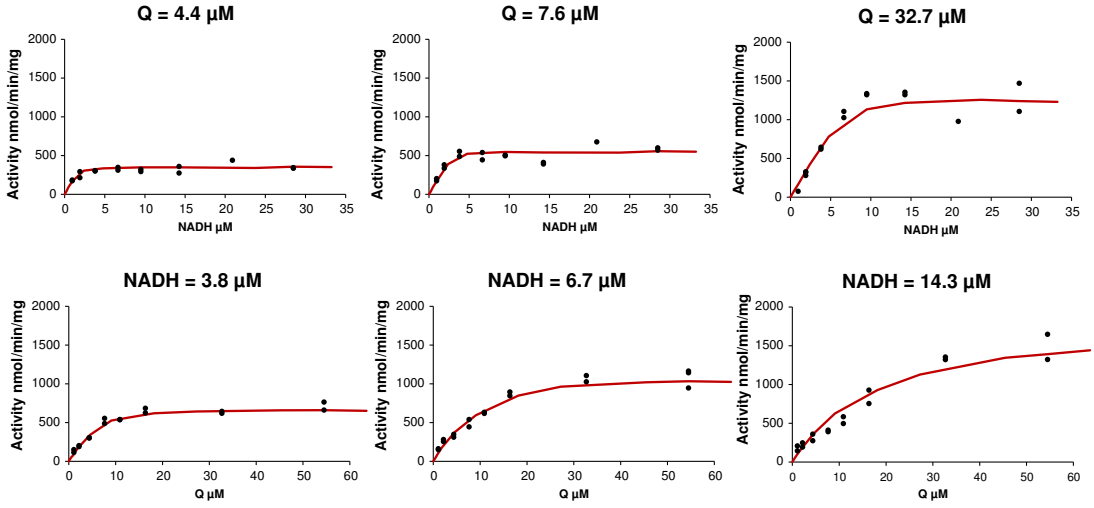

NADH and reduction of Q, occur independently of each other, and do not correspond to any traditional enzyme mechanism at steady state.

A double reciprocal plot which is classically used to identify binding orders is shown in figure 2.17. It reveals that with one substrate fixed neither a ping pong mechanism nor an ordered mechanism can be pointed out since $1/v = f(1/substrate)$ is first of all not linear. Thus the second condition that the required linear lines should be either parallel (ping pong mechanism) or intercepting in a common point (ordered mechanism) is definitely not obtained. Still it is thinkable that under certain combinations of substrate and product concentrations steady state kinetics could resemble a ping pong mechanism. This is the situation, where most probably, after two electron has been fed into the redox center chain by oxidizing NADH, an Q is reduced.

Inhibition by quinone

The stochastic model can so far not reproduce the effect of an inhibition by Q or Q_{tot} observed at higher concentrations. As already discussed above in section 2.3.2 a plausible explanation for this inhibition might be that Q and QH_2 could obstruct the path guiding them to and from the binding site. Such an obstruction was taken into account by the following modification of the model: A second Q binding site was introduced where the ubiquinones and ubiquinols have to bind on their way to the catalytic site and on their way out, too. The step from the new binding site to the catalytic site was implemented as a transfer reaction. If Q or QH_2 is bound at the second Q binding site, another Q or QH_2 cannot pass by, and thus the higher is the Q_{tot} concentration, the more it is probable that QH_2 is blocked on its way out of the catalytic site and the higher the QH_2 concentration the higher is the probability that the second binding site is occupied by a QH_2 that hinders Q to enter the catalytic site.

It should be emphasized at this point that such a second binding site probably does not exist, but it is a simple, very reasonable and illustrative approach to model an obstruction of the path. And indeed, the results show a good agreement with the experimental data. The inhibition at higher concentrations by Q and the strong inhibition by the product QH_2 can be well described with this approach, as shown in figure 2.16.

Being an intrinsic feature of the model, the plateau behavior remains as it has been observed for the original model (not shown). Additional to the parameters describing the binding and release of the substrates, the transfer between the inhibiting binding site and the catalytic site needed to be parameterized. For sake of simplicity, the binding rates were assumed to be independent of whether a Q or QH_2 molecule already occupied the catalytic site. The corresponding parameter values are given in table 2.8.

It is worth noting that in both cases, with or without inhibition, the K_d for QH_2 is smaller than the K_d for Q, which shows that QH_2 has a high affinity and may exert a strong negative regulation on the catalytic activity of complex I.

Figure 2.16.: Stochastic model with inhibition. The obstruction of the access path to the catalytic Q-site is modeled via a second Q-binding site, as illustrated in a). QH_2 binding at the site B can block the way for Q to reach the catalytic site A. Further Q or QH_2 bound at site A hinder QH_2 to leave the catalytic site. In b) the possible interactions are schematized. The pathway in the middle of the scheme is ideal for quinone reduction. c) The model can now describe the data where an inhibition at higher concentrations of Q is observed and can reproduce well the strong inhibition by QH_2

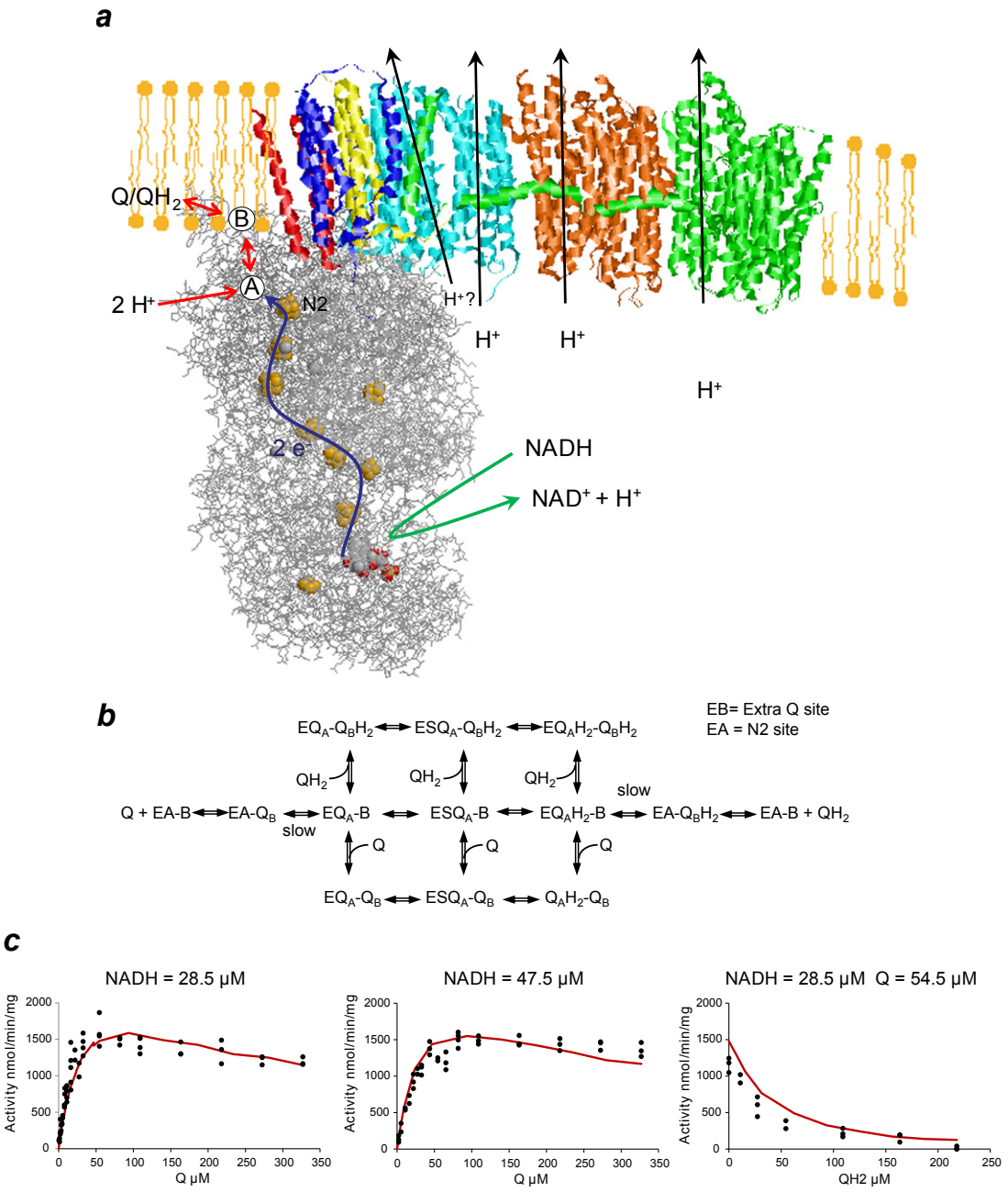

Figure 2.17.: Double reciprocal plots of the simulated initial velocities. The plots excludes clearly a classical enzyme mechanism, where a linear relationship between 1/v and 1/substrate should be given, and the lines resulting from different fixed concentrations of the second substrate would be expected to be parallel for a ping pong mechanism and intersecting in one common point in case of an ordered mechanism. The figure is taken from Ransac et al. [2012]

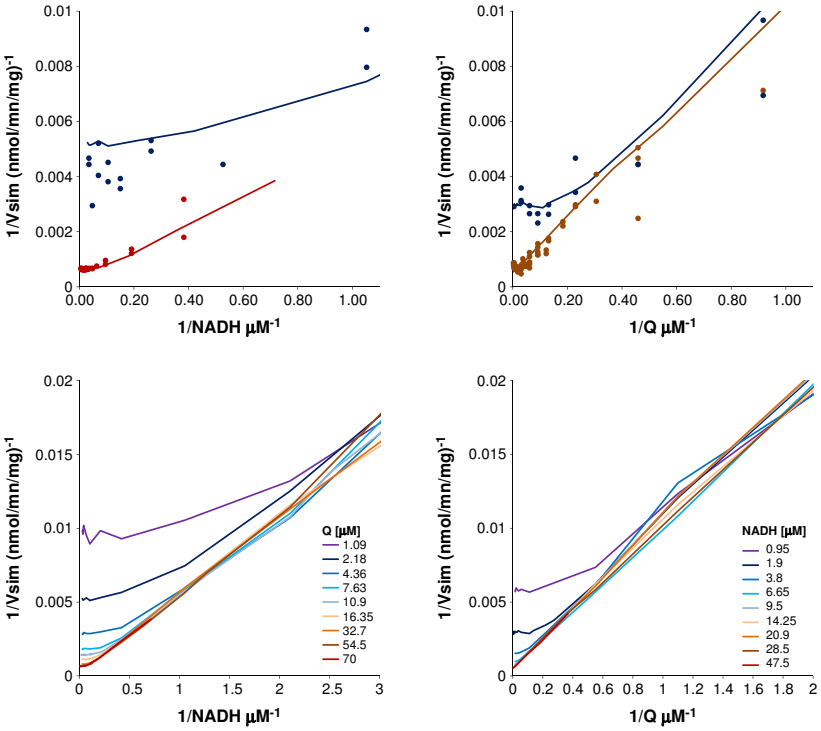

Table 2.8.: Rate constants of substrate and product binding and release used in the modified 2-Q-site stochastic model of complex I.

	k_{ON} [$M^{-1} s^{-1}$]	k_{OFF} [s^{-1}]	K_d [M]	E [V]
NADH	16,500,000	400	$24\ 10^{-6}$	− 0.285
NAD	2,800,000	1800	$643\ 10^{-6}$	− 0.198
Q	15,000,000	2700	$180\ 10^{-6}$	− 0.107
QH_2	20,000,000	1200	60.10^{-6}	− 0.137

	$k_{A \Longrightarrow B}$ [s^{-1}]	$k_{B \Longrightarrow A}$ [s^{-1}]	K_{eq}
Q	500	2550	5.1
QH_2	800	1500	1.9

2.4. Rate equation for complex II

Complex II catalyzes the 2-substrate 2-product reaction

$$\text{succinate} + \text{Q} \rightleftharpoons \text{fumarate} + \text{QH}_2 \tag{2.38}$$

With the given experimental method, we encountered problems concerning the experiments that are essential for the determination of the products K_m values. We developed thus an approach for estimating the influence of QH_2 on complex II activity which kept the same experimental conditions as had been used for analyzing the rate dependency on the substrate concentrations. However, with the given experimental setup the strength of product inhibition by fumarate could not be determined (for both issues see section 2.2.5).
All above listed equations are in principal possible candidates to describe the kinetics of complex II. However, such an incomplete data set would not allow for a good parametrization of the non-simplified rate laws, thus solely the simplified and general rate equations were considered.

2.4.1. Fitting to experimental data

The fitting procedure for complex II was split up into two, because of the different types of experimental data obtained by different means: At first, initial rate measurements where the substrates succinate and ubiquinone have been varied in absence of the products were used to determine the specific activity and the K_m values of both substrates (see figure 2.18 a-d). Afterwards K_{QH_2} was estimated from time course data, using two different approaches: one was to fit directly these progress curves by integrating the given rate equations (see figure 2.18 e-j), the other was to fit the parameters using the initial velocities approximated from the progress curves (see figure 2.18 k).
For the estimation of K_{QH_2} the other parameter values were fixed to the previously determined values, and since the K_m for fumarate could not be determined, we set $K_{fum} = K_{suc}$; this relationship has been found before for isolated complex II from bovine heart mitochondria [Grivennikova et al., 1993, Tushurashvili et al., 1985].

In the experimental series where Q was varied, we found a small activity for Q = 0 μM. A direct reduction of quinone or DCIP by succinate however was not observed and therefore we assigned this offset to a residual concentration of quinones. Hence we have accorded a small 'corrective' concentration of 1 μM to the concentrations used in the experiments, which improved the accuracies of fits. This correction could have also been done for complex I, but there the K_Q and K_{QH_2} values were higher than for complex II, so the effect of a contingent residual Q concentration should only have a minor effect.

The estimated parameter values are listed in table 2.9. All equations show a good agreement for the data description. Satisfactory results were also obtained with EMA but significantly less precisely when compared to the other rate equations. Figure 2.18 shows the data description by PPMs and EMA. In total, the simplified ping pong (PPMs)

Figure 2.18.: Complex II: fit to experimental data. Using the simplified ping pong equation (PPMs) good results are obtained (red line). Fitting the data points with the extended mass action equation (EMA, dashed line) is less good but for most cases still satisfactory. However EMA fails for the description of the initial velocities when QH_2 is varied in absence of fumarate (figure k): The product expression in the denominator of the equation becomes zero because it contains as factor the concentration of fumarate (=0) and thereby no influence of the QH_2 concentration on the forward velocity can be simulated. For estimating the parameters of EMA, the succinate and fumarate concentrations were considered in mM, while for the Q and QH_2 concentrations the unit μM was used. This was done in order to compensate for the large difference in their K_m values of about three orders of magnitude.Thermodynamics are thereby not violated because in each, forward and backward term, the units μM and mM occur once and hence for the calculation of the K_{eq} the factor 1000 for the conversion from mM to μM is cleared. In the EMA equation itself the different units are considered by the constants C_S and C_P. The parameter values for PPMs and EMA are listed in table 2.9. The substrate concentrations in the experimental series e) to j) were succinate = 200 mM and Q = 140 μM.

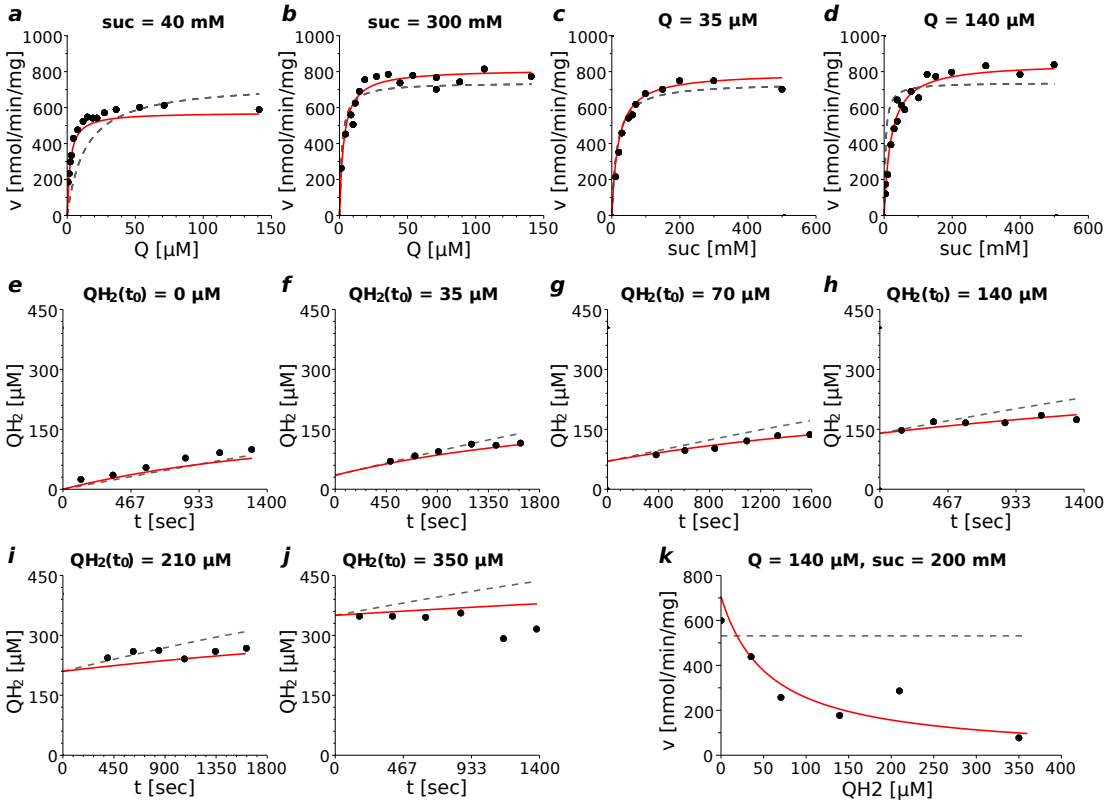

equation shows the best results; the values for K_{QH_2} obtained by the two different approaches are in good agreement. It is remarkable that K_{QH_2} is here about 10 times lower than K_Q, indicating strong affinity of QH_2 for the binding site.
The difference in accuracy to PPMs is rather small for the other rate equations. Since the determination of the substrate K_ms and the k_{cat}^+ were performed in absence of the product concentrations, the denominators of all rate equations but EMA and PPMs are equal and consequently the same values are found for these kinetic parameters. In contrast to that, the values for the K_{QH_2} vary within two orders of magnitude, the two different methods for their determination always lead to results in the same order. This shows again impressively how different the apparent K_m values can be according to the different rate equations.

For complex II, no inhibition by Q or Q_{tot} was observed, the strong inhibition effect of QH_2 is thus purely due to the normal product inhibition.
Like complex I, also complex II has some redox centers between the two binding sites, albeit less. If an electron buffering effect exists, it should be much less pronounced, and the steady state mechanism should be close to ping pong. Indeed, this mechanism lead to somewhat better accuracies than the other mechanisms.

For EMA, the relatively good agreement was only possible because succinate (and fumarate) were considered in mM whilst for Q and QH_2 the unity was μM. This seems to be inconvenient but the unities are balanced by its global Michaelis-Menten constants C_S and C_P, and further in the Haldane equation 2.15 the unities are cleared since 'mM' occurs once in the nominator and denominator and the same for 'μM', thus it is consistent with thermodynamics. This approach compensates for the very different affinities of quinone and succinate, their K_m being three orders of magnitude apart. Taking mM for succinate compensates for this big difference, since the more the K_m of the substrates or the K_m of the products are different, the lower is the accuracy of the equation. This is a another weak point of the EMA equation. The disadvantage of the correction is that the concentration changes this must be taken into account when the equation is used in an differential equation system.
Since for the determination of C_P only QH_2 has been varied, the results for the description of the corresponding data are quite good. However the value obtained for C_P is to regard with caution since the influence of fumarate on this parameters has not been tested.

Comparison to literature data

If not noted otherwise, the literature data that are cited in the following refer to bovine heart mitochondria.
The specific activities that have obtained with the rate equations are comparable with the results of Tushurashvili et al. [1985] who measured on intact mitochondria a specific activity of 700 nmol/min/mg. Grivennikova et al. [1993] found that the forward specific activity of complex II was 40 times the reverse specific activity. This relationship is

Table 2.9.: Complex II: parameter values. Three values are given for the RMSD: the first value refers to the fits to the initial velocity measurements for the variation of succinate and Q in absence of the products. The second and third values refer to the estimation of the K_{QH_2}, for fitting to time course data points (see figure 2.18 e-j) and therefrom estimated initial velocity measurements (see figure 2.18 k). K_{fum} was not determined experimentally and was set set equal to K_{suc}. *The $kcat^-$ were calculated using the Haldane relationship 2.15 (and 2.15 for EMA), see also section 2.2.7.

equation	**RMSD** * / ** / *	$\mathbf{k^+_{cat}}$	$\mathbf{k^-_{cat}}$	$\mathbf{K_{suc}}$*	$\mathbf{K_Q}$	$\mathbf{K_{fum}}$*	$\mathbf{K_{QH_2}}$
		nmol/min/mg		[μM]	[μM]	[μM]	[μM]
PPMs	39.6 / 21.5 / 76.2	869	40.3	20721	3.3	20721	0.47 / 0.23
OMs 'SQFQ'	42.1 / 21.6 / 92.9	852	1109	18796	2.5	18796	10.0 / 4.21
OMs 'QSQF'	42.1 / 24.3 / 92.9	852	4357	18796	2.5	18796	39.3 / 48.3
OMs 'QSFQ'	42.1 / 21.2 / 92.9	852	202	18796	2.5	18796	1.82 / 0.86
OMs 'SQQF'	42.1/ 23.1 / 92.9	852	4733	18796	2.5	18796	42.7 /44.9
RBs	42.1 / 21.2 / 92.9	852	202	18796	2.5	18796	1.82 / 0.86
CK	42.1 / 21.2 / 92.9	852	17.7	18796	2.5	18796	0.16 / 0.07
EMA	116 / 25.2 / -	738	0.06	$C_S = 531\,mM\,\mu M$		$C_P = 0.14\,mM\,\mu M$	

* [nmol/min/mg], ** [μM]

approximately fulfilled for PPMs and CK.

The K_{suc} value that we measured was, at around 20 mM, significantly elevated compared to literature data where the values ranged from 0.020 - 1.5 mM [Tushurashvili et al., 1985, Vinogradov et al., 1989, McLean et al., 2009, Yang et al., 1996]. The protocol we used for this enzyme assay is taken from the French Mitochondrial diseases network, with slight modifications. From the work that has been done by means to find optimal conditions for the complex II assay, a K_{suc} of roughly 5 mM can be estimated [French Mitochondrial Diseases Network].
Hence there might be a problem with components in the reaction mix. Since the maximal activity seems to be correct, an inhibitor would act competitively. But none of its components could be identified as problematic compared to other protocols. Another reason might be an insufficient disruption of the mitochondrial membranes because then the access of succinate to the respective binding site could be blocked. However, since for complex I the access of NADH to its binding site seems correct - the K_m values for NADH were reasonable - presumably there should be no problem with respect to the accessibility. The reason for the high K_{suc} remains unclear.

Tushurashvili et al. [1985] determined a K_Q of 0.5 μM, which is roughly in the range of the K_Q estimated for PPMs, RBs, CK but not all OMs. Many entries for Ecoli were found in the BRENDA database ranging from 0.0025 mM to 0.2 mM, the interval covering also most of the other microorganism listed there. But since the structure of the membrane integral parts of complex II which contains the ubiquinone binding site is relatively variable among the species, it is questionable whether these values can be referred to the bovine complex II.
For the reverse reaction in Ecoli, a K_m around 5 μM for both, Q_1H_2 and Q_2H_2 has been

determined, very similar to the $K_m = 2\ \mu M$ for Q_1 and Q_2 with respect to the forward reaction [Maklashina and Cecchini, 1999], the authors were using the coupled system of [Grivennikova et al., 1993], as described above in section 2.2.5. Again this is in good agreement with PPMs, RBs, CK but not all OMs.

K_Q and K_{QH_2} have apparent values because they are referred to the added amount of quinones in the reaction mix. However the real concentration of quinones having access to the Q-binding site is the amount of quinones in the membrane, in equilibrium with the quinones in the water phase and those organized in micelles. Also the type of quinone may influence their binding affinities, see also section 2.2.6. For complex II we can consider that the Q-binding site is well integrated in the membrane and thus the natural more hydrophobic long chain quinones should access easier, and their apparent K_Q and K_{QH_2} being consequently lower.

2.5. Rate equation for complex III

Complex III catalyzes via the Q-cycle mechanism of the following net reaction:

$$QH_2 + 2cytc_{ox} + 2H^+_x \rightleftharpoons Q + 2cytc_{red} + 4H^+_{is} \tag{2.39}$$

Two Q-binding sites are involved in this mechanism, the QH_2 reduction site Q_o, close to the intermembrane space, and the Q oxidation site Q_i, located on the matrix side of the membrane. When considering all participating components, the reaction is

$$2QH_2(o) + 2cytc_{ox} + Q(i) + 2H^+_x \rightleftharpoons 2Q(o) + 2cytc_{red} + QH_2(i) + 4H^+_{is} \tag{2.40}$$

This representation shows also clearly that ubiquinones and ubiquinols are both, substrates and products. The functioning of complex III cannot be assigned to any classical steady state kinetics. The following approaches could be made to model complex III kinetics:

Derivation of a rate equation via King-Altmann method. Here, the exact binding sequence must be known, and the resulting equation would be more complex than the above cited mechanism based equations, which is not in our interest. One could than simplify the expression, by assuming that reduced and oxidized complex III would have same binding properties and by setting the K_i equal to their corresponding K_m.

The fact that complex I kinetics are well approached by simplified Michaelis-Menten equations suggest that for complex III there will be not much benefit of such an intricate proceeding, compared to using a generic Michaelis-Menten rate equation.

Separation of the reaction steps. Due to the Q-cycle mechanism one could split the reaction into two steps (or more), e.g.

step 1:

$$E + QH_2(0) + cytc_{ox} + Q(i) \rightleftharpoons E : SQ + Q(o) + cytcred + 2H^+_{is} \tag{2.41}$$

step 2:

$$E : SQ + QH_2(0) + cytc_{ox} + 2H+_x \rightleftharpoons E + Q(o) + cytc_{red} + QH_2(i) + 2H^+_{is} \tag{2.42}$$

where E represents the enzyme complex and E:SQ is its reduced form with a bound semiquinone (SQ). The letters 'o' and 'i' signify the two different Q-binding sites. These two steps could then be treated as two separate enzymatic reactions, one being catalyzed by E and the other by E:SQ. However, one would have to find a way how to include the energy difference between E and E:SQ into the equilibria of these reactions. Further the constraint that the total concentration of complex IV is $E_{tot} = E + E : SQ$ would have to be considered.

Omitting the binding and release at the Q_i-site , assuming that it has only minor effects on the kinetics. A two substrates - two products reaction would be the result, with QH_2 and $cytc_{ox}$ as substrates, and Q and $cytc_{red}$ as products, following first order kinetics for both, cytochrome c and the quinone species. However, a huge disadvantage is that the equilibrium calculated via the Haldane equation represents not the true equilibrium and thus the equation violates thermodynamics:

$$K_{eq} \neq \frac{K_Q \cdot K_{cytc_{red}}}{K_{QH_2} \cdot K_{cytc_{ox}}} \tag{2.43}$$

Simple but thermodynamically correct rate equations . Here, the candidates are CK, the generalized RBs equation and EMA. For each, one can consider two types of equations, in the following presented on the example of RBs equation:

- Describing the net reaction scheme .

$$v = \frac{q_r^{n/2} \cdot c_o^n - q_o^{n/2} \cdot c_r^n}{(1 + q_o + q_r)^{n/2} \cdot (1 + c_o + c_r)^n} \tag{2.44}$$

- Describing the detailed reaction scheme .

$$v = \frac{q_r(o)^n \cdot c_o^n \cdot q_o(i)^{n/2} - q_o(o)^n \cdot c_r^n \cdot q_r(i)^{n/2}}{(1 + q_o(o) + q_r(o))^n \cdot (1 + c_o + c_r)^n \cdot (1 + q_o(i) + q_r(i))^{n/2}} \tag{2.45}$$

n is the reaction order of cytochrome c, the reaction order(s) for the quinone(s) arise from the equations above. We will consider n = 1 and n = 2.

The basic representation of CK does not allow for the incorporation of non integer stoichiometric factors. To overcome this problem we modified here the expression

for a concentration c in the denominator as follows: $(1+c)^{\nu}$ for $\nu < 1$ (cases with non integer stoichiometric factor > 1 were not considered).

2.5.1. Fitting to initial rate measurements

Despite the particular mechanism of complex III, with the generalized and simplified rate equations we achieved an acceptable description of the initial rate measurements, therefore it was not necessary to make more complicated approaches, at least in a first attempt.

The equations in which the Q_i site is ignored revealed an interesting aspect: PPMs described the experimental data better than the OMs equations or the generalized equations. Moreover it showed also better results than the general rate equations describing the net reaction scheme. It was even comparable with the precision of the generalized rate equations describing the detailed reaction scheme , although the latter feature two additional parameters. The results of the different equation types are summarized in table 2.10 a-c).
It is thus probable, that the apparent steady state kinetics of complex III is very close to a ping pong behavior whereupon the influence of substrate binding and product release at the Q_i-site plays only a minor role. This is consistent with the findings of Esposti et al. [1986] who suggested a ping pong mechanism for complex III.
Despite these good results, we need to consider thermodynamically correct equations, because PPMs is not suitable for the subsequent introduction of the membrane gradient, where K_{eq} is an important feature (see above).

Among the equations describing the net reaction scheme 2.5.1, the only equation that has acceptable results is RBs where cytochrome c and the quinones at the Q_o site are second order. When additionally fitting the order, the parameters were underdetermined. The results are shown in table 2.10 b).

Better results were achieved when the detailed reaction scheme 2.5.1 was the basis for the rate equations. But here, parameter values could not be precisely determined; the high uncertainties concerned in most cases only the product K_m. Also here RBs reproduced best the experimental data, with second order for cytochrome c and the quinones at the Q_o site. Its very high value for k_{cat}^{-} seems however not reasonable. When additionally fitting the reaction order n, the data description did not improve but higher uncertainties in the parameter values were obtained.
The parameter fit for the equations following the detailed reaction scheme 2.5.1, entailed an approximation of a residual concentration of Q in the SMP, which we set to $Q_0 = 1\mu M$ (corresponding to the value that has been used when the kinetic parameters of complex II were estimated). This is because Q acts also as substrate: without this correction one would theoretically obtain zero activity for the initial rate measurements where no Q was added.
For all equations K_Q(i) was found to be very low which on one hand is due to the low

Table 2.10.: Complex III: Parameter values for the different reaction schemes. *The kcat$^-$ were calculated using the Haldane relationship 2.15 (and 2.15 for EMA), see also section 2.2.7.

a) First order for both, cytochrome and quinone (thermodynamically not correct, hence k^-_{cat} cannot be calculated via the Haldane equation.)

Equation	**RMSD**	$\mathbf{k^+_{cat}}$	$\mathbf{K_{QH_2}}$	$\mathbf{K_{cytc_{ox}}}$	$\mathbf{K_Q}$	$\mathbf{K_{cytc_{red}}}$
	[nmol/min/mg]		μM	μM	μM	μM
PPMs	399	17316	443	80.7	1022	1266
OMs, CQCQ	421	8900	142	23.2	292	1657
OMs, CQQC	414	8792	142	21.7	598	293
OMs, QCCQ	419	8760	137	22.9	347	995
OMs, QCQC	421	9052	147	23.3	544	628
RBs	414	8635	138	21.6	341	296
CK	414	8624	138	21.5	124	117
EMA	540	5174	$C_S = 5392\mu M^2$		$C_P = (4.72 \pm 3.38) \cdot 10^6 \mu M^2$	

b) One Q-site: second order for cytochrome, first order for quinones, RBs

Equation **Order**	**RMSD**	$\mathbf{k^+_{catf}}$	$\mathbf{k^-_{cat} * b}$	$\mathbf{K_{QH_2}}$	$\mathbf{K_{cytc_{ox}}}$	$\mathbf{K_Q}$	$\mathbf{K_{cytc_{red}}}$
	[nmol/min/mg]			μM	μM	μM	μM
RBs, n = 1	473	22239	133	3644	22.8	271	403
RBs, n = 2	421	8090	10.3	138	7.7	323	312
CK, n = 1	474	21937	31.7	3544	22.7	78.8	382
CK, n = 2	492	7570	0.015	137	10.2	17.1	72.5
EMA n = 1	676	6103	7.29	$C_S = 678\mu M^2$		$C_P = (2.45 \pm 3.05) \cdot 10^6 \mu M^2$	
EMA, n = 2	748	3967	0.066	$C_S = 98406\mu M^2$		$C_P = (4.95 \pm 2.90) \cdot 10^6 \mu M^2$	

c) 2 Q-sites. The reaction order for quinone at the Q_o-site and for cytochrome c is n, for quinone at the Q_i-site n/2. A residual concentration of $Q_0 = 1\mu$M has been assumed to avoid zero activity for Q = 0.

Equation **Order**	**RMSD**	$\mathbf{k^+_{cat}}$ $\mathbf{k^-_{cat}}$*	$\mathbf{K_{QH_2}(o)}$ $\mathbf{K_Q(o)}$	$\mathbf{K_Q(i)}$ $\mathbf{K_{QH_2}(i)}$	$\mathbf{K_{cytc_{ox}}}$ $\mathbf{K_{cytc_{red}}}$
		[nmol/min/mg]	μM	μM	μM
RBs	405	11452 ± 362	188 ± 8	0.011 ± 0.002	21.8 ± 0.2
n = 1		3727	267 ± 5	6.7 ± 1.7	352 ± 43
CK	414-416	11093 ± 317	140 ± 7	0.64 ± 0.1	17.7 ± 1.1
n = 1		27.5	3.0 ± 0.3	334 ± 356	156 ± 72
RBs	393-396	8264 ± 240	48.8 ± 1.9	0.025 ± 0.021	7.6 ± 0.1
n = 2		$1.05 \cdot 10^6$	300 ± 11	82.9 ± 97.4	420 ± 182
CK	396-409	6226 ± 201	54.2 ± 1.0	0.027 ± 0.029	10.1 ± 0.5
n =2		0.027	0.85 ± 0.39	33.5 ± 36.9	66.0 ± 72.7
EMA	998	2901	$C_S = 1574 \pm 3\mu M^2$		
n = 1		5.15	$C_P = (8.46 \pm 2.65) \cdot 10^6 \mu M^2$		
EMA	1005	2651	$C_S = 2.56 \cdot 10^6$		
n = 2		$7.84 \cdot 10^{-4}$	$C_P = 2.29 \cdot 10^6 \mu M^2$		

Figure 2.19.: Complex III: Fit to initial rate measurements. Blue line: simplified random binding (RBs) equation describing the net reaction scheme 2.5.1 with second order for cytochrome c and first order for QH_2. Red line: RBs describing the detailed reaction scheme 2.5.1 with second order for cytochrome c and QH_2 at the Q_o site and first order for QH_2 at the Q_i site. The dashed gray line shows the extended mass action (EMA) with first order for cytochrome c and 0.5 order for the QH_2 equation, following the net reaction scheme 2.5.1. RBs show for both cases satisfactory results, while the simple generic EMA is much more inaccurate.

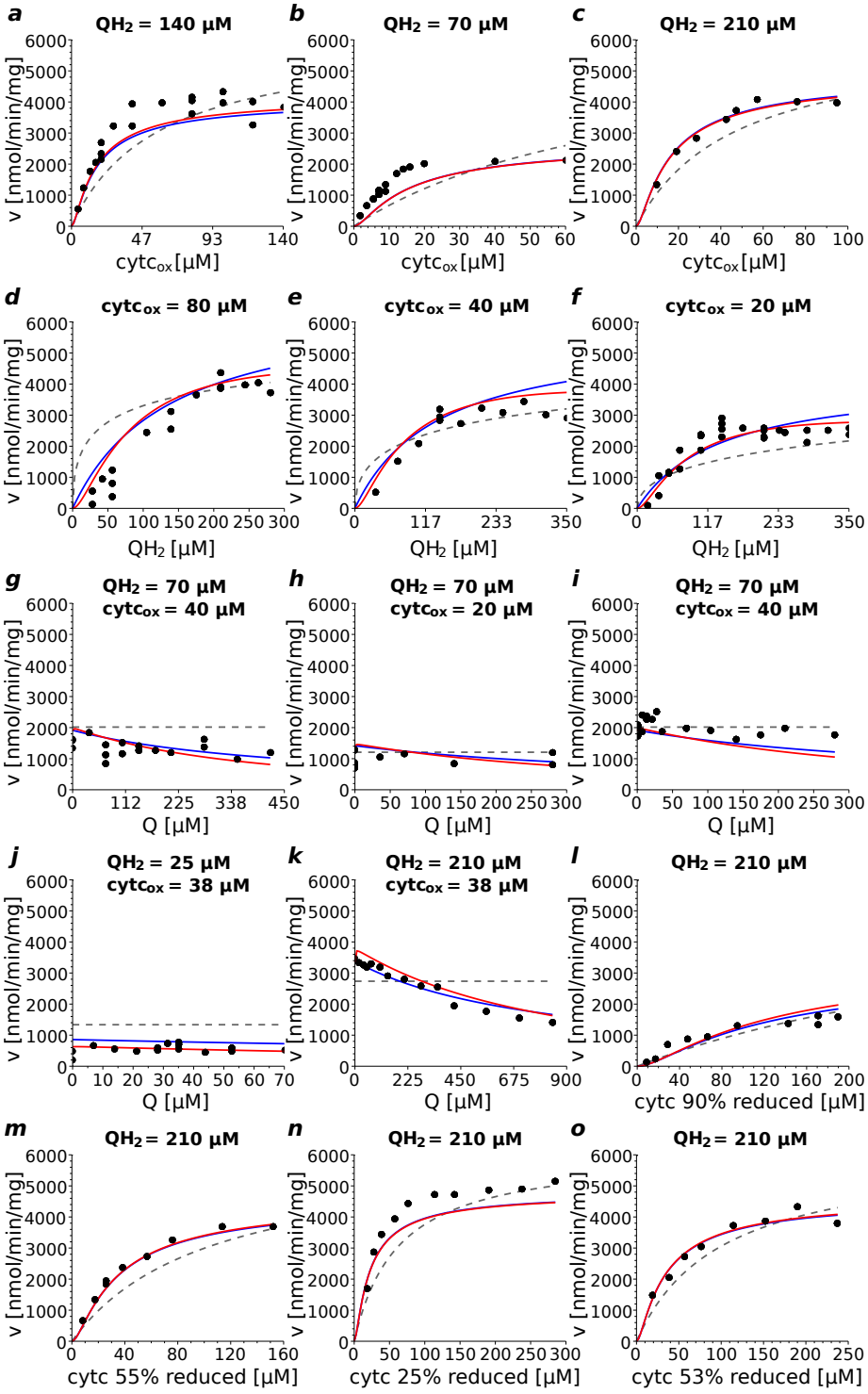

concentration of Q_0. This concentration could be set a little higher, because we found retrospectively that QH_2 was not 100 % reduced (supposedly between 95 -98 %). On the other hand, we could see upon PPMs, that the Q_i-site seems not to interfere much in the kinetics, such that its affinity for Q should indeed be very high (low $K_Q(i)$).

The values found for k_{cat}^- were in all cases higher than those of the other proton pumping complexes I and IV. This is on the one hand due to complex III having a lower standard Gibbs energy of the reaction DeltaG$_0$ in absence of the membrane gradient. On the other hand, since k_{cat}^- is calculated via the Haldane relationship 2.15 which relates the kinetic parameters, its elevated value is also a consequence of the low $K_Q(i)$ value. This is in particular the case when Q(i) has the reaction order 2 and consequently the square of $K_Q(i)$ appears in the Haldane equation.

Figure 2.19 shows the experimental data and their description by RBs 'net' and 'detailed'. Also the results of EMA 'net' are shown. This simple rate equation reproduced less good the experimental data, but was still well suited for a rough approach

Analysis of a possible inhibition by quinones and quinols

Having two Q binding sites, and also since the Michaelis-Menten like equations fail at some points to accurately describe the experimental data, we analyzed briefly whether by employing a Q, QH_2 or Q_{tot} inhibition term, a significant higher accuracy might be achieved. Therefore we tested simple non-competitive and steric inhibition upon the RBs 'net' and 'detailed' equations. In no case did an inhibition by Q alone improve the results, at least not significantly. As before, RBs with second order for cytochrome c and Q at the Q_o site describe best the data points, in particular when assuming steric inhibition by Q_{tot} at the Q_o site. However, the values of k_{cat}^- are extremely high being not reasonable at all. The accuracies improved only little when Q and QH_2 had a separate inhibition constant. The uncertainties of the parameter values were comparable to those that have been found without inhibition.

.

Table 2.11 summarizes the most significant results. In figure 2.20. RBs 'detailed' with second order for cytochrome c and quinones (Qo site) is plotted versus the initial rate measurements, a comparison is made between steric inhibition and no inhibition. For most experimental series the simulated curves were close. In the series were QH_2 has been varied (d-f) the equation with inhibition reproduce better the shape of the experimental curves.
But it is questionable whether in reality an inhibition occurs. The discrepancies in the data reproduction may simply be due to the fact that the Q-cycle mechanism is not reflected in the equations. This idea is supported by the elevated values imposed on k_{cat}^- by the Haldane equation, indicating that something is missing in the description of complex III kinetics when using Michaelis-Menten like kinetics. But still these equations are a good compromise between simplicity and accuracy, the data points being satisfactory

Table 2.11.: Complex III: Fit to initial rates assuming inhibition by quinones. a-c) the simplified random binding (RBs) equation with its different reaction orders and a simple inhibition term either steric or non competitive inhibition, has been analyzed. The best results were obtained for RBs describing the detailed reaction scheme 2.5.1 with second order for cytochrome c and for steric inhibition at the Q_o-site, see c). b) For the accuracy of data description when employing the RBs based on the detailed reaction scheme with first order for cytochrome c the inhibition terms improved the accuracies only very little. When both Q sites have been considered in the equation, also the steric inhibition refers only to one of them, as indicated below. *The $kcat^-$ were calculated using the Haldane relationship 2.15, see also section 2.2.7.

a) One Q-site: second order for cytochrome and first order for quinones

Inhibition	**RMSD**	$\mathbf{k_{cat}}^+$ [nmol/min/mg]	$\mathbf{k_{cat}^-}$*	$\mathbf{K_{QH_2}}$ μM	$\mathbf{K_{cytc_{ox}}}$ μM	$\mathbf{K_Q}$ μM	$\mathbf{K_{cytc_{red}}}$ μM	**Ki** μM
$I_{nc} = \frac{1}{1+\frac{Q_{tot}}{Ki}}$	402	18338	785	344	7.5	30000(ul)	289	492
$I_{nc} = \frac{1}{1+\frac{QH_2}{Ki}}$	401	21592	13	404	7.5	481	294	406
$I_s = 1 + \frac{Q_{tot}}{Ki}$	379	30000(ul)	279	692	7.2	15415	256	112

b) 2 Q-sites: first order for cytochrome c and quinones at the Q_o -site and 0.5 order for quinones at the Q_i-site A residual concentration of $Q_0 = 1\mu$M has been assumed to avoid zero activity for Q = 0.

Inhibition	**RMSD**	$\mathbf{k_{cat}^+}$ $\mathbf{k_{cat}^-}$* [nmol/min/mg]	$\mathbf{K_{QH_2}(o)}$ $\mathbf{K_Q(o)}$ μM	$\mathbf{K_Q(i)}$ $\mathbf{K_{QH_2}(i)}$ μM	$\mathbf{K_{cytc_{ox}}}$ $\mathbf{K_{cytc_{red}}}$ μM	**Ki** μM
$I_{nc} = \frac{1}{1+\frac{Q_{tot}}{Ki}}$	391	27243 ± 1819	477 ± 36.1	0.031 ± 0.035	21.2 ± 0.2	463 ± 26
		166138	8154 ± 8167	54.4 ± 78.7	314 ± 44	
$I_{nc} = \frac{1}{1+\frac{QH_2}{Ki}}$	393	22033 ± 4986	379 ± 866	0.048 ± 0.046	21.3 ± 0.4	652 ± 253
		16497	390 ± 45.8	252 ± 537	372 ± 95	
$I_s = 1 + \frac{Q_{tot}}{Ki}$ (Q_o)	374	30000 (ul)	635 ± 4	0.023 ± 0.015	20.2 ± 0.1	1332 ± 5
		236307	9998 ± 3978	111 ± 8	253 ± 11	
$I_s = 1 + \frac{Q_{tot}}{Ki}$ (Q_i)	397	20675 ± 1562	350 ± 25	0.045 ± 0.038	21.5 ± 0.25	265 ± 57.2
		25479	1374 ± 465	51.2 ± 51.9	348 ± 69.8	

c) 2 Q-sites: second order for cytochrome c and quinones at the Q_o site and first order for quinones at the Q_i site A residual concentration of $Q_0 = 1\mu$M has been assumed to avoid zero activity for Q = 0.

Inhibition	**RMSD**	$\mathbf{k_{cat}^+}$ $\mathbf{k_{cat}^-}$* [nmol/min/mg]	$\mathbf{K_{QH_2}(o)}$ $\mathbf{K_Q(o)}$ μM	$\mathbf{K_Q(i)}$ $\mathbf{K_{QH_2}(i)}$ μM	$\mathbf{K_{cytc_{ox}}}$ $\mathbf{K_{cytc_{red}}}$ μM	**Ki** μM
$I_{nc} = \frac{1}{1+\frac{Q_{tot}}{Ki}}$	362	18854 ± 553	94.7 ± 2.3	0.036 ± 0.020	7.3 ± 0.0	327 ± 10.3
		$2.05 \cdot 10^9$	28624 ± 1918	97.5 ± 70.3	266 ± 2	
$I_{nc} = \frac{1}{1+\frac{QH_2}{Ki}}$	362	30000 (ul)	122 ± 1	0.042 ± 0.006	7.2 ± 0.0	155 ± 1
		$1.41 \cdot 10^8$	585 ± 1.6	1883 ± 3039	267 ± 1	
$I_s = 1 + \frac{Q_{tot}}{Ki}$ (Q_o)	355	20649 ± 3096	115 ± 13	0.046 ± 0.034	7.1 ± 0.1	546 ± 85
		$3.52 \cdot 10^{10}$	26568 ± 5047	3285 ± 6907	261 ± 53.2	
$I_s = 1 + \frac{Q_{tot}}{Ki}$ (Q_i)	362	19523 ± 423	95.7 ± 1	0.063 ± 0.022	7.2 ± 0.0	310 ± 12
		$1.85 \cdot 10^9$	28984 ± 1503	145 ± 71.3	265 ± 4.35	

Figure 2.20.: Complex III: Fit to initial rates assuming inhibition by quinones. The effect of including an inhibition term is exemplary shown on the random binding equation following the detailed reaction scheme 2.5.1 with second order for cytochrome c and quinones at the Q_o site and first order for quinones at the Q_i site. Blue line: steric inhibition by Q_{tot} at the Q_o-site. Red dashed line: no inhibition. A slight improvement of the data fits due to the inhibition can be seen on the curves where Q has been varied (g-l) and in particular for the variation of QH_2 (d-f)

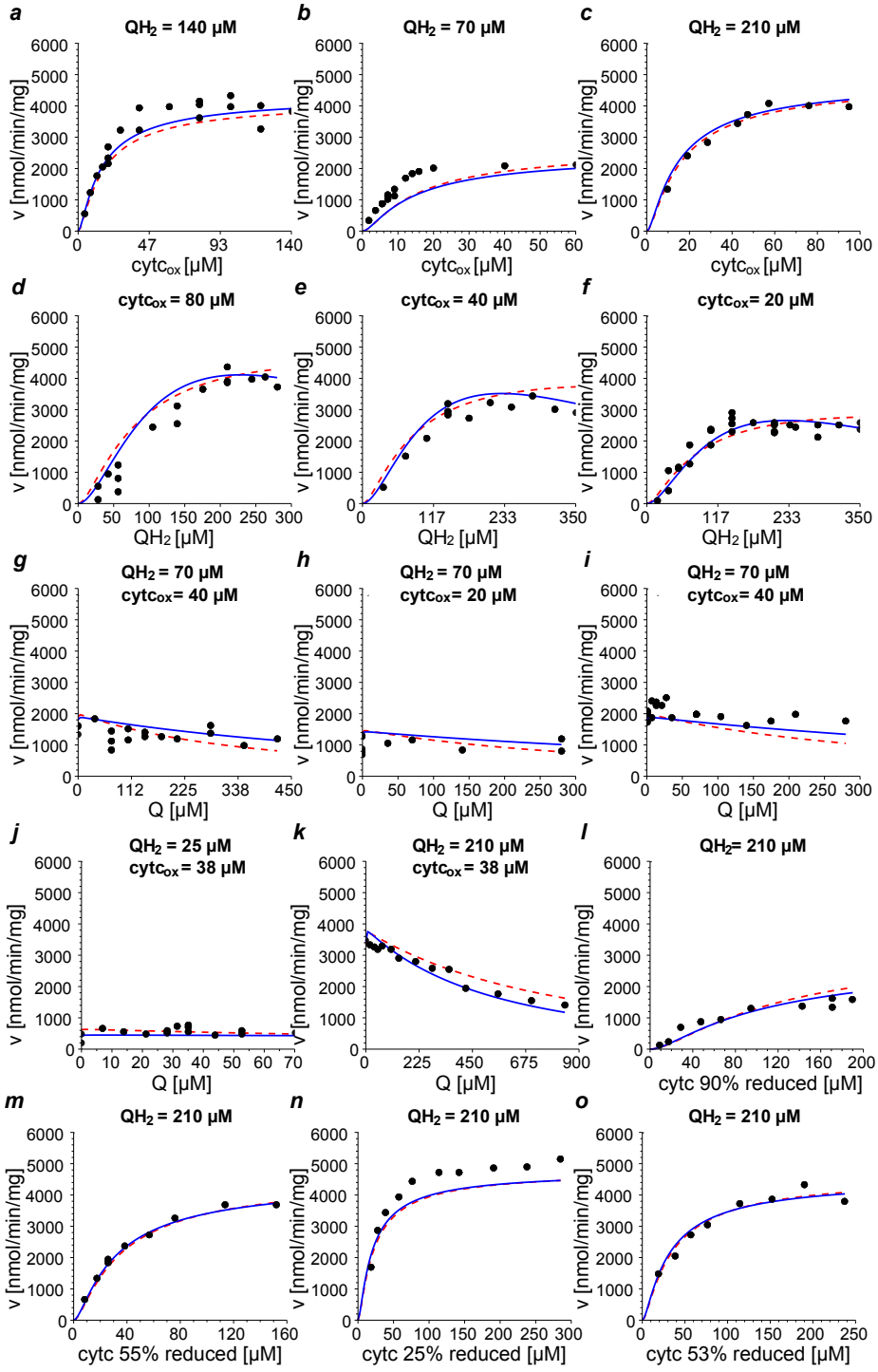

described.

Comparison to literature data

The literature data below refer exclusively to bovine heart mitochondria. The values of the equations were the Q_i-site has been neglected are taken as reference, because the substrates are both in first order and this is what is classically measured.

Esposti et al. [1986] reported a specific activity of 2610 nmol/min/mg. The theoretical maximal values that we determined were about three times higher, however the highest activity that was indeed found among our experimental data points was around 5000 nmol/min/mg. The activities were difficult to measure, since a direct reduction of cytochrome c by QH_2 was observed, this side reaction was quite active and perturbing the measurements, so that it may explain a certain discrepancy.

The K_m values for oxidized cytochrome c with the different equations types are comparable to the literature values determined by Brandt and Okun [1997] and Esposti et al. [1986], i.e. 6 and 13.6 μM. In contrast, the K_{QH_2} around 140 μM that we have determined is elevated: for different types of ubiquinols, the literature values ranged within 1.2 - 3.8 μM [Usui et al., 1990, Speck and Margoliash, 1984, Esposti et al., 1986], but also higher values, 10 and 13 μM [Brandt and Okun, 1997] and 72 μM [Pember et al., 2005] have been found. The measured deviation could partially be due to the fact that ubiquinol seems to be slightly inhibitory at higher concentrations. It may also have its origin in the difficulty of determining the activities of complex III in the presence of a strong side reaction.

Values of the products K_m were so far not reported in literature nor K_ms referred to the different Q-binding sites.

2.6. Rate equation for complex IV

The stoichiometry of complex IV is particular: Four reduced cytochrome c are oxidized in order to reduce one molecule of oxygen to two molecules of water:

$$4\,\mathrm{cytc_{red}} + \mathrm{O_2} + 4\,\mathrm{H^+} \rightleftharpoons 4\,\mathrm{cytc_{ox}} + 2\,\mathrm{H_2O} \tag{2.46}$$

The proton pumping is here not included.

Complex IV is quasi irreversible even in presence of the membrane potential difference, its forward reaction can be subdivided in the following steps: Successively, two molecules of cytochrome c bind, transfer their electron to complex IV, and leave the binding site. A water molecule leaves the oxygen binding site and a molecule of oxygen binds to it, and becomes reduced by the two electrons. Again two molecules of cytochrome c transfer their electrons onto the complex and oxygen becomes completely reduced.

Water being omnipresent at a concentration of approximately 56 M is quasi constant and classically not included in the kinetic expressions nor does it occur in the expressions of Gibbs energies. Still, none of the classical rate equations listed above can describe this complex process. One could derive an rate equation using the King-Altmann method, but such an equation would be complex and have many more parameters.

The overall reaction could also be seen as catalyzed by at least four different enzymes, having different redox states and catalytic properties with each electron that is transfered to complex IV. At quasi constant and saturating oxygen concentrations and assuming that the subsequent reducing steps have the same kinetic properties, one can then approximate the reaction to a one substrate one product reaction, consisting of the binding of reduced cytochrome c and the release of oxidized cytochrome c, i.e. a first order reaction. However, in order to obey thermodynamics and to take into account situations where oxygen is not constant any longer, the concentration of oxygen has to be included. We propose the following equation for complex IV, which is derived from the simplified random binding equation:

$$v = \frac{k_{cat}^{+} \cdot c_r^n \cdot o_2^{0.25 \cdot n} - k_{cat}^{-} \cdot c_o^n}{(1 + c_r + c_o)^n \cdot (1 + o_2)^{0.25 \cdot n}} \tag{2.47}$$

where n is the reaction order for cytochrome c.
Since our experimental set up did not permit varying the amount of oxygen, we set $K_{O2} = 1\,\mu$M corresponding to literature data: Bienfait et al. [1975] found a K_{O_2} of 1-3 μM or even $< 0.1\ \mu M$, depending on the experimental conditions. The oxygen concentration during the initial velocity measurement is quasi constant, the reaction mix was exposed to air. The O_2 concentration in the buffer solution is around 200 μM. At this oxygen concentration complex IV is largely saturated and hence equation 2.47 can be approximated by

$$v \approx \frac{k_{cat}^{+} \cdot c_r^n}{(1 + c_r + c_o)^n.} \tag{2.48}$$

.
Therefore exact values of the K_{O_2} and the O_2 concentration are not necessary for the determination of k_{catf}, K_{cred} and K_{cox}, as long as it is sure that the enzyme is highly oxygen saturated. If necessary, K_{O_2} can be adapted later without decreasing accuracy. The number of the experimental series that we have produced for complex IV was lower than for complex I and III, but this should be sufficient because only three kinetic parameters had to be estimated and moreover we made no search to distinguish between the catalytic mechanisms, as mentioned above.

Table 2.12 shows the results of the parameter estimation for equation 2.47 for different orders. As expected, first order shows good results, see also figure 2.21. When additionally the reaction order is included into the parameters estimation, a value of n = 0.97 has been obtained, confirming the assumption that the kinetics should follow first order reaction. Further fixing higher orders resulted in much higher root mean square

Table 2.12.: Complex IV: Parameter values. The table lists the parameters values resulting from fitting RBs, CK and EMA to the data from initial velocity measurements (see figure 2.12. The k^-_{cat} has been calculated using the Haldane relationship 2.15. The K_{eq} was calculated from $\Delta G_0 = n \cdot 117.01/2kJ/moL$, with n being the reaction order for cytochrome c. (R = 8.314 KJ/mol/K, T = 310 K).

equation	**order**	**RMSD**	$\mathbf{k^+_{cat}}$ [nmol/min/mg]	$\mathbf{k^-_{cat}}$	$\mathbf{K_{cred}}$ [μM]	$\mathbf{K_{cox}}$ [μM]	$\mathbf{K_{O_2}}$ [μM]
RBs	0.97	390	14010	$1.07 \cdot 10^{-7}$	71	56	1
RBs	1	390	13738	$5.20 \cdot 10^{-8}$	65.0	56.1	1
CK	1	390	13790	$2.13 \cdot 10^{-10}$	65.0	0.23	1
EMA	1	390	13721	$4.38 \cdot 10^{-7}$	$C_S = 244\mu M^2$	$C_P = 56.3\mu M^2$	
RBs	2	469	10869	$1.07 \cdot 10^{-18}$	16.3	56.0	1
RBs	4	549	9933	$2.80 \cdot 10^{-26}$	6.1	55.4	1

deviations. In addition to equation 2.47,a modified CK equation has also been fitted, adapted to the case of a non integer stoichiometric factor:

$$v = \frac{k_{catf} \cdot c_r^n \cdot o_2^{0.25 \cdot n} - k_{catb} \cdot c_o^n}{(1 + c_r)^n \cdot (1 + o_2)^{0.25 \cdot n} + (1 + c_o)^n - 1} \tag{2.49}$$

The accuracy for first order for cytochrome c is the same as for equation 2.12, and also here the accuracy decreased with the order for cytochrome c (not shown). The approximation 2.48 is not valid for the CK equation, thus the value of the oxygen solubility could have a greater influence on the parameter values.
For CK, K_{cox} is very small compared to K_{red} which is physiologically less probable, since this is not favorable for the reaction. Compared to this, for the simplified random binding the values for K_{cox} and K_{cred} are in the same range, which is more plausible.

Comparison to literature data

If not otherwise noted, the literature values refer to bovine heart mitochondria.

It is worth remarking that two kinetic phases have been reported for complex IV: For reduced cytochrome c a high affinity K_m mostly in the range of 0.02- 1 μM was found and besides a low affinity K_m that ranged from 1- 65 μM was reported [Büge and Kadenbach, 1986, Merle and Kadenbach, 1982, Sinjorgo et al., 1987]. The rates assigned to the low affinity K_m were with 11220-15504 nmol/min/mg under all conditions significantly higher than the rates for the high affinity K_m with 1469-6120 nmol/min/mg (the specific activities were taken and converted from Merle and Kadenbach [1982]).
The values that we have determined for first order kinetics for cytochrome c (see table 2.12) correspond well to the low affinity kinetic parameters. Moreover, Sinjorgo et al. [1987] found that at high ionic strength (I = 270mM) the kinetics becomes monophasic with $K_{cred} = 23\mu M$. Also at high ionic strength Lee and Lee [1995] found $K_{cred} = 32 - 44\mu M$ and Büge and Kadenbach [1986] a K_m of 64 μM (though for the latter a biphasic behavior has been observed). These values close to the value that we have

Figure 2.21.: Complex IV: Fit to experimental data. Below, the data from the initial velocity measurements are well described using equation 2.47 assuming first order for cytochrome c. The corresponding fits for CK and EMA resulted in the same curves for first order (not shown). In a) - c) the reduction state of cytochrome c was kept constant, to the value indicated above the figures. In d) - f), a fixed concentration of reduced cytochrome c was present, and oxidized cytochrome c was added.

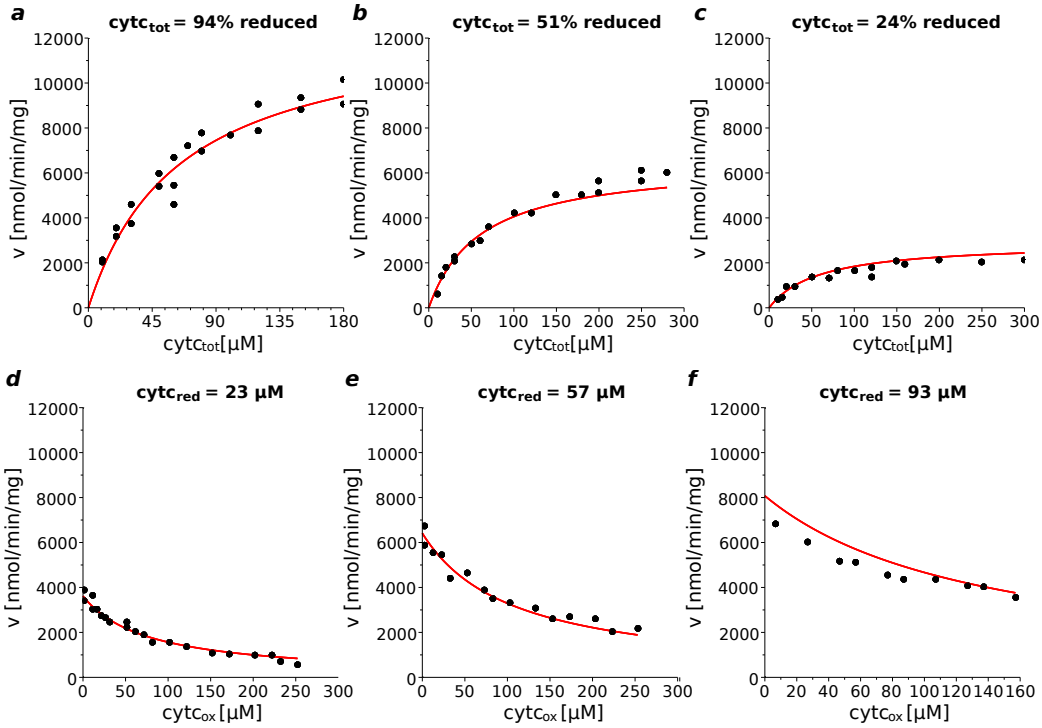

obtained at I ≈ 200. High ionic strength corresponds to intracellular conditions, for comparison, for human red blood cells I = 200 mM has been estimated Mouat and Manchester [1998].
Further Reimann et al. [1993] reported that the presence of oxidized cytochrome c shifts the biphasic behavior into a monophasic behavior. It seems that under physiological conditions the role of high affinity K_m is thus rather underpart, and that hence our results are reasonable.

As for the other three respiratory chain complexes, literature data on the K_i or K_m of the product, here oxidized cytochrome c were rare. It has been found that oxidized cytochrome c is competitive with its reduced counterpart in the high affinity phase yet non-competitive in the low affinity phase and support thereby that complex IV could have additionally a regulative binding site [Reimann et al., 1993]. However such a non-competitive behavior is not reflected in our experimental data, at least they can be well reproduced with normal product inhibition.

2.7. Rate equation for F1Fo-ATPsynthase

Since in the beginning of the work our focus was in particular on the respiratory chain complexes, we did not perform initial rate measurements on the ATPsynthase. For the complexes of the respiratory chain we have so far made the experience that rate equations of the type Michalis-Menten are well suited for their general kinetic description despite their different mechanisms. We therefore assume that the reversible kinetics of the ATPsynthase in absence of an electrochemical gradient can be sufficiently described by the random binding equation:

$$v_{rev} = E_t \cdot \frac{k^+_{cat} \cdot atp - k^-_{cat} \cdot adp \cdot p_i}{(1 + adp + atp)\,(1 + pi)} \tag{2.50}$$

where $adp = \frac{[ADP]}{K_{ADP}}$, $atp = \frac{[ATP]}{K_{ATP}}$ and $p_i = \frac{[P_i]}{K_{[}P_i]}$.

Literature data

For ATP hydrolysis, Vinogradov [2000] reported a K_m for magnesium bound ATP of 0.1 mM, and the K_i for ADP was found to be 0.3 mM.

2.8. Consideration of the whole system and discussion

Mass action law and near equilibrium rate equations cannot describe the kinetics of the respiratory complexes. We have tested a variety of rate equations that feature saturation kinetics on their ability to describe the behavior of the respiratory chain complexes in absence of the membrane gradient. The underlying experiments were performed in equal conditions for each complex which allowed us to yield consistent sets of parameters, which

is a very beneficial pre-condition for modeling the whole system, also in regard of data from literature are often diverging and have been acquired under different conditions.

2.8.1. Experimental data

The experiments of choice were initial rate measurements that we have performed on complexes I - IV exclusively on the forward reaction because the complexes are quasi irreversible in absence of the electrochemical gradient, except for complex II. Thus the estimated K_m for the products do not necessarily correspond to their real K_m values and hence represent rather K_i-constants.
For complex II the influence of the products on the catalytic activity could not be determined with initial rate measurements without changing considerably the experimental conditions. Hence we have developed a new method based on progress curves to overcome this problem for QH_2. With this relatively time intensive approach we could produce reasonable results. However, it was not possible to determine K_{fum}, the application of an inhibitor for the fumarase which was not available would make this measurement possible.

Except for this case, progress curves turned out to be not suitable for the application on the respiratory chain complexes. One reason is the difficult handling of noise, which especially for complex III is a big problem because here we observed a high direct reduction rate of cytochrome c by QH_2. Also the background noise for complex I is not negligible. The latter is the only respiratory complex where we collected such data and used them for fitting. Here the parameter values were insufficiently determined, the extended mass action equation derived in this context to reduce the number of parameters, described the data less accurately, the parameters showed still considerable variations albeit smaller. For complex II assays, commonly an artificial electron acceptor is used which becomes reduced by ubiquinol for making detectable the reaction. This additional component makes difficult the acquisition of time course data resulting from the complex II activity. Eventually for complex IV one would encounter the problem that the oxygen concentration could not be measured or set constant in the given experimental setup.

2.8.2. Fitting rate equations featuring saturation kinetics

Despite of the intricate functioning of the respiratory chain complexes, principally with all of the simplified or generalized Michaelis-Menten like rate equations the experimental kinetic data were described satisfactory. These equations exhibit maximal forward and backward velocity and a K_m for each substrate and product. For complex I the *original, non simplified Michaelis-Menten like rate equations* did not improve the results. Here parameters were underdetermined. With a greater set of experimental data one might resolve this problem. However our object is to have a relatively simple, good and robust description of the kinetics. In contrary, using the simpler *extended mass action equation*, the data description becomes inaccurate. We have derived the EMA rate equation to lower the number of parameters but still describing saturation kinetics.

Like the Michaelis-Menten like rate laws, this equation features maximal forward and reverse rate, but summarizes the K_m of all substrates in one global constant C_S, the same for the products, C_P. This explains why the equation shows acceptable results when the affinities of the substrates are in the same order and likewise for the products, and why the accuracies decrease with increasing number of substrates and products. Yet the extended mass action equation is in any case a good compromise with respect to mass action or near equilibrium thermodynamics.

The *simplified and generic Michaelis-Menten* like rate equations are thus a good choice, even if not all experimental series were well described. This can partially be due to the fact that for each respiratory complex all experimental series have been fitted simultaneously (except for complex II). Hence if for any individual series there was a small deviation in enzyme or substrate concentration, this series would be less well described. But a more important aspect is supposedly that the mechanisms of the respiratory chain complexes do not correspond to the classical steady state mechanisms. Hence with the Michaelis-Menten like rate equations they can at most be approximated. This may also be the reason why in general we did not observe significant differences in the simulation of the experimental data using the different rate equations. Amongst the similar accuracies, one could not point out the most suitable equation type.

2.8.3. Comparing the results of the simplified Michaelis Menten like rate equations

Despite the similar accuracies among the simplified Michaelis-Menten like equations one have to chose with caution. It is remarkable, that the determined product K_ms varied largely among the rate equations, and herein is a great advantage of having performed our own experiments, because this permitted us to determine these values properly for each equation. Employing literature K_i values is in this regard critical.

Especially for the *simplified ordered mechanism*(sOM) the product K_m values vary largely depending on the binding sequence and some of them are very probably not appropriate for data description because they seem much too high. Knowing that with respect to the reverse reaction these constants denote the concentration where the backward rate is at half of its maximal activity, the assumption of ordered mechanism is very delicate in particular for the reversible complexes I and II as well as the ATP-synthase. Generally one can assert that if kinetic data are only available on the forward reaction but the reaction is principally reversible, ordered mechanism should be employed for fitting these data only if the binding and release sequences of the substrates and products are known. In contrary to this, for *convenience kinetics* (CK) the product K_m values are assumably too small: for both complex I and complex II the values of K_{QH_2} are well below K_Q, which would mean that the products have a much higher affinity as the substrates. In case of complex IV the same can be observed, here $K_{cox} << K_{red}$.
Data on both, forward and reverse reaction can help point out the reaction mechanism or in case of convenience kinetics help to avoid an underestimation of the product K_m

values.

The *simplified ping-pong mechanism* (sPPM) showed reasonable product K_m values for complex I, II, and III. Further, with the stochastic model of Ransac et al. [2010] we could show that due to the internal 'electron buffer' the NADH and Q binding to complex I are to a large extent independent of each other, thus a formation of a ternary complex, i.e. both substrates are bound simultaneously on the enzyme, is not necessary for the catalysis. sPPM does not include a ternary complex and may thus well approach the real steady state kinetics of complex I, however it still has a fixed binding order which makes it different.
One can also expect that the situation for complex II is similar, since also here there are several redox centers between the binding sites of succinate and quinone, albeit their number is lower. Complex III functions completely different and can be described well by sPPM but only if Q binding on the Q_i site is neglected. This however violates thermodynamic constraints. Complex IV was best described with first order for cytochrome c and thus fits not in the scheme of sPPM.

Applicable throughout, and with reasonable product K_m-values, is the *simplified random binding mechanism* (sRB) and its generalized form. The latter also takes into account other than 2-substrate-2 product reactions. Thereby this equation type is a good choice for modeling the respiratory chain complexes. Since it describes well very different types of mechanisms we suppose that it is also well suitable for the ATPsynthase. For this OXPHOS complex however we did not perform experiments to confirm this, our focus was at first on the respiratory chain complexes.
Compared to CK which is also based on random binding, the RBs equation does not exclude simultaneous binding of a substrate on one binding site with a product on the other binding site, which may explain the more realistic K_m values obtained for RBs. At least for complex I and II one can assume independence for the substrate and product binding at the different binding sites and thereby one may explain the better performance of RBs.

2.8.4. Comparison of the kinetic parameters along the respiratory chain and their relation to the quinone pool and cytochrome c pool

The results of fitting RBs to the experimental data of all respiratory chain complexes are summarized in table 2.13.

The electron entry at complex I and II

Compared to NADH, NAD_+ has a weak affinity for its binding site on complex I, since $K_{NADH} << K_{NAD}$ and hence the concentration of NAD^+ affects the activity of this enzyme much less than does the reduced form. With the stochastic model of Ransac et al. [2010] we could show that under most conditions the oxidation of NADH is not

Table 2.13.: Comparison of the kinetic parameters along the respiratory chain. The parameters listed below were all obtained by the simplified random binding equation or its generalized form. This equation type shows throughout the respiratory chain complexes reasonable parameter values. Additionally the specific activities of the complexes are listed, for comparison they are expressed in nmol e^-/min/mg. For complex III, two possibilities are given: (a) refers to the reaction order first order for cytochrome c and quinone at the Q_o site and 1/2-order for quinone at the Q_i-site, whereas in (b) the net reaction with second order for cytochrome c and first order for quinones is given. The value for K_{fum} was set equal to K_{suc} because it could not be determined with the given experimental method. The K_m in bold are those of the substrates.

Complex	$\mathbf{k^+_{cat}}$ nmol/min/mg	$\mathbf{K_{NADH}}$ [μM]	$\mathbf{K_{NAD}}$ [μM]	$\mathbf{K_{suc}}$ [μM]	$\mathbf{K_{fum}}$ [μM]	$\mathbf{K_{QH_2}}$ [μM]	$\mathbf{K_Q}$ [μM]	$\mathbf{K_{c_{red}}}$ [μM]	$\mathbf{K_{c_{ox}}}$ [μM]
I	3582	**4.3**	780			5.3	**9.7**		
II	1704			**18796**	(18796)	1.8	**2.5**		
III(a)	11452					**188** (o) 6.7 (i)	267 (o) **0.011** (i)	352	**21.8**
III(b)	8090					**138**	323	312	**7.7**
IV	13783							**65.0**	56.3

rate limiting for complex I. The regulation of its activity should thus emanate via the availability of quinone.
For complex II K_{suc} is much higher the values found in literature. An explanation for could not be found, although the experimental protocol seems to be correct, some changes might be tried out. It was not possible to determine K_{fum} with the given experimental setup and the constant was set equal to K_{suc}. An interpretation of these values is thus not possible at this point.

The Q-pool, the interface between the complexes I, II and III

It is worth considering that the size and the reduction state of the quinone pool may have a regulative effect on the respiratory chain or vice versa: Complex I and complex II experience a strong inhibition by their product QH_2 since for both we have $K_{QH_2} \approx K_Q$. This could ensure that even in case of high concentrations of NADH and succinate, Q is always available for complex III besides QH_2. This is an important aspect since due to the Q-cycle mechanism both, reduced and oxidized quinones, act as substrates and products for complex III.

For complex I, an inhibition by the substrate Q has been observed at higher concentrations. A plausible explanation for this is an obstruction of the access path to the quinone binding site of complex I by both, Q and QH_2. For the simplified random binding equations as well as in the stochastic model, the consideration of such an inhibition lead to more accurate results. It is however questionable whether this inhibition could be important enough to contribute to the regulation of the Q-pool or of the complexes activities, amongst other because of the use of decylubiquinone instead of the physiolog-

ical coenzyme Q.

Complex III features two Q binding sites and hence the possible regulative role of complex III is more intricate: On one hand for the QH_2 oxidizing Q_o-site K_Q is in the range of K_{QH_2}, hence Q being well competitive with QH_2. On the other hand Q has a very high affinity to the Q_i site, while here its respective product QH_2 is less competitive. This suggests that the reduction of Q at the Q_i site has only very little influence on the kinetics of complex III. This idea is supported by the fact that with PPMs one can well describe the complex III kinetics when neglecting the Q_i site.
The K_Q and K_{QH_2} of the Q_o site of complex III are both a magnitude higher that that of complex I, suggesting that when complex I is just saturated with quinones complex III might still be sensitive to changes of the Q and QH_2 concentrations.
For complex III the data are slightly better described when employing an inhibition term with QH_2 or Q_{tot} as inhibitor. But in reality an inhibition is questionable, and the small improvement may be simply due to the employment of an additional parameter, resulting in a better description of the kinetic behavior produced by the Q-cycle mechanism. The latter is indeed not reflected in the structure of the Michaelis-Menten like equations, this could also be the reason for the elevated values of k_{kat}^{-}, imposed by the haldane relationship 2.15.

The interplay of the Q-pool and the respiratory chain deserves further analysis. It should also be considered that the lipophilic physiological CoQ may behave differently to the amphiphilic decylubiquinone that has been employed in the experiments, with respect to a possible inhibition but also in regard to the Q and QH_2 affinities to their binding sites.
Here one can suspect that K_Q and K_{QH_2} have been estimated somewhat too low for complex I, because the Q-binding site is in an hydrophobic environment, and for complexes II and III somewhat too high because the binding sites are situated well in the membrane. It should be pointed out, that K_Q and K_{QH_2} are apparent values because they are referred to the total reaction volume, but the effective concentrations are the amount of ubuquinones and ubuquinoles accumulated in the membrane volume.
With respect to some mitochondrial diseases where the size of the Q pool is too low for an efficient electron transfer, the oral intake of CoQ is an approach for treatment. A model that can take into account different binding affinities of different quinols could help determining the optimal type of quinone for an efficient electron transport or help finding a good compromise between efficiency in electron transport and with regard to the ability of an external quinone to reach the inner mitochondrial membrane.

The connection of the complexes III and IV via cytochrome c and the reduction of oxygen

The affinity of oxidized cytochrome c to its binding site on complex III is much higher than that of its reduced form, thus product inhibition should play only a minor role. On the contrary, for complex IV we found that $K_{cox} \approx K_{cred}$ so that here oxidized and

reduced cytochrome c are very competitive, the reduction state of the cytochrome c pool should thus significantly influence the complex IV activity.
The K_m of oxygen with respect to this complex was not determined because its concentration could not be varied with the given experimental setup nor measured spectrometrically. The constant was set to $1\mu M$ according to literature data and therefor the enzyme was highly saturated with an oxygen concentration at around 200 μM. No conclusions on this parameter are possible upon our experiments.

The K_m values allow for a first insight in the interplay of the respiratory complexes via the quinone and cytochrome c pools. Indeed, in rat heart tissue, the Q-pool is reduced only to a small extent while the cytochrome c pool is reduced to about two third, but the relations can be quite different for other tissues, as was demonstrated by Benard et al. [2006], see also figure 2.22 and probably also with respect to other species. The author mentioned also the possibility of the existence of more than one Q-pool. The formation of supercomplexes may entail local Q-pools.

The specific activities and their influence on the reduction states of the respiratory chain intermediates

Another important aspect of the interplay of the respiratory chain complexes and the Q-pool(s) and the cytochrome c pool are certainly the specific activities, which are listed in table 2.13. The relation between these maximal rates shows a considerable increase along the respiratory chain with $C_I + C_{II} : C_{III} : C_{IV} \approx 0.65 : 1 : 1.7$. Here the complex III activity for the net reaction with second order for cytochrome c and first order for quinone has been employed and the rates are normalized to this value. It is more suitable for comparison because the maximal rate for the detailed reaction compensates for Q and QH_2 being substrates and products at the same time and thus it can never be achieved in reality.

It is remarkable that even though complex IV has largely the highest activity, the cytochrome c pool is reported to be more than half reduced [Benard et al., 2006], this may be partially due to the high product inhibition exerted by oxidized cytochrome c, however this should reduce its rate not more than half. Thus complex III would have to work close to its maximal turnover in order to maintain the reduction state of the cytochrome c pool at steady state. Yet this cannot be the case because the Q-pool is oxidized to a large extent and Q was found to compete strongly with QH_2 for the Q_o-site, slowing down the complex III activity. On the other side, saturation with Q and the very weak presence of QH_2 is optimal for the activity of complexes I and II, and if one accorded generously to complex III that its rate was reduced only to that that of complex I + II, at least the reduction state of the Q-pool could be explained.
A possible explanation for these contradictory observations is that the activities of the respiratory chain complexes are influenced by the membrane gradient, and to a different degree, at least complex II is not coupled to the membrane gradient while the other complexes are. The activities could thereby be shifted such that they become compat-

Figure 2.22.: Physiological diversity of oxidative phosphorylation. In their homonymous publication, Benard et al. [2006] investigated the diversity of the OXPHOS system CII + CIII + CIV and illustrated their results in the figure shown below (the figure was slightly modified for better readability). The size of the gray rectangles present the amounts of the respiratory chain complexes, the color intensity is proportional to their specific activity. The surface of the blue rectangles show the abundance of quinone (CoQ) and cytochrome c (cyt c), the reduced fraction is encoded in dark blue. The amount of mitochondria (represented by the citrate synthesis activity) is illustrated by the yellow rectangles. All amounts are referred to the tissues' weight.

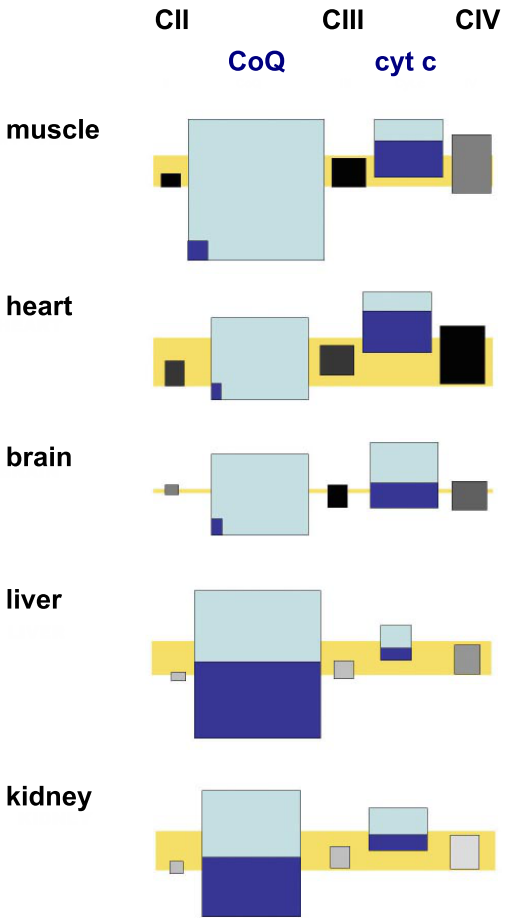

ible with the reduction states of the Q and cytochrome c pool. Also a proton gradient induced change in Michaelis-Menten constants could contribute.

As mentioned before, the existence of two or more Q-pools is discussed [Benard et al., 2006], the effective Q-pool for OXPHOS may thus be reduced to a higher extent. Another aspect is the formation of supercomplexes, especially I + III_2 may considerably contribute to the catalytic performance: The quinones could be channeled between these complexes or at least the path of diffusion could be shortened and besides a delimited small Q-pool might reduce the competition for the binding sites such that the interplay between these complexes would be optimized. Further it is known that complex I is stabilized by complex III, which may increase its activity. It should also be remarked that the Q pool and cytochrome c reduction states were discussed upon rat heat mitochondria, the situation in beef heart mitochondria could thus be different. The solution is certainly not not given by one of these issues alone, rather it is probable that several aspects together may explain the discrepancies.

2.8.5. The influence of ethanol on complex I activity

A completely different aspect in this chapter is the experiment which revealed the inhibitive influence of ethanol on complex I activity: At 2% ethanol concentration, the activity of complex I is decreased to half of its maximum. This is interesting with respect to *Saccharomyces cerevisiae* which does not contain complex I but alternative NADH dehydrogenases, which also reduce quinone but without being coupled to proton pumping. Knowing that this yeast produces ethanol via fermetation, the question arises whether the loss of complex I during evolution might be an adaptation to bear higher alcohol concentrations and having thus an advantage in competition with other organisms. However, in absence of ethanol the absence of complex I is probably a disadvantage since the ATP yield via oxidative phosphorylation is lower.

2.9. Summary

Initial rate measurements have been performed on the respiratory complexes. A method to estimate the inhibitory effect of QH_2 on the complex II activity was established. We could show with a stochastic model that complex I does not follow a classical enzyme mechanism, its chain of redox centers seems to function as an electron buffer and allows the oxidation of NADH and the reduction of Q to appear independently of each other.
Although the respiratory complexes have very different and complex catalytic mechanisms, we could show that their kinetics can be well approached by Michaelis-Menten like rate equations. It is hence probable that the kinetics of the ATP synthase can also be represented well by these kind of rate equations. In particular the simplified and generalized random binding mechanism was well suited, the fits of this simple and flexible rate law delivered reasonable parameter values for all respiratory complexes.
These parameter values give an intuitive insight in a possible regulation of respiratory enzyme activity. However the size and reduction state of the quinone and cytochrome

c pool are necessary to analyze further the entire system. A crucial point is also the influence of the electrochemical gradient on the OXPHOS complexes activities, which is treated in the next chapter.

3. Introduction of the electrochemical gradient into the rate equations

3.1. Introduction

Under physiological conditions, the respiratory chain establishes an electrochemical proton gradient over the inner mitochondrial membrane: the complexes I, III and IV translocate protons from the mitochondrial matrix into the inner membrane space using the energy released from redox reactions. Depending on the physiological conditions the gradient changes its magnitude which influences the proton pumping and thereby the respiratory complexes activities which act reciprocally on the gradient. Moreover also the activity of the F_1F_o-ATPsynthase is governed strongly by the proton gradient. This makes it necessary to integrate the gradient as a state variable into the rate equations. However, as we show in the following, the means to integrate the gradient is not obvious: the approximation of a linear flux force relationship, as has been done e.g. in the model of Korzeniewski [2001], is only valid for near equilibrium conditions and already physiological changes in ΔpH and $\Delta\Psi$ can exceed the valid area of linear thermodynamics.
In this chapter, we propose a flexible method to integrate the gradient which is consistent with thermodynamics. We first present the thermodynamic basics and then we discuss the way in which the proton gradient may influence the kinetics of the OXPHOS complexes, and further how this may affect the parameter values of the Michaelis-Menten like rate equations. A distribution among all parameters is then proposed as a simple approach; in particular a focus is put on the forward and backward rate constants which present mostly the enzyme internal, catalytic steps.

3.2. General thermodynamical considerations

3.2.1. Flux-force relationship

In general, the Gibbs energy that drives a reaction, ΔG_R, can be calculated from the equilibrium of the reaction, described by the equilibrium constant, and the concentrations of substrates and products.
We consider the general reversible reaction

$$\sum_{i=1}^{m} \nu_i S_i \rightleftharpoons \sum_{j=1}^{n} \eta_j P_j \tag{3.1}$$

where ν_i and η_j are the stoichiometric constants of the substrate S_i and product P_j,

respectively. The parameter Γ is defined as the ratio of the substrates and products concentrations:

$$\Gamma = \frac{\prod_{j=1}^{n} [P_j]^{\eta_j}}{\prod_{i=1}^{m} [S_i]^{\nu_i}} \tag{3.2}$$

and the standard Gibbs energy is linked to the equilibrium of the reaction with

$$\Delta G_0 = -RT \ln K_{eq} = -RT \ln \Gamma_{eq} \tag{3.3}$$

with R = 8.314 J/(mol K) the universal gas constant and T the temperature in K.
Now we can express ΔG_R as follows:

$$\Delta G_R = \Delta G_0 + RT \cdot \ln \Gamma \tag{3.4}$$

We consider also the reactions catalyzed by all OXPHOS complexes as reversible. Here we have a particular situation since they are coupled to proton translocation and these additional processes are shifting the equilibria of the reactions. We denote the energy that is due to proton translocation from the matrix into the inner membrane space with ΔG_H and extend equation 3.4

$$\Delta G_R = \Delta G_0 + \Delta G_H + RT \cdot \ln \Gamma. \tag{3.5}$$

Equation 3.5 allows us to define the new equilibrium of the reaction being now dependent on $\Delta G_0 + \Delta G_H$:

$$K_{eq} = (\Gamma)_{eq} = \exp\left(-\frac{\Delta G_0 + \Delta G_H}{RT}\right) \tag{3.6}$$

The net reaction flux v is defined as the difference of the forward flux and the backward flux, $v = v^+ - v^-$. Note that when ΔG_R is negative, the net reaction is driven in forward direction, and if it is positive the net reaction takes place in backward direction. At equilibrium where $\Delta G_R = 0$ there is no net reaction, i.e. forward and backward fluxes are equal.
The Ussing-equation relates the forward and backward fluxes thermodynamically to the driving force ΔG_R:

$$\frac{v^+}{v^-} = \exp\left(-\frac{\Delta G_R}{RT}\right) = \exp\left(-\frac{\Delta G_0 + \Delta G_H}{RT}\right) \cdot \Gamma^{-1} \tag{3.7}$$

However it is not possible to conclude anything from ΔG_R about the steady state kinetics of an enzyme. Indeed, for the OXPHOS complexes we have an idea of the kinetics in absence of the electrochemical gradient, but this equation points out the difficulty of integrating the latter into kinetic rate equations:

- The relationship v^+/v^- describes only the relative changes of the forward and

backward velocities with respect to ΔG_R and thus with respect to the gradient. It contains no information about the absolute values of the net velocity and thus no information about how the gradient and the translocated protons will be reflected in the kinetics.

- Furthermore, the gradient is composed of an electrical and a chemical part which supposedly influence the enzyme kinetics in a different way.

We combine now the very general relationship 3.7 with the Michaelis-Menten-like rate equations that we have presented in chapter 2.1 via the Haldane equation 2.15. The latter links the kinetic parameters of these equations with the equilibrium constant, at least in absence of the gradient. In presence of an electrochemical potential difference we have thus for the general reaction 3.1

$$K_{eq} = \underbrace{\frac{V^+_{max}}{V^-_{max}} \cdot \frac{\prod_{j=1}^{n} K_{P_j}^{\eta_j}}{\prod_{i=1}^{m} K_{S_i}^{\nu_i}}}_{\mathrm{K_{eq}\ at\ \Delta G_H=0}} \cdot \exp\left(-\frac{\Delta G_H}{RT}\right) \tag{3.8}$$

Using further relationship 3.3 which establishes the relation between the equilibrium constant K_{eq} and the standard Gibbs energy ΔG_0, we can express the Ussing relationship 3.7 as follows:

$$\frac{v^+}{v^-} = \underbrace{\frac{V^+_{max}}{V^-_{max}} \frac{\prod_{j=1}^{n} K_P^{\eta_j}}{\prod_{i=1}^{m} K_S^{\nu_i}} \cdot \Gamma^{-1} \cdot}_{\text{kinetics at } \Delta G_H = 0} \underbrace{\exp\left(-\frac{\Delta G_H}{RT}\right)}_{\text{contribution of the } H^+ \text{ gradient}} \tag{3.9}$$

Below we will discuss whether and which kinetic parameters might be affected by the electrochemical gradient.

3.3. The electrochemical gradient

In this section we consider in which respect the translocation of protons against or along the electrochemical gradient may influence the kinetics of the OXPHOS complexes. The electrical and chemical potential difference have a different nature and may thus differently influence the enzymes' behavior. Additionally, we also include in this consideration the scalar protons, i.e. protons that are involved directly as substrate or product in the redox reactions.

For the impact of the proton gradient on the kinetic parameters two main cases can be discussed:

Case 1: The kinetic parameters are not influenced by the electrochemical gradient. The proton pumping is seen as an external process which is coupled to the redox reaction. It can slow down or accelerate the reaction, but never beyond the maximal enzyme rate. In other words: the gradient is seen as an external force which does not influence the internal qualities of the enzyme.

Case 2: The kinetic properties of the enzyme are influenced by the electrochemical gradient. The proton pumping is seen as an internal process. Any of the kinetic parameter values determined in absence of the gradient could then be affected by the gradient.

In this work we focus on case 2, i.e. we assume that the proton pumping is an internal process of the enzyme and tightly coupled. We assume further that the reactions catalyzed by the OXPHOS complexes are all reversible, which is facilitating the introduction of the proton gradient into the rate equations.
Indeed complex IV is supposedly irreversible, a reversal would mean that water would be split into hydrogen and oxygen, a highly endergonic reaction. From a thermodynamic point of view within the physiological OXPHOS system the electrochemical gradient cannot achieve values such that the ΔG_R of the reaction could attain positive values. However not being able to achieve such high values it is not in contradiction with a theoretical reversibility for complex IV.

We suppose that under the influence of the proton gradient the reactions catalyzed by the OXPHOS complexes can be still be represented by Michaelis-Menten like rate equations such that we can write:

$$\begin{aligned} K_{eq} &= \frac{V^+_{max}(\Delta G_H)}{V^-_{max}(\Delta G_H)} \frac{\prod_{j=1}^{n} K^{\eta_j}_{P,j}(\Delta G_H)}{\prod_{i=1}^{m} K^{\nu_i}_{S,i}(\Delta G_H)} = \exp\left(\frac{\Delta G_0}{RT}\right) \cdot \exp\left(\frac{\Delta G_H}{RT}\right) \\ &= \frac{V^+_{max}(0)}{V^-_{max}(0)} \cdot \frac{\prod_{j=1}^{n} K^{\eta_j}_{P_j}(0)}{\prod_{i=1}^{m} K^{\nu_i}_{S_i}(0)} \cdot \exp\left(\frac{\Delta G_H}{RT}\right) \end{aligned} \tag{3.10}$$

Therefrom the question arises how the term $\exp(\Delta G_H/RT)$ is distributed among the kinetic parameters.

3.3.1. The electrical gradient

The electric potential difference should have a strong impact on the catalytic steps that are linked to the translocation of charges, i.e. the transfer of electrons or the pumping of protons. This can be attributed to the enzyme internal steps, while the binding and release of substrates and products should only be slightly influenced by the electrical

gradient.
In a first approximation we could hence propose to split the $\Delta\Psi$ between the forward and backward rate constant. However it should also be considered that the K_ms are a combination of several rate constants, among them also the catalytic steps [Segel, 1993a], which represent internal transfers of electrons and protons. Thus these constants may also be affected by the eletric potential difference.

3.3.2. The chemical gradient

The chemical part of the membrane gradient ΔpH may have a very different impact compared to its electrical counterpart: The proton translocation should not be, or only slightly, influenced by the chemical gradient under the presumption that there is no 'proton concentration' and thus chemical gradient inside the enzyme. At least, there cannot be an open channel with a homogeneous gradient. If such existed, there would be no way to create or maintain a ΔpH between the matrix and the intermembrane space, because any difference would be rapidly equilibrated by this open connection since the transfer of H^+ not limited by diffusion, but transferred by very rapidly changing water bonds. Therefore, the binding or dissociation of the protons on both sides of the membrane should be the crucial step with respect to the chemical gradient.
Consequently, these vectorial protons should be included into the equation like any other substrates and products, normalized to their own dissociation constant(s). However, the determination of such constants would be extremely difficult or impossible with the classical approaches for enzyme kinetics: it would require for instance measurements of the complex I activity with different pH values on both sides of the membrane and at the same time as constant $\Delta\Psi$.

Another aspect is that in general enzyme activity is influenced by the pH, whether protons intervene in the catalyzed reaction or not. This is manifested in an enzyme's pH optimum and range. Moreover for the special case of the proton translocating OXPHOS complexes, the optimum is even a function of two pH values: the matrix pH (pH_x) and the intermembrane space pH (pH_{is}). Alberty [2008] analyzed the influence of the pH on 2 product-2 substrate reactions and thereby provided complex equations but they are too detailed with respect to our modeling aim and do not take into account the two different pH values.

It is evident that these circumstances entail simplifications in the modeling of the OXPHOS complexes. We thus make the following simplifications: we neither take into account the indirect dependence of their activities on (pH_x) and (pH_{is}), nor do we integrate into the rate equations Michaelis-Menten constants for both, H_x^+ and H_{is}^+. However we consider the thermodynamical contribution of the ΔpH.
The model may later be extended in order to correct for these simplifications. For example one could approximate the general pH dependency by a function describing the particular case where the enzymes' activities are dependent on $pH_x = pH_{is}$. This situation is experimentally easy to realize by working on fragmented mitochondrial membrane

particles, which means in absence of a membrane gradient.

3.3.3. Scalar protons

For reasons of simplicity, we have not yet discussed the scalar protons i.e. protons that are directly implied in the redox reactions. In our experiments the pH was fixed to 7.5. Being constant, the concentration of scalar protons was integrated into the standard Gibbs free energies of the reactions, ΔG_0 (pH 7.5), which served in chapter 2 for the determination of the parameter k^-_{catf} via the Haldane relationship 2.15. They now have to be 'extracted'.

For the general *chemical* reaction $S + j\,H^+ = P + k\,H^+$, that takes place in one compartment, we have

$$\Delta G_0(pH_{ref}) \rightarrow \Delta G_0(pH_{ref}) + j \cdot RT \ln(H_{ref}) - k \cdot RT \ln(H_{ref}) \tag{3.11}$$

Here $\Delta G_0(pH_{ref})$ is the Gibbs standard energy of reaction at the given reference proton concentration H_{ref}.

For simplicity and not being able to determine Michaelis-Menten constants for the scalar protons, we will include their concentrations into the energetic expression.

3.3.4. Energetic terms of the complexes

The Gibbs energy that is required to translocate one proton against the electrochemical potential difference from the mitochondrial matrix into the inter membrane space consists of an electrical and a chemical part:

$$\Delta\tilde{\mu}_H = \underbrace{F\Delta\Psi}_{\text{el. grad.}} + \underbrace{RT \ln\left(\frac{[H^+]_x}{[H^+]_{is}}\right)}_{\text{chem. grad.}} \tag{3.12}$$

where the indexes 'x' and 'is' denote the matrix and the intermembrane space, respectively. F = 96485 C/mol is the Faraday constant, R = 8.314 J/(mol K) the universal gas constant and T the temperature in K. The electric potential difference over the inner membrane is defined as $\Delta\Psi = \Psi_x - \Psi_{is}$ and is negative under physiological conditions.

In the following, we present the energetic term ΔG_H for each of the OHPHOS complexes, except for complex II. The latter is not subject of proton translocation and no scalar protons intervenes in the redox reaction it catalyzes.

Complex I: Due to the oxidation of one molecule NADH 5 protons are taken from the matrix space per turnover, of which 4 protons are pumped into the intermembrane

space:

$$NADH + Q + 5\,H_x^+ \rightleftharpoons NAD^+ + QH_2 + 4\,H_{is}^+ \tag{3.13}$$

The Gibbs energy for the proton translocation and the scalar proton is

$$\Delta G_H^{C1} = -RT \ln\left(\frac{[H^+]_x}{H_{ref}}\right) - 4 \cdot \Delta\tilde{\mu}_H \tag{3.14}$$

Complex III: Per completion of the Q-cycle four protons are released into the intermembrane space and two protons are taken up from the matrix, while two electrons are transfered against the electric gradient from the Q_o-site to the Q_i-site. This corresponds net to a transfer of two protons from the matrix into the intermembrane space and two scalar protons as products:

$$QH_2 + 2\,cytc_{ox} + 2\,H_x^+ \rightleftharpoons Q + 2\,cytc_{red} + 4\,H{+}_{is} \tag{3.15}$$

We obtain thereby the following energetic term for the proton translocation

$$\Delta G_H^{C3} = -2 \cdot RT \ln\left(\frac{H_{ref}}{[H^+]_{is}}\right) - 2 \cdot \Delta\tilde{\mu}_H \tag{3.16}$$

Complex IV: For the oxidation of one molecule cytochrome c one electron is driven against the electric gradient which serves together with a proton coming from the matrix to reduces $\frac{1}{4}O_2$. Additionally, one proton is pumped from the matrix into the intermembrane space.

$$cytc_{red} + \frac{1}{4}\,O_2 + 2H_x^+ \rightleftharpoons cytc_{ox} + 1\,H_{is}^+ + \frac{1}{2}\,H_2O$$

A complete turnover of the reaction catalyzed by complex IV involves 4 cytochrome c which reduce one molecule of oxygen. Usually the reaction is referred to the transfer of two electrons which corresponds to 2 cytochrome c. But since the kinetics of complex IV is best described with cytochrome c in first order we refer it to only one electron, and the energy that this 'quater' reaction releases for proton pumping is

$$\Delta G_H^{C4} = -1 \cdot RT \ln\left(\frac{[H^+]_x}{H_{ref}}\right) - 1 \cdot F \cdot \Delta\Psi - 1 \cdot \Delta\tilde{\mu}_H. \tag{3.17}$$

Note that the negative sign in this expression is due to $\Delta\Psi$ being negative, the more depolarized is the membrane the higher is ΔG_H.

F1Fo-ATP-synthase: The phosphorylation of 1 molecule of ADP, is driven by n_A protons following the electrochemical gradient from the intermembrane space into the

matrix:

$$ADP^{3-} + P_i^{2-} + n_A\, H_{is}^{+} + H_x^{+} = ATP^{4-} + H_2O + (n_A - 1)\, H_x^{+}$$

The stoichiometric ratios between the c and β subunits of the ATPsynthase can vary among the mechanism and suggest for yeast $n_A = 10/3$ [Stock et al., 1999] and for bovine heart $n_A = 8/3$ [Watt et al., 2010]. However deviations from these structural constraints were found in experiments, suggesting that one can not deduce from the stoichiometric ratios the exact number of the proton/ATP ratio [Petersen et al., 2012]. The energetic term for the proton translocation via the ATPsynthase is

$$\Delta G_H^{F1} = -RT \ln\left(\frac{[H^+]_x}{H_{ref}}\right) + n_A \cdot \Delta\tilde{\mu}_H. \tag{3.18}$$

3.4. Introduction of the electrochemical gradient into Michaelis-Menten-like equations

In this section we propose a way to introduce the electrochemical gradient into the Michealis-Menten like rate equations. We analyze different repartitions among the kinetic parameters. For all simulations that are done in this section, the (modified) simplified random binding rate equation have been employed. For complex III, the reaction based on the net reaction scheme for cytochrome c in second order has been used. The kinetic parameters $\mathrm{V_{max}}$ and $\mathrm{K_m}$ (at $\Delta\mu_H = 0$) are given in table 2.13. The simulations have been performed using Scilab 5.3.0 [Scilab Enterprises, 2012].

3.4.1. A simple approach to model the influence of the proton gradient on the kinetic parameters

In section 3.3 we decided to integrate the gradient into the rate equations, assuming that the kinetic parameters are directly affected by the gradient. Basically all of them, the V_{max} and the K_m, can be concerned, in a different extent. Equation 3.10 shows how the equilibrium constant is related to the kinetic parameters and to the energetic term describing the proton translocation $\Delta\mathrm{G_H}$. According to this equation we propose to split the term $\exp(\Delta G_H/RT)$ in the following way:

$$X(\Delta G_H) = X^0 \cdot e^{-\beta_X \cdot \frac{(\Delta G_H)}{RT}} \tag{3.19}$$

where X^0 is the parameter in absence of the gradient and β_X defines the fraction of ΔG_H effecting X^0.

We define now as couples of parameters: the couple of maximal rates (V_{max}^{+} & V_{max}^{-}) and the couples of Michaelis-Menten constants of the oxidized and reduced form of a

component (K_{NADH} & K_{NAD}, K_Q & K_{QH_2}, $K_{cytc_{ox}}$ & $K_{cytc_{red}}$) and, in case of the ATP-synthase, the Michaelis-Menten constants of the twofold and threefold phosphorylated adenosine (K_{ADP} & K_{ATP}), respectively.
There are exceptions for the following components: In the rate equation for complex IV, the redox partner of O_2 does not appear since it is H_20. In the rate equation for the ATPsynthase P_i is an additional partner of ATP, however K_{ATP} is already assigned to K_{ADP}. For simplicity, we assume at first that these two 'non couple' parameters are not influenced by the electrochemical gradient. If necessary, this simplification will be annihilated.
We introduce the parameters ζ_j in order to distribute ΔG_H among the n parameter couples of a given equation:

$$\Delta G_H = \sum_{j=1}^{n} \zeta_j \cdot \Delta G_H \tag{3.20}$$

And hence

$$\sum_{j=1}^{n} \zeta_j = 1. \tag{3.21}$$

The impact of the gradient on a redox couple is then split between the two partners by the constant $\gamma_i \, \epsilon \, [0, 1]$. They are implemented such that $\gamma_j = 1$ (0) means that the gradient is playing exclusively on the forward (backward) velocity constant or on the Michaelis-Menten constants of the substrates (products), respectively.
For the velocity constants, we have thereby

$$V^+_{max} = V^+_{max}(0) \cdot \exp\left(\gamma_V \cdot \left(-\zeta_V \cdot \frac{\Delta G_H}{RT}\right)\right) \tag{3.22}$$

$$V^-_{max} = V^-_{max}(0) \cdot \exp\left((\gamma_V - 1) \cdot \left(-\zeta_V \cdot \frac{\Delta G_H}{RT}\right)\right) \tag{3.23}$$

We use the fact that in the generic rate equations all concentrations are normalized by their K_M -values and define

$$s_j(\Delta G_H) = \frac{[S_j]}{K_{S_j}(\Delta G_H)} = [S_j] \cdot \frac{\exp\left(\frac{\gamma_j}{\nu_j} \cdot \left(-\zeta_j \cdot \frac{\Delta G_H}{RT}\right)\right)}{K^0_{S_j}}; \tag{3.24}$$

$$p_j(\Delta G_H) = \frac{[P_j]}{K_{P_j}(\Delta G_H)} = [P_j] \cdot \frac{\exp\left(\left(\frac{\gamma_j - 1}{\nu_j}\right) \cdot \left(-\zeta_i \cdot \frac{\Delta G_H}{RT}\right)\right)}{K^0_{P_j}} \tag{3.25}$$

The indexes for the substrates and products are now both 'j' which expresses that they occur in couple where the partners of each couple have the same stoichiometric factor ν_j. We define further

$$a = \frac{[A]}{K_A} \text{ and } b = \frac{[B]}{K_B}$$

for a substrate A and a product B which have no partner or where the partner is not occurring within the rate equation. As mentioned before, K_A and K_B may be rendered sensitive to the gradient if necessary.
The general rate equation is now dependent on the electrochemical proton gradient. On the example of the simplified and generalized random binding equation 2.12 it reads

$$v = \frac{V^+_{max}(\Delta G_H) \cdot a^{\nu_a} \cdot \prod_{j=1}^{n} s_j^{\nu_j}(\Delta G_H) - V^-_{max}(\Delta G_H) \cdot b^{\nu_b} \cdot \prod_{j=1}^{n} p_j^{\nu_j}(\Delta G_H)}{\prod_{j=1}^{n} (1 + s_i(\Delta G_H) + p_j(\Delta G_H))^{\nu_j} \cdot (1+a) \cdot (1+b)} \tag{3.26}$$

This is the basic rate equation for the introduction of the gradient into the Michaelis-Menten like rate equations. It has the same structure as the generalized random binding equation and is equal for $\Delta \mathrm{G_H} = 0$.

3.4.2. Repartition of the proton gradient's influence among the kinetic parameters

We suppose that all ζ_j are positive respecting the constraint 3.21 and further that all $0 \leq \gamma \leq 1$.

Figure 3.1 shows that the impact of the electrochemical gradient on a Michaelis-Menten constant should be relatively small because otherwise the values of these constants can become extremely high (K_S) or low (K_P) with increasing $\Delta\tilde{\mu}_\mathrm{H}$. This implies that a large part of ΔG_H should weigh on V^+_{max} and V^-_{max} which is in line with our expectations: since one can roughly say that these parameters represent the catalytic steps and thereby the steps involved in proton and electron translocation, they should be in particular sensitive to the electrochemical gradient.
A general exclusion of an influence on the binding steps is still not reasonable because the binding and dissociation steps may involve a charge transfer in an electrical field. Moreover, the expressions for the $\mathrm{K_m}$ which are obtained by a formal derivation of this parameter based on a reaction scheme, see e.g. Segel [1993a], contain besides the corresponding binding rate constants also the catalytic rate constants. Since the latter are thought to be sensitive to $\Delta\tilde{\mu}_H$, the same must be true for the $\mathrm{K_m}$.

Equal influence of the proton gradient on the forward and backward rate constants

It has been proposed that the impact of an electrical gradient on a reaction step should be symmetrically distributed on its forward and backward direction [Reynolds et al., 1985, Läuger, 1984]:

$$k_j^+ = k_j^{+0} \cdot e^{0.5 \cdot \zeta_j \cdot \frac{F \Delta \Psi}{RT}} \tag{3.27}$$

$$k_j^- = k_j^{-0} \cdot e^{-0.5 \cdot \zeta_j \cdot \frac{F \Delta \Psi}{RT}} \tag{3.28}$$

Figure 3.1.: Influence of the electrochemical gradient on the Michaelis-Menten constants. For simplicity, we set $\Delta pH = 0$ and consequently we have $\Delta\tilde{\mu}_H = \Delta\Psi$.
a) Substrate K_m as a function of $\Delta\Psi$: $K_S = K_S^0 \cdot \exp((\beta \cdot \Delta G_H)/(RT))$
b) Product K_m as a function of $\Delta\Psi$: $K_P = K_P^0 \cdot \exp((-\beta \cdot \Delta G_H)/(RT))$
The figure shows that one can expect a low influence of the proton gradient on the Michaelis-Menten constants. Else their values would change extremely with $\Delta\Psi$. Note that depending on the proton stoichiometry of the reaction, the effect of $\Delta\Psi$ on a K_m can be more or less strong for the same repartition constant β, see also the ΔG_H values in section 3.3.4. For instance complex I pumps 4 protons per reduction of one molecule of NADH. If here $\beta = 0.05$, then $\beta \cdot \Delta G_H \approx 0.2 \cdot \Delta\tilde{\mu}_H$. But if for complex III or IV a given K_m shall experience approximately the same influence, β has to be set to 0.1, because these complexes are transferring only 2 charges per (net) oxidation of one QH_2 or one cytochrome c, respectively.

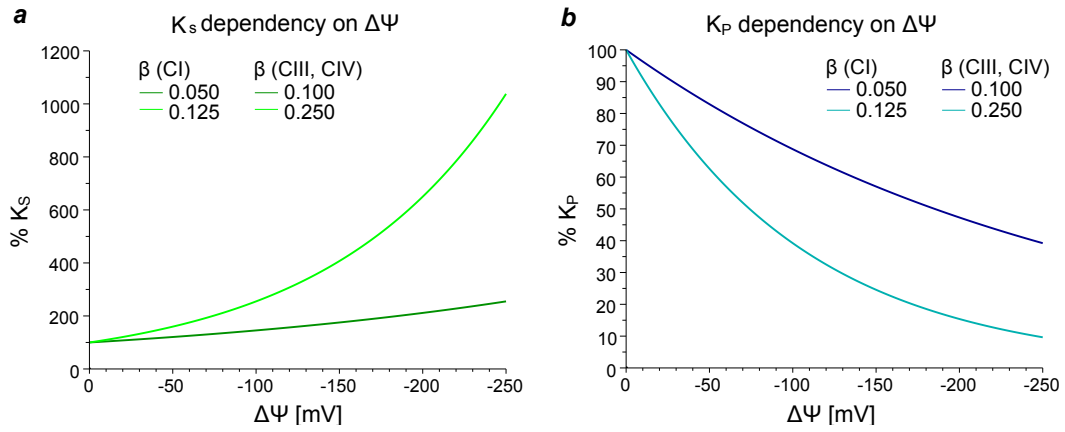

Where k_j^+ and k_j^- are the rate constants of the reaction step j with ζ_j determining the fraction of ΔG_H that is affecting the reaction step j. The index 0 denotes the absence of an electrochemical gradient.
Accordingly, since we reduce the ensemble of forward catalytic steps and the ensemble of backward catalytic steps into one step each, represented by V_{max}^+ and V_{max}^-, we can set $\gamma_V = 0.5$ in the first instance.

For the K_m the situation is different. One can roughly compare them to the dissociation constants K_D. The latter can be expressed as the release rate constant k_{off} of a component divided by its respective binding rate constant k_{on}. Under influence of a proton gradient one can thus write according to equations 3.27 and 3.28

$$K_m \approx K_D(\Delta G_H) = \frac{k_{off}^0 \cdot e^{0.5 \cdot \beta_K \cdot \frac{\Delta G_H}{RT}}}{k_{on}^0 \cdot e^{-0.5 \cdot \beta_K \cdot \frac{\Delta G_H}{RT}}} = K_D^0 \cdot e^{\beta_K \cdot \frac{\Delta G_H}{RT}} \tag{3.29}$$

where β_K designates the fraction of ΔG_H affecting a K_m. Above we have defined γ_i as the parameter that splits the gradient's impact between the partners of a K_m couple. However, we cannot estimate whether the gradient would more or less influence the binding and release of the reduced or oxidized (or two fold and three fold phosphorylated) component. Thus we set also here $\gamma_i = 0.5$. Note that this has not the same meaning as for γ_V.

As an example we analyze the case of complex I for the combination $\gamma_V = 0.5$ and $\gamma_i = 0.5$. Figure 3.2 illustrates that either the respiratory rate is strongly repressed at physiological values for $\Delta\tilde{\mu}_H$, even at substrate saturation in absence of any product. Or the influence of the proton gradient on the V_{max} is only very little, meaning that the K_m are highly affected which is not reasonable.
This result is not surprising: [Reynolds et al., 1985] showed that the effects of $\Delta\Psi$ on several steps are not additive, and depending on how much the gradient influences the steps within an enzyme, the overall flux-force relationships can be quite different. [Boork, 1984] supposed that for summarized reaction steps the gradient may not be symmetrically distributed on the backward and forward reaction but that this repartition was rather dependent on where the transition state of an enzyme was located with respect to the binding sites. One can thus conclude that setting strictly $\gamma_V = 0.5$ is not reasonable.

Uneven influence of the proton gradient on the forward and backward rate constants

For $\gamma_V < 0.5$ it is possible to achieve adequate fluxes at physiological values of $\Delta\tilde{\mu}_H$, while changing the Michaelis-Menten constants only a little (ζ_i relatively small). This is shown in figure 3.3 on the example of complex I. However, when simulating the rate equations under conditions where the reaction of an OXPHOS complex becomes reversed, this asymmetric distribution of the gradient on V_{max}^+ and V_{max}^- entails an extreme in-

Figure 3.2.: Even repartition of the impact of the electrochemical gradient on the rate constants, i.e. $\gamma_V = 0.5$.Below are shown the rate dependencies on $\Delta\Psi$ for different distributions of ΔG_H among the kinetic parameters. We suppose that for each value ζ_V, the rest of the ΔG_H is equally distributed among the K_m such that $\sum_j \zeta_j = 1$, with all $\gamma_j = 0.5$. For simplicity, we set Δ pH = 0 and thus $\Delta\tilde{\mu}_H = \Delta\Psi$. In the curves a) - c) the product concentrations are set to zero and the substrate concentration are set to $100 \cdot K_m^0$, where K_m^0 is the value of the K_m at $\Delta\tilde{\mu}_H = 0$. a) $\zeta_V = 1$. Only the V_{max} are influenced by the proton gradient. In this case, it is clear that even at low $\Delta\Psi$ (around -100 mV), the activity of all the complexes is close to zero. b) $\zeta_V = 0.5$. The activities are higher in physiological conditions of state 3 (around -100 to -140 mV) and zero at state 4 (around -150 to -200 mV) except for complex I for which the activity is low in all cases. c) Case of complex I for different ζ_V-values. For all values of ζ_V there is a rapid decrease in activity except when the V_{max}^+ and V_{max}^- of complex are not affected by $\Delta\tilde{\mu}_H$ ($\gamma_V = 0$). d) Case of complex I for different ζ_V-values, but in this case the substrates values are set to 100 times their actual $K_m(\Delta\Psi)$, always in the absence of products. Despite higher values of substrate concentrations, reasonable velocities are only obtained for values of $\gamma_V \leq 0.2$. These figures show that an equal repartition of the ΔG_H between the rates ($\gamma_V = 0.5$) and the K_m will lead, most of the time, to a too abrupt decrease of the respiratory complexes activities with $\Delta\Psi$.

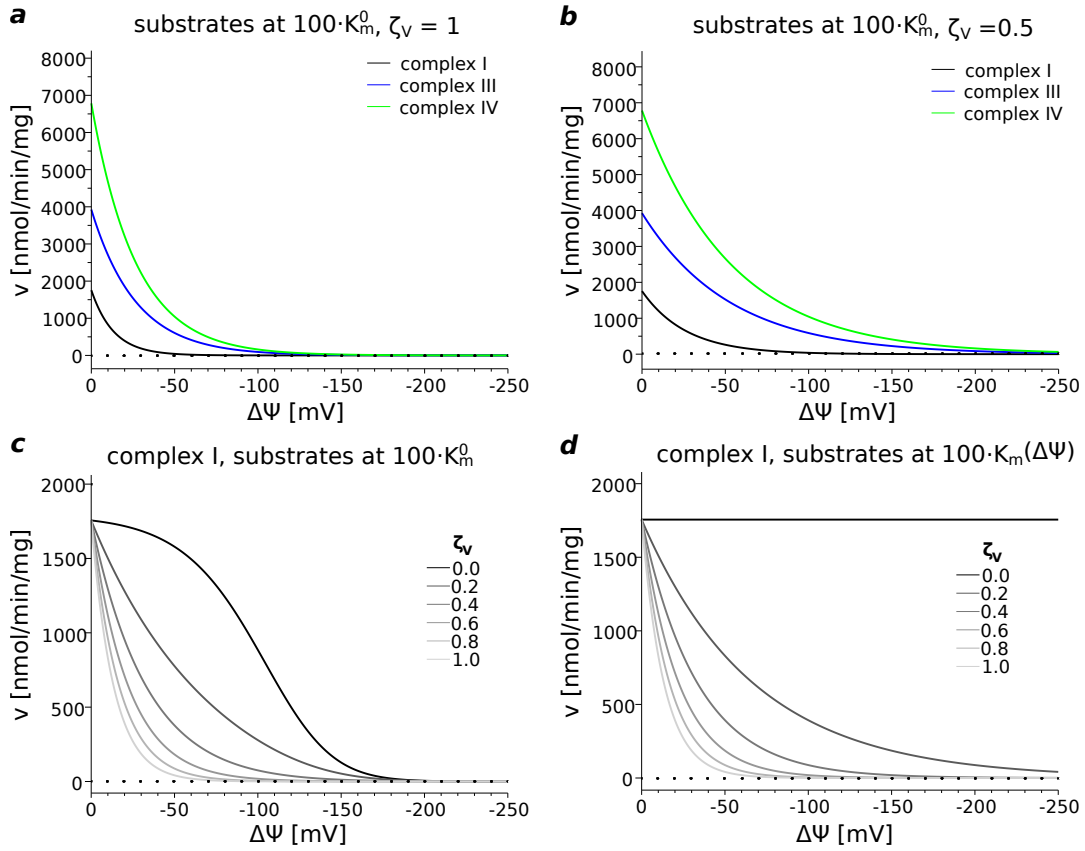

crease of the net (backward) velocity with the gradient becoming more negative, and this even relatively close to the $\Delta\Psi$ of the reversal point. This behavior is not consistent with enzyme kinetics.

Indeed under most physiological conditions, the OXPHOS complexes operate in forward direction, but there are exceptions:

- Complex I has been found reversible in *in vitro* experiments [Löw and Vallin, 1963] and there are indications that under special conditions this can also be true in vivo [Zoccarato 2007, Muller 2008].
- The ATPsynthase is reversible [Fillingame, 1997] and its reaction sense is dependent on the proton motive force. At low membrane potential, e.g. under anoxic conditions, the enzyme hydrolyzes ATP [St-Pierre et al., 2000].

These aspects can become important in particular when analyzing special physiological and pathological situations, and hence extreme backward velocities would not allow for adequate simulations.

3.4.3. Concept of the internal energy

In the following we propose a way for modeling the OXPHOS complexes under influence of $\Delta\tilde{\mu}_H$ which allows also for a reasonable backward velocity. We define as *internal energy* ΔG_{int} the energy that is driving an enzyme's catalytic i.e. 'internal' steps . In the absence of the electrochemical gradient it shall be given by

$$\Delta G^0_{int} = -RT \cdot \ln\left(\frac{V^+_{max}}{V^-_{max}}\right) = \Delta G'_0 + RT \ln\left(\frac{\prod_j K^{\nu_j}_{P_j}}{\prod_i K^{\nu_i}_{S_i}}\right) \tag{3.30}$$

For $\Delta G_H \neq 0$ the internal energy becomes

$$\Delta G_{int} = \Delta G^0_{int} + \zeta_V \cdot \Delta G_H \tag{3.31}$$

with ζ_V the fraction of the gradient influencing the internal steps. Note that the actual substrate and product concentrations are not part of ΔG_{int}. We can thereby define as 'external energy' the energy arising from the substrate and product concentrations and their corresponding K_M.

We express now the maximal velocities as functions of ΔG_{int}:

$$V^+_{max}(\Delta G_{int}) = k \cdot e^{\gamma_V \cdot \left(-\frac{\Delta G_{int}}{RT}\right)} \tag{3.32}$$

$$V^-_{max}(\Delta G_{int}) = k \cdot e^{(\gamma_V - 1) \cdot \left(-\frac{\Delta G_{int}}{RT}\right)} \tag{3.33}$$

Figure 3.3.: Uneven repartition of the impact of the electrochemical gradient on the kinetic constants. Below the catalytic rates are shown as a function of the membrane potential, for different values of γ_V. This parameter decides in which extent the part of ΔG_H, which is influencing the rate constants, is distributed among V^+_{max} and V^-_{max}. Here $\gamma_V = 1$ (0) means that exclusively the forward (reverse) rate is affected. In all simulations, the influence of ΔG_H on the rate constants is given by $\zeta_V = 0.8$. The rest is equally distributed among the K_m of substrates and products. For simplicity Δ pH was assumed to be zero, and hence $\Delta\tilde{\mu}_H = \Delta\Psi$. a) $\gamma_V = 0.3$ and b) $\gamma_V = 0.1$. The activities of complexes I, III and IV are shown as a function of $\Delta\Psi$. The simulations were done in absence of products and with substrates concentrations 100 times higher than their K^0_m , i.e. their K_m in the absence of effect of $\Delta\tilde{\mu}_H$. It appears that the parameter γ_V importantly regulates the complexes activities and thus will be central in experiments fittings (with low values of this parameters especially for complex I). c) The activity of complex I is plotted for different γ_V values as a function of $\Delta\Psi$ in conditions where substrates and products concentrations are set K^0_m. In these conditions the reaction always reverse around - 150 mV. d) Same conditions as in c) but zoomed out. It reveals the large disadvantage of this asymmetric repartition of the $\Delta G_H(\Delta\Psi)$ on V^+_{max} and V^-_{max}. When $\Delta G_R > 0$, the backward velocity increases dramatically (except for $\gamma_V = 1$).

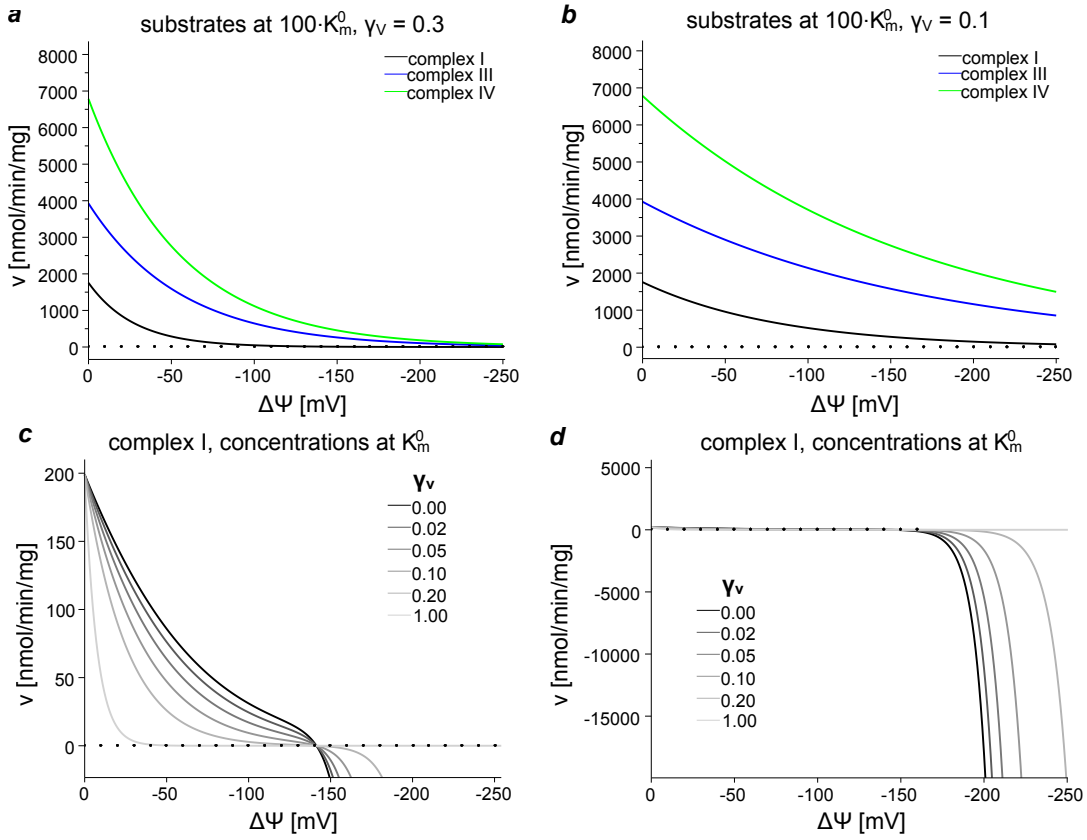

with

$$k = V^{+}_{max}(0) \cdot e^{\gamma_V \cdot \frac{\Delta G^0_{int}}{RT}} \tag{3.34}$$

where $V^{+}_{max}(0)$ is the maximal velocity in absence of the gradient.

We have seen that for $\gamma_V < 0.5$ it is possible to achieve satisfactory rates as long as the total energy of reaction ΔG_R is negative. To overcome the problem of extreme backward velocities for $\Delta G_R > 0$ we consider that there must be a rate limiting step for the forward as well as for the backward direction among the internal reaction steps. Which of these steps is limiting may depend on the actual $\Delta\tilde{\mu}_H$ and hence it may be possible that the step limiting the overall forward velocity is different to the one restricting the backward velocity. It is thus difficult to estimate the effect of $\Delta\tilde{\mu}_H$ on the apparent V^{+}_{max} and V^{-}_{max} and therefore we assume simply that the dependency of these parameters on the internal energy shall be symmetric, i.e.

$$V^{+}_{max}\left(-\Delta G_{int}\right) = V^{-}_{max}\left(\Delta G_{int}\right) \tag{3.35}$$

which means that when the external energies are zero, which is e.g. given when the substrate and product concentrations are at their actual K_M, we have

$$v\left(-\Delta G_{int}\right) = -v\left(\Delta G_{int}\right) \tag{3.36}$$

To achieve such a behavior, the following constraint must be fulfilled:

$$\gamma_V\left(\Delta G_{int}\right) = 1 - \gamma_V\left(-\Delta G_{int}\right) \tag{3.37}$$

If γ_V was constant, the equation can only be resolved for $\gamma_V = 0.5$, but since we have excluded this possibility above, $\gamma_V \,\epsilon\, [0,1]$ cannot be constant and must hence be a function of ΔG_{int}. This is in agreement with rate limiting steps depending probably on $\Delta\tilde{\mu}_H$ and also with the effects of $\Delta\tilde{\mu}_H$ on single internal steps not being additive with respect to the overall rate. Consequently, the repartition of ΔG_H on the apparent V^{+}_{max} and V^{-}_{max} via γ_V, can be dependent on $\Delta\tilde{\mu}_H$ and thereby on ΔG_{int}.

A function that fulfills the condition 3.37 is

$$\gamma_V(\Delta G_{int}) = \beta + (0.5 - \beta) \cdot \left(1 + \tanh\left(\frac{\Delta G_{int}}{c}\right)\right) \tag{3.38}$$

where $\beta \,\epsilon\, [0, 0.5]$. The function is plotted in figure 3.4. It can be adapted to produce a more or less smooth transition between the values of γ_V at $\Delta G_{int} < 0$ and $\Delta G_{int} > 0$. Here the constant c regulates the steepness of the function. When choosing high values of c, the curves show non-physiological peaks in the area where $\Delta G_{int} \approx 0$. These 'artifacts' vanish for $c \to 0$.
Thereby, function 3.38 becomes a step-function and can be replaced by the following

Figure 3.4.: The repartition of the proton gradient's influence on the rate constants as a function of the internal energy. a) γ_V as a function of ΔG_{int}. The absolute value of γ_V is determined by γ_V*. The constant c regulates the steepness of the curve, here $c = 10kJ$. b) Complex I activity as a function of $\Delta\Psi$ for different γ_V*. For simplicity, ΔpH was set zero, hence $\Delta\tilde{\mu}_H = \Delta\Psi$. For ΔG_{int} being close to zero, high values for c result in an non physiological peak . Besides this exception, the curves for high and low c are very similar. For $c \to 0$, γ_V approximates a step function, see equation 3.39.

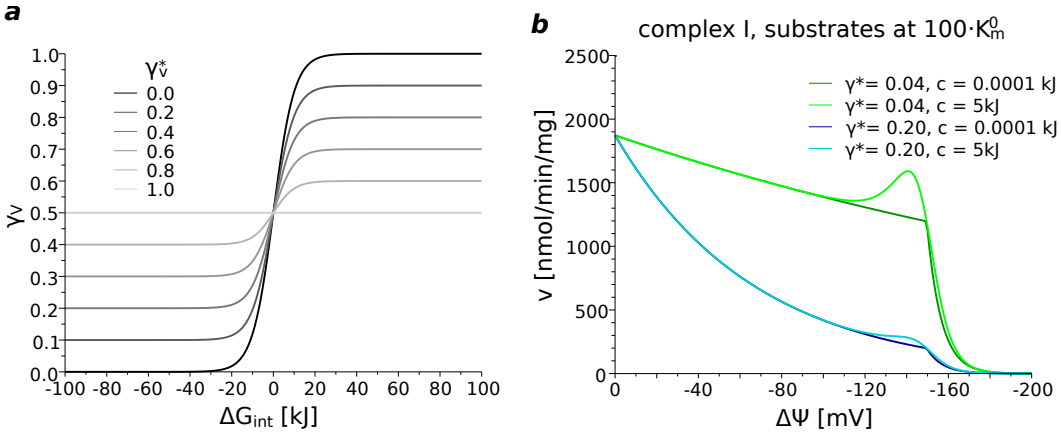

simple approach:

$$\gamma_V(\Delta G_{int}) = \begin{cases} \gamma^* & \text{if } \Delta G_{int} < 0, \\ 0.5 & \text{if } \Delta G_{int} = 0, \\ 1-\gamma^* & \text{if } \Delta G_{int} > 0. \end{cases} \tag{3.39}$$

with $\gamma^* \epsilon [0, 1]$

We replace equations 3.32 and 3.33 now by

$$V^+_{max}(\Delta G_H) = k \cdot e^{\gamma_V(\Delta G_{int})\cdot\left(-\frac{\zeta_V\cdot\Delta G_{int}}{RT}\right)} \tag{3.40}$$

$$V^-_{max}(\Delta G_H) = k \cdot e^{(\gamma_V(\Delta G_{int})-1)\cdot\left(-\frac{\zeta_V\cdot\Delta G_{int}}{RT}\right)} \tag{3.41}$$

Due to $\gamma_V(\Delta G_{int})$ being a step function, k can be calculated using equation 3.34 with $\gamma_V = \gamma^*$.

With the $\Delta\tilde{\mu}_H$-dependent expressions for the V_{max} and the K_M (equations 3.24,3.25, 3.40 and 3.41) inserted into the basic rate equation structure (equation 3.26), we have now a $\Delta\tilde{\mu}_H$-dependent generic rate equation for the OXPHOS complexes: figure 3.5 shows that with a ΔG_{int} dependent repartition of the proton gradient's influence on V^+_{max} and V^-_{max}, adequate rates at physiological values of the gradient can be achieved,

and that the maximal velocities are restricted for both cases $\Delta G_R \leq 0$ and $\Delta G_R > 0$ within a large interval.

The new rate equations, on the example of the simplified random binding equation as basic equation, are listed in table 3.1 for both alternatives, with and without γ_V as a function of ΔG_{int}.

3.5. Summary and Discussion

In order to achieve a more realistic kinetic representation of the OXPHOS complexes the electrochemical membrane potential difference was introduced into the Michaelis-Menten like rate equations. Therefore the assumption was made that in presence of the proton gradient, their steady state kinetics can also be well approached with this type of rate law. The introduction of $\Delta\mu_H$ was implemented such that the new rate equations can describe the OXPHOS complexes kinetics in absence and in presence of the membrane gradient. This is a new aspect for the modeling of the oxidative phosphorylation: so far equations have been used that do not cover such a wide range of membrane gradient, and in most cases do not even account for saturation kinetics. Further the approach conforms to thermodynamic laws.

The new rate equations are flexible, since the approach can take into account as basis every type of Michaelis-Menten like equations (ordered mechanism, ping-pong mechanism, etc, and also extended mass action equation) as long as Haldane equation is valid.

3.5.1. Introduction of the gradient

The equilibrium of the reactions catalyzed by the OXPHOS complexes is shifted under the influence of the membrane gradient. Since the kinetic parameters are related to the equilibrium constant K_{eq} via the Haldane equation 3.10, it is concluded that their values must be sensitive to changes in the proton gradient.
K_{eq} is an exponential function of the standard Gibbs energy of the reaction, which in turn is dependent on the energy needed for the proton translocation ΔG_H. We have made the simple approach that also the kinetic parameters values are exponential functions of ΔG_H

Of particular interest is the influence of the proton gradient on the maximal forward and backward rates, since they are mostly representing the inner catalytic steps to which the energy of proton transfer is attributed. We found that when charging these two constants evenly, the catalytic rates achieved for physiological $\Delta\mu_H$ were much too low. We thereby concluded, that the forward and backward rate constants should be differently charged by the gradient. Hereby we achieved adequate rates. However, with increasing $\Delta\mu_H$ extremely high backward velocities were observed, not being compatible with typical enzyme behavior. This is not acceptable if the model shall be valid also for

Figure 3.5.: Internal energy dependent repartition of the electrochemical gradient on the rate constants. Below the catalytic rates are shown as a function of the membrane potential, for different values of γ_V*. This parameter determines the absolute value of γ_V. The latter is now a function of the internal energy ΔG_{int} and thus dependent on $\Delta\tilde{\mu_H}$, see equation 3.39. In all simulations, the influence of ΔG_H on the rate constants is given by $\zeta_V = 0.8$. The rest is equally distributed among the K_m of substrates and products. ΔpH was assumed to be zero, and hence $\Delta\tilde{\mu}_H = \Delta\Psi$. a) $\gamma_V* = 0.3$ and b) $\gamma_V* = 0.1$. The now ΔG_{int} dependent influence of ΔG_H on V^+_{max} and V^-_{max} changes the shapes of the curves: at the point, where ΔG_{int} becomes positive, a sudden decrease of the forward velocity can be observed, since here the internal catalytic steps are in favor of the backward reaction, while the substrates push the whole reaction further in the forward direction. Reasonable rates can be obtained in the physiological range (-100 to -180 mV). The simulations were done in absence of products and with substrates concentrations 100 times higher than their K^0_m , i.e. their K_m in the absence of effect of $\Delta\tilde{\mu}_H$. c) Activity of complex I for different γ_V* values as a function of $\Delta\Psi$. Here the substrates and products are set to their actual $K_m(\Delta\Psi)$. This means that no net driving force results from the substrate and product concentrations, and hence one can observe the symmetry of the forward and backward rates with respect to $\Delta\Psi$, as it has been stated as condition (see equation 3.36) in order to avoid extremely high backward rates. d) Activity of complex I for different γ_V* values as a function of $\Delta\Psi$. All concentrations are set to their K^0_m. Since with decreasing $\Delta\Psi$ the K_m-values of the substrates increase and those of the products decrease, the backward rates are stronger than the forward rates, but in no case they attain extreme values.

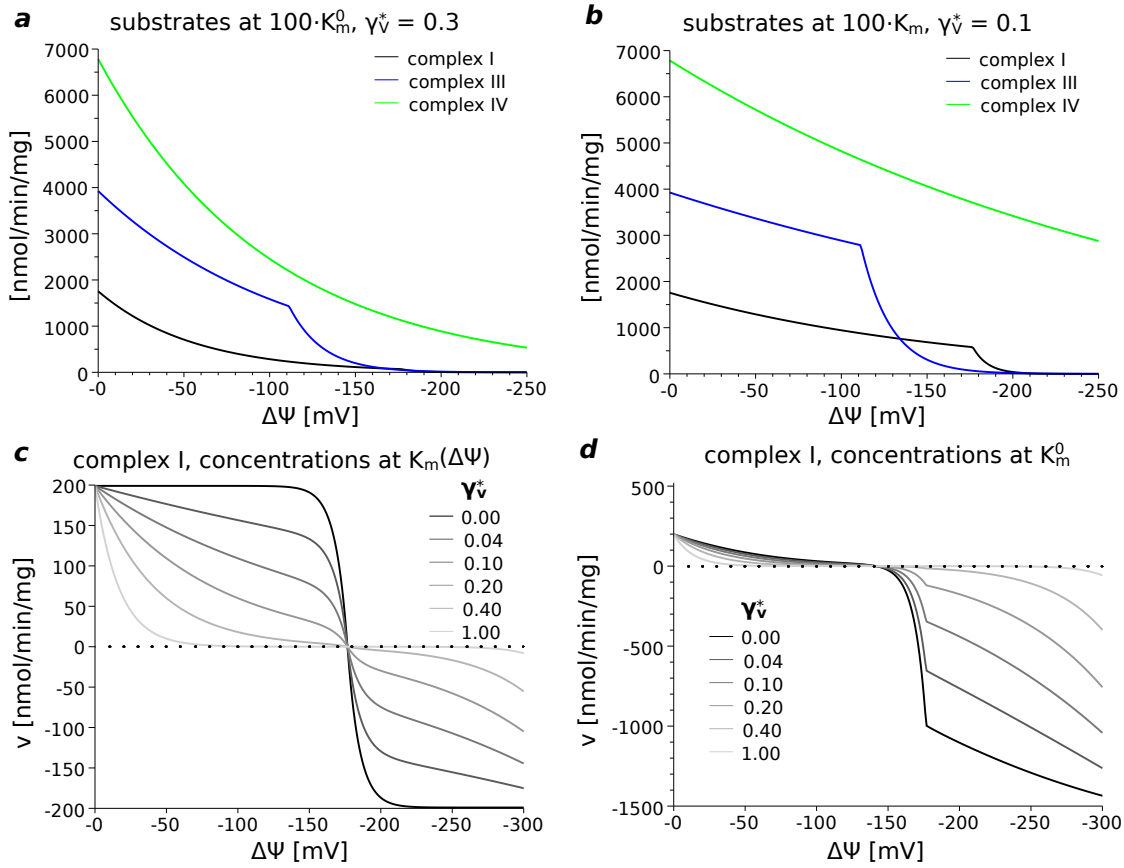

Table 3.1.: The new rate equations for the proton translocating OXPHOS complexes are shown below on the example of the (modified) simplified random binding equation. The V^{+}_{max} and the V^{-}_{max} are presented for both approaches, γ_V constant and γ_V as a function of ΔG_{int}. The way we integrate the proton pumping into the equations is very flexible since any of the Michaelis-Menten-like rate equations can be used as basis, thus the kinetic expressions can be rendered more precise later if needed. The rate equation for Complex III is presented based on the net reaction scheme. ΔG_{int} and $\gamma_V(\Delta G_{int})$ are calculated via equations 3.31 and 3.39, respectively.

complex I: $v = \frac{V^{+}_{max} \cdot n_r \cdot q_o - V^{-}_{max} \cdot n_o \cdot q_r}{(1+n_o+n_r)\cdot(1+n_r+n_o)}$

$n_o = \frac{[NAD]}{K^0_{NAD}} \cdot e^{(\gamma_N - 1)\cdot\zeta_N \cdot \left(-\frac{\Delta G^{C1}_H}{RT}\right)}$

$n_r = \frac{[NADH]}{K^0_{NADH}} \cdot e^{\gamma_N \cdot \zeta_N \cdot \left(-\frac{\Delta G^{C1}_H}{RT}\right)}$

$q_o = \frac{[Q]}{K^0_Q} \cdot e^{\gamma_Q \cdot \zeta_Q \cdot \left(-\frac{\Delta G^{C1}_H}{RT}\right)}$

$qh_r = \frac{[QH_2]}{K^0_{QH_2}} \cdot e^{(\gamma_Q - 1)\cdot\zeta_Q \cdot \left(-\frac{\Delta G^{C1}_H}{RT}\right)}$

complex III: $v = \frac{V^{+}_{max} \cdot q_r \cdot c_o^2 - V^{-}_{max} \cdot q_o \cdot c_r^2}{(1+q_o+q_r)\cdot(1+c_o+c_r)^2}$

$c_o = \frac{[cytc_{ox}]}{K^0_{cytc_{ox}}} \cdot e^{\gamma_C \cdot \frac{\zeta_C}{2} \cdot \left(-\frac{\Delta G^{C3}_H}{RT}\right)}$

$c_r = \frac{[cytc_{red}]}{K^0_{cytc_{red}}} \cdot e^{(\gamma_C - 1)\cdot \frac{\zeta_C}{2} \cdot \left(-\frac{\Delta G^{C3}_H}{RT}\right)}$

$q_o = \frac{[Q]}{K^0_Q} \cdot e^{(\gamma_Q - 1)\cdot\zeta_Q \cdot \left(-\frac{\Delta G^{C3}_H}{RT}\right)}$

$q_r = \frac{[QH_2]}{K^0_{QH_2}} \cdot e^{\gamma_Q \cdot \zeta_Q \cdot \left(-\frac{\Delta G^{C3}_H}{RT}\right)}$

complex IV: $v = \frac{V^{+}_{max} \cdot c_r \cdot o_2^{0.25} - V^{-}_{max} \cdot c_o}{(1+c_o+c_r)\cdot(1+o_2)^{0.25}}$

$c_r = \frac{[cytc_{red}]}{K^0_{cytc_{red}}} \cdot e^{\gamma_C \cdot \zeta_C \cdot \left(-\frac{\Delta G^{C4}_H}{RT}\right)}$

$c_o = \frac{[cytc_{ox}]}{K_{cytc^0_{ox}}} \cdot e^{(\gamma_C - 1)\cdot \zeta_C \cdot \left(-\frac{\Delta G^{C4}_H}{RT}\right)}$

$o_2 = \frac{[O_2]}{K^0_{O2}} \cdot e^{\frac{\zeta_O}{0.25} \cdot \left(-\frac{\Delta G^{F1}_H}{RT}\right)}$

($\zeta_O = 0$ in section 3.4)

ATP Synthase: $v = -\frac{V^{+}_{max} \cdot atp - V^{-}_{max} \cdot adp \cdot pi}{(1+adp+atp)(1+p_i)}$

$adp = \frac{[ADP]}{K^0_{ADP}} \cdot e^{(\gamma_A - 1)\cdot\zeta_A \cdot \left(-\frac{\Delta G^{F1}_H}{RT}\right)}$

$atp = \frac{[ATP]}{K^0_{ATP}} \cdot e^{\gamma_C \cdot \zeta_A \cdot \left(-\frac{\Delta G^{F1}_H}{RT}\right)}$

$p_i = \frac{[P_i]}{K^0_{P_i}} \cdot e^{-\zeta_P \cdot \left(-\frac{\Delta G^{F1}_H}{RT}\right)}$

($\zeta_P = 0$ in section 3.4)

all complexes:

γ_V constant

$V^{+}_{max} = k \cdot e^{\gamma_V \cdot \zeta_V \cdot \left(-\frac{\Delta G_{int}}{RT}\right)}$

$V^{-}_{max} = k \cdot e^{(\gamma_V - 1)\cdot\zeta_V \cdot \left(-\frac{\Delta G_{int}}{RT}\right)}$

γ_V as a function of ΔG_{int}

$V^{+}_{max} = k \cdot e^{\gamma_V(\Delta G_{int})\cdot\zeta_V \cdot \left(-\frac{\Delta G_{int}}{RT}\right)}$

$V^{-}_{max} = k \cdot e^{((\gamma_V(\Delta G_{int}) - 1)\cdot\zeta_V)\cdot \left(-\frac{\Delta G_{int}}{RT}\right)}$

extreme conditions: complex I and the F_1F_0-ATP synthase are known to be reversible in case of a high and respectively low, membrane gradient.
To overcome the problem of extreme backward rates, the concept of the inner energy ΔG_{int} was introduced, i.e. the total energy available to realize all catalytic steps inside the enzyme. The repartition of the gradient among the maximal forward and backward rates was then modeled as simple function of ΔG_{int}, not requiring any additional parameter.

This method of introducing the electrochemical potential is a new aspect in modeling the respiratory chain complexes. In the model of Beard [2005], the electrochemical potential acts exclusively on the forward velocity, as well as in the quite complex model of Jin and Bethke [2002]. In the model of Bohnensack [1981] it acts only on the backward velocity. In the model of Korzeniewski [2001], the velocity does not result from the difference of a forward and a backward velocity, thus here the integration of the gradient is different.

3.5.2. Sensitivity of the Michaelis-Menten constants to the membrane gradient

In a first simple approach one could attribute the K_m exclusively to the binding affinities and the V_{max} exclusively to catalytic steps, and further assume that then the relevant steps for proton and electron translocation would be purely represented by the V_{max}. However, as emphasized above, in order to obtain reasonable values for the complexes activities under physiological $\Delta\mu_H$, the substrates and products K_m values need also to be sensitive to the proton gradient, such that the substrates K_m increase and the products K_m decrease with increasing $\Delta\mu_H$.
There are some experimental indications in this direction. Bienfait et al. [1975] showed that for oxygen binding to complex IV K_{O_2} is increased at higher $\Delta\mu_H$. Further it has been reported for the reverse reaction of complex I, thus at high $\Delta\mu_H$, that the K_i of NADH is higher than its K_m for the forward reaction, and similarly that the K_i for NAD in the forward reaction is higher than its K_m in the reverse reaction [Vinogradov, 1993, 2008]. But here it must be remarked that the K_i-values have to be regarded with caution: depending on the rate equation that has been used for determining the K_i, the real enzyme's mechanism might not be sufficiently well described and this can lead to discrepancies between the apparent K_m and their respective K_i (see also the discussion in chapter II, section 2.8).
These differences suggest that the dependencies of the classical kinetic parameters K_m, K_i and V_{max} on $\Delta\mu_H$ may be complex. This is not surprising when considering that here the intricate functionalities of the OXPHOS complexes are represented by the simple Michaelis-Menten like equations: the latter are derived from a simple reaction scheme taking into account the binding and release of substrate and products and *one* catalytic step, representing catalytic processes. These kinetic expressions may be well suited to describe an OXPHOS complex at a fixed $\Delta\mu_H$, but the incorporation of a change in $\Delta\mu_H$ into the rate equations is not obvious. However, our relative simple approach of integrating the $\Delta\mu_H$ in the rate equations seems to be promising, since without

distributing much of the proton gradients influence on the K_m-values, we can achieve adequate rates at physiological $\Delta\mu_H$, while in any case the enzymes activities are well described in absence of the proton gradient. In how far this is also true when simulating the system of OXPHOS, where $\Delta\Psi$, ΔpH as well as substrate and product concentrations are variable will be analyzed in chapter 4.

3.5.3. Further considerations

There is a strong simplification in summarizing ΔpH, the $\Delta\Psi$ and the scalar protons within one energetic expression, since all these components may influence differently the kinetics of the OXPHOS complexes. In this regard, for instance, one could later extend the rate equations for a general pH dependency of the activity, such that it directly influences the kinetics and does not only appear in the energetic terms.

A stochastic model of each complex that includes all catalytic steps [Ransac et al., 2008, 2010], and which takes into account the effect of $\Delta\Psi$ and the matrix and intermembrane space pH, at the place where they occur, could be very helpful: to study the dependencies of the K_m and V_{max}, and thus to evaluate the model, to adapt the distribution of the the proton gradients influence among the parameters, and if necessary, to improve the integration of the proton gradients influence on these parameters.

Experimental data of the dependency of an isolated OXPHOS complex' activity on $\Delta\Psi$ and the matrix and intermembrane space pH would as well allow for testing the suitability of the new rate equations and for adapting the parameter values that are responsible for the distribution of the proton gradient on the K_m and V_{max}. In particular kinetic experiments for the determination of the K_m at different membrane potentials would be very helpful. Unfortunately such experiments are difficult to realize. Literature data are mostly referred to the whole system, regarding the respiration rate as a function of $\Delta\Psi$ and ΔpH in physiological ranges. In the next chapter we will compare a model taking account the system of the OXPHOS complexes, represented by the new rate equations, to such experimental data.

The model includes many simplifications also with respect to activation energies and the degree of efficiency of coupling proton translocation to redox reactions. Further the possible slippage of electrons [Pietrobon, 1986] is not considered. But despite all these simplifications, the model is very promising. The distribution of the gradients impact among the kinetic parameters provides a flexibility for adapting the flux-$\Delta\mu_H$-dependency. The rate equations link the well described kinetics in the absence of the proton gradient, suitable for a wide range of substrate and product concentrations, to the kinetics in the presence of an electrochemical potential difference, where adequate rates can be achieved at physiological $\Delta\mu_H$.

4. Modeling the system of oxidative phosphorylation

4.1. Introduction

For the simulation of OXPHOS with our new rate equations, we need to set them in the context of a mitochondrial environment, e.g. we need to distinguish between matrix and intermembrane space in order to take into account the proton gradient that is established over the inner membrane. For this purpose we chose a framework model that employs the same components as the OXPHOS model of Beard [2005]. The new model is then used to evaluate our new rate equations and for simulations. For instance the effect of inhibiting an OXPHOS complex on the global system is analyzed, and the time courses of the respiratory rate are simulated.

4.2. The framework model

A schematic representation of the framework model is shown in figure 4.1. The model takes into account the mitochondrial matrix, the intermembrane space and the external space, which will be denoted 'x', 'is' and 'e', respectively.
In order to clarify the basis of the simulations and analyses we provide the entire framework model: the system of differential equations is shown in table 4.1 and the constraints are given in table 4.2; the rate equations are listed in the appendix A.
For steady state simulations, the concentrations in the external space are set constant and thus do not appear in the ordinary differential equation system. For the simulation of time courses, these external concentrations will later appear as state variables.

The model uses the same components as has been used before in the OXPHOS model of Beard [2005]; most of them were however already part of the OXPHOS model of Korzeniewski [2001], albeit in the latter in many cases other kinetic expressions and more constraints were used.
In the following we shortly describe the elements that are part of the framework model besides the respiratory complexes I, III and IV and the F_1F_o-ATPsynthase. Complex II was originally not included in the model and will be introduced only later.

The proton-leak through the inner membrane ($\rightarrow J_{H_{le}}$).

$$H_{is}^{+} \rightleftharpoons H_{x}^{+} \tag{4.1}$$

Figure 4.1.: Schematic representation of the OXPOS model. The components are the same as for the model of Beard [2005]. Besides the proton pumping respiratory chain complexes (CI, CIII, and CIV) and the F_1F_0-ATP-synthase the inner membrane contains also the adenine nucleotide transporter* (ANT), the proton coupled phosphate transport* (PiH) and the K^+H^+-exchanger (KH). The H^+ and K^+ leak fluxes through this membrane are further considered. The Krebs cycle in the matrix is represented by a 'dehydrogenase' (DH) reaction and the adenylate kinase* (AK) is situated in the intermembrane space. For the outer membrane, the permeation of P_i and the adenine nucleotides are taken into account. ATP and ADP appear in free and Mg^{2+} bound form (mATP, fATP, mADP, fATP). Most of the here listed components appeared already in the model of [Korzeniewski, 2001], the equations for the enzyme catalyzed reactions labeled by * had the same kinetic expressions.

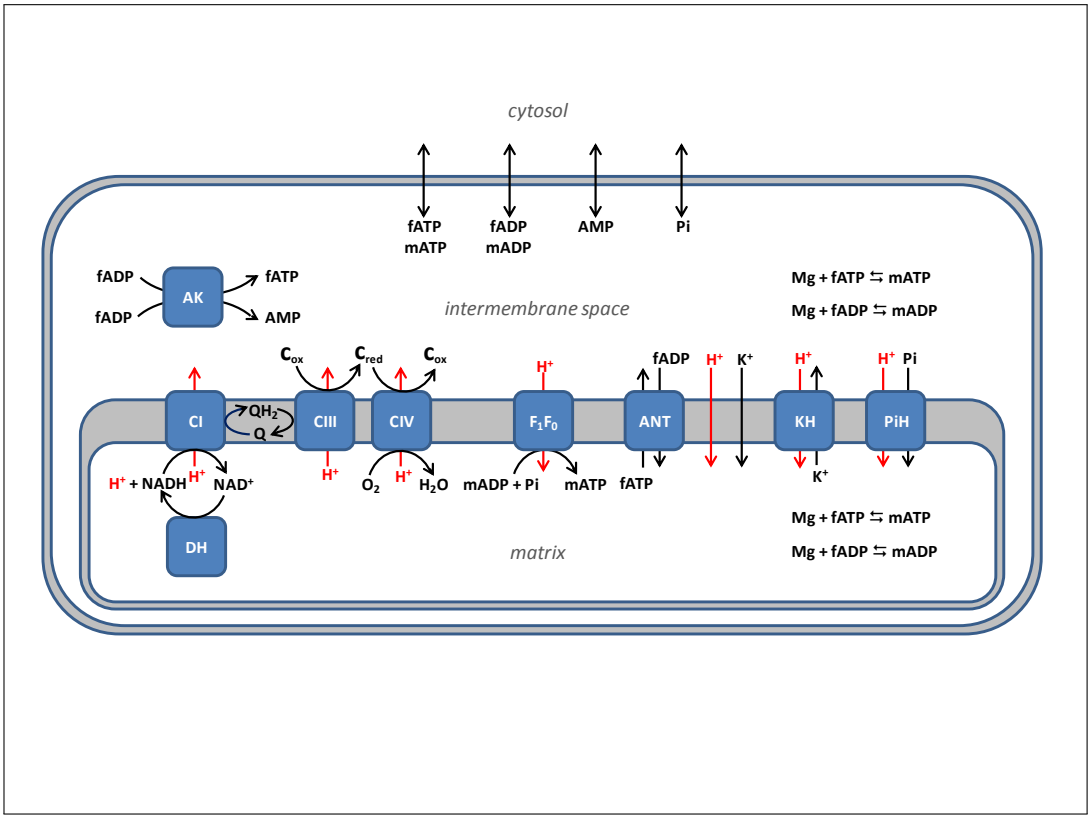

Although the inner membrane is highly impermeable there is a proton leak flux driven by the high proton gradient between the intermembrane space and the matrix. Further protons may leak via membrane standing proteins and in particular there may be a slippage during the proton pumping of the respiratory chain complexes. These features are comprised in the expression $J_{H_{le}}$. It is an essential component in the modeling of the OXPHOS system, because it permits the achievement a steady state also under conditions where the ATP-Synthase activity is zero as it is the case in vivo (state 4). Otherwise one would have to set constant $\Delta\Psi$ and the matrix proton concentration (the intermembrane and external proton concentrations are assumed to be constant).

The dehydrogenase reaction ($\rightarrow J_{DH}$)

$$NAD^+ \rightleftharpoons NADH \tag{4.2}$$

The dehydrogenase reaction represents the Krebs cycle wherein NAD^+ becomes reduced to NADH. The reaction allows for treating NADH as state variable.

ATP consumption. This is a complementary process to the production of ATP via the F_1F_o-ATP-synthase. In the model, this feature is realized in a very simple way, by setting to zero the external ATP concentration.

Adenine nucleotides play a central role in this OXOPHOS model. It is taken into account that ADP and ATP exist in Mg^{2+} bound and free form, denoted by 'f' and 'm', respectively. AMP is considered only in its free form, although it exists also in Mg^{2+} bound form [Rose, 1968]. However the only reaction where Mg^2+ bound AMP could intervene in this model is the adenylate kinase. But here the simplification is made that the enzyme takes into account only the free forms of adenine nucleotides, see also below.

The F_1F_o-ATP-synthase ($\rightarrow J_{F_1}$) shall be mentioned again at this point, because this OXPHOS complex accepts exclusively Mg^{2+} bound ADP (mADP) and ATP (mATP) as substrate and product, respectively.

$$mADP + n_A\, H^+_{is} + P_iH^+ \rightleftharpoons mATP + (n_A - 1)\, H^+_x \tag{4.3}$$

In the simulations, we set $n_A = 3$ unless otherwise noted.

The adenine-nucleotide transporter ($\rightarrow J_{ANT}$)

$$fATP_x + fADP_{is} \rightleftharpoons fADP_x + fATP_{is} \tag{4.4}$$

This transporter is situated in the inner membrane and mediates the exchange of fADP against fATP between the inner membrane space and the matrix. Because fATP has four negative charges and fADP only three, this exchange is electrogenic.

The adenylate kinase ($\rightarrow J_{AK}$)

$$2\,fADP \rightleftharpoons fATP + AMP \tag{4.5}$$

The adenylate kinase is located in the inner membrane space. It catalysis the reaction of two ADP molecules into one ATP and one AMP, and vice versa. Here, only the free forms are considered. It is so far not arising from literature, whether this catalysis is restricted to the free forms, but including both, free and Mg^{2+} bound forms would lead to several possibilities how the reaction could take place, e.g. ADP_m could interact with ATP_f, and moreover each of these reactions would have their own equilibrium constants because the dissociation constants for AMP_m, AMP_m and AMP_m differ in one to two orders of magnitude [Rose, 1968]. Since the adenylate kinase is not in the focus of this model, for the sake of simplicity we decided to refrain from taking into account the Mg^{2+}-bound adenine nucleotides for its catalysis.

Mg^{2+} binding to ADP and ATP ($\rightarrow J_{MgADP}$, J_{MgATP}) .

$$ADP_x + Mg_x \rightleftharpoons mADP_x \tag{4.6}$$
$$ATP_x + Mg_x \rightleftharpoons mATP_x \tag{4.7}$$
$$ADP_{is} + Mg_{is} \rightleftharpoons mADP_{is} \tag{4.8}$$
$$ATP_{is} + Mg_{is} \rightleftharpoons mATP_{is} \tag{4.9}$$

In the model the binding is considered in the matrix as well as in the intermembrane space. In the external space concentrations are considered to be constant and hence the mADP concentration is calculated via a fixed mathematical expression.

Permeation of adenin nucleotids through the outer membrane ($\rightarrow J_{AMP}$, J_{fADP}, J_{mADP}, J_{fATP}, J_{mATP}).

$$fADP_e \rightleftharpoons fADP_{is} \tag{4.10}$$
$$mADP_e \rightleftharpoons mADP_{is} \tag{4.11}$$
$$fATP_e \rightleftharpoons fATP_{is} \tag{4.12}$$
$$mATP_e \rightleftharpoons mATP_{is} \tag{4.13}$$

The big pores of the outer membrane permit adenine nucleotides to diffuse quasi freely between the inner membrane space and the external space. In the original model only the diffusion for the free forms was possible. This has been corrected in the present work so that now also mADP and mATP can permeate. The same diffusion constant was assumed for all adenine nucleotides.

Protons have a particular role in the OXPHOS. But besides them also other ions are considered:

Phosphate-proton cotransporter ($\rightarrow J_{PiHt}$)

$$H_2PO^-_{4,is} + H^+_{is} \rightleftharpoons H_2PO^-_{4,x} + H^+_x \tag{4.14}$$

This transporter is situated in the inner membrane. The symport is electroneutral because dihydrogen phosphate ($H_2PO_4^-$) is transported together with one proton. Therefore an instant equilibrium between hydrogen (HPO_4^{2-}) and dihydrogen phosphate ($H_2PO_4^-$) is assumed in the model so that $H_2PO_4^-$ can be expressed as a function of $P_i = H_2PO_4^- + HPO_4^{2-}$.

(In Beard 2005 the equation of P_i-transport was wrong)

The potassium leak ($\rightarrow J_K$).

$$K^+_{is} \rightleftharpoons K^+_x \tag{4.15}$$

The rate constant of the potassium leak was set to zero in the original model, we did the same in the present work.

Permeation of phosphate through the outer membrane ($\rightarrow J_{Pi}$) . The permeation is quasi free and the diffusion constant was set to high values such that this process cannot be rate limiting for other model internal reactions.

The potassium-proton exchanger ($\rightarrow J_{KH}$)

$$K^+_{is} + H^+_x \rightleftharpoons K^+_x + H^+_{is} \tag{4.16}$$

This antiport is electroneutral, but is strongly dependent on the chemical proton gradient.

4.3. Incorporation of the new OXPHOS rate equations

We build the dynamical model in the same way as Beard [2005] did, but with using the new rate equations for the OXPHOS complexes. But before the model can be used for simulations, we have to consider the following two issues:

1. The rate constants k have to be converted in order to fulfill the model conditions: in the framework model enzyme activities are referred to mitochondrial volume and fluxes are expressed in mol/(L mito Volume sec), while the V^+_{max} that we have determined for the calculation of the k is given in nmol/min/mg protein.

Table 4.1.: Differential equation system of the OXPHOS model, taken from Beard [2005]. We corrected the expression for the time dependent change of $[mADP]_x$ and of $[mATP]_x$ by considering the flux through the ATP-synthase since only the Mg^{2+} bound species is the true substrate and product, respectively. The differential equations for $[ADP]_i$, $[ATP]_i$, $[mADP]_i$, $[mATP]_i$ were extended for the permeation of the Mg^{2+} bound species through the outer membrane, assuming that they diffuse in the same extend as their free counterparts. The corrections are marked in bold. Flux names are explained in the text, x_{buff} is the buffering capacity and C the membrane electric capacity. V_x, V_i, V_m, are the volumes of the matrix, the intermembrane space and the inner membrane, respectively.

$$\frac{d[H^+]_x}{dt} = \frac{x_{buff} \cdot [H^+]_x}{V_x} \cdot \begin{pmatrix} +J_{DH} - 5\,J_{C_1} - 2\,J_{C_3} - 4\,J_{C_4} \\ +(n_A - 1)\,J_{F_1} + 2\,J_{PiHt} + J_{H_{le}} - J_{KH} \end{pmatrix} \tag{4.17}$$

$$\frac{d[K]_x}{dt} = (J_{KH} + J_K)\,/V_x \tag{4.18}$$

$$\frac{d[Mg]_x}{dt} = (-J_{MgATPx} - J_{MgADPx})\,/V_x \tag{4.19}$$

$$\frac{d[NADH]_x}{dt} = (+J_{DH} - J_{C_1})\,/V_x \tag{4.20}$$

$$\frac{d[QH_2]}{dt} = (+J_{C_1} - J_{C_3})\,/V_m \tag{4.21}$$

$$\frac{d[cytc_{red}]}{dt} = (+2\,J_{C_3} - 2\,J_{C_4})\,/V_{is} \tag{4.22}$$

$$\frac{d[ATP]_x}{dt} = (+J_{F_1} - J_{ANT})\,/V_x \tag{4.23}$$

$$\frac{d[mATP]_x}{dt} = (J_{MgATPx} \boldsymbol{+ J_{F_1}})\,/V_x \tag{4.24}$$

$$\frac{d[mADP]_x}{dt} = (J_{MgADPx} \boldsymbol{- J_{F_1}})\,/V_x \tag{4.25}$$

$$\frac{d[Pi]_x}{dt} = (-J_{F_1} + J_{PiHt})\,/V_x \tag{4.26}$$

$$\frac{d[ATP]_i}{dt} = \left(+J_{ATP_f} \boldsymbol{+ J_{ATP_m}} + J_{ANT} + J_{AK}\right)/V_{is} \tag{4.27}$$

$$\frac{d[ADP]_i}{dt} = \left(+J_{ADP_f} \boldsymbol{+ J_{ADP_m}} - J_{ANT} - 2J_{AK}\right)/V_{is} \tag{4.28}$$

$$\frac{d[AMP]_i}{dt} = (+J_{AMP} + J_{AK})\,/V_{is} \tag{4.29}$$

$$\frac{d[ATP_m]_i}{dt} = (+J_{MgATPi} \boldsymbol{+ J_{ATP_m}})\,/V_{is} \tag{4.30}$$

$$\frac{d[ADP_m]_i}{dt} = (+J_{MgADPi} \boldsymbol{+ J_{ADP_m}})\,/V_{is} \tag{4.31}$$

$$\frac{d[Pi]_i}{dt} = (-J_{PiHt} + J_{Pi})\,/V_i \tag{4.32}$$

$$\frac{d\Delta\Psi}{dt} = \frac{1}{C} \cdot (4\,J_{C_1} + 2\,J_{C_3} + 4\,J_{C_4} - n_A \cdot J_{F_1} - J_{ANT} - J_{H_{le}} - J_K) \tag{4.33}$$

Table 4.2.: Constraints. Below are listed the constraints that have been used in the model, if not otherwise noted, e.g. for the time course simulations, the external concentrations are turned into state variables.

$$[NAD]_x = N_{tot_x} - [NADH]_x \tag{4.34}$$
$$[Q] = Q_{tot} - [QH_2] \tag{4.35}$$
$$[cytc_{ox}] = C_{tot} - [cytc_{red}] \tag{4.36}$$
$$[ADP]_x = A_{tot_x} - [ATP]_x \tag{4.37}$$
$$[fATP]_x = [ATP]_x - [mATP]_x \tag{4.38}$$
$$[fADP]_x = [ADP]_x - [mADP]_x \tag{4.39}$$
$$[fATP]_{is} = [ATP]_{is} - [mATP]_{is} \tag{4.40}$$
$$[fADP]_{is} = [ADP]_{is} - [mADP]_{is} \tag{4.41}$$
$$[mADP]_e = \frac{1}{2}\left((K_{ADP} + [ADP]_e + Mg_{tot}) - \sqrt{\begin{array}{l}(K_{ADP} + [ADP]_e + Mg_{tot})^2 \\ -4(Mg_{tot} \cdot [ADP]_e)\end{array}}\right) \tag{4.42}$$
$$[fADP]_e = [ADP]_e - [mADP]_e \tag{4.43}$$
$$[Mg]_e = Mg_{tot} - [mADP]_e \tag{4.44}$$
$$[H]_{is} = [H]_e \tag{4.45}$$
$$[Mg]_{is} = [Mg]_e \tag{4.46}$$
$$[K]_{is} = [K]_e \tag{4.47}$$
$$[H_2PO_4^-]_x = \frac{[H^+]_x \cdot [P_i]_x}{[H^+]_x + Kd_{PiH}} \tag{4.48}$$
$$[H_2PO_4^-]_{is} = \frac{[H^+]_{is} \cdot [P_i]_{is}}{[H^+]_{is} + Kd_{PiH}} \tag{4.49}$$

We make the rough estimation that 1 μL of mitochondrial volume contains 0.8 mg of mitochondrial proteins.

$$V^+_{max}\left[\frac{M}{sec}\right] = k^+_{cat}\left[\frac{nmol}{min \cdot mg}\right] \cdot \frac{1min}{60sec} \cdot 10^{-3}\frac{\mu mol}{nmol} \cdot 0.8 \cdot \frac{mgprot.}{\mu L(\text{mito. Vol.})} \quad (4.50)$$

2. Beard [2005] used the model to describe experimental data of the basic respiratory chain features in dependency on the external phosphate concentration, taken from Bose et al. [2003]. For an appropriate description of these data, the author introduced a factor that accounts for an activation of complex III by phosphate. This activation factor reads

$$f_{PiC3} = \frac{1 + \frac{[P_i]}{k_{pi3}}}{1 + \frac{[P_i]}{k_{pi4}}} \quad (4.51)$$

where $f_{PiC3} = 1$ for $P_i = 0$ and $f_{PiC3} = \frac{k_{Pi_4}}{k_{Pi_3}}$ for $P_i \to \infty$, with k_{Pi_3} and k_{Pi_4} parameterizing the activation. Since our experimental data on complex III kinetics have been performed in a buffer with saturating phosphate concentration, we can conclude that the V^+_{max} that we have determined for complex III activity is also maximal with respect to the phosphate concentration. Further, experimental data from the French Mitochondrial Diseases Network suggest that the activity of complex III is rather close to zero for $P_i = 0$. For these reasons we do not use equation 4.51 but change this factor to

$$f_{PiC3} = \frac{[P_i]}{[P_i] + k_{P_i}} \quad (4.52)$$

We finally corrected the temperature in the model to $37°C = 310K$, which corresponds to the temperature used in the Bose experiments and also in our experiments.

4.4. Estimation of parameter values upon basic respiratory chain features

About half of the parameters in the Beard model are fixed to values taken from literature or previous models, see table 4.3. The adjustable parameters have been determined by fitting the experimental data of Bose et al. [2003]. This data set includes quasi steady state measurements of respiration rate, the $\Delta\Psi$, the ΔpH and the reduction states of NADH and cytochrome c, all for phosphorylating (state 3) and non phoshorylating (state 4) conditions and in dependency on inorganic phosphate (P_i) concentration. Covering essential features of the OXPHOS, the data are well suitable for controlling the general integrity of our new rate equations and for determining the parameter values of our new model.
Moreover, stemming also from heart mitochondria these data sets are comparable with

Table 4.3.: Fixed parameters of the models. The parameter values have been taken from the model of , beard2005 where literature values have been employed or some parameters been arbitrarily fixed. In some cases there are minor discrepancies with respect to the publication which arose from the fact that for establishing this model, a Matlab code kindly provided by Dr. Dan Beard as well as the corresponding model on in the CellML model collection (http://www.cellml.org/) have been used. L_{mito} signifies liters of mitochondrial volume. *In Beard's model, the inner membranes volume was not taken into account and the quinones were referred to the matrix volume. We adopted this simplification by setting $V_m = V_x$.

parameter	value	unit	remark
R	8.314	$J\,mol^{-1}\,K^{-1}$	universal gas constant
T	310	K	temperature
F	96.484	$J\,mol^{-1}\,mV^{-1}$	Faraday constant
ΔG^0_{C1}	-69370	J	standard reaction energy for $NADH + Q = NAD^+ + QH_2$
ΔG^0_{C3}	-32530	J	standard reaction energy for $QH_2 + 2\ cytc_{ox} = Q + 2\ cytc_{red}$
ΔG^0_{C4}	-122940	J	standard reaction energy for $2\ cytc_{red} + \frac{1}{2}\ O_2 = 2cytc_{ox}$
$\Delta G^0_{F_1}$	36.03	J	standard reaction energy for $ADP + Pi = ATP$
n_A	3	nondimensional	number of protons for the generation of one molecule ATP
pH_e	7.1	nondimensional	cytolsolic pH
H_e	10^{-pH_e}	M	cytolsolic proton concentration
K_e	0.15	M	cytosolic potassium concentration
ATP_e	0	M	cytosolic ATP concentration
AMP_e	0	M	cytosolic AMP concentration
Kd_{PiH}	$10^{-6.75}$	M	$H_2PO_4^-$ dissociation constant
Kd_{MgATP}	$24e-6$	M	mATP dissociation constant
Kd_{MgADP}	$347e-6$	M	mADP dissociation constant
K_{AK}	0.4331	nondimensional	equilibrium constant for $2\ ADP = AMP + ATP$
V_{mito}	0.72376	ml water / ml mito	mitochondrial water space
V_x	$0.9 \cdot V_{mito}$	ml water / ml mito	matrix water space
V_{is}	$0.1 \cdot V_{mito}$	ml water / ml mito	IM water space
V_m*	$0.9 \cdot V_{mito}$	ml water / ml mito	innermembrane space
γ	5.99	μm^{-1}	outer membrane area per mito volume
N_{tot_x}	$2.97e-3$	M	total nicotinamide adenine dinucleotide concentration
Q_{tot}	$1.35e-3$	M	total quinone concentration
C_{tot}	$2.7e-3$	M	total cytochrome c concentration
A_{tot_x}	0.01	M	total matricial adenin nucleotid concentration
x_{buff}	100	nondimensional	buffer capacity factor
x_{AK}	1e6	$mol\,s^{-1}\,M^{-2}L^{-1}_{mito}$	rate constant of adenylate kinase
x_{MgA}	1e6	$mol\,s^{-1}\,M^{-2}L^{-1}_{mito}$	rate constant of Mg binding to adenine nucleotides
ρ_A	85.0	$\mu msec^{-1}$	mitochondrial outer membrane permeability to adenine nucleotides
ρ_{Pi}	327.00	$\mu msec^{-1}$	mitochondrial outer membrane permeability to organic phosphate
k_{O_2}	$120e-6$	M	binding constant of O_2 to complex IV
k_{ADP}	$3.50e-6$	M	$fADP_f$ binding constant for ANT

our experimental data. However Bose performed his experiments on porcine heart mitochondria while we have used bovine heart mitochondria. It is to keep in mind that the same tissues but from different species may have different energy demands and thus different compositions and activities of the OXPHOS complexes.
Besides estimating the parameters for our new model, we additionally refitted the parameters of Beard's model since it shall serve as reference. The refit was necessary because some modifications have been introduced in Beard's model, see above and table 4.1.

4.4.1. Objective function and fitting routine

For an optimal data description, we searched to minimize the sum of the weighted *coefficients of variation* (CV) of the *root mean square deviation* (RMSD) of each series j, i.e.

$$f_{obj} = \sum_j W_j \cdot CV_j(RMSD_j) \tag{4.53}$$

The weights W_j of the experimental series j are given in table 4.4. The coefficient of variation is

$$CV(RMSD) = \frac{n_i}{\sum_j x_{exp}(j,i)} \cdot RMSD_j \tag{4.54}$$

and the root mean square error is

$$RMSD_j = \sqrt{\frac{\sum_i \left(x_{exp}(j,i) - x_{sim}(j,i)\right)^2}{n_j}} \tag{4.55}$$

with $x_{exp}(j,i)$ and $x_{sim}(j,i)$ are the i^{th} points in the experimental respectively simulated series j. $n(j)$ is the number of points of the series j. The fitting was done using a genetic algorithm. The initial population size was set to 3000, the following generations had a population size of 300. The reproduction was modeled with crossover of the genes of two parents out of the 60 best individuals of the precedent generation. The probability of mutation was set to 1/10 per gene. The ten best results have been refined using a local search routine and thereof the best result was eventually taken. The fitting procedure has been repeated 8 times. Since for the simulation of the models we encountered numerical problems with Scilab 5.3.0 [Scilab Enterprises, 2012], the models were implemented in Matlab R2012b [MathWorks, 2012]. We have also implemented the genetic algorithm; for local refinement a build-in function ('fmincon') was used.

4.4.2. Problems concerning the parameter estimation

The parameter estimation turned out to be not evident for both models. For the experimental data of $\Delta\Psi$ under phosphorylating conditions, either the tendency of the values was well described, realized by fitting by hand and resulting in a high RMSD, or after using the above described fitting procedure, the RMSD was minimized but the model

Table 4.4.: Weight on each experimental series. In principally, the weight was to account for the number of data points for an experimental series. For both series of $\Delta\Psi$, phosphorylating (state 3) and non phosphorylating (state 4), the weight was doubled.

data	$\Delta\Psi$		pH_x		v_{O_2}		NADH (norm.)		cytc % red.	
state	3	4	3	4	3	4	3	4	3	4
weight	2	2	0.25	0.25	1	-	1	1	0.25	0.25

failed to describe the tendency of $\Delta\Psi$ at low P_i concentrations. In the experiments $|\Delta\Psi|$ increases with increasing P_i until a concentration of $\approx 3mM$ and remains constant afterwards (hyperbolic curve). In contrast, for the simulations using an optimized parameter set $|\Delta\Psi|$ starts at a relatively high value in Beard's model. In our model a more complex behavior is observed with three phases: (i) rapid increase from zero culminating to a maximum at low Pi values then (ii) decrease to a minimum value and (iii) finally an increase to a maximal value for higher Pi values.
The explanation for this discrepancy is that in the models, the matrix P_i concentration will go to zero at steady state when the external P_i concentration is zero. Under this condition, the ATP-synthase cannot phosphorylate ADP and hence does not consume the $\Delta\Psi$. In Beard's model, the dehydrogenase reaction (DH) and complex III are activated by P_i but still show an activity in its absence, explaining the high $\Delta\Psi$ under this condition contrary to the experimentally observed low $|\Delta\Psi|$. In our model, the activation of complex III by P_i is modeled such that at $P_i = 0$ the complex III activity is zero. Hence the respiratory chain is blocked, and $\Delta\Psi$ drops close to zero. But since here the experimentally measured $\Delta\Psi$ is around -145 mV, the RMSD becomes high for the data points at low concentrations of P_i, and by minimizing the RMSD the parameters are adjusted such that the $\Delta\Psi$ increases immediately and extremely for low P_i concentrations, not matching the first data points.
The fitting problem could not be resolved by weighting differently each experimental series or by weighting differently the initial points of the $\Delta\Psi$ curves. Neither did we achieve good results by taking in to account also/or exclusively the distance to the experimental data with respect to the Pi- concentration of the first $\Delta\Psi$data points.

It can be expected that in reality the matrix P_i concentration will not go to zero when the external P_i concentration is zero. Based on this idea, the following two approaches have been tried out for the parameter estimation:

Minimal matrix phosphate concentration We have accorded a minimal matrix phosphate concentration Pi_x^0 to the reactions catalyzed by the following components: dehydrogenase, complex III and F_1F_o -ATPsynthase. The phosphate-proton symport (PiHt)over the inner membrane has not been taken into account, since for external $P_i = 0$, there would always be an outward flux. This is also the reason why Pi_x^0 could not directly be set as constraint for the state variable Pi_x. But still, negative Pi_x for $Pi_e = 0$ occurred during integration of the model (using Matlab), albeit the constraint was set that all concentrations must be ≥ 0.

Table 4.5.: Adjustable parameters of the models. The parameter values have been estimated using a genetic algorithm and a subsequent refinement by a local fitting routine, see also section 4.4.1.

parameter	Beard's model	our model	unit	remark
r	6.0551	12.751		equilibrium constant of dehydrogenase reaction (simplified Krebs cycle)
k_{Pi_1}	0.00029908	0.0006305	M	Pi activation of dehydrogenase reaction
k_{Pi_2}	0.001296	0.0027854	M	Pi activation of dehydrogenase reaction
k_{Pi_3}	0.00065249	0.005663*	M	Pi activation of complex III
k_{Pi_4}	0.72235		M	Pi activation of complex III
k_{PiHt}	0.40709	3.3946	M	H_2Pi_i-binding constant on Pi/H^+ symporter
x_{DH}	0.079819	0.040316	$mol\,s^{-1}\,M^{-1}L_{mito}^{-1}$	rate constant of dehydrogenase reaction
x_{Krebs}		0.020158	$mol\,s^{-1}\,M^{-1}L_{mito}^{-1}$	rate constant of dehydrogenase reaction with respect to succinate production
x_{C_1}	0.73192		$mol\,s^{-1}\,M^{-1}L_{mito}^{-1}$	rate constant of complex I
x_{C_3}	0.12192		$mol\,s^{-1}\,M^{-1}L_{mito}^{-1}$	rate constant of complex III
x_{C_4}	7.1691e-05		$mol\,s^{-1}\,M^{-1}L_{mito}^{-1}$	rate constant of complex IV
x_{F_1}	478.4798		$mol\,s^{-1}\,M^{-2}L_{mito}^{-1}$	rate constant of F_1F_O-ATPsynthase
x_{ANT}	0.0077587	316.04	$mol\,s^{-1}\,M^{-1}L_{mito}^{-1}$	rate constant of adenine nucleotid transport
x_{PiHt}	253940000	10^9	$mol\,s^{-1}\,M^{-1}L_{mito}^{-1}$	rate constant of phosphat-proton symport
x_{KH}	10^9	267090000	$mol\,s^{-1}\,M^{-2}L_{mito}^{-1}$	rate constant of K^+/H^+-exchanger
x_{H_le}	336.7397	441.4929	$mol\,s^{-1}\,mV^{-1}\,M^{-1}L_{mito}^{-1}$	rate constant of proton leak
x_K	set to 0	set to 0	$mol\,s^{-1}\,mV^{-1}\,M^{-1}L_{mito}^{-1}$	rate constant of potassium leak
x_{AK}	100000	1000000	$mol^{-1}\,s^{-1}$	rate constant of adenylate kinase
Pi_e^0	6.013e-06	0.00017319	M	minimal external Pi concentration

Minimal external phosphate concentration We assumed that in the external medium a small Pi_e^0 concentration is generally present, which is added to each experimental Pi_e-value, i.e. the Pi_e-axes is slightly shifted. Estimating the parameters under this assumption resulted in a very good data description with our model. For the Beard model there was no benefit, which is due to the different activation factors for complex III.

4.4.3. Description of the experimental data

Applicability of the new rate equations

We have at first refitted the parameters of the Beard model. The experimental data of Bose are well reproduced, with exception of $\Delta\Psi$ for lower P_i concentrations, see figure 4.2. The fitted parameters are listed in table 4.5 and the fixed parameters in table 4.3. Then we used these parameter values except those involved in the respiratory complex rate functions to analyze the general applicability of our new rate equations 2. Therefore we employed the new rate equations for complexes I, III and IV, keeping the V_{max} and

K_m that we have obtained in absence of $\Delta\mu_H$. We made the simple and arbitrary assumption that for the repartition of the gradients impact ΔG_H among the parameter pairs the impact should correspond approximately to the fraction that each parameter pair contributes to the ΔG_0 in absence of the gradient:
ΔG_0 can be represented by the logarithmic Haldane equation

$$\Delta G_0 = RT \cdot \ln\left(\frac{V^+_{max}(0)}{V^-_{max}(0)}\right) + \sum_{j=1}^{n}\left(RT \cdot \ln\left(\frac{K_{P_j}(0)}{K_{S_j}(0)}\right)\right) - RT \cdot \ln K_A(0) + RT \cdot \ln K_B(0) \tag{4.56}$$

where K_A and K_B are Michaelis-Menten that do not occur in a parameter couple and for which we assumed in a first time that they may not be affected by the proton gradient. The arbitrary repartition of the gradient on the parameter couples was then realized by

$$\zeta_j = RT \ln\left(\frac{(K_{S_j}(0)}{K_{P_j}(0)}\right) / \Delta G_0 \tag{4.57}$$

and if this expression was negative, we set $\zeta_j = 0$. The ζ_V were calculated by

$$\zeta_V = 1 - \sum_{j=1}^{n} \zeta_j \tag{4.58}$$

The Bose data set was then simulated for various values of γ_V*, which splits the gradients impact between V^+_{max} and V^-_{max}, According to the simulations in figure 3.5 we restricted the variation of γ_V to the interval [0, 0.2]. The simulations confirm that the new rate equations are in general suitable to describe the Bose experiments, as shown in figure 4.2 where the colored area correspond to the ensemble of simulated curves. Already without fitting any parameter, employing the new rate equations for the complexes I, III and IV lead to a good approximation of the values for $\Delta\Psi$, matrix pH, the respiratory rate and the reduction states of NADH and cytochrome c.
It is to emphasize that hereby it is demonstrated that these equations can establish the link of the kinetic constants obtained for the isolated complexes in absence of a membrane potential and the comportment of the OXPHOS system in the presence of the proton gradient. For this analysis we did not take into account a new rate equation for the ATPsynthase because for this enzyme we have not performed measurements in absence of the gradient and thus we kept the Beard's equations.

When fitting the parameter values of the new rate equations for the complex I, III, IV and the ATPsynthase, expectedly, a very good data description could be achieved, see 4.3. Also the $\Delta\Psi$ values for low P_i concentrations were reproduced correctly.
For the sake of completeness, we allowed the proton gradient to influence also the K_m not appearing in a parameter couple, namely K_{O_2} and K_{P_i} (ATPsynthase). The obtained parameter values are listed in the tables 4.5 and 4.6, the fixed parameters where the same as taken for Beard's model 4.3. To simplify matters, we have assumed that γ_V* has the same value for all OXPHOS complexes. This parameter defines the repartition

Figure 4.2.: General suitability of the new rate equations. The red line represents the fit of the original model (Beard), whereof the full lines are in presence of 1.3 mM ADP (phosphorylating) and the dashed lines are in absence of ADP (non-phosphorylating). We then used the same parameters but replacing complexes I, III and IV by the new rate equations. The green and blue stripes, meaning in presence and absence of ADP, respectively, are obtained by varying the parameter $\zeta*$. This parameter has been varied between 0 and 0.2, i.e. from darker to lighter colors in the figures. Here 0 (1) signifies that the only the backward (forward) velocity is influenced by the gradient for $\Delta G_{int} < 0$ ($\Delta G_{int} > 0$). The impact of the gradient on a Michaelis-Menten constants couple has been roughly approximated by setting $\zeta_i = RT \ln(K_{S_j}/K_{P_j})/\Delta G_0$ if positive, else zero, and $\zeta_V = 1 - \sum_j \zeta_i$. *complex I:* $\zeta_N = 0.22$, $\zeta_Q = 0$, $\zeta_V = 0.78$; *complex III:* $\zeta_Q = 0.05$, $\zeta_C = 0.48$, $\zeta_V = 0.47$; *complex IV:* $\zeta_C = 0$, $\zeta_V = 1.00$. (Remark: the minimal external phosphate concentration in these simulations was $Pi_e^0 = 0.006$ mM. Although this is a relatively low concentration, one cannot see anymore the immediate increase of $|\Delta\Psi|$ from zero high values, which can be observed when applying our rate equations and when starting to increase the external Pi concentration from zero. See section 4.4.2 for more explanations to the behavior of $\Delta\Psi$ at low phosphate concentrations.)

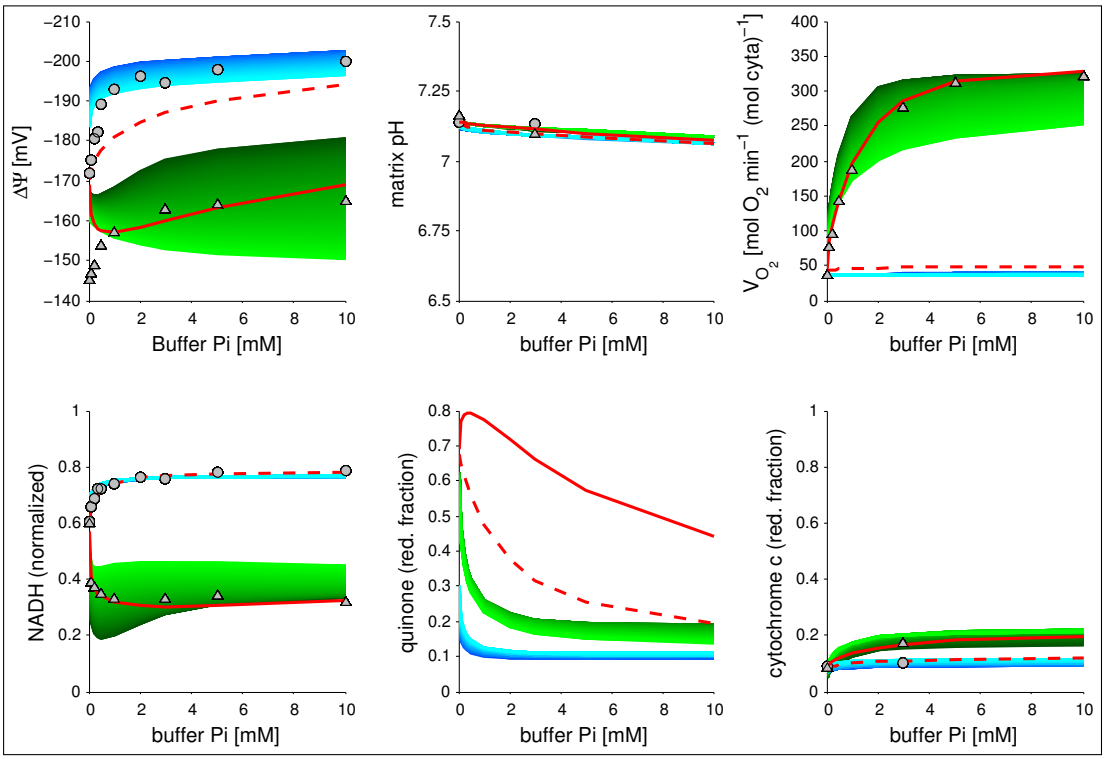

of the gradients impact between the backward and forward velocity constant. It was estimated to $\gamma_V* = 0.0443$, the value being in agreement with the analysis in figure 3.5. If required, a γ_V* could be determined for each complex. All K_m were found to be effected by the gradient. The estimated influence on each K_m value was in all cases in an acceptable range, see table 4.6 and compare to figure 3.1. For complex I and III they correspond surprisingly well to the simple and arbitrary assumption that we have made above, see equations 4.57 and 4.58.

Figure 4.3.: Results of fitting the new model to the Bose data set. The blue lines result from the fits to the combined model, where the original equations of the complexes I, III and IV have been replaced by the new rate equations. The combined model describes well the experimental data, especially now it is possible to reproduce the values of $\Delta\Psi$ for low phosphate concentrations. The dashed lines signify the non-phosphorylating state while the full lines signify the phosphorylating state.

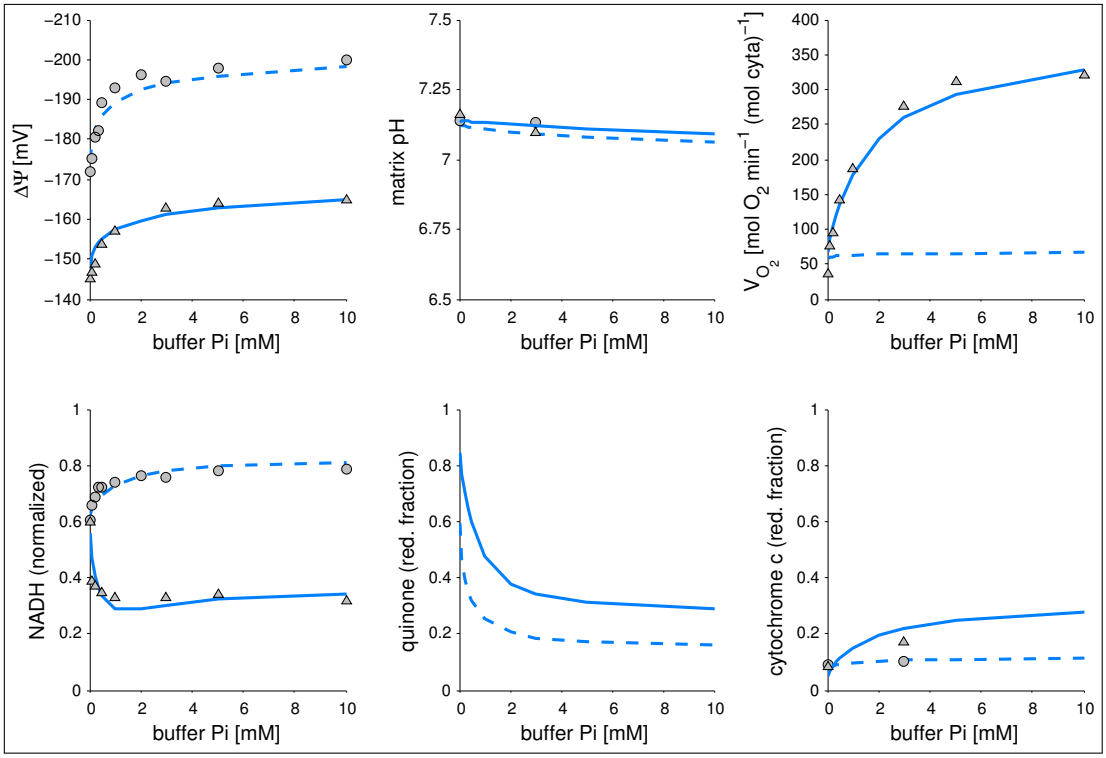

Table 4.6.: Parameters of the new OXPHOS rate equations. The table summarizes the parameters obtained via the initial rate measurements (V_{max} and K_m in chapter 2 and the parameters estimated by fitting to the data of Bose et al. [2003] (ζ and γ). For all complexes the simplified (and generalized) random binding equations has been employed. For complex III, the equation following the net reaction scheme 2.5.1 was taken, with cytochrome c in second order and Q in first order. Complex IV was modeled with first order for cytochrome c. The rate constants k_{C_x} have been calculated by the respective V^+_{max} and V^-_{max} using equation 3.34. The activities of the respiratory chain complexes are referred to the transfer of two electrons (nmol e^-/min/mg prot). The constant $\gamma = 0.5$ was fixed for all Michaelis-Menten constants occuring in pairs (oxidized/reduced). The ΔG_0 were calculated for pH 7.5 for all respiratory chain complexes since the basic kinetic parameters have been determined under this condition. The basis therefore were the ΔG_0 values at pH 7 used in the model of Beard [2005]. For the ATP-synthase we have $\Delta G_0 = 36.03 kJ/mol$kJ/mol for free ATP and ADP, at pH 7.0. But it has to be considered that the ATPsynthase uses exclusively Mg^{2+} bound ATP and ADP, so that $\Delta G_0 \rightarrow \Delta G_0 - RT \ln(K_{MgATP}/K_{MgADP})$. The K_m values from the ATP synthase were taken from Vinogradov [2000]. Note that here the forward reaction corresponds to the hydrolysis of ATP. *For complex II, the K_{suc} that we have determined experimentally was about 2 orders of magnitude higher compared to literature values, see section 2.4. We therefore divided these values by 100 and kept the approximation $K_{suc} = K_{fum}$.

	parameter	value	unit	parameter	value	unit
Complex I	V^+_{max}	1791	nmol/min/mg	ζ_N	0.1757	
	V^-_{max}	$1.1 \cdot 10^{-6}$	nmol/min/mg	ζ_Q	0.0261	
	k_{C_1}	0.0178	M/sec	ζ_V	0.7982	
	K_{NADH}	$4.3 \cdot 10^{-6}$	M	γ_N	0.5	
	K_{NAD}	$780 \cdot 10^{-6}$	M	γ_Q	0.5	
	K_Q	$9.7 \cdot 10^{-6}$	M	γ_V*	0.0443	
	K_{QH2}	$5.3 \cdot 10^{-6}$	M	ΔG_0 (pH 7.5)	-66.4	kJ/mol
Complex II	V^+_{max}	852	nmol/min/mg			
	V^-_{max}	202	nmol/min/mg			
	K_{suc}	$18.796 \cdot 10^{-6}$*	M			
	K_{fum}	$18.796 \cdot 10^{-6}$*	M			
	K_Q	$2.5 \cdot 10^{-6}$	M			
	K_{QH_2}	$1.8 \cdot 10^{-6}$	M	ΔG_0 (pH 7.5)	- 2.9	kJ/mol
Complex III	V^+_{max}	8090	nmol/min/mg	ζ_Q	0.0582	
	V^-_{max}	10.3	nmol/min/mg	ζ_C	0.49386	
	k_{C_3}	0.0582	M/sec	ζ_V	0.44799	
	K_Q	$323 \cdot 10^{-6}$	M	γ_Q	0.5	
	K_{QH_2}	$138 \cdot 10^{-6}$	M	γ_C	0.5	
	$K_{c_{ox}}$	$7.7 \cdot 10^{-6}$	M	γ_V*	0.0443	
	$K_{c_{red}}$	$312 \cdot 10^{-6}$	M	ΔG_0 (pH 7.5)	-38.46	kJ/mol
Complex IV	V^+_{max}	13738/2	nmol/min/mg	ζ_C	0.0806	
	V^-_{max}	$5.2 \cdot 10^{-8}/2$	nmol/min/mg	ζ_{O_2}	0.1516	
	k_{C_4}	0.0745	M/sec	ζ_V	0.7628	
	$K_{c_{ox}}$	$56.1 \cdot 10^{-6}$	M	γ_C	0.5	
	$K_{c_{red}}$	$65.0 \cdot 10^{-6}$	M	γ_V*	0.0443	
	K_{O_2}	$1 \cdot 10^{-6}$	M			
				ΔG_0 (pH 7.5)	-117.01	kJ/mol
ATP synthase	V^+_{max}	4836	nmol/min/mg	ζ_A	0.0668	
	V^-_{max}	$1.78 \cdot 10^{-4}$	nmol/min/mg	ζ_P	0.0902	
	k_{F_1}	0.0552	M/sec	ζ_V	0.8430	
	K_{ADP}	$300 \cdot 10^{-6}$	M	γ_A	0.5	
	K_{ATP}	$100 \cdot 10^{-6}$	M	γ_V*	0.0443	
	K_{Pi}	$1000 \cdot 10^{-6}$	M			
				ΔG_0 (pH 7.0)	-29.15	kJ/mol

4.5. Analysis and Simulations

In this section, the model is analyzed and used for simulations. In both cases, the results are not complete since the work is still under progress. But already the present status gives a good idea of the performance of the new model. All simulations were performed using Matlab R2012b [MathWorks, 2012].

4.5.1. Complex II as electron entry point

We kept the same parameter values as for the previous simulation but used complex II instead of complex I as electron entry point into the respiratory chain. We modeled the recycling of fumarate into succinate similar as it is done for the dehydrogenase reaction for the NADH recycling:

$$J_{Krebs} = x_{Krebs} \cdot (r \cdot [fum]_x - [suc]_x) \cdot \frac{1 + \frac{[P_i]_x}{k_{Pi_1}}}{1 + \frac{[Pi]_x}{k_{Pi_2}}} \tag{4.59}$$

.
Since the dehydrogenase reaction is representing the Krebs cycle, one can make the rough approximation that for the degradation of one molecule of pyruvate 4 NAD^+ and one molecule of succinate are produced. Hence we set the rate constant $\mathrm{X_{Krebs}} = 0.25 \cdot \mathrm{X_{DH}}$. The inclusion of complex II entails only minor changes for the ODE system 4.1: We need to introduce an ODE for succinate and adjust the ODE for QH_2.

$$\frac{d[suc]}{dt} = (+J_{Krebs} - J_{C_2}) / V_x \tag{4.60}$$

$$\frac{d[QH_2}{dt} = (+J_{C_1} + J_{C_2} - J_{C_3}) / V_m \tag{4.61}$$

$$\tag{4.62}$$

Further we add the following entry to the list of constraints, see table 4.2:

$$[fum] = S_{tot} - [suc] \tag{4.63}$$

where S_{tot} is the total concentration of succinate and fumarate.
For the simulations with complex II, we set $J_{C_1} = J_{DH} = 0$. Figure 4.4 shows that the system complex II + III + IV produces under phosphorylating conditions oxygen consumption rates similar to those of the system with complex I as electron entry point. $\Delta\Psi$ is a little lower. Under non-phosphorylating conditions, we obtain however a higher gradient and consequently a higher proton leak flux.

At least for the model, one can state, that both systems are comparable with respect to their performance. But it has also to be considered that complex II is not pumping protons. Hence the higher gradient and higher leak-flux under non phosphorylating conditions (state 4) must be accompanied by a higher turnover of complex III and IV,

thus complex II is pushing the system stronger. On the contrary complex I is here rate limiting. This is also consistent with our finding that complex I has the slowest catalytic activity of the three proton pumping complexes in absence of the gradient, see table 2.13, but it has also to be considered that the V_{max} decreases when $\Delta\mu_H$ increases, and the extent may vary among the complexes.

Figure 4.4.: Electron entry into the respiratory chain via complex II. The results of the simulations are similar to those obtained for complex I as electron entry point. For comparison, we replotted the experimental points obtained for complex I as electron entry, see also figure 4.3. Under non phosphorylating conditions (dashed lines) the values for $\Delta\Psi$ are higher, resulting in a higher proton leak flux which explains the higher oxygen consumption rate. This indicates that complex II can push the system stronger than complex I. Under phosporylating conditions (full lines), a similar respiratory rate is obtained, while $|\Delta\Psi|$ is nearly 10 mV lower. For the simulations the same parameters have been used as for the system complexes I + III + IV. Except the rate constants for the dehydrogenase reaction and complex I, i.e. x_{DH} and k_{C1} have been set to zero. The recycling of fumarate into succinate was modeled in analogy to the dehydrogenase reaction, see 4.59. Its rate constant x_{Krebs} was set to $0.25 \cdot x_{DH}$, in order to account for the rough approximation that per molecule of pyruvate four NAD^+ are reduced but only one succinate is produced. For the simulations we set the sum of the succinate and fumarate concentrations to 100 times K_{suc}.

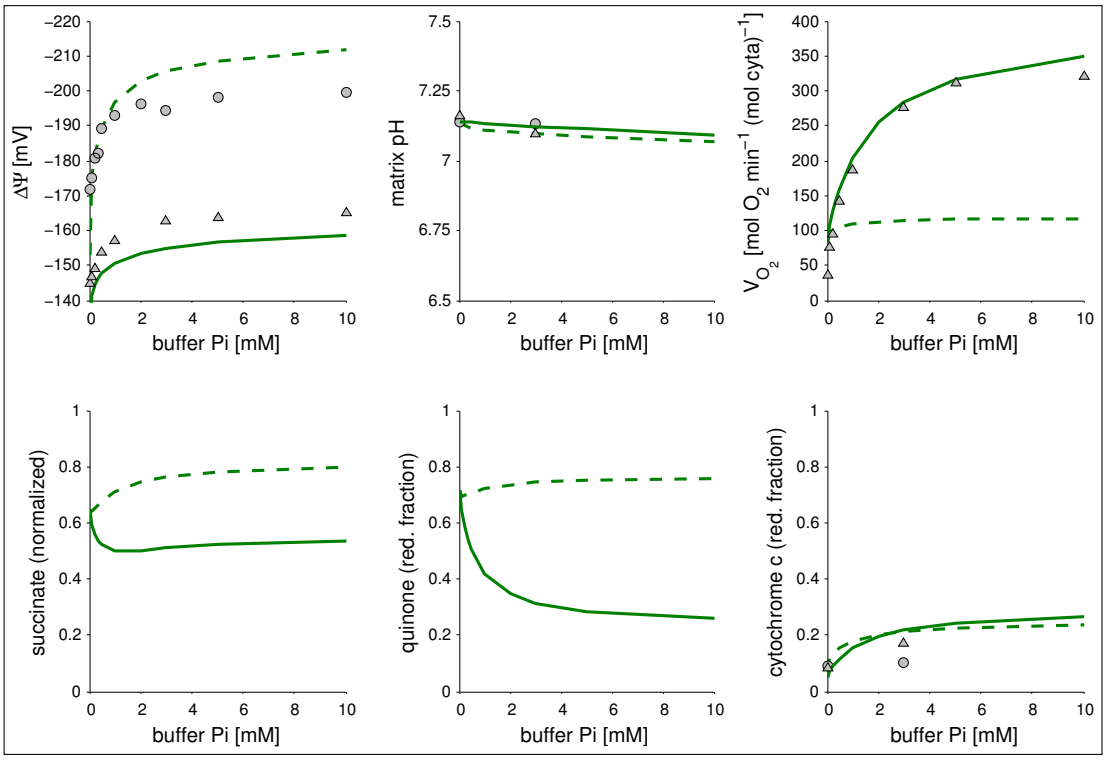

4.5.2. Robustness of the model with respect to the apparent Michaelis-Menten constants of the quinones and quinols

The values for the K_Q and K_{QH_2} that we have determined in chapter 2 for the respiratory complexes I, II and III are apparent K_m. Their values referred to the volume of the reaction medium. However the real K_Q and K_{QH_2} should refer to the Q and QH_2 concentrations that were indeed in the inner membrane fragments, because this presents the real concentration at the Q binding sites. Further we have discussed in section 2.2.6 that quinones used for kinetic assays may have other properties than the physiological coenzyme Q_{10} which may change their affinity to the binding sites.
It is thus worth to examine the robustness of the model with respect to the K_Q and K_{QH_2} values, which we have done for complex I and III. We have assumed that for a given complex, K_Q and the respective K_{QH_2} change in the same extent, which corresponds to a given factor between apparent and real concentrations. This is necessary in order to respect the Haldane equation 3.10 and hence thermodynamics.

Under non phosphorylating conditions (state 4), the K_m for complex I has practically no influence over a very wide range, for complex III the K_m start having an effect only when increasing them more then 100 times, see figure 4.5. Under conditions where phosphorylation takes place (state 3), the respiratory chain features are still insensitive to the variations of the K_m for complex I, but changes in the K_m for complex III is now important: With increasing K_m, the respiration rate and $|\Delta\Psi|$ decrease significantly, see figure 4.6.

The total quinone pool size used in the model is with 1.35 mM largely above the values of the K_Q and K_{QH_2}: two orders of magnitude higher with respect to complex I and one order of magnitude higher with respect to complex III. Hence a certain robustness is not surprising. Fato et al. [1996] estimates the quinone K_m in the membranes to be much higher which would render the models much more sensitive to the K_m.

4.5.3. Flux-inhibition curves

In a metabolic network, the decrease of an enzyme's activity results in a decline of the global flux through the corresponding part of the system. The way the latter responds to this perturbation is dependent on the network structure and on the kinetic properties of the involved enzymes. The flux inhibition as a function of the enzyme inhibition can present different shapes between two extremes. A proportional decrease of the flux or a threshold curve, i.e. a slow decrease until a threshold (threshold in enzyme inhibition) and then a rapid decrease to zero.
In our case, we consider the respiration rate at steady state as a function of the inhibition of an OXPHOS complex. In addition to a classical enzyme system, the inhibition curves are further influenced by the $\Delta\Psi$ and ΔpH that they are maintaining. We consider in this work threshold curves at state 3 and state 4 respiration, i.e. the system is phosphorylating ADP or not, respectively.

Figure 4.5.: Variation of the Michaelis-Menten constants for quinone and quinols at non phosphorylating state. The models turns out to be very robust with respect to changes in the values of K_Q and K_{QH_2} for complex I and III. For a given complex, these parameters have been varied in the same extent, in order to keep to the thermodynamical constraint given by the Haldane equation 3.10. The x- and y-coordinates represent the factor that is applied on K_{Q_2} and K_Q of complex I and complex III respectively, their originally values correspond thus to the (x,y) coordinate (1,1).

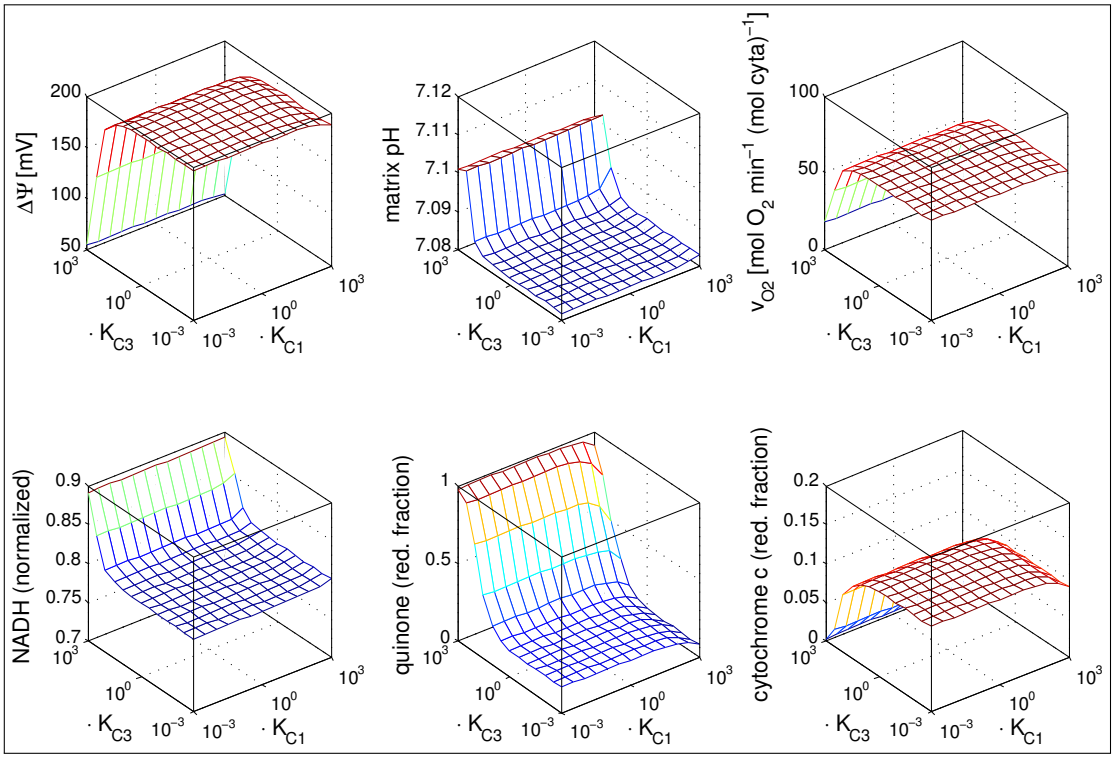

Figure 4.6.: Variation of the Michaelis-Menten constants for quinone and quinols under phosphorylating conditions. In comparison to non-phosphorylating conditions, the model becomes sensitive to K_Q and K_{QH_2} for complex III. See figure 4.5 for more explanations.

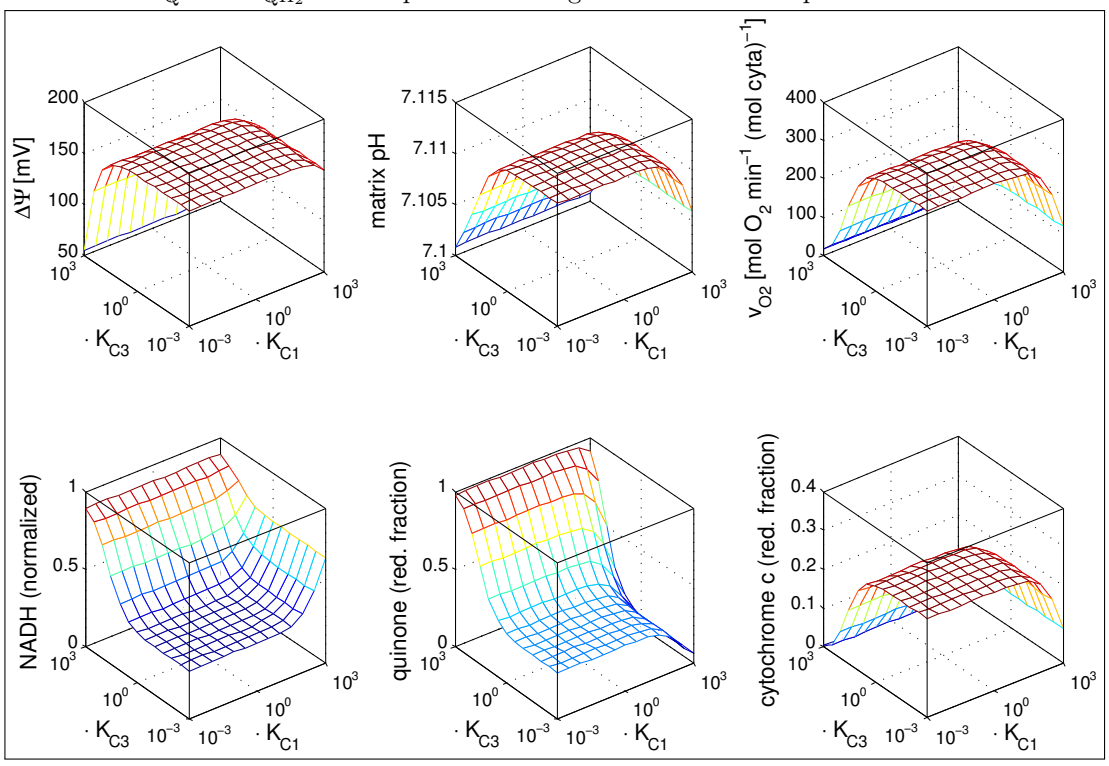

For a given enzyme complex, within the same species but for different tissues, the shapes of inhibition curves can vary significantly for state 3 respiration [Rossignol et al., 1999] as shown in figure 4.7 on the example of complex IV and the ATP synthase. This may be explained by the OXPHOS system being adjusted to the distinct energy demands of the tissues, reflected in the relative amount of the single OXPHOS complexes, their activities and the abundance of the intermediates and their reduction states, which are compared in the work of Benard et al. [2006].

Figure 4.7.: Shapes of threshold curves. Within one species and for a distinct OXPHOS complex, the shapes of the threshold curves can vary significantly, here shown on complex IV and the ATPsynthase for heart and skeleton muscle, brain, liver and kidney at respiratory state 3, i.e under phosphorylating conditions. The images are taken from Rossignol et al. [1999] and were edited for better readability.

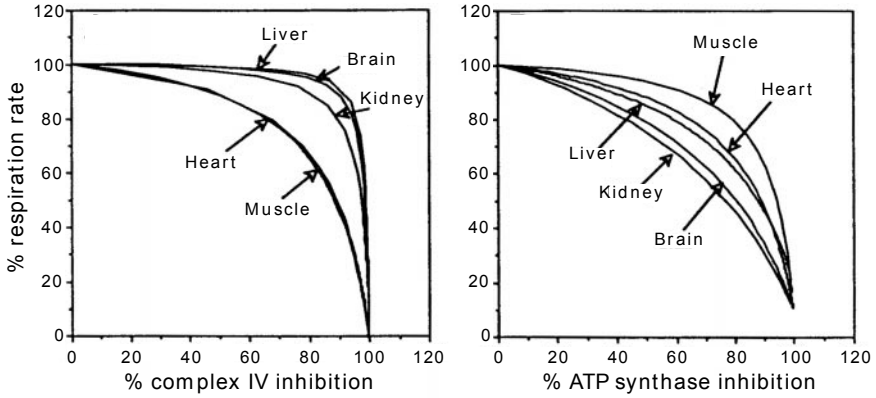

But besides the threshold shaped inhibition curves also proportional relationships between respiration rate and inhibition of a given OXPHOS complex have been revealed [Genova et al., 2008]. This behavior is probably due to substrate channeling between the complexes which can assemble to supercomplexes. We have started to regard this issue and have developed two models to analyses the supercomplexes kinetics. The results are preliminary and are listed in the Appendix B.

Inhibition curves for the subsystem CI + CIII + CIV

The inhibition curves simulated with our model for the system CI + CIII + CIV reproduces well the observed experimental threshold curves at *state 3* recorded by [Rossignol et al., 1999] on rat heart mitochondria, see figure 4.8. It shall be pointed out that the used parameters are those fitted in section 4.3, with Bose's data.
All simulated curves have a similar threshold shape: in each case pronounced threshold is found. The simulations with our model reveal further, that until 90% of inhibition of a given respiratory chain complex the $\Delta\Psi$ decreases only very little, but after the threshold a strong decrease is observed. Expectedly, the inhibition of the ATPsynthase shows an

Figure 4.8.: Simulation of threshold curves at state 3. a) Beard's model (black line) cannot reproduce the respiration rates as a function of complex I, III, IV or ATP synthase inhibition, respectively. b) With our model, the threshold curves for the respiration rates are well described, with a minor discrepancy for complex III. Besides the respiration rate, also $\Delta\Psi$ and the matrix pH are plotted versus the inhibition of the OXPHOS complexes. It is remarkable that both remain constant over a very wider range. The experimental data on rat heart mitochondria are taken from Rossignol et al. [1999]. The data points were extracted from the figures using the digitizing software *engauge* (http://digitizer.sourceforge.net). For complex IV and the ATP synthase the threshold curves were only sketched (see figure 4.7). Here we took just some points that permit to have representation of these curves.

a

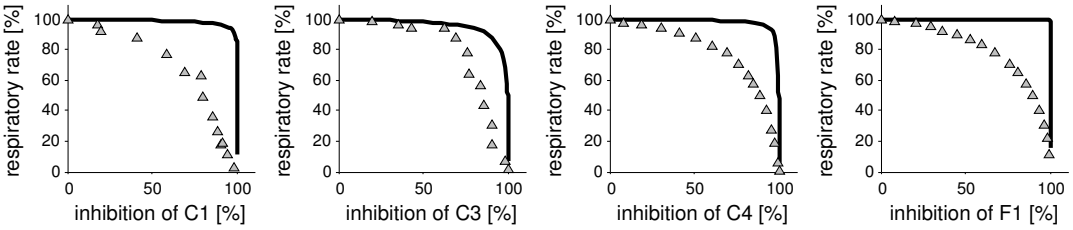

b

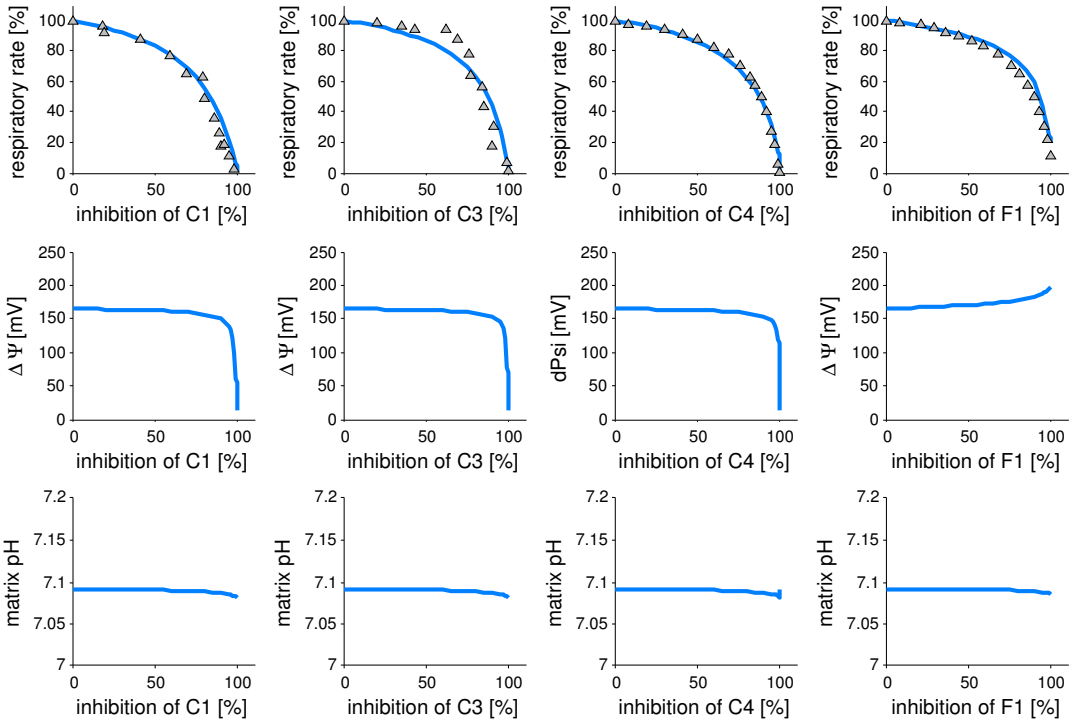

inverse effect: a slow increase somewhat more pronounced after 90% of inhibition finally reaching the $\Delta\Psi$ value of state 4 respiration. For all complexes the matrix pH decreases also very slightly, which is obvious because there is only a small latitude with respect to the cytosolic pH.
In contrast, with Beard's model, extremely high thresholds for each OXPHOS complex are observed and do not at all reproduce the experimental data. This large discrepancy is very probably due to the kinetics of the OXPHOS complexes modeled with mass action law. Shapes of inhibition curves that are similar to those obtained experimentally are only possible with Beard's model when the rate constants of the complexes are set to very small values. But then the respiratory chain features, represented by the data set of Bose et al. [2003],see figure 4.59, cannot be approached at all (not shown).

At state 4 respiration the shapes of the inhibition curves change completely exhibiting a very high threshold, see figure 4.9. This is in good agreement with the tendency observed experimentally by Genova et al. [2008] for complexes I and III in rat liver mitochondria and by Quarato et al. [2011] for complex IV in the human hepatic cancer cell line HepC2. However these experimental data show lower thresholds at state 3 and 4 than we obtained with our model. An explanation may be the difference in tissue, see also figure 4.7. Further the model takes so far not into account the formation of supercomplexes, which can significantly influence the shapes of the threshold curves. A preliminary modeling approach for supercomplexes can be found in the appendix B.

Figure 4.9.: Threshold curves at state 4. High thresholds are observed for the inhibition of complex I, III and IV, respectively. This indicates that when the system is not phosphorylating, the control on the respiration rate is highly exerted by the proton leak flux. As expected, the inhibition of the ATPsynthase does not influence the respiration rate at state 4.

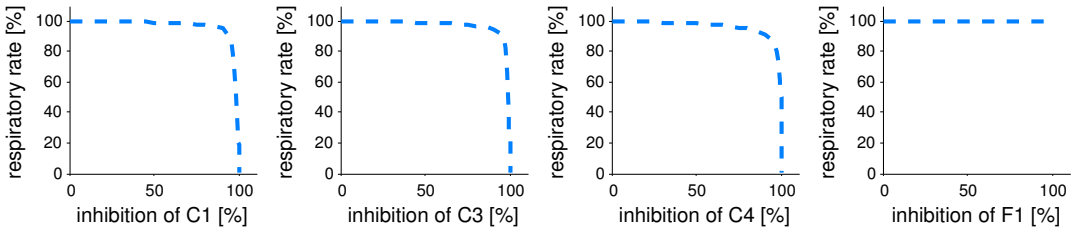

The steeper the slope of decrease of the respiration rate with the inhibition of a complex, the higher is the control on the global rate by the latter. A linear decrease throughout from 100% to 0% activity corresponds to a flux control coefficient of 1. The curves show that at state 3 initially none of the complexes have a strong control, but the control is rising constantely with increasing inhibition of the complex, the control coefficient is finally approaching 1. At state 4, we find nearly up to complete inhibition a very low control, which changes quasi instantly after the point of threshold to a high control. This threshold shift due to the transition from state 3 to state 4 respiration is expected since to maintain state 4 respiration a much lower number of respiratory chain complexes is

necessary, thus the inhibition becomes only remarkable at over 95 %. Here the control is mostly excerted by the proton leak flux.

Inhibition curves for the subsystem CII + CIII + CIV

The threshold curves arising from the system with complex II as electron entry point are shown in figure 4.10. With respect to the complexes III and IV the behavior is similar compared to that of the subsystem with complex I as electron entry point. In contrast the inhibition curve of complex II under phosphorylating conditions is closer to a linear shape. This indicates a stronger control exerted by complex II than by complex I, although the respiration rates themselves are very similar for the two electron entry points, compare figures 4.3 and 4.4. The simulations show that it is mostly the ATPsynthase that compensates with a lower control (high threshold) the higher control of complex II (low threshold).

Figure 4.10.: Threshold curves of the system CII + CIII + CIV. Under phosphorylating conditions (full line) the inhibition of the complexes III and IV show similar threshold curves compared to the system with complex I as electron entry point. In contrast, the threshold curve of complex II is closer to a linear dependency than that for complex I, indicating a higher control. This is compensated by the inhibition curves for the ATP synthases, where a higher threshold is exerted in case of the system CI + CIII + CIV. At state 4 (dashed line), the threshold curves for the respiratory chain complexes are very high. This means that over a large extend of inhibition they have nearly no control on the respiration rate. Expectedly, under non phosphorylating condition the inhibition of the ATP synthase does not show an effect on the respiratory rate

.

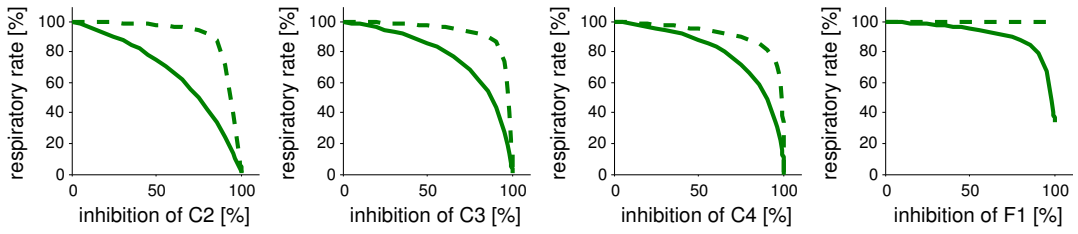

Inhibition curves for uncoupled mitochondria

We simulated uncoupled mitochondria by setting the rate of the proton leak flux to a very high value ($x_{Hle} = 5 \cdot 10^5\, s^{-1}\, mV^{-1}$), see figure 4.11. In absence of the proton gradient, the threshold curves do not significantly differ whether ADP is present or not. Since the ATPsynthase only phosphorylates ADP when a physiological important membrane potential is given, and since the absence of ATP did not allow for ATP hydrolyzes, this enzyme was not of interest in these simulations.

For both systems, i.e. with complex I or complex II as electron entry point, one can see that generally the thresholds are more pronounced than in presence of the gradient.

This was expected, since in this conditions the respiratory complexes have much higher capacities with respect to their rates, and hence they have to be strongly inhibited in order to obtain a decrease of the respiratory rate.
Further the thresholds are increasingly pronounced in the order CI/CII - CIII - CIV, see figure 4.11. This hierarchy vanishes in presence of the membrane potential, and for the system C1 + C3 + C4 the gradient causes a similar control strength among the complexes when the system is at state 3 respiration. The inhibition curve for complex II only slightly changes its behavior whether the proton gradient is present or not and its relatively high control remains. This is in agreement with complex II kinetics not being influenced by the gradient.

Figure 4.11.: Threshold curves in absence of the electrochemical gradient. a) System CI + CIII + CIV. b) System CII + CIII + CIV. Expectedly for both systems the thresholds of the complexes are more pronounced in absence of the gradient, since their capacities are large with respect to their maximal rates, not being slowed down by the gradient. Only the complex II inhibition curve does not change much whether the gradient changes or not This consistent with this enzyme not being influenced by the proton gradient. Its relatively high control remains. For both systems, with increasing order of the enzyme, the thresholds are more pronounced.

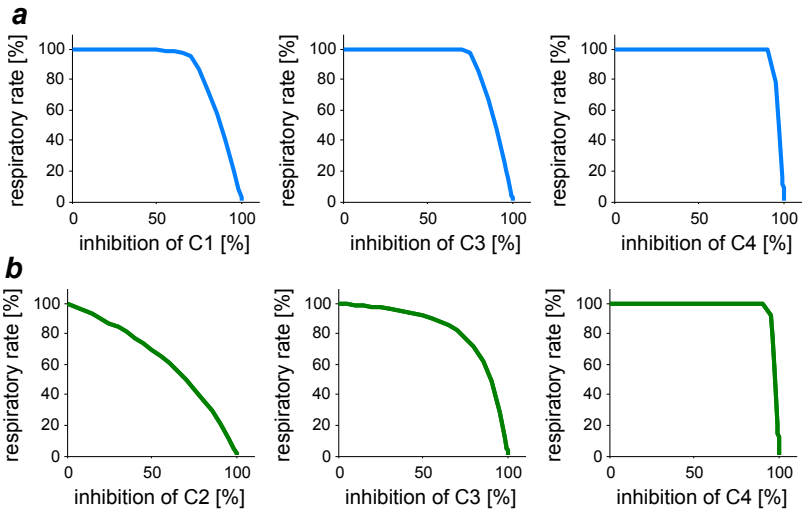

4.5.4. The proton/ATP ratio of the ATPsynthase

Until now the ratio of H^+/ATP (n_A) has been set to 3, as it has been done in the model of Beard [2005]. However, this stoichiometry can differ across species Watt et al. [2010], von Ballmoos et al. [2009]. Structural constraints suggest for yeast is $n_A = 10/3$ [Stock et al., 1999] and for bovine tissue $n_A = 8/3$ Watt et al. [2010]. As mentioned before deviations from these structural constraints were found in experiments, and hence one can not deduce thereof the exact number of the proton/ATP ratio [Petersen et al., 2012]. Despite the uncertainty, it is worth to consider the aspect of differences in the number of protons/ATP among the different species. The value of n_A has a non-negligible effect

on the thermodynamics since it shifts the Gibbs energy available by proton transfer to drive the phosphorylation of ADP: while - if the structural constraints are respected - in yeast the energy of 10 vectorial protons are used to drive the phosphorylation of three molecules of ADP, in bovine tissues this driving force must be met by only 8 vectorial protons. That means that if in both organisms the same total energy per synthesis of one molecule of ADP shall be provided, the electrochemical gradient in bovine tissues would have to be 10/8 times stronger than in yeast.

Figure 4.12.: Variation of the proton/ATP ratio of the F_1F_0-ATP-synthase. Simulation of the Bose data for $n_A = 9/3$ (blue), $n_A = 10/3$ (black) and $n_A = 8/3$ (red), all other parameters are fixed to the same values. For yeast ($n_A = 10/3$) $|\Delta\Psi|$ is decreased and the oxygen consumption rate is elevated, while in bovine tissue ($n_A = 8/3$) the contrary can be observed.

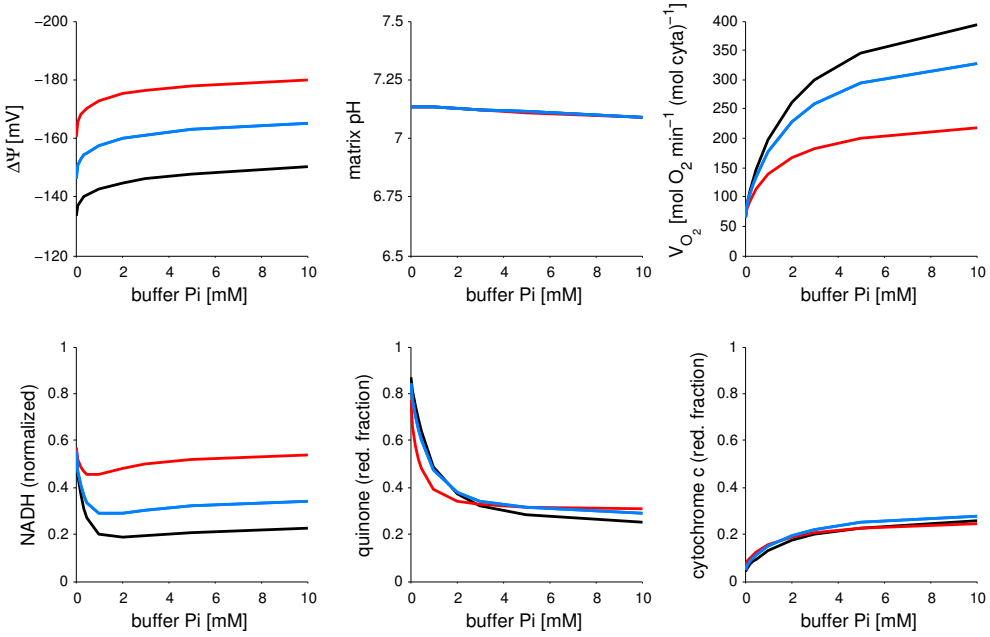

In figure 4.12 the effects of setting n_A to 8/3 and 10/3 are compared to $n_A = 3$ are illustrated. All other parameter values remained fixed. The plots show that the proton/ATP ratio can strongly influence the comportment of OXPHOS. The elevated $|\Delta\Psi|$ in case of $n_A = 8/3$ is in agreement with our considerations above. The respiratory rate is here slower. For $n_A = 10/3$ the contrary can be observed. However this behavior is of course also dependent on the other adjustable parameters of the model. A new estimation of their values should reduce the effects.

It would be interesting to compare the performance of the OXPHOS in both species, taking into account the relative amounts of OXPHOS complexes. For instance, here we have not considered that *saccaromyces cerevisiae* does not contain complex I but alternative

NADH dehydrogenases, catalyzing the same reaction as complex I but without coupling them to proton translocation. The comparison would be in particular interesting to investigate these systems with respect to energy efficiency and metabolic rate.

4.5.5. Simulation of time courses

So far, only the model behavior with respect to steady states has been analyzed. We examine now the models ability to reproduce time courses. Therefore some modifications have to be done.

Modifications of the model for the simulation of time courses

For the time course simulations the oxygen concentration is no longer fixed, as well as the concentrations in the surrounding medium are treated as state variables, this concerns ATP_e, ADP_e and their Mg^{2+} bound forms as well as AMP_e, Pi_e and Mg_e. Further in the intermembrane space, Mg_i has been set variable.
The ODE system 4.1 has been extended for the following components:

$$\frac{d[O_2]}{dt} = -0.5 \cdot J_{C_4}/(W_x + W_m + W_i + W_e) \tag{4.64}$$
$$\frac{d[ATP]_e}{dt} = (-J_{ATPm} - J_{ATPf})/W_e \tag{4.65}$$
$$\frac{d[ADP]_e}{dt} = (-J_{ADPm} - J_{ADPf})/W_e \tag{4.66}$$
$$\frac{d[AMP]_e}{dt} = -J_{AMP}/W_e \tag{4.67}$$
$$\frac{d[mATP]_e}{dt} = (-J_{ATPm} + J_{MgATPe})/W_e \tag{4.68}$$
$$\frac{d[mADP]_e}{dt} = (-J_{ADPm} + J_{MgADPe})/W_e \tag{4.69}$$
$$\frac{d[Pi]_e}{dt} = -J_{Pi2}/W_e \tag{4.70}$$
$$\frac{d[Mg]_i}{dt} = (-J_{MgATPi} - J_{MgADPi} + J_{Mg})/W_i \tag{4.71}$$
$$\frac{d[Mg]_e}{dt} = (-J_{MgATPe} - J_{MgADPe} - J_{MgAMPe} - J_{Mg})./W_e \tag{4.72}$$

W_e represents the external volume and was set to $W_e = 1000 \cdot W_m$. The external fluxes of the Mg^{2+} binding to ATP and ADP, i.e. J_{MgATPe} and J_{MgADPe}, were modeled as their counterparts in the intermembrane space and in the matrix. The same diffusion law between the intermembrane space and the external medium as for Pi has been applied for Mg^{2+}.
With respect to the constraints listed in table 4.2 the following items were removed:

4.42, 4.44, 4.45, and 4.46. Further, one constraint was added:

$$fATP_e = ATP_e - mATP_e \tag{4.73}$$

Time course simulations

Figure 4.13 shows time courses of $\Delta\Psi$ where complex IV was stepwise inhibited under phosphorylating and non phosphorylating conditions. They could be well reproduced. It could also be simulated that when ATP is present, gained from the phosphorylation of ADP during the experiment, the depolarization of $\Delta\Psi$ was less strong. To model the inhibition of complex IV by hydrogen cyanide (KCN) we assumed non-competitive inhibition and multiplied the complex IV rate with the following factor:

$$f_i = \frac{Ki_{KCN}}{Ki_{KCN} + [KCN]} \tag{4.74}$$

For the simulations we used $Ki_{KCN} = 5\mu$M and the KCN concentrations were the same as applied in the experiments.

Figure 4.13.: The electric gradient at state 3 and 4 and the effect of inhibiting complex IV. a) Experimental data taken from Quarato et al. [2011]. b) Simulations. The time courses of $\Delta\Psi$ for a stepwise inhibition of complex IV could be well reproduced under phosphorylating and non phosphorylating conditions, but when finally adding a decoupler, simulated by increasing the proton leak flux rate constant $x_{H_{le}}$ 1000 fold, we observed a strong drop of $\Delta\Psi$ in the model however this was not observed experimentally. Interestingly, when ATP is present, gained from the phosphorylation of ADP during the experiment, the depolarization of $\Delta\Psi$ was less strong. Remark: the time scales of the simulation is different and can be corrected by adjusting the volume of mitochondrial/external volume.

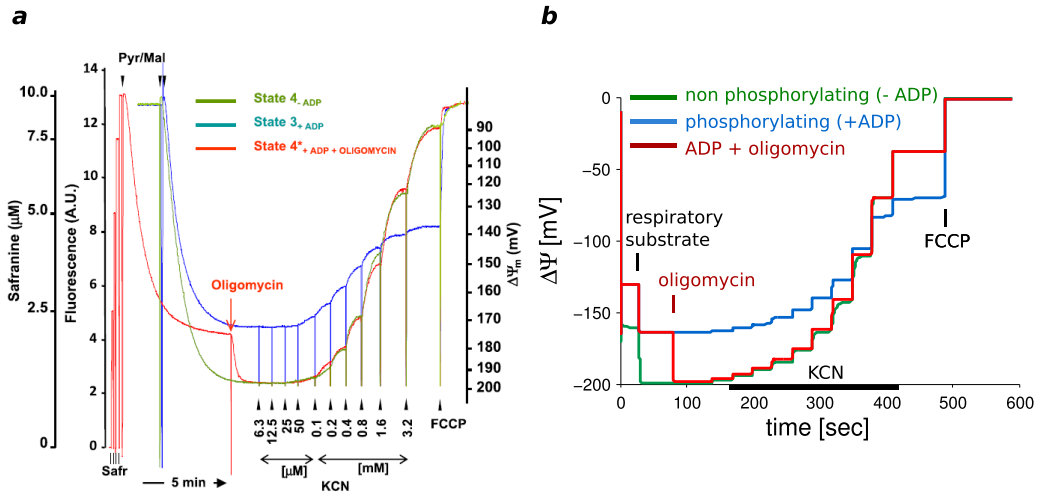

When an uncoupler was added, which makes the membrane well permeable for protons, $\Delta\Psi$ reaches about -70 mV. In the simulations, where the uncoupling is modeled by in-

creasing the proton leak rate constant $x_{H_{le}}$ 1000 fold, we observed a strong drop of $\Delta\Psi$ to near zero. Expectedly, our model cannot account for the resting potential of the membrane: the latter is due to impermeable charged particles like proteins, but such components are not considered so far.

We have further simulated a classical respiration time course which we took from Bose et al. [2003], this time course is one of those which have been used to obtain the data for the above shown general respiratory chain features. The time course data describe the behavior of oxygen consumption after subsequent addition of respiratory substrate, P_i and eventually ADP until all oxygen has been consumed. Also the corresponding data for $\Delta\Psi$ and the normalized NADH concentration were available. We modeled the addition of the respiration substrates glutamate and malate by setting the rate constant x_{DH} of the NADH-dehydrogenase reaction from a low value (0.0042 sec^{-1}) to a high value (0.0403 sec^{-1}).

Our simulations are in good agreement with most of the data. The oxygen consumption rates are well reproduced, only the rate in presence of ADP is described somewhat too low. However the simulated rate is in good agreement with the steady state rates (e.g. figure 4.3) for the given conditions (Pi = 3 mM, ADP = 1.3 mM). The normalized NADH concentrations could be simulated correctly. The values of $\Delta\Psi$ were met with exception of two situations: at the beginning before the addition of respiratory substrate and at the end in anoxia where the simulated values are much too low, see figure 4.14. The fact the resting potential cannot be described with our model can only partly explain this high deviation. In the experiments, the $\Delta\Psi$ in anoxia is presumably maintained by ATP hydrolysis by the reverse ATPsynthase, although the ATPsynthase is under these conditions inhibited by the inhibitory subunit F_1, but the extent of inhibition depends on the organism and is up to around 90 % [St-Pierre et al., 2000].

Simply changing values of the parameters could not resolve this problem. Further we estimate that the discrepancy is not due to the rate equations for the OXPHOS complexes. Indeed the way the ATPsynthase is modeled permits to have reasonable activities when the ADP phosphorylation inverses to ATP hydrolyzes, which is the case in anoxia. This means that that either some other rate equations in the system are not appropriate for the description in the case of anoxia in vitro or that there must be other components play an essential role but are not implemented in the model. The following points may play a role in the maintenance of the proton gradient in anoxia:

- The proton leak flux has generally an important influence on $\Delta\Psi$. The flux taken from the original model is not symmetrical for the influx with respect to the efflux. Further the proton influx has a quite linear flux-$\Delta\Psi$ dependency, however it was experimentally observed to be rather exponential [Divakaruni and Brand, 2011, O'Shea et al., 1984] This issue needs to be investigated further in the modeling.
- The ATP/ADP exchanger (ANT) works only with free ATP and ADP whereas the ATPsynthase involves only the Mg^{2+} bound forms. Thereby also the equilibrium

Figure 4.14.: Time courses: respiration, $\Delta\Psi$ and normalized NADH. a) Experimental data, taken from Bose et al. [2003], for P_i = 3 mM and ADP = 1.3 mM. b) Our simulations were in good agreement with the experimental time course data, with the following exceptions: (i) The value for the oxygen consumption rate after addition of ADP was slower than the experimentally observed one, however it corresponds well to the that given e.g. in figure 4.2, which is from the same publication. (ii) $|\Delta\Psi|$ is too low in absence of respiratory substrate and under anoxia. The numbers above the respiration curves denote the measured oxygen fluxes given in mol O_2/min/mol cyta. The discrepancies for the absolute oxygen concentration indicate that an more precise adjustment of the external volume is necessary, for a higher volume the oxygen concentration decreases less fast.

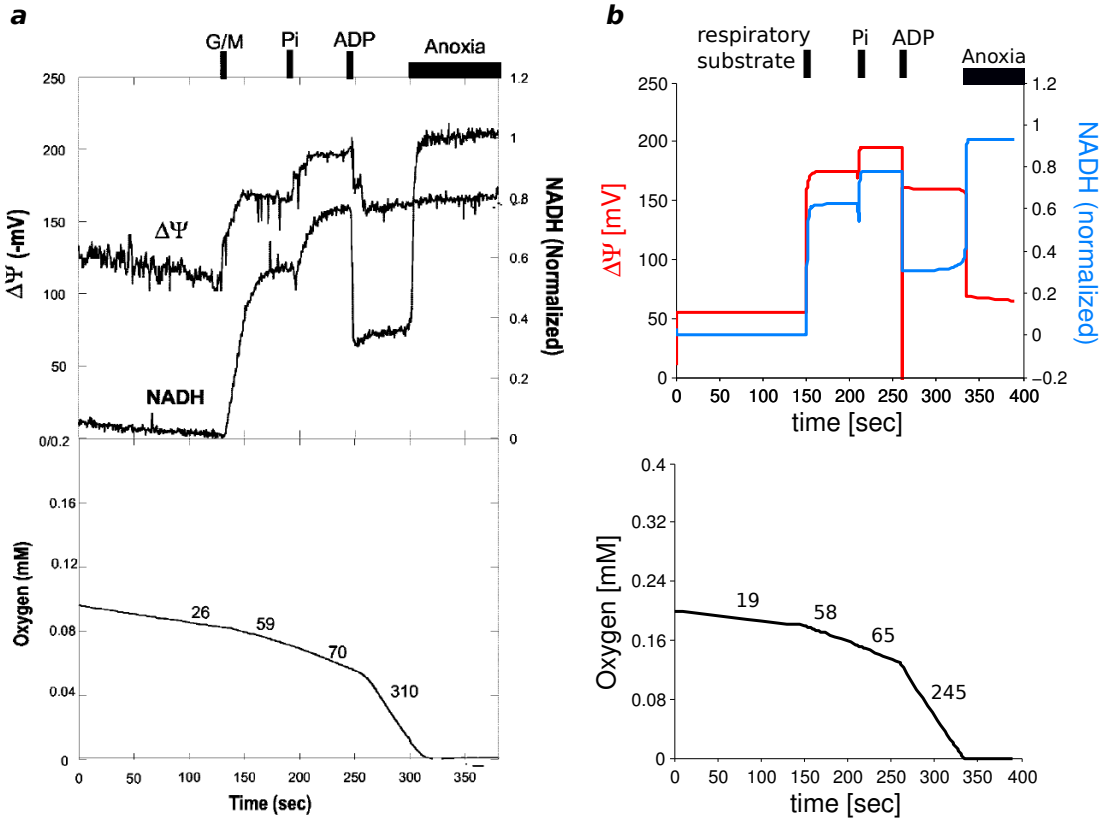

between the bound and free ADP and ATP may play a role. For the ANT it is further to consider that the import of ATP into the mitochondrial matrix corresponds to the net important of a negative charge, hence contributing directly on one hand to the establishment of the gradient but on the other hand, since this transport is not favored by the proton gradient, it will will slow down and thereby slow down the supply of ATP for the ATP hydrolysis.

- Another component that may play in maintaining $\Delta\Psi$ in anoxia is a net transport of mATP into the matrix: This is mediated by the electroneutral phosphate-mATP transporter [Joyal and Aprille, 1992].

- Ions are not considered in the model but may also play a role in maintaining the gradient, e.g. mitochondria are known to be able to uptake large quantities of Ca^{2+}. Further Cl^{-} may also be involved.

4.6. Summary and discussion

We have integrated the new OXPHOS rate equations into the context of a framework model, that contains the same features as the OXPHOS model of Beard [2005] except for some modifications. The simulations that we have done were in some cases preliminary and require further investigations. But we have so far achieved promising results which show that the model is suitable as a tool for addressing a variety of questions.

Applicability of the new rate equations

We could show that the new equations were applicable for the description of the data set of Bose et al. [2003] which covers essential features of the respiratory chain at state 3 and state 4 respiration: $\Delta\Psi$, the matrix pH, the respiration rate and the reduction state of NADH and cytochrome c, all in dependency on the buffer phosphate concentration.
It confirms that the equations are suitable to link the single complexes kinetics in absence of the proton gradient with the behavior of the OXPHOS system in presence of a physiological proton gradient. This is a new point in OXPHOS modeling since all relatively simple equations that have so far been used in OXPHOS models were not able to account for such a wide span of $\Delta\mu_H$.
Between zero and the physiological $\Delta\mu_H$ we have not yet evaluated the OXPHOS complexes activities as a function of $\Delta\mu_H$ or vice versa. But since the data of Bose, covering a broad interval of $\Delta\Psi$, ranging from -140 mV to -200 mV, could be well described, one can suppose that the respiration rate in the non physiological range of $\Delta\Psi$ is at least reasonably approached. However this should be confirmed with experimental data.
The estimated influence of the gradient on the K_m value was in all cases reasonable, see table 4.6 and compare to figure 3.1. This is an important prerequisite for the analysis of mutations affecting the binding affinities and their consequences to the whole system.

Simulations

A good validation of the new model was the simulation of the respiratory rates in dependence on the degree of inhibition of an OXPHOS complex: without adapting any parameter (after the parameter estimation based on the Bose data), the experimental curves could be precisely reproduced. The model of [Beard, 2005] could not reproduce the inhibition curves and [Korzeniewski and Mazat, 1996] needed to modify the rate equations for the respiratory chain complexes in order to make possible the simulation of such inhibition curves.
The system was robust to changes in K_{QH_2} and K_Q of the complexes I and III, in particular for state 4 respiration, due to a highly saturating total concentration of quinone. This can compensate to a certain extent (i) the use of decylubiquinone instead of the natural CoQ in the experiments, having different properties and (ii) the probably underestimated values of the apparent K_{QH_2} and K_Q , since in the measurements the quinone concentrations were referred to the whole reaction volume and not to the volume of the membrane. Fato et al. [1996] estimates that the difference of the apparent Q concentrations to the real concentration in the membrane can be quite large (factor 100), so that at state 3 respiration, the system might be indeed sensitive to the K_m of the quinones, which would then be important for the regulation of the system.

This might also be an explanation for the elevated fraction of reduced quinones in the simulations: in both systems, with complex I or complex II as electron entry point, and for phosphorylating and non phosphorylating conditions, the reduction state of quinone is around 20 % up to much higher values, but the values that have been observed experimentally are much below for rat heart mitochondria, i.e. around 1.9 % [Benard et al., 2006]. The author states that not all of the quinones might be engaged in the respiratory chain and mentionned the possibility of different Q pools.

The simulations with complex II as electron entry point showed that at state 4, this enzyme complex can push the system to higher values of $|\Delta\Psi|$ and higher respiration rates, because it is not sensitive to the proton gradient. This indicates that under this condition complex I is rate controlling. At state 3, $\Delta\Psi$ was lower for the system CII + CIII + CIV while the respiration rate was similar, which is coherent with the fact that here 4 protons are lacking per 2 electrons entering the respiratory chain.
It would be very interesting, to analyze the competition between these complexes. The availability of NADH and succinate is interdependent because both are linked to the Krebs cycle. It is also important for respiration of fatty acids because their degradation (β-oxidation) gives simultaneously NADH and $FADH_2$ Hence an integration of this metabolic pathway into the model would be necessary to reproduce a realistic basis for analyzing this problem. A good basis to model this aspect could be the simple Krebs cycle model that we have proposed before Nazaret et al. [2009], or the more extensive model of Wu et al. [2007].
In this regard it is also necessary to take into account different (combinations of) respiratory substrates, which favor either complex I or complex II [Gnaiger, 2009]. This would

however require the integration of respective transporters over the inner membrane, for glutamate, malate, succinate , etc.

The simulations of the consequences of using for the synthesis of ATP either a proton/ATP stoichiometry of $n_A = 10/3$ or $n_A = 8/3$, which are suggested by the structures of yeast and bovine ATPsynthase, respectively, showed that for the lower ratio one can expect higher values for $|\Delta\Psi|$ and a lower respiration rate, while for the higher ratio the inverse is the case. This is consistent with the fact that if less protons are used to catalyze the reaction, they must be more 'energetic'. It has been stated that one cannot conclude directly from the structure of the ATPsynthase to the real stoichiometry, since also smaller n_A values have been measured experimentally than those indicated by the structure [Petersen et al., 2012]. But the large difference within the organisms, from a 'structural' $n_A = 8/3$ to $15/3$, suggests still an adaptation to the $\Delta\tilde{\mu_H}$.
It would be interesting to compare different organisms with different proton/ATP ration in the background of their energy demand and find out which benefits and disadvantages the systems can have, in particular with respect to the two competing strategies of energy efficiency and time efficiency.

Limits of the model

Most parts of the experimental time courses of the respiratory rate, $\Delta\Psi$, and the reduction state of NADH could be well reproduced with our model. However these simulations also pointed out the limits of the model, which are the incapacity to reproduce $\Delta\Psi$ for the following situations: (i) the shortage of respiratory substrate, (ii) anoxic conditions, and (iii) the presence of an uncoupler. These are situations where the respiratory chain is either restricted by substrate supply, completely blocked or where the effect of proton pumping is nullified, respectively. Here, the simulated $|\Delta\Psi|$ was significantly too low.

In uncoupled mitochondria, a membrane potential around -60 to -70 mV is observed, which can also be seen in figure 4.13 a). Charged proteins, Ca^{2+} and other ions are involved in this basal membrane potential. The model needs to be extended in this regard, which would solve point (iii). This would also contribute to improve the situations for the first two points, but could still not explain the high $|\Delta\Psi|$ in anoxia. Under anoxic conditions, one can assume a contribution to $\Delta\Psi$ by the ATPsynthase pumping protons driven by ATP hydrolysis [St-Pierre et al., 2000]. But also other components are linked to this process: the adenine nucleotide-exchanger, the proton leak, and other ions. A modification or extension of the model might be necessary for a proper description of $\Delta\Psi$ in anoxia. In this regard it would be interesting to consider the innermembrane integral electroneutral mATP-Pi exchanger [Joyal and Aprille, 1992]. This would generally bring new aspects, since it renders variable the total adenonsine phosphate concentration in the matrix.

It must be pointed out that our that these problems do not arise from our new rate equations which were proved to be suitable for a wide range of applications. Rather the

framework model needs to be extended for a correct description of the particular cases cited above. However, in most simulations that we made, the framework model was sufficient to achieve good results.

5. Conclusion

We have built a model of oxidative phosphorylation based on a system of ordinary differential equations. The focus was put on the derivation of rate expressions for the isolated OXPHOS complexes, which describe their kinetics over a wide range of substrate and product concentrations as well as a large interval of the electrochemical potential difference (proton gradient). These equations were then combined with a framework model, constituted of the components given by Beard [2005]. The model is well suited to reproduce the extensive data set of Bose et al. [2003]. The latter covers the essential respiratory chain features $\Delta\Psi$, matrix pH, respiration rate, and the reduction states of NADH and cytochrome c, that have been measured as a function of the buffer phosphate concentration under phosphorylating and non-phosphorylating conditions (state 3 and state 4 respiration).

Bottom up approach, validation of the rate equations at different levels

The bottom-up approach permitted to analyze and to validate the rate equations on three levels, which will be described in the following.

At first, the kinetics of the OXPHOS complexes were considered in the absence of the proton gradient. We showed that here simple reversible Michaelis-Menten like rate equations, containing a forward and backward V_{max} and further a K_m for each substrate and product, are appropriate. Although the functioning of each complex is different and intricate, the steady state kinetics of the complexes I, II and III are supposedly close to a ping pong behavior. Good results for these three complexes were also achieved with the simplified (and generalized) random binding mechanism, which was furthermore suitable for the description of complex IV kinetics. For both equation types, reasonable product K_m values were found which was mostly not the case for the simplified ordered mechanism and convenience kinetics. The non simplified mechanism based rate equations did not lead to better results but to underdetermined parameters, the saturation kinetics of the extended mass action (EMA) equation allows for a rough data description, but not precise enough in all cases.
The equations were analyzed based on initial rate measurements that we have performed on bovine heart mitochondria. For all respiratory complexes the experimental conditions were similar, which allowed us to provide coherent parameter sets. Since only the forward reactions could be measured, the K_m values of the products were highly dependent on the equation type. In this regard there is a big advantage of fitting directly to experimental data than using of literature values data.

Because of their simplicity and flexibility to describe all respiratory complexes, we chose the simplified and generalize random binding mechanism as a basis of the new rate equations.

In the second step, we examined the introduction of the proton gradient into the kinetic expressions in a thermodynamic coherent way. Here we assumed that for any electrochemical potential difference, the kinetics can be represented by Michaelis-Menten kinetics which entails that the kinetic parameters must depend on the proton gradient. We described the dependency of these parameters upon the proton gradient by an exponential function, distributed among all kinetics constants (V_{max} and K_m). Reasonable results could only be achieved when (i) the rate constants were unevenly affected by the gradient, and when (ii) this uneven repartition was a function of $\Delta\mu_H$ itself. The first point allows for appropriate rates at physiological $\Delta\tilde{\mu_H}$ without affecting too much the K_m and the second point avoids extreme backward rates in the case of the reactions reverse.

Here we have demonstrated that with these new rate equations, it is possible to link the respiratory chain complexes kinetics in absence of the proton gradient with the appropriate rates at physiological $\Delta\tilde{\mu}_H$.

The third step consisted of simulating the ensemble of the OXPHOS rate equations in the context of the framework model mentioned above. Here our new rate equations were confronted with interdependent $\Delta\Psi$, matrix pH and substrate concentrations. The data set of Bose et al. [2003] was well reproduced. It includes data points of $\Delta\Psi$ ranging from -140 to - 200 mV depending on the phosphate concentration and the respiration state. This confirms that the new rate equations can reproduce the rates at a physiological proton gradient, and moreover over a wide range under different conditions. A further confirmation of the validity of our rate equations was that the respiration rate in dependence of the degree of inhibition of an OXPHOS complex is well described without changing any parameter (threshold curves). This is important since this shows that the response of the global system to a local perturbation can be well described.

In contrast to the OXPHOS equations used in the models of Beard [2005] and Korzeniewski [2001], our rate equations can well reproduce the kinetics of the isolated OXPHOS complexes, and the parameters K_m and V_{max} have a biological meaning and can thereby be easier handled (in case of a mutation, for instance). As does our model, the Beard model describes well the data set of Bose et al. [2003], but when confronted with different degrees of inhibition of an OXPHOS complex, the model fails to simulate the effects on the respiration rate. Korzeniewski and Mazat [1996] could describe such inhibition curves, but therefor the OXPHOS equations had to be adapted in an arbitrary way: instead of their rates being linear to the Gibbs energy of reaction ΔG_R, they showed now a saturation behavior as a function of ΔG_R. Thus our equations have the clear advantage that they are valid for a much larger scope being able to respond correctly to greater perturbations.

Simplifications

We have generally proved the applicability of the equations. But it is to keep in mind, that several simplifications have been made.
The simplified and generalized random binding equations describe well the observed steady state kinetics of the OXPHOS complexes, but do not represent their mechanisms. If more details are required, these basic rate equations can be adapted: as long as they obey the Haldane relationship, the way how we introduced the gradient into the rate equations is still valid. This renders flexible the adaptation of the equations to different conditions.

The V_{max} summarizes several catalytic steps. These are supposedly influenced by the proton gradient in a different extent, and the thereof resulting rate dependency on the proton gradient may be more complex than a simple exponential function, because the effects of the different steps are not necessarily additive [Reynolds et al., 1985]. The use of stochastic models taking into account the single catalytic steps [Ransac et al., 2008, 2010] could shed light into the effects of a proton gradient on the steady state kinetics, if the effect of the proton gradient on the individual redox reactions was included.

We did not differentiate between the influence of the electrical and that of the chemical part of the gradient and also the contribution of the scalar protons was put in the same energetic expression ΔG_H. They may however affect differently the kinetics. With respect to the Bose data, the pH difference between the matrix and the surrounding buffer solution was very small, $\Delta pH < 0.1$, so that in this case the problem is negligible. But also in general, in mitochondria the electrical part of the gradient is much higher, which justifies this simplification. If high changes in pH are to expect, the equations could be extended for a factor that approximates their general rate pH dependency.

Limits of the model

The simulated values for $|\Delta\Psi|$ were significantly too low in situations where the respiratory chain is either restricted by substrate supply, completely blocked or when the proton gradient is uncoupled, respectively. However this is not a consequence of the OXPHOS rate equations, but rather of the system: the model does not take into account non permeable charged particles which are necessary for the establishment of a basal membrane potential which can be measured when the protons are uncoupled. Also other ions like Ca^2+ and Cl^- play an important role of the dynamics of $\Delta\Psi$, and the way the proton leak flux is modeled requires an improvement, in order to account for the exponential leak flux - $\Delta\Psi$ relationship. These are important aspects which should be considered in a future model.
In anoxia, the electroneutral mATP-P_i antiporter [Joyal and Aprille, 1992] could be significant for the ATP supply of the ATPsynthase. This enzyme now hydrolyzes ATP, maintaining thereby a certain proton gradient [St-Pierre et al., 2000]. Since net transport of ATP renders variable the total concentration of adenine nucleotides in the mitochon-

drial matrix, this may also bring new aspects.

The model was robust to changes in K_{QH_2} and K_Q for the complexes I and III, in particular for state 4 respiration. However, the measurements of the decylubiquinone concentrations were referred to the whole reaction volume and not to the volume of the membrane, and thereby their apparent K_m are probably significantly underestimated [Fato et al., 1996]. Consequently the system could be indeed sensitive to the K_m of the quinones and thereby attributing them a regulative role. This issue needs to be clarified.

Perspectives

In the following, possible applications for the model are shortly described.

The respiratory chain complexes can assemble to supercomplexes, with variable stoichiometries: CI_{0-1}+$CIII_2$+$C4_{0-2}$ [Dudkina et al., 2010, Genova et al., 2008]. These assemblies may facilitate substrate channeling and thus enhance the electron transfer through the respiratory chain. Analysis of flux control coefficients and rate-inhibitor titration curves show evidence for a functional assembly of complex I and III [Genova et al., 2008]. The authors suggest that here the electron transfer between the complexes takes place either by diffusion in a small Q-pool or by channeling of electrons within the quinones.
Our model provides a good basis for the investigation of kinetic properties of supercomplexes: it describes well the isolated complexes kinetics, which is necessary to distinguish kinetics arising from assembled complexes. In particular our model reproduces well the inhibition curves, their shapes giving information about the degree of channeling between two complexes [Lenaz and Genova, 2009]. We have started to do some theoretical analysis on supercomplexes, where in a first attempt we have built two models of supercomplex CI+$CIII_2$: a model considering tight channeling, treating the assembly as one single enzyme, and a second model taking into account a separate Q pool between complex I and complex III. For the latter, we assumed as a first example a channel between the Q-site of complex I and the Q_o-site of complex III, but also the Q_i-site should later be taken into consideration. So far only the volume and the redox states have been considered. The diffusion of quinone is not included yet but seems to be also an important feature for a future model. Preliminary results are presented in the appendix B.
It would be worth to investigate whether the channeling of electrons between complex I and complex III can explain why we have found a much higher reduction state of quinones in our simulations without supercomplexes (mostly over 20 %) compared to the low values that Benard et al. [2006] found in rat heart tissue (around 2 %).
These data are part of a much vaster data set of Benard et al. [2006] which show for different tissues the abundance and activity of the respiratory chain complexes II, III and IV as well as the sizes and the reduced fractions of their quinone and cytochrome c pools (see also figure 2.22). On one hand these data can be used to test our model on different tissues by taking into account the given amounts and activities of the complexes and see

whether thereby the reduction states of quinone and cytochrome c can be matched, with or without taking into account supercomplexes. On the other hand one could analyze the performance of the OXPHOS system of different tissues with respect to their capacity of establishing a proton gradient and of responding to diverse energy demands (ATP consumption). This can help understanding the phenotypes of mitochondrial diseases which are often multisystemic, the tissues being affected in different extends.

Another task for which our model is well suited, is to analyze the regulation of complex IV by ADP and ATP. The allosteric inhibition by ATP [Arnold and Kadenbach, 1997] allows for a feedback loop from the synthesis of ATP back to the establishment of the proton gradient by the cytochrome c oxidase. There are at least ten binding sites that are involved in this regulation, whereof 3 are specific to ADP. Further it has been found that additional to the ATP/ADP-ratio in the matrix, complex IV is also affected by the cytosolic ATP/ADP-ratio [Napiwotzki and Kadenbach, 1998]. Modeling it is certainly an important approach for a better understanding of this highly complex regulation.

The feedback of the ATP/ADP ratio on $\Delta\tilde{\mu_H}$ may further contribute to keep the production of reactive oxygen species (ROS) within limits. The main sites of ROS production are the Q-site of complex I and the Q_o-site of complex III. Here, the ROS production is increasing with increasing membrane gradient [Rottenberg et al., 2009, Tahara et al., 2009]. Among other components, ROS damages mitochondrial DNA, which provokes mutations. One consequence is that the assembly and functioning of the OXPHOS complexes can be affected and may lead to an increased production of ROS, which closes the circuit. The accumulation of ROS induced damaged is hypothesized to play a crucial role in aging.
A theoretical approach could reveal the consequences of this circuit with regard to the development of the ATP production in time, taking into account that on one hand dysfunctioning complex I and III might indeed produce more ROS but on the other hand they will contribute less or not to the proton gradient. Hence it will be necessary to extend the model for ROS production at the Q-sites of complexes I and III. In a next step, repair mechanisms should be included into this system (mitophagy and ROS scavenging). Further the ATP and $\Delta\tilde{\mu_H}$ levels are influenced by energy consumption and substrate supply; it would be interesting to simulate the ROS dynamics as a response to the latter.

The respiratory chain is fueled by NADH and succinate. Both substrate levels are further dependent on the Krebs cycle activity where succinate is a direct intermediate. The competition between the two entry points is not only dependent on the concentrations but also on the actual membrane potential, since complex II is not sensitive to it. The system becomes more complicated when considering that the uptake of the Krebs cycle intermediates pyruvate and glutamate is directly coupled to the proton gradient while other Krebs cycle intermediates are transported over the inner membrane by electroneutral exchangers, as summarized in Wu et al. [2007]. The Krebs cycle model of the latter includes also the OXPHOS model of Beard [2005]. Hence it is tenting to integrate our new rate equations in this model, in order to analyze the role of different

Krebs cycle substrates on the competition of the electron entry points and the dynamics of $\Delta\tilde{\mu_H}$, under phosphorylating and non-phosphorylating conditions. Since the model of Wu et al. [2007] is very extensive, alternatively the simple Krebs-cycle model that we have established [Nazaret et al., 2009] could be employed. The role of complex II is of particular interest, since it is member of the Krebs cycle *and* the respiratory chain. A dysfunctioning of this enzyme ('tumor supressor') has been found in the context of cancer [King et al., 2006, Ralph et al., 2011].

An important result of our work was also the dependency of the respiratory rate and the membrane potential upon the stoichiometry of ATPsynthase due to the number of subunits in the c-ring which governs to a certain extent the number of protons per ATP produced. A high number of c subunits may permit ATP synthesis at low $\Delta\tilde{\mu}_H$ and vice-versa. A conflict between energy efficiency and high rate of ATP synthesis could also be the reason for the different number of subunits in the c-ring and this question can be addressed with our model.

To sum it up, we have developed a model of oxidative phosphorylation which in the same time gives a good representation of the kinetics of the individual complexes over a wide range of conditions, and when the kinetics are assembled, gives a relevant description of the OXPHOS behavior in many different conditions. The interest of such a model is that it is possible to understand or to predict how a precise defect in a complex or different arrangements of the complexes may influence the global performances of the oxidative phosphorylation. This model may be of great help to understand the increasingly recognized role of mitochondria in many cell processes such as ROS production, aging, diabetes, cancer, mitochondrial pathologies etc.

A. Rate equations of the framework model

As framework model for our simulations we have used rate equations from the OXPHOS model of Beard [2005]. For completeness, they are listed below. For the simulations of the new model, the rate equations for the complexes I, III and IV are replaced by our new OXPHOS equations.

Respiratory chain complexes and F_1F_0-ATPsynthase

Energy to translocate a proton across the inner mitochondrial membrane

$$\Delta\tilde{\mu}_H = F\Delta\Psi + RT\log\left(\frac{[H]_x}{[H]_i}\right) \tag{A.1}$$

Complex I

$$J_{C_1} = x_{C_1}\cdot(\exp_{C_1}\cdot[NADH]_x - [NAD]_x) \tag{A.2}$$

$$\text{where } \exp_{C_1} = e^{-\frac{1}{RT}\left(\Delta G^0_{C_1} - RT\log\left(\frac{[H^+]_x}{10^{-7}}\right) - RT\log\left(\frac{[Q]}{[QH_2]}\right) - 4\Delta\tilde{\mu}_H\right)} \tag{A.3}$$

Complex III

$$J_{C_3} = x_{C_3}\cdot\left(\frac{1+\frac{Pi_x}{k_{Pi_3}}}{1+\frac{Pi_x}{k_{Pi_4}}}\right)\cdot(\exp_{C_3}\cdot[cytc_{ox}] - [cytc_{red}]) \tag{A.4}$$

$$\text{where } \exp_{C_3} = e^{-\frac{1}{2RT}\left(\begin{array}{l}\Delta G^0_{C_3} + 2RT\log\left(\frac{[H^+]_x}{10^{-7}}\right)\\ -RT\log\left(\frac{[QH_2]}{[Q]}\right) - 4\Delta\tilde{\mu}_H + 2F\Delta\Psi\end{array}\right)} \tag{A.5}$$

Complex IV

$$J_{C_4} = x_{C_4}\cdot\frac{1}{1+\frac{k_{O_2}}{O_2}}\cdot\frac{cytc_{red}}{C_{tot}}\cdot\left(\exp_{C_4}\cdot[cytc_{red}] - [cytc_{ox}]\cdot e^{\frac{F\Delta\Psi}{RT}}\right) \tag{A.6}$$

$$\text{where } \exp_{C_4} = e^{-\frac{1}{2RT}\left(\Delta G^0_{C4} - 2RT\log\left(\frac{[H^+]_x}{10^{-7}}\right) - \frac{RT}{2}\log([O_2]) - 2\Delta\tilde{\mu}_H\right)} \tag{A.7}$$

F_1F_0-ATPsynthase

$$J_{F_1} = x_{F_1} \cdot \left(\exp_{F_1} \cdot \frac{K_{DD}}{K_{DT}} \cdot [mADP]_x \cdot [Pi]_x - [mATP]_x \right) \tag{A.8}$$

$$\text{where } \exp_{F_1} = e^{-\frac{1}{RT}\left(\Delta G^0_{F_1} + n_A . * \Delta\tilde{\mu}_H - RT . * \log\left(\frac{[H^+]_x}{10^{-7}}\right)\right)} \tag{A.9}$$

Reactions in the matrix

Dehydrogenase reaction

$$J_{DH} = x_{DH} \cdot (r \cdot [NAD]_x - [NADH]_x) \cdot \frac{1 + \frac{[Pi]_x}{k_{Pi_1}}}{1 + \frac{[Pi]_x}{k_{Pi_2}}} \tag{A.10}$$

Magnesium binding on adenosine nucleotides

$$J_{MgATP_x} = x_{MgA} \cdot ([fATP]_x \cdot [Mg]_x - K_{MgATP} \cdot [mATP]_x) \tag{A.11}$$

$$J_{MgADP_x} = x_{MgA} \cdot ([fADP]_x \cdot [Mg]_x - K_{MgADP} \cdot [mADP]_x) \tag{A.12}$$

Transport processes over the inner mitochondrial membrane

ANT-transporter
for $[ADP_f]_i > 10^{-12}$ and $[ATP_f]_i > 10^{-12}$

$$J_{ANT} = x_{ANT} \cdot \left(\begin{array}{c} \frac{[fADP]_i}{[fADP]_i + [fATP]_i \cdot e^{-\frac{F\Psi_i}{RT}}} \\ - \frac{[fADP]_x}{[fADP]_x + [fATP]_x \cdot e^{-\frac{F\Psi_x}{RT}}} \end{array} \right) \cdot \frac{[fADP]_i}{[fADP]_i + k_{ADP}] } \tag{A.13}$$

with $\Psi_x = -0.65\Delta\Psi$; $\Psi_i = +0.35\Delta\Psi$
else $J_{ANT} = 0$
Phosphate-proton symport

$$J_{PiHt} = x_{PiHt} \cdot \frac{[H]_i \cdot [H_2Pi]i - [H]_x \cdot [H_2Pi]_x}{[H_2Pi]i + k_{PiHt}} \tag{A.14}$$

with $[H_2Pi]_i = [Pi]_i \cdot \frac{[H]_i}{[H^+]_i + k_{HPi}}$ and $[H_2Pi]_x = [Pi]_x \cdot \frac{[H]_x}{([H^+]_x + k_{HPi}}$

Proton leak flux

$$J_{H_le} = x_{H_le} \cdot \Delta\Psi \cdot \frac{[H^+]_i \cdot e^{\frac{F\Delta\Psi}{RT}} - [H^+]_x}{e^{\frac{F\Delta\Psi}{RT}} - 1} \tag{A.15}$$

Potassium leak flux

$$J_K = x_K \cdot \Delta\Psi \cdot \frac{[K]_i \cdot e^{\frac{F\Delta\Psi}{RT}} - [K]_x}{e^{\frac{F\Delta\Psi}{RT}} - 1} \tag{A.16}$$

Potassium proton antiport

$$J_{KH} = x_{KH} \cdot \left([K]_i \cdot [H^+]_x - [K]_x \cdot [H^+]_i\right) \tag{A.17}$$

Reactions in the intermembrane space

Adenylate kinase

$$J_{AK} = x_{AK} \cdot (K_{AK} \cdot [fADP]_i \cdot [fADP]_i - [AMP]_i \cdot [fATP]_i) \tag{A.18}$$

Magnesium binding to ADP and ATP

$$J_{MgATPi} = x_{MgA} \cdot (fATP_i \cdot Mg_i - K_{MgATP} \cdot mATP_i) \tag{A.19}$$
$$J_{MgADPi} = x_{MgA} \cdot (fADP_i \cdot Mg_i - K_{MgADP} \cdot mADP_i) \tag{A.20}$$

Transport processes over the outer membrane

Transport of adenine nucleotides

$$J_{AMP} = \gamma \cdot \rho_A \cdot ([AMP]_e - [AMP]_i) \tag{A.21}$$
$$J_{fADP} = \gamma \cdot \rho_A \cdot ([fADP]_e - [fADP]_i) \tag{A.22}$$
$$J_{mADP} = \gamma \cdot \rho_A \cdot ([mADP]_e - [mADP]_i) \tag{A.23}$$
$$J_{fATP} = \gamma \cdot \rho_A \cdot ([fATP]_e - [fATP]_i) \tag{A.24}$$
$$J_{mATP} = \gamma \cdot \rho_A \cdot ([mATP]_e - [mATP]_i) \tag{A.25}$$
$$\tag{A.26}$$

Transport of phosphate

$$J_{Pi} = \gamma \cdot \rho_{Pi} \cdot ([Pi]_e - [Pi]_i) \tag{A.27}$$

B. Modeling supercomplexes

The respiratory chain complexes can assemble to supercomplexes, different compositions have been evidenced with the following stoichiometries CI_{0-1}+$CIII_2$+$C4_{0-2}$ [Dudkina et al., 2010, Genova et al., 2008]. Complex I is essentially stabilized by a complex III dimer [Schägger et al., 2004, Stroh et al., 2004], Supercomplexes may facilitate substrate channeling. However, when assembled, the Q sites in complex I and complex III are not so close. It is suggested that here the electron transfer could be either mediated by diffusion in a small Q-pool or by channeling of electrons within the quinones [Genova et al., 2008].
It is thus worth to model supercomplex kinetics. Since CI_1+$CIII_2$ seems to be very stable and CI_1 was found to be stabilized by the complex III dimer, we investigate the possible kinetic role of this complex.
It is assumed, that about 2/3 of complex III is in complexed form with complex I and that rather all complex I is assembled with complex III dimers [Genova et al., 2008]. Thus our kinetic analyses of supercomplexes versus free complexes integrates the following constraints:

$$\mathrm{CI_{sc}} = \mathrm{f_{sc}} \cdot \mathrm{CI_{tot}} \tag{B.1}$$

$$\mathrm{CIII_{sc}} = \mathrm{f_{sc}} \cdot \frac{2}{3} \cdot \mathrm{CIII_{tot}} \tag{B.2}$$

$$\tag{B.3}$$

where the index 'sc' denotes the complexes assembled in supercomplexes and f_{sc} is the factor that appoints the fraction of complex I being assembled in supercomplex with complex III. The corresponding distributions chosen for the simulations are summarized in table B.1.

Table B.1.:
Supercomplex distributions used for simulations

CI (sc)	CI (free)	CIII (sc)	CIII (free)
0 %	100 %	0 %	100 %
50 %	50 %	33 %	67 %
90 %	10 %	60 %	40 %
100 %	0 %	67 %	33 %

Figure B.1 illustrates how the respiratory rate should behave as a function of a complexes'

inhibition when substrate channeling occurs. Different types of inhibition curves have been observed: Genova et al. [2008] and Quarato et al. [2011] and showed a linear rate-inhibition dependency for complexes I and III, and complex IV respectively, at state 3, while the threshold curves obtained by Rossignol et al. [1999] showed different types of inhibition curves, depending on the tissue with more or less pronounced thresholds. This can be the result of a more drastic isolation procedure of mitochondria, which destroy the supercomplex architecture.

Figure B.1.: Supercomplexes: Shapes of inhibition curves. On the example of the complexes I and III the expected inhibition curves for a) no substrate channeling and b) substrate channeling between complex I and III are shown.

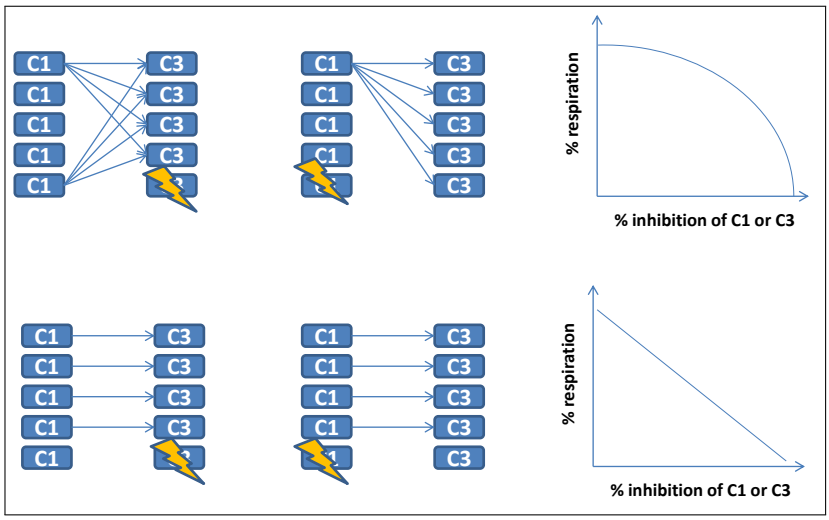

In the following we will analyze possible properties of supercomplexes and their effects on the kinetics. We have modeled the supercomplexes with two different approaches. The 'strict channeling model' and the 'partial channeling model'. They are illustrated in figure B.2 and described below.

B.1. Supercomplex CI + $CIII_2$ modeled with strict channeling

Here, we assume that the supercomplex $CI + CIII_2$ is assembled so tightly, that the channeling of the electrons between the complexes can be considered like another step in the catalytic process, i.e. we model $CI + CIII_2$ as a single enzyme.
We assume therefore that reduced quinones from complex I are directly transfered to the Q_o-site of complex III, where they become oxidized. Hence there is no Q-concentration playing on these sites: The quinones act like intermediate redox centers. In contrast, the Q_i site of complex III is still sensible to the concentration and redox state of the quinones. Thus the quinones that have been reduced at the Q_i-site can only be reoxidized by the free complex III dimers, as illustrated in figure B.2.

Figure B.2.: Scheme of the virtual supercomplexes. a) Strict channeling model and b) partial channeling model

.

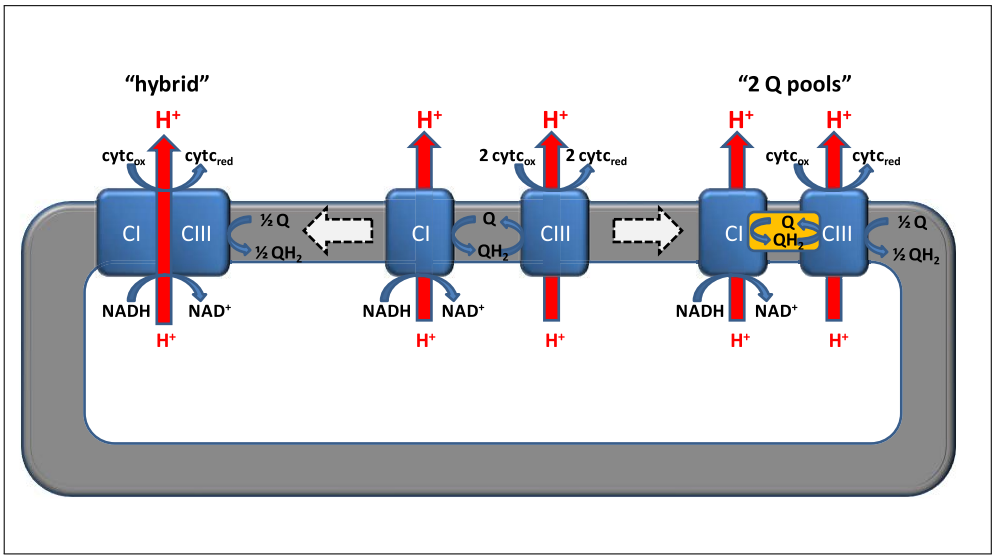

Modifications of the framework model

In order to describe this strict channeling supercomplex, a new equation has to be conceived. By merging the two reaction schemes for complex I

$$NADH + Q + 5H_x^+ = NAD + QH_2 + 4H_i^+ \tag{B.4}$$

and for complex III

$$QH_2(o) + \frac{1}{2}Q(i) + cytc_{ox} + H_x^+ = Q(o) + \frac{1}{2}QH_2(i) + cytc_{red} + 2H_i^+ \tag{B.5}$$

(Q cycle respected), we obtain the overall reaction scheme for CI+$CIII_2$ supercomplex:

$$NADH + cytc_{ox} + \frac{1}{2}Q(i) + 6H_x^+ = NAD + cytc_{red} + \frac{1}{2}QH_2(i) + 6H_i^+ \tag{B.6}$$

Complex I transfer 4 charges over the inner membrane, complex III (referred to the reaction scheme B.5) transfers one charge) so that the supercomplex transfers in total 5 charges. Additionally a proton is taken up from the matrix and another proton is released in the intermembrane space. For the strict channeling supercomplex, the Gibbs energy for proton and charge translocation is thus

$$\Delta G_H^{C13} = 5 \cdot \Delta\mu_H - RT \cdot log\frac{H_x}{H_i} \tag{B.7}$$

The generalized simplified random binding equation for the reaction scheme B.6 reads

$$v_{C13} = E_t \cdot k \cdot \frac{\begin{bmatrix} e^{\gamma_k(\beta,\Delta G_{int})\cdot\left(-\frac{\Delta G_{int}}{RT}\right)} \cdot nadh \cdot c_{ox} \cdot (q^i)^{0.5} \\ -e^{(\gamma_k(\beta,\Delta G_{int})-1)\cdot\left(-\frac{\Delta G_{int}}{RT}\right)} \cdot nad \cdot c_{red} \cdot (q^i)^{0.5} \end{bmatrix}}{(1 + nad + nadh) \cdot (1 + c_{ox} + c_{red}) \cdot \left(1 + q^i + qh_2^i\right)^{0.5}} \tag{B.8}$$

where

with

$$\Delta G_{int} = \Delta G^0_{int} + \zeta_V \cdot \Delta G_H^{C13}$$
$$\Delta G^0_{int} = \Delta G_0^{C13} - RT \cdot \ln\left(\frac{K_{NADH}^{C13}}{K_{NAD}^{C13}}\right) - 0.5 \cdot RT \cdot \ln\left(\frac{K_{Qi}^{C13}}{K_{QH_2i}^{C13}}\right) - RT \ln\left(\frac{K_{cox}^{C13}}{K_{red}^{C13}}\right).$$

We have also to consider, that the standard Gibbs energy is now composed of ΔG_0^{C1} and ΔG_0^{C3}. Since we have referred these values to the reaction schemes 3.13 and 3.15, respectively, only half of ΔG_0^{C3} is to take into account in order to calculate the Gibbs standard energy of reaction for the reaction scheme of the strict channeling supercomplex B.6:

$$\Delta G_0^{C13} = \Delta G_0^{C1} + \frac{1}{2} \cdot \Delta G_0^{C3} \tag{B.9}$$

The rate constant k is calculated corresponding to equation 3.34.

To allow for a better comparison between supercomplex and isolated complexes, the generalized and simplified random binding equation for free complex III is based on reaction scheme B.5, i.e. both q binding sites are considered and first order for cytochrome c and Q at the Q_o site and 0.5 order for Q at the Q_i site is assumed. The kinetic parameters V_{max} and K_m for this rate equation have been determined in section 2.5. The parameters concerning the distribution of the proton gradients effect on the kinetic parameters were approximated for complex III as it has been done for the preliminary simulations in figure 4.2, according equations 4.57 and 4.58. The resulting values are listed in table B.2. The K_m of the supercomplex CI + CIII were identical with those of the isolated complexes CI and CIII, but the repartition of the gradient's impact on the parameters was different, because the pairs among which the $\Delta G_H(C_{13})$ is distributed are different.

For the simulations, the V^+_{max} for the supercomplex CI+CIII was varied in the range of the V^+_{max} of CI and CIII.

The following ODEs are those which have been modified with respect to the ODE system 4.1.

Table B.2.: Parameters of the strict and partial channeling models. For both models, the rate equation considering both Q binding sites have been employed based on reaction scheme 2.5.1. Also here the generalized random binding equation was used, with first order for cytochrome c and the Q at the Qo site and 0.5 order for Q at the Qi site. The parameters for the distribution of the proton gradients impact on the K_m and V_{max} have not been fitted but roughly approximated as done for the simulations in figure 4.2. For further explanations see table 4.6.

parameter	value	unit	parameter	value	unit
Complex III					
V^+_{max}	11452/2	nmol/min/mg	ζ_{Q_o}	0.0407	
V^-_{max}	$x \cdot 10^{-y}$	nmol/min/mg	ζ_{Q_i}	0.4296	
k_{C_3}	0.0912	M/sec	ζ_C	0.3728	
$K_{Q(o)}$	$267 \cdot 10^{-6}$	M	ζ_V		
$K_{QH_2(o)}$	$188 \cdot 10^{-6}$	M	γ_{Q_o}	0.5	
$K_{Q(i)}$	$0.011 \cdot 10^{-6}$	M	γ_{Q_i}	0.5	
$K_{QH_2(i)}$	$6.7 \cdot 10^{-6}$	M	γ_C	0.5	
K_{c_ox}	$21.8 \cdot 10^{-6}$	M	γ_V*	0.0443	
K_{c_red}	$352 \cdot 10^{-6}$	M	ΔG_0 (pH 7.5)	-38.46/2	kJ/mol
complex I + III					
$V^+_{max}(1)$	1791	nmol/min/mg	$V^+_{max}(2)$	3759	nmol/min/mg
$V^-_{max}(1)$	$x \cdot 10^{-y}$	nmol/min/mg	$V^-_{max}(2)$	$x \cdot 10^{-y}$	nmol/min/mg
$k_{C_{13}}(1)$	0.0109	M/sec	$k_{C_{13}}(2)$	0.0228	M/sec
$V^+_{max}(3)$	5736	nmol/min/mg	ζ_N	0.2018	
$V^-_{max}(3)$	$x \cdot 10^{-y}$	nmol/min/mg	ζ_{Q_i}	0.0965	
$k_{C_{13}}(3)$	0.0348	M/sec	ζ_C	0.0837	
K_{NADH}	$4.3 \cdot 10^{-6}$	M	ζ_V		
K_{NAD}	$780 \cdot 10^{-6}$	M	γ_{Q_o}	0.5	
$K_{Q(i)}$	$0.011 \cdot 10^{-6}$	M	γ_{Q_i}	0.5	
$K_{QH_2(i)}$	$6.7 \cdot 10^{-6}$	M	γ_C	0.5	
K_{c_ox}	$21.8 \cdot 10^{-6}$	M	γ_V*	0.0443	
K_{c_red}	$352 \cdot 10^{-6}$	M	ΔG_0 (pH 7.5)	-38.46/2	kJ/mol

$$\frac{d[NADH]}{dt} = \left(+J_{DH} - J_{C_1} - J_{C_{13}}\right)/W_x \tag{B.10}$$

$$\frac{d[QH_2]}{dt} = \left(+J_{C_1} + J_{C_2} - J_{C_3} + \frac{1}{2}J_{C_{13}}\right)/W_m \tag{B.11}$$

$$\frac{d[cytc_{red}]}{dt} = \left(+2J_{C_3} - 2J_{C_4} + J_{C_{13}}\right)/W_i \tag{B.12}$$

$$\frac{d[H^+]_x}{dt} = \frac{x_{buff} \cdot [H^+]_x}{W_x} \cdot \begin{pmatrix} +J_{DH} - 5J_{C_1} - 2J_{C_3} - 4J_{C_4} - 6J_{C_{13}} \\ +(n_A - 1)J_{F_1} + 2J_{Pi_1} + J_{H_{le}} - J_{KH} \end{pmatrix} \tag{B.13}$$

$$\frac{d\Delta\Psi}{dt} = \frac{1}{C}\left(4J_{C_1} + 2J_{C_3} + 4J_{C_4} + 5J_{C_{13}} - n_A J_{F1} - J_{ANT} - J_{H_{le}} - J_K\right) \tag{B.14}$$

For the simulations, J_C2 and J_{Krebs} are set to zero. The percentages of supercomplexes are given in table B.1 were respected for calculating the fluxes J_{C1}, J_{C3} and J_{C13}. All simulations have been performed with Pi_e = 10 mM, Mg_e = 5 mM. For state 3 we set ADP_e = 1.3 mM, for state 4 it was set to 0.
The constraints given in table 4.2 were not modified.

Simulations of the strict channeling model

At first we investigated, whether with the strict channeling model one could reproduce a linear rate-inhibition dependency with respect to inhibition of complex I and III, as predicted in figure B.2. The fraction of inhibited supercomplexes was always the same as either for free complex I or III. In order to account for the effect of a higher stability due to supercomplex formation, we chose to set the maximal velocity of isolated complex I to half of the measured value, i.e. $V^+_{max}(C_1, \text{iso}) = 0.5 \cdot V^+_{max}(C_1)$.
Indeed due to the supercomplex formation one can approached the expected behavior, see figure B.3. However, for relatively high maximal velocity of the supercomplex CI+$CIII_2$, the inhibition curves show a sigmoidal shaped decrease of velocity with increasing inhibition. This is due to their higher rate capacity, which allows to compensate better for the inhibition. But in the same time it may also be a consequence of the different repartitions of the gradient among the parameters of the supercomplex and of the free complexes I and III.

We have then analyzed the effect the supercomplex formation has on the absolute value of the respiration rate. Further we tested the model with respect to a possible time efficiency when changing from non phosphorylating state to phosphorylating state and vice versa. In figure B.4 it is shown that the strict channeling model of the supercomplex does not contribute to a faster state transition between phosphorylating and non-phosphorylating model.
We found that here the supercomplex formation can only be beneficial for the respiration rate, when the maximal rate of the supercomplex is much higher than that of the isolated complex I, e.g. when it corresponds to the rate measured for free complex III. However no benefit could be ascribed to the strict channeling complex in regard of accelerating the transition between state 3 and state 4 and vice versa.

B.2. Supercomplex CI + $CIII_2$ modeled with partial channeling

In this approach, we assume for the supercomplex CI+$CIII_2$ that the Q binding site of complex I is close to the Q_o binding site of complex III such that a cavity is formed and they would share a common Q-pool, see figure B.2. This Q_o-pool may be accessible by diffusion from the surrounding Q_i-pool. We investigated, whether this arrangement can be beneficial for the global respiratory rates and reproduce a linear relationship between respiration rate and inhibition of complex I or III.

Modifications of the framework model

For this model we must employ an equation for complex III that takes into account the two Q binding sites of complex III. We have decided to employ the same rate equation as for the strict channeling model, i.e. the generalized and simplified random binding equation with first order for cytochrome c.

Figure B.3.: Strict channeling model: inhibition curves at state 3. A linear up to a sigmoidal decline of the respiration rate as a function of inhibition of complex I or III can be observed. The inhibition curves have been simulated for different fractions of supercomplexes, where the full/dashed/point-dashed lines represent 0%,50% and 90% of CI assembled in supercomplexes. Further the maximal velocity of the supercomplex was varied. Here, the red, blue and green lines correspond to $V^+_{max}(C_{13}) = V^+_{max}(C_1)$, $V^+_{max}(C_{13}) = (V^+_{max}(C_1) + V^+_{max}(C_3))/2$ and $V^+_{max}(C_{13}) = V^+_{max}(C_3)$, respectively. In order to account for the effect of a higher stability due to supercomplex formation, we chose to set the maximal velocity of isolated complex I to half of the measured value, i.e. $\mathrm{V^+_{max}(C_1, iso) = 0.5 \cdot V^+_{max}(C_1)}$. This assures also that the system is not yet at its maximum performance, because then one would probably not observe a beneficial effect of the supercomplex formation.

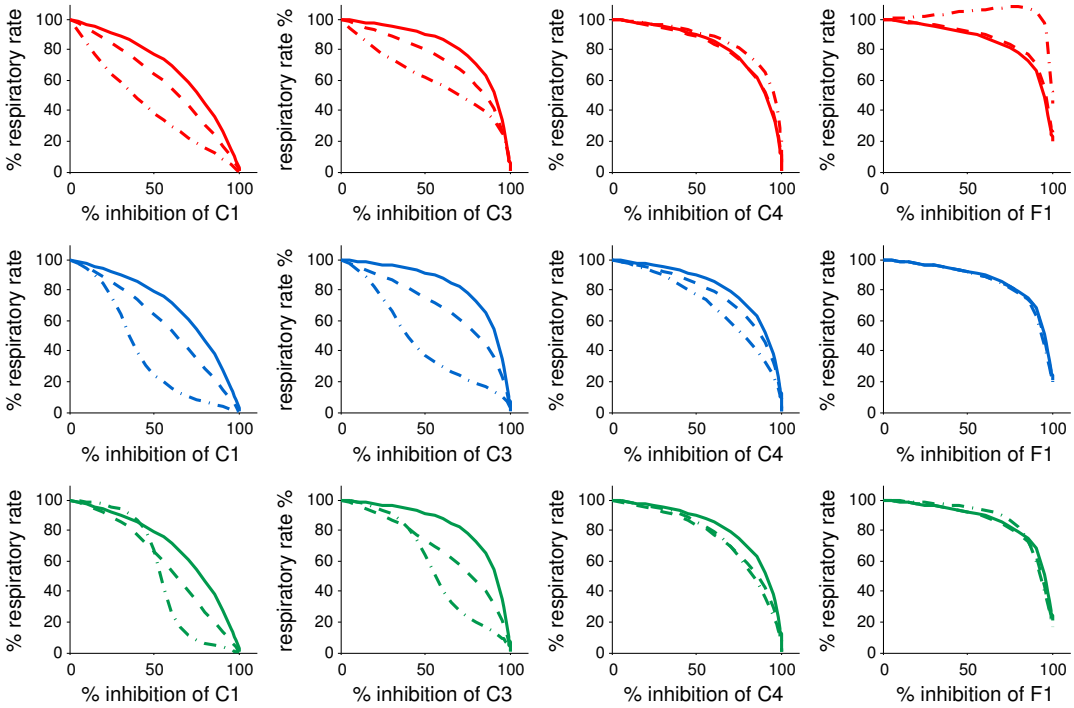

Figure B.4.: Strict channeling model: state transition and respiration rate. a) The strict channeling supercomplex does not lead to a significant time difference for the state transition. The full and dashed lines indicate that 0% or respectively /90% of CI assembled in supercomplexes. The rate constant for the ADP-ATP exchanger x_{ANT} was set to 0.01, if not the system reacted with a strong overshoot when the conditions were changed, i.e. sudden addition/privation of ADP. b) Depending on the maximal supercomplex activity, the assembly of complex I with complex III can increase the respiration rate. The red, blue and green lines correspond to $V^+_{max}(C_{13}) = V^+_{max}(C_1)$, $V^+_{max}(C_{13}) = (V^+_{max}(C_1) + V^+_{max}(C_3))/2$ and $V^+_{max}(C_{13}) = V^+_{max}(C_3)$, respectively.
.

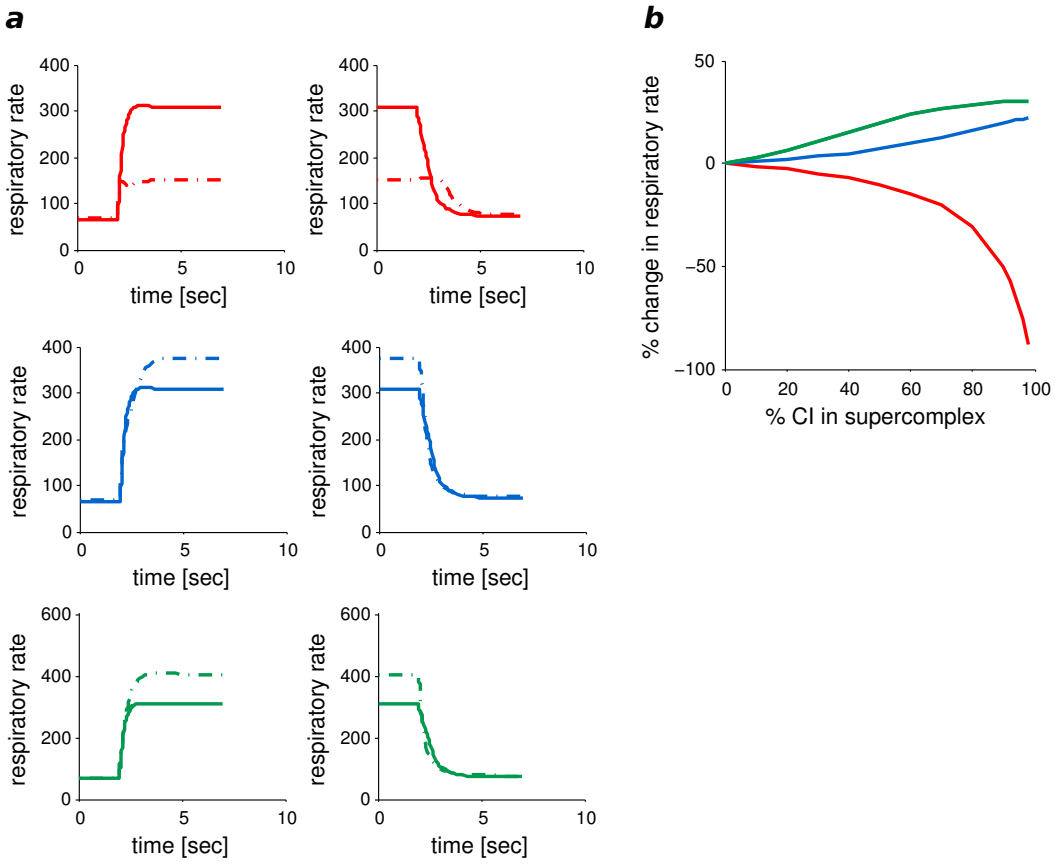

Two rate equations were implemented for each, complexes I and III, one for the isolated ('iso') and one for the assembled form ('sc'), so that the respective Q-pool could be assigned ($J^{iso}_{C_1}$, $J^{sc}_{C_1}$, $J^{iso}_{C_3}$, $J^{sc}_{C_3}$).

$$\frac{d[NADH]}{dt} = \left(+J_{DH} - J^{iso}_{C_1} - J^{sc}_{C_1}\right)/W_x \tag{B.15}$$

$$\frac{d[QH_2]_i}{dt} = \left(+J^{iso}_{C_1} + J_{C_2} - J^{iso}_{C_3} + J^{sc}_{C_3} + J^{dif}_{QH_2}\right)/V_m \tag{B.16}$$

$$\frac{d[Q]_o}{dt} = \left(-J^{sc}_{C_1} + 2J^{sc}_{C_3} - J^{dif}_{QH_2}\right)/V_o \tag{B.17}$$

$$\frac{d[QH_2]_o}{dt} = \left(+J^{sc}_{C_1} - 2J^{sc}_{C_3} - J^{dif}_{QH_2}\right)/V_o \tag{B.18}$$

$$\frac{d[cytc_{red}]}{dt} = \left(+2J^{iso}_{C_3} + 2J^{sc}_{C_3} - 2J_{C_4}\right)/V_{is} \tag{B.19}$$

$$\frac{d[H^+]_x}{dt} = \frac{x_{buff}\cdot[H^+]_x}{W_x}\cdot\begin{pmatrix} +J_{DH} - 5\left(J^{iso}_{C_1} + J^{sc}_{C_1}\right) - 2\left(J^{iso}_{C_3} + J^{sc}_{C_3}\right) \\ -4J_{C_4} + (n_A - 1)J_{F_1} + 2J_{Pi_1} + J_{H^le} - J_{KH} \end{pmatrix} \tag{B.20}$$

$$\frac{d\Delta\Psi}{dt} = \frac{1}{C}\begin{pmatrix} 4\left(J^{iso}_{C_1} + J^{sc}_{C_1}\right) + 2\left(J^{iso}_{C_3} + J^{sc}_{C_3}\right) + 4J_{C_4} \\ -n_A\cdot J_{F_1} - J_{ANT} - J_{H^le} - J_K \end{pmatrix} \tag{B.21}$$

Further we accounted for a possible diffusion of quinone in its oxidized and reduced form using simple mass action equations:

$$J^{dif}_Q = k_{dif}\cdot(r_{dif}\cdot[Q]_o - [Q]_i) \tag{B.22}$$

$$J^{dif}_{QH_2} = k_{dif}\cdot(r_{dif}\cdot[QH_2]_o - [QH_2]_i) \tag{B.23}$$

where k_{dif} is the diffusion constant - assuming an equal diffusion coefficient for Q and QH_2 - and r_{dif} the equilibrium between the concentrations in the two Q-pools. If it is set to values greater than 1 the Q_o-pool has a preference to 'hold' quinones. This may be the case if the Q_o-pool is very small and interactions between the supercomplex and the quinones would occur.
Constraint 4.35 was replaced by the following expression

$$Q = Q_{tot} - QH_2(i) - (QH_2(o) + Q(o))\cdot\frac{V_o}{V_m} \tag{B.24}$$

Simulations of the partial channeling model

We have examined the influence of the 2 different Q pools on the kinetics of the oxidative phosphorylation, and the effect of varying the concentration and volume of the Q_o-pool. We set the maximal rate of complex I to half of the measured value, for both the free (C^{iso}_1) and assembled (C^{sc}_1) form. This permits to start the analyses at a point where the system is not already at its full performance but lets open the possibility to achieve

higher rates with increasing supercomplex formation. Since the effect of two Q-pools can be better determined when no diffusion takes place, we set $k_{dif} = 0$ for the investigations.

In general, no effect could be observed when decreasing the volume of the Q_o-pool to 1/100 of the Q_i-pool. The inhibition curves did not change their shape when the concentration in the Q_o-pool was higher than that of the Q_i-pool. A shift to a more linear behavior could only be observed, when smaller Q concentrations in the Q_o-pool were assumed, see figure B.5.
For the state transition from phosphorylating to non-phosphorylating state and vice versa, the formation of supercomplexes was not beneficial, as shown in figure B.6 (a). Moreover, a higher concentration of Q in the Q_o-pool did only very slightly increase the respiratory flux, while a lower concentration decreased significantly the rate with increasing fraction of complex I assembled in supercomplexes, see figure B.6 (b).

Figure B.5.: Partial channeling model: inhibition curves at state 3 respiration. a) Variation of the concentration in the Q_o-pool with respect to the surrounding Q_i-pool. In the simulations 90 % of complex I were assembled in supercomplexes. The behavior is shifted towards a linear functioning if the Q_o concentrations is much smaller than the Q_i- concentration.$[Q]_o = x \cdot [Q]_i$, with red full line and dashed line: 1 and 0.1; blue: 0.01; black full and dashed line 0.0001 and 0.001. In order to avoid a saturation effect for the respiratory rate, the complex I activity was set to half of its measured value. The volume of the Q_o-pool was set to 1/100 of the Q_i-pool volume. However, an effect due to a variation of the Q_o-pool volume was not observed. b) The concentration in the Q_o-pool was set to 100 times below that of the Q_i-pool. The shapes of the inhibition curve for complex I does only slightly change with increasing fraction of supercomplexes, more effect can be seen for complex III but even for the 100 % C1 assembled in supercomplexes, the rate-inhibition dependency is not linear. The full/dashed/point-dashed/pointed lines represent 0%,50%, 90% and 100 % of CI assembled in supercomplexes.

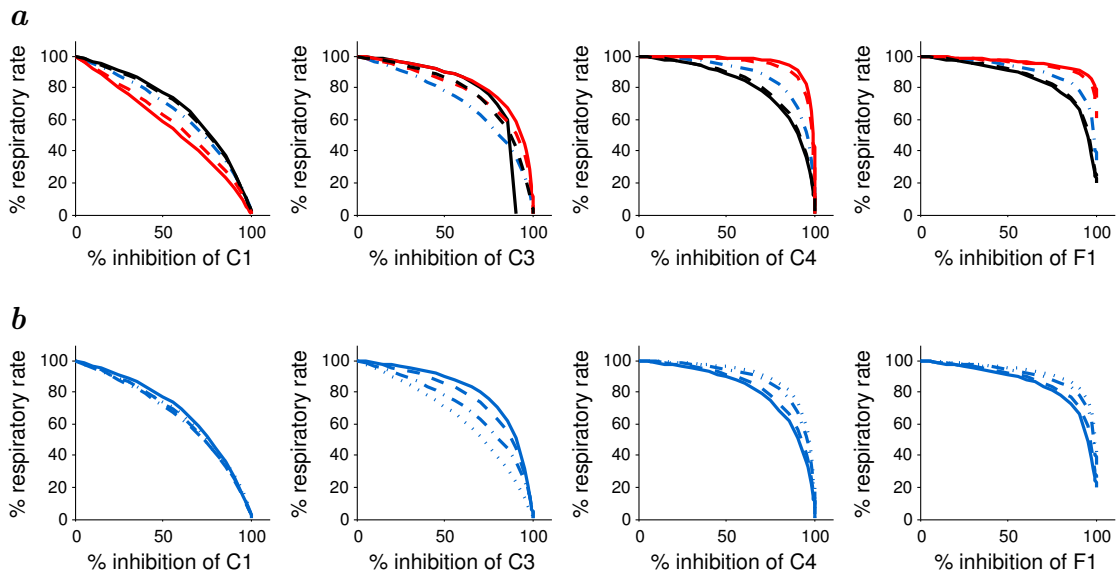

Figure B.6.: Partial channeling model: state transition and respiratory rate. a) No beneficial effect of supercomplex formation was observed with respect to a time difference in changing from phosphorylating state to non phosphorylating state and vice versa. 90 % of complex I was assembled in supercomplexes for this simulation. The concentration in the Q_o-pool was set to 1/100 of the concentration in the Q_i-pool. The rate constant for the ADP-ATP exchanger x_{ANT} was set to 0.01, if not the system reacted with a strong overshoot when the conditions were changed, i.e. sudden addition/privation of ADP. b) The plot of the respiration rate versus the fraction of supercomplexes reveals that a higher concentration in the Q_o-pool than in the Q_i-pool is only very little beneficial, while a lower concentration leads to a significant decrease of the respiratory rate. Red line: $[Q]_o$ is 100 times $[Q]_i$, black: factor 1, blue factor 1/100. In both simulations the complex I activity was set to half of its measured value, in order to avoid a saturation effect for the respiratory rate. The volume of the Q_o-pool was set to 1/100 of the Q_i-pool volume. Here as well, an effect due to a variation of the Q_o-pool volume was not observed.

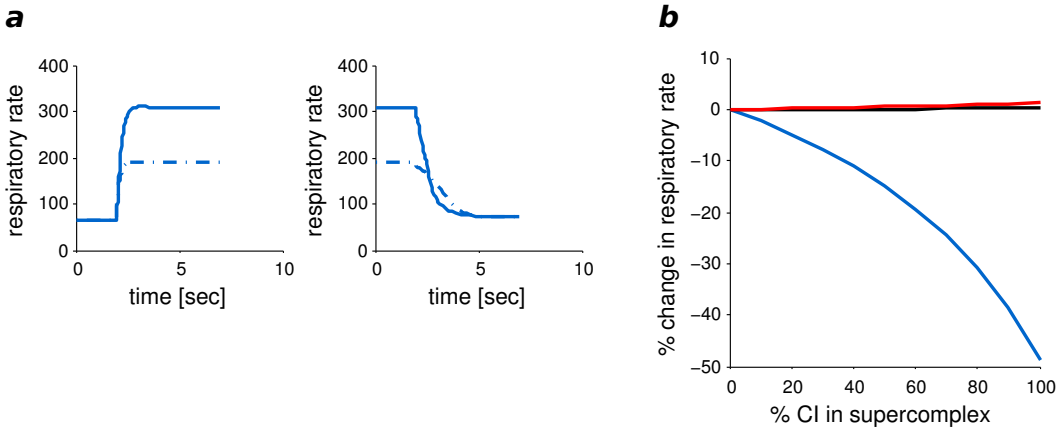

This is consistent with the system being basically at saturating Q-concentrations. It explains why only for lower Q concentrations in the Q_o-pool the inhibition curves are closer to a linear rate-inhibition dependency because here supercomplex become rate limiting, and hence has a higher control. But the effect on the respiratory rate is negative. As it has already been mentioned, the measured K_Q and K_{QH_2} for complexes I, II and III are apparent values and are supposed to be higher in reality (see 2.2.6 and for analysis 4.5.2). This could mean that the Q concentrations are in reality not saturating, an thus a higher concentration in the Q_o-pool may have indeed a positive effect on the OXPHOS kinetics. The increase of velocity, albeit very small, for increasing supercomplex assembly that we observed for higher concentrations in the Q_o-pool than in the Q_i-pool reinforces the idea of a potentially positive effect under these conditions. However, considering the trend that with increasing concentrations in the Q_o-pool the threshold is more pronounced, one can expect that this approach cannot explain the linear rate-inhibition dependencies.

But before to conclude, this has to be challenged by simulations. To render more realistic the properties of the Q_o-pool, the model should be extended to take into account the diffusion distance within the Q_o-pool and the Q_i-pool, e.g. by relating these distance to the volumes of these pools. This aspect would certainly contribute positively to the kinetics of OXPHOS.

Bibliography

J. P. Abrahams, A. G. W. Leslie, R. Lutter, and J. Walker. Structure at 2.8 A resolution of F1-ATPase from bovine heart mitochondria. *Nature*, 370:621–628, 1994.

R. A. Alberty. Rapid-equilibrium rate equations for the enzymatic catalysis of A+B=P+Q over a range of pH. *Biophys Chem*, 132(2-3):114–26, Feb. 2008. ISSN 0301-4622. doi: 10.1016/j.bpc.2007.10.015.

M. Aliev and V. Saks. Compartmentalized energy transfer in cardiomyocytes: use of mathematical modeling for analysis of in vivo regulation of respiration. *Biophysical journal*, 73:428–445, 1997.

H. Angerer, H. R. Nasiri, V. Niedergesäß, S. Kerscher, H. Schwalbe, and U. Brandt. Tracing the tail of ubiquinone in mitochondrial complex I. *Biochim Biophys Acta*, 1817(10):1776–84, Oct. 2012. ISSN 0006-3002. doi: 10.1016/j.bbabio.2012.03.021.

S. Arnold and B. Kadenbach. Cell respiration is controlled by ATP, an allosteric inhibitor of cytochrome-c oxidase. *Eur J Biochem*, 249:350–354, 1997.

H. Atamna and W. H. Frey. Mechanisms of mitochondrial dysfunction and energy deficiency in Alzheimer's disease. *Mitochondrion*, 7:297–310, 2007. doi: 10.1016/j.mito.2007.06.001.

J. N. Bazil, G. T. Buzzard, and A. E. Rundell. Modeling mitochondrial bioenergetics with integrated volume dynamics. *PLoS Comput Biol*, 6(1):e1000632, Jan. 2010. ISSN 1553-7358. doi: 10.1371/journal.pcbi.1000632.

D. Beard. A Biophysical Model of the Mitochondrial Respiratory System and Oxidative Phosphorylation. *PLoS Comput Biol*, 1(4):e36, 2005. ISSN 1553-734X. doi: 10.1371/journal.pcbi.0010036.eor.

G. Benard, B. Faustin, E. Passerieux, A. Galinier, C. Rocher, N. Bellance, J.-P. Delage, L. Casteilla, T. Letellier, and R. Rossignol. Physiological diversity of mitochondrial oxidative phosphorylation. *Am J Physiol Cell Physiol*, 291(6):C1172–82, Dec. 2006. ISSN 0363-6143. doi: 10.1152/ajpcell.00195.2006.

P. Bénit, A. Slama, and P. Rustin. Decylubiquinol impedes mitochondrial respiratory chain complex I activity. *Mol Cell Biochem*, 314(1-2):45–50, July 2008. ISSN 0300-8177. doi: 10.1007/s11010-008-9763-z.

E. Berry, M. Guergova-Kuras, L. Huang, and C. AR. Structure and function of cytochrome bc complexes. *Annu Rev Biochem*, 69:1005–1075, 2000.

H. F. Bienfait, J. M. C. Jacobs, and E. C. Slater. Mitochondrial oxygen affinity as a function of redox and phosphate potentials. *Biochim Biophys Acta*, 376:446–457, 1975.

R. M. Bock and R. A. Alberty. Studies of the enzyme fumarase. I. Kinetics and equilibrium. *J Am Chem Soc*, 75(8):1921 – 1925, 1953.

R. Bohnensack. Control of energy transformation in mitochondria. Analysis by a quantitative model. *Biochim Biophys Acta*, 634:203–218, 1981.

R. Bohnensack, U. Küster, and G. Letko. Rate-controlling steps of oxidative phosphorylation in rat liver mitochondria. A synoptic approach of model and experiment. *Biochim Biophys Acta*, 680(3):271–80, June 1982. ISSN 0006-3002.

J. Boork. The influence of membrane potentials on reaction rates. Control in free-energy-transducing systems. *Biochim Biophys Acta*, 767(2):314–320, Nov. 1984. doi: 10.1016/0005-2728(84)90201-9.

S. Bose, S. French, F. J. Evans, F. Joubert, and R. S. Balaban. Metabolic network control of oxidative phosphorylation: multiple roles of inorganic phosphate. *J Biol Chem*, 278(40):39155–65, Oct. 2003. ISSN 0021-9258. doi: 10.1074/jbc.M306409200.

G. Brändén, R. B. Gennis, and P. Brzezinski. Transmembrane proton translocation by cytochrome c oxidase. *Biochim Biophys Acta*, 1757(8):1052–63, Aug. 2006. ISSN 0006-3002. doi: 10.1016/j.bbabio.2006.05.020.

U. Brandt. A two-state stabilization-change mechanism for proton-pumping complex I. *Biochim Biophys Acta*, 1807(10):1364–9, Oct. 2011. ISSN 0006-3002. doi: 10.1016/j.bbabio.2011.04.006.

U. Brandt and J. G. Okun. Role of deprotonation events in ubihydroquinone:cytochrome c oxidoreductase from bovine heart and yeast mitochondria. *Biochemistry*, 36(37):11234–40, Sept. 1997. ISSN 0006-2960. doi: 10.1021/bi970968g.

G. E. Briggs and J. B. S. Haldane. A note on the kinetics of enzyme action. *Biochem Journal*, 19(2):338–339, 1925.

P. S. Brookes, D. W. Kraus, S. Shiva, J. E. Doeller, M.-C. Barone, R. P. Patel, J. R. Lancaster, and V. Darley-Usmar. Control of mitochondrial respiration by NO*, effects of low oxygen and respiratory state. *J Biol Chem*, 278(34):31603–9, Aug. 2003. ISSN 0021-9258. doi: 10.1074/jbc.M211784200.

G. Brown. Nitric oxide regulates mitochondrial respiration and cell functions by inhibiting cytochrome oxidase. *FEBS letters*, 369:136–139, 1995.

G. C. Brown and C. E. Cooper. Nanomolar concentrations of nitric oxide reversibly inhibit synaptosomal respiration by competing with oxygen at cytochrome oxidase. *FEBS letters*, 356(2-3):295–8, Dec. 1994. ISSN 0014-5793.

U. Büge and B. Kadenbach. Influence of buffer composition, membrane lipids and proteases on the kinetics of reconstituted cytochrome-c oxidase from bovine liver and heart. *Eur J Biochem*, 161(2):383–90, Dec. 1986. ISSN 0014-2956.

G. Burger, B. F. Lang, M. Reith, and M. W. Gray. Genes encoding the same three subunits of respiratory complex II are present in the mitochondrial DNA of two phylogenetically distant eukaryotes. *Proc Natl Acad Sci*, 93(6):2328–32, Mar. 1996. ISSN 0027-8424.

E. Cadenas and A. Boveris. of superoxide radicals and hydrogen peroxide by NADH-ubiquinone reductase and ubiquinol-cytochrome c reductase from beef-heart mitochondria. *Archives of biochemistry ...*, 180:248–257, 1977.

E. Cadenas and K. A. Davies. Mitochondrial free radical generation, oxidative stress, and aging. *Free radical biology & medicine*, 29:222–230, 2000.

C. Camello-Almaraz, P. J. Gomez-Pinilla, M. J. Pozo, and P. J. Camello. Mitochondrial reactive oxygen species and Ca 2+ signaling. *American Journal of Cell Physiology*, 291:C1082–1088, 2006. doi: 10.1152/ajpcell.00217.2006.

R. Capaldi. Structure and function of cytochrome c oxidase. *Annu Rev Biochem*, 59: 569–596, 1990.

P. Cardol. Mitochondrial NADH:ubiquinone oxidoreductase (complex I) in eukaryotes: a highly conserved subunit composition highlighted by mining of protein databases. *Biochim Biophys Acta*, 1807(11):1390–7, Nov. 2011. ISSN 0006-3002. doi: 10.1016/j.bbabio.2011.06.015.

J. Carroll, I. M. Fearnley, J. M. Skehel, R. J. Shannon, J. Hirst, and J. E. Walker. Bovine complex I is a complex of 45 different subunits. *J Biol Chem*, 281(43):32724–7, Oct. 2006. ISSN 0021-9258. doi: 10.1074/jbc.M607135200.

G. Cecchini. Function and structure of complex II of the respiratory chain. *Annu Rev Biochem*, 72:77–109, Jan. 2003. ISSN 0066-4154. doi: 10.1146/annurev.biochem.72.121801.161700.

B. Chance and G. Hollunger. Energy-linked reduction of mitochondrial pyridine nucleotide. *Nature*, 185:666–672, 1960. doi: 10.1038/185666a0.

D. T. W. Chang and I. J. Reynolds. Differences in mitochondrial movement and morphology in young and mature primary cortical neurons in culture. *Neuroscience*, 141 (2):727–36, Aug. 2006. ISSN 0306-4522. doi: 10.1016/j.neuroscience.2006.01.034.

T. Clason, V. Zickermann, T. Ruiz, U. Brandt, and M. Radermacher. Direct localization of the 51 and 24 kDa subunits of mitochondrial complex I by three-dimensional difference imaging. *Journal of structural biology*, 159(3):433–42, Sept. 2007. ISSN 1047-8477. doi: 10.1016/j.jsb.2007.05.002.

I. Collinson, M. van RaaiJ, M. Runswick, I. Fearnley, J. Skehel, G. Orriss, B. Miroux, and J. Walker. ATP Synthase from Bovine Heart Mitochondria: In Vitro Assembly of a Stalk Complex in the Presence of F1-ATPase and in its Absence. *J Mol Biol*, 242: 408–421, 1994.

S. Cortassa, M. a. Aon, E. Marbán, R. L. Winslow, and B. O'Rourke. An integrated model of cardiac mitochondrial energy metabolism and calcium dynamics. *Biophys J*, 84(4):2734–55, Apr. 2003. ISSN 0006-3495. doi: 10.1016/S0006-3495(03)75079-6.

S. Cortassa, M. a. Aon, B. O'Rourke, R. Jacques, H.-J. Tseng, E. Marbán, and R. L. Winslow. A computational model integrating electrophysiology, contraction, and mitochondrial bioenergetics in the ventricular myocyte. *Biophys J*, 91:1564–1589, Aug. 2006. ISSN 0006-3495. doi: 10.1529/biophysj.105.076174.

A. R. Crofts and S. Rose. Marcus treatment of endergonic reactions: a commentary. *Biochimica et biophysica acta*, 1767(10):1228–32, Oct. 2007. ISSN 0006-3002. doi: 10.1016/j.bbabio.2007.06.006.

A. R. Crofts and Z. Wang. How rapid are the internal reactions of the ubiquinol : cytochrome c2 oxidoreductase ? *Photosyn Res*, 22:69–87, 1989. doi: 10.1007/BF00114768.

L. E. A. de Wit, L. Spruijt, G. C. Schoonderwoerd, I. F. M. de Coo, H. J. M. Smeets, H. R. Scholte, and W. Sluiter. A simplified and reliable assay for complex I in human blood lymphocytes. *J Immunol Meth*, 326(1-2):76–82, Sept. 2007. ISSN 0022-1759. doi: 10.1016/j.jim.2007.07.009.

A. S. Divakaruni and M. D. Brand. The regulation and physiology of mitochondrial proton leak. *Physiology (Bethesda, Md.)*, 26:192–205, June 2011. ISSN 1548-9221. doi: 10.1152/physiol.00046.2010.

N. V. Dudkina, R. Kouril, K. Peters, H.-P. Braun, and E. J. Boekema. Structure and function of mitochondrial supercomplexes. *Biochim Biophys Acta*, 1797(6-7):664–70, 2010. ISSN 0006-3002. doi: 10.1016/j.bbabio.2009.12.013.

K. S. Echtay, D. Roussel, J. St-Pierre, M. B. Jekabsons, S. Cadenas, J. a. Stuart, J. a. Harper, S. J. Roebuck, A. Morrison, S. Pickering, J. C. Clapham, and M. D. Brand. Superoxide activates mitochondrial uncoupling proteins. *Nature*, 415(6867):96–9, Jan. 2002. ISSN 0028-0836. doi: 10.1038/415096a.

R. G. Efremov and L. a. Sazanov. Structure of the membrane domain of respiratory complex I. *Nature*, 476(7361):414–420, Aug. 2011. ISSN 0028-0836. doi: 10.1038/nature10330.

R. G. Efremov and L. A. Sazanov. The coupling mechanism of respiratory complex I - A structural and evolutionary perspective. *Biochim Biophys Acta*, 1817(10):1785–95, Oct. 2012. ISSN 0006-3002. doi: 10.1016/j.bbabio.2012.02.015.

R. G. Efremov, R. Baradaran, and L. a. Sazanov. The architecture of respiratory complex I. *Nature*, 465(7297):441–5, May 2010. ISSN 1476-4687. doi: 10.1038/nature09066.

M. Esposti, E. Avitabile, M. Barilli, G. Schiavo, C. Montecucco, and G. Lenaz. Comparative biochemistry of the ubiquinol-cytochrome c oxidoreductase (EC 1.10.2.2) isolated from different heart mitochondria. *Comp Biochem Physiol*, 85(3):543 – 552, 1986.

M. Esposti, A. Ngo, A. Ghelli, and B. Benelli. The interaction of Q analogs, particularly hydroxydecyl benzoquinone (idebenone), with the respiratory complexes of heart mitochondria. *Arch Biochem Biophys*, 330(2):395–400, 1996.

N. Exner, A. K. Lutz, C. Haass, and K. F. Winklhofer. Mitochondrial dysfunction in Parkinson's disease: molecular mechanisms and pathophysiological consequences. *EMBO J*, 31:3038–3062, 2012. ISSN 0261-4189. doi: 10.1038/emboj.2012.170.

R. Fato, E. Estornell, S. Di Bernardo, F. Pallotti, G. Parenti Castelli, and G. Lenaz. Steady-state kinetics of the reduction of coenzyme Q analogs by complex I (NADH:ubiquinone oxidoreductase) in bovine heart mitochondria and submitochondrial particles. *Biochemistry*, 35(8):2705–16, Feb. 1996. ISSN 0006-2960. doi: 10.1021/bi9516034.

S. Ferguson-Miller, C. Hiser, and J. Liu. Gating and regulation of the cytochrome c oxidase proton pump. *Biochim Biophys Acta*, 1817(4):489–94, Apr. 2012. ISSN 0006-3002. doi: 10.1016/j.bbabio.2011.11.018.

R. H. Fillingame. Coupling H+ transport and ATP synthesis in F1F0-ATP synthases: glimpses of interacting parts in a dynamic molecular machine. *J Exp Biol*, 200(Pt 2): 217–24, Jan. 1997. ISSN 0022-0949.

R. H. Fillingame, C. M. Angevine, and O. Y. Dmitriev. Mechanics of coupling proton movements to c-ring rotation in ATP synthase. *FEBS Letters*, 555(1):29–34, Nov. 2003. ISSN 00145793. doi: 10.1016/S0014-5793(03)01101-3.

French Mitochondrial Diseases Network. Homepage. URL `http://lbbma.univ-angers.fr/lbbma.php?id=57`.

C. Frieden. Slow transitions and hysteric behavior in enzymes. *Annu Rev Biochem*, 48: 471–489, 1979.

T. Friedrich, K. Steinmüller, and H. Weiss. The proton-pumping respiratory complex I of bacteria and mitochondria and its homologue in chloroplasts. *FEBS letters*, 367 (2):107–11, June 1995. ISSN 0014-5793.

A. Galkin, S. Dröse, and U. Brandt. The proton pumping stoichiometry of purified mitochondrial complex I reconstituted into proteoliposomes. *Biochim Biophys Acta*, 1757(12):1575–81, Dec. 2006. ISSN 0006-3002. doi: 10.1016/j.bbabio.2006.10.001.

A. S. Galkin, V. G. Grivennikova, and A. D. Vinogradov. –>H+/2e- stoichiometry in NADH-quinone reductase reactions catalyzed by bovine heart submitochondrial particles. *FEBS letters*, 451(2):157–61, May 1999. ISSN 0014-5793.

F. Gellerich, R. Bohnensack, and W. Kunz. Control of mitochondrial respiration. The contribution of the adenine nucleotide translocator depends on the ATP- and ADP-consuming enzymes. *Biochim Biophys Acta*, 222(2):381–391, 1983.

M. L. Genova, A. Baracca, A. Biondi, G. Casalena, M. Faccioli, a. I. Falasca, G. Formiggini, G. Sgarbi, G. Solaini, and G. Lenaz. Is supercomplex organization of the respiratory chain required for optimal electron transfer activity? *Biochim Biophys Acta*, 1777(7-8):740–6, 2008. ISSN 0006-3002. doi: 10.1016/j.bbabio.2008.04.007.

R. W. Gilkerson, J. M. Selker, and R. a. Capaldi. The cristal membrane of mitochondria is the principal site of oxidative phosphorylation. *FEBS Letters*, 546(2-3):355–358, July 2003. ISSN 00145793. doi: 10.1016/S0014-5793(03)00633-1.

E. Gnaiger. Capacity of oxidative phosphorylation in human skeletal muscle: new perspectives of mitochondrial physiology. *Int J Biochem Cell Biol*, 41(10):1837–45, Oct. 2009. ISSN 1878-5875. doi: 10.1016/j.biocel.2009.03.013.

J. Greenhut, H. Umezawa, and F. Rudolph. Inhibition of fumarase by S-2, 3-dicarboxyaziridine. *J Biol Chem*, 260(11):6684–6686, 1985.

V. G. Grivennikova, E. V. Gavrikova, A. A. Timoshin, and A. D. Vinogradov. Fumarate reductase activity of bovine heart succinate-ubiquinone reductase. New assay system and overall properties of the reaction. *Biochim Biophys Acta*, 1140(3):282–92, Jan. 1993. ISSN 0006-3002.

V. G. Grivennikova, A. N. Kapustin, and A. D. Vinogradov. Catalytic activity of NADH-ubiquinone oxidoreductase (complex I) in intact mitochondria. Evidence for the slow active/inactive transition. *J Biol Chem*, 276(12):9038–44, Mar. 2001. ISSN 0021-9258. doi: 10.1074/jbc.M009661200.

A. K. Groen, R. J. A. Wanders, H. V. Westerhoff, R. van der Meer, and J. M. Tagers. Quantification of the contribution of various steps to the control of mitochondrial respiration. *J Biol Chem*, 257(6):2754–2757, 1982.

C. Hägerhäll. Succinate: quinone oxidoreductases. Variations on a conserved theme. *Biochim Biophys Acta*, 1320(2):107–41, June 1997. ISSN 0006-3002.

C. Hägerhäll and L. Hederstedt. A structural model for the membrane-integral domain of succinate: quinone oxidoreductases. *FEBS letters*, 389(1):25–31, June 1996. ISSN 0014-5793.

N. Hano, Y. Nakashima, K. Shinzawa-Itoh, H. Terada, and S. Yoshikawa. Effect of pH on the steady state kinetics of bovine heart NADH: coenzyme Q oxidoreductase. *J Bioenerg Biomembr*, 35(5):419–25, Oct. 2003a. ISSN 0145-479X.

N. Hano, Y. Nakashima, K. Shinzawa-Itoh, and S. Yoshikawa. Effect of the side chain structure of coenzyme Q on the steady state kinetics of bovine heart NADH: coenzyme Q oxidoreductase. *J Bioenerg Biomembr*, 35(3):257–65, June 2003b. ISSN 0145-479X.

R. Heinrich and T. A. Rapoport. A linear steady-state treatment of enzymatic chains. General properties, control, effector strength. *Eur J Biochem*, 42:89–95, 1974.

S. Helling, S. Vogt, A. Rhiel, R. Ramzan, L. Wen, K. Marcus, and B. Kadenbach. Phosphorylation and kinetics of mammalian cytochrome c oxidase. *Molecular & cellular proteomics : MCP*, 7(9):1714–24, Sept. 2008. ISSN 1535-9484. doi: 10.1074/mcp.M800137-MCP200.

J. Hirst. Why does mitochondrial complex I have so many subunits? *The Biochemical journal*, 437(2):e1–3, July 2011. ISSN 1470-8728. doi: 10.1042/BJ20110918.

J. Hirst, M. S. King, and K. R. Pryde. The production of reactive oxygen species by complex I. *Biochem Soc Trans*, 36(Pt 5):976–80, Oct. 2008. ISSN 0300-5127. doi: 10.1042/BST0360976.

H.-G. Holzhütter, W. Henke, W. Dubiel, and G. Gerber. A mathematical model to study short-term regulation in mitochondrial energy transduction. *Biochim Biophys Acta*, 810:252–268, 1985.

C. Hunte, H. Palsdottir, and B. L. Trumpower. Protonmotive pathways and mechanisms in the cytochrome bc1 complex. *FEBS Letters*, 545(1):39–46, June 2003. ISSN 00145793. doi: 10.1016/S0014-5793(03)00391-0.

S. Iwata. Complete Structure of the 11-Subunit Bovine Mitochondrial Cytochrome bc1 Complex. *Science*, 281(5373):64–71, July 1998. doi: 10.1126/science.281.5373.64.

A. T. Jagendorf and J. Neumann. Effect of uncouplers on the light-induced pH rise with spinach chloroplasts. *J Biol Chem*, 240(7):3210–3214, July 1965. ISSN 0021-9258.

S.-Y. Jeong and D.-W. Seol. The role of mitochondria in apoptosis. *BMB reports*, 41 (1):11–22, Jan. 2008. ISSN 1976-6696.

W. Jiang and R. H. Fillingame. Interacting helical faces of subunits a and c in the F1Fo ATP synthase of Escherichia coli defined by disulfide cross-linking. *Proc Natl Acad Sci*, 95(12):6607–12, June 1998. ISSN 0027-8424.

Q. Jin and C. M. Bethke. Kinetics of electron transfer through the respiratory chain. *Biophys J*, 83(4):1797–808, Oct. 2002. ISSN 0006-3495. doi: 10.1016/S0006-3495(02) 73945-3.

J. L. Joyal and J. R. Aprille. The ATP-Mg/Pi carrier of rat liver mitochondria catalyzes a divalent electroneutral exchange. *J Biol Chem*, 267(27):19198–203, Sept. 1992. ISSN 0021-9258.

B. Kacser and J. A. Burns. The control of flux. *Symp Soc Exp Biol*, 27:65–104, 1973.

A. King, M. A. Selak, and E. Gottlieb. Succinate dehydrogenase and fumarate hydratase: linking mitochondrial dysfunction and cancer. *Oncogene*, 25:4675–4682, 2006. doi: 10.1038/sj.onc.1209594.

T. Klimova and N. S. Chandel. Mitochondrial complex III regulates hypoxic activation of HIF. *Cell Death Diff*, 15(4):660–6, Apr. 2008. ISSN 1350-9047. doi: 10.1038/sj.cdd.4402307.

K. Kobayashi, T. Yamanishi, and S. Tuboi. Physicochemical, catalytic, and immunochemical properties of fumarases crystallized separately from mitochondrial and cytosolic fractions of rat liver. *J Biochem*, 89(6):1923–31, June 1981. ISSN 0021-924X.

S. Koene and J. Smeitink. *Mitochondrial Medicine. A clinical guideline*. Khondrion BV, Nijmegen, first edit edition, 2011. ISBN 978-90-817737-0-6.

B. Korzeniewski. An extended dynamic model of oxidative phosphorylation. *Biochim Biophys Acta*, 1060(2):210–223, 1991.

B. Korzeniewski. Regulation of ATP supply during muscle contraction: theoretical studies. *Biochem J*, 330:1189–1195, Mar. 1998. ISSN 0264-6021.

B. Korzeniewski. Theoretical studies on the regulation of oxidative phosphorylation in intact tissues. *Biochim Biophys Acta*, 1504(1):31–45, Mar. 2001. ISSN 0006-3002.

B. Korzeniewski. Regulation of oxidative phosphorylation through parallel activation. *Biophys Chem*, 129(2-3):93–110, Sept. 2007. ISSN 0301-4622. doi: 10.1016/j.bpc.2007.05.013.

B. Korzeniewski and W. Froncisz. Theoretical studies on the control of the oxidative phosphorylation system. *Biochim Biophys Acta*, 1102(1):67–75, 1992.

B. Korzeniewski and J.-P. Mazat. Theoretical studies on the control of oxidative phosphorylation in muscle mitochondriq: application to mitochondrial deficiencies. *Biochem J*, 319:143–148, 1996.

B. Korzeniewski and J. A. Zoladz. A model of oxidative phosphorylation in mammalian skeletal muscle. *Biophys Chem*, 92(1-2):17–34, Aug. 2001. ISSN 0301-4622.

A. Kowald. The Mitochondrial Theory of Aging. *Biol Signals Recept*, 10:162–175, 2001.

A. V. Kulikov, E. S. Shilov, I. A. Mufazalov, V. Gogvadze, S. A. Nedospasov, and B. Zhivotovsky. Cytochrome c: the Achilles' heel in apoptosis. *Cell Mol Life Sci*, 69 (11):1787–97, June 2012. ISSN 1420-9071. doi: 10.1007/s00018-011-0895-z.

P. Läuger. Thermodynamic and kinetic properties of electrogenic ion pumps. *Biochim Biophys Acta*, 779(3):307–341, 1984.

M. Lazarou, D. R. Thorburn, M. T. Ryan, and M. McKenzie. Assembly of mitochondrial complex I and defects in disease. *Biochim Biophys Acta*, 1793(1):78–88, Jan. 2009. ISSN 0006-3002. doi: 10.1016/j.bbamcr.2008.04.015.

J. Y. Lee and S. J. Lee. Enzymatic properties of cytochrome oxidase from bovine heart and rat tissues. *J Biochem Mol Biol*, 28(3):254–260, 1995.

G. Lenaz and M. L. Genova. Mobility and function of coenzyme Q (ubiquinone) in the mitochondrial respiratory chain. *Biochimica et biophysica acta*, 1787(6):563–73, June 2009. ISSN 0006-3002. doi: 10.1016/j.bbabio.2009.02.019.

G. Lenaz, P. Pasquali, E. Bertoli, and G. Parenti-Castelli. The inhibition of NADH oxidase by the lower homologs of coenzyme Q. *Arch Biochem Biophys*, 169(1):217–26, 1975.

G. Lenaz, A. Baracca, R. Fato, M. L. Genova, and G. Solaini. New insights into structure and function of mitochondria and their role in aging and disease. *Antioxid Redox Signal*, 8(3 & 4):417–437, 2006.

R. L. Lester and F. L. Crane. The natural occurrence of coenzyme Q and related compounds. *The Journal of biological chemistry*, 234(8):2169–75, Aug. 1959. ISSN 0021-9258.

C. Li and R. M. Jackson. Reactive species mechanism of cellular hypoxia-reoxygenation injury. *Am J Physiol Cell Physiol*, 282:C227–C241, 2002.

W. Liebermeister and E. Klipp. Bringing metabolic networks to life: integration of kinetic, metabolic, and proteomic data. *Theor Biol Mol Model*, 3:42, Jan. 2006. ISSN 1742-4682. doi: 10.1186/1742-4682-3-42.

D. C. Logan. The mitochondrial compartment. *J Exp Bot*, 57(6):1225–43, Jan. 2006. ISSN 0022-0957. doi: 10.1093/jxb/erj151.

H. Löw and I. Vallin. Succinate-linked Diphosphopyridine Nucleotide Reduction in Submitochondrial Particles. *Biochim Biophys Acta*, 69:361–364, 1963.

O. H. Lowry, N. J. Rosebrough, R. Randall, and A. L. Lewis. Protein measurment with the folin phenol reagent. *Anal Biochem.*, 203(1):121–6, 1951.

E. Maklashina and G. Cecchini. Comparison of catalytic activity and inhibitors of quinone reactions of succinate dehydrogenase (Succinate-ubiquinone oxidoreductase) and fumarate reductase (Menaquinol-fumarate oxidoreductase) from Escherichia coli. *Arch Biochem Biophys*, 369(2):223–32, Sept. 1999. ISSN 0003-9861. doi: 10.1006/abbi.1999.1359.

E. Margoliash and N. Frohwirt. Spectrum of horse-heart cytochrome c. *Biochem J*, 71 (3):570–2, Mar. 1959. ISSN 0264-6021.

V. Massey. Studies on Fumarase. The effect of inhibitors on fumarase activity. *Biochemical Journal*, 55:172–177, 1953.

MathWorks. *Matlab*. MathWorks, Massachusetts, USA, 2012. URL `http://www.mathworks.de/products/matlab/`.

J. P. Mazat, M. Aimar, B. Faustin, T. Letellier, M. Malgat, C. Nazaret, and R. Rossignol. Modeling of electron transport, Chap 8-3 Vol 5 in , A. Lajtha ed. , Kluwer Academic/ Plenum Publishers 2006. In Kluwer Academics, editor, *Handbook of Neurochemistry and Molecular Neurobiology*, chapter 8-3. Plenum Publishers, 2006. ISBN 978-0-387-30366-6.

S. McLean, S. M. Richards, S.-L. Cover, S. Brandon, N. W. Davies, J. P. Bryant, and T. P. Clausen. Papyriferic acid, an antifeedant triterpene from birch trees, inhibits succinate dehydrogenase from liver mitochondria. *J Chem Ecol*, 35(10):1252–61, Oct. 2009. ISSN 1573-1561. doi: 10.1007/s10886-009-9702-9.

P. Merle and B. Kadenbach. Kinetic and structural differences between cytochrome c oxidases from beef liver and heart. *Eur J Biochem*, 125(1):239–44, June 1982. ISSN 0014-2956.

L. Michaelis, M. L. Menten, K. a. Johnson, and R. S. Goody. The original Michaelis constant: translation of the 1913 Michaelis-Menten paper. *Biochemistry*, 50(39):8264–9, Oct. 2011. ISSN 1520-4995. doi: 10.1021/bi201284u.

P. Mitchell. Coupling of phosphorylation to electron and hydrogen transfer by a chemi-osmotic type of mechanism. *Nature*, 191:188–148, 1961.

P. Mitchell. Metabolism, Transport, and Morphogenesis:. *J Gen Microbiol*, 29:25–37, 1962.

P. Mitchell. The protonmotive Q-cycle: a general formulation. *FEBS letters*, 59(2): 137–139, 1975.

P. Mitchell. Chemiosmotic coupling in oxidative and photosynthetic phosphorylation. 1966. *Biochim Biophys Acta*, 1807(12):1507–38, Dec. 2011. ISSN 0006-3002. doi: 10.1016/j.bbabio.2011.09.018.

P. Mitchell and J. Moyle. Evidence discriminating between the chemical and the chemiosmotic mechanisms of electron transport phosphorylation. *Nature*, 208(5016):1205–1206, 1965.

N. Morgner, V. Zickermann, S. Kerscher, I. Wittig, A. Abdrakhmanova, H.-D. Barth, B. Brutschy, and U. Brandt. Subunit mass fingerprinting of mitochondrial complex I. *Biochim Biophys Acta*, 1777(10):1384–91, Oct. 2008. ISSN 0006-3002. doi: 10.1016/j.bbabio.2008.08.001.

C. C. Moser, T. a. Farid, S. E. Chobot, and P. L. Dutton. Electron tunneling chains of mitochondria. *Biochim Biophys Acta*, 1757(9-10):1096–109, 2006. ISSN 0006-3002. doi: 10.1016/j.bbabio.2006.04.015.

M. F. Mouat and K. L. Manchester. The intracellular ionic strength of red cells and the influence of complex formation. *Comparative Haematology International*, 8:58–60, 1998.

Y. Nakashima, K. Shinzawa-Itoh, K. Watanabe, K. Naoki, N. Hano, and S. Yoshikawa. The second coenzyme Q1 binding site of bovine heart NADH: coenzyme Q oxidoreductase. *J Bioenerg Biomembr*, 34(2):89–94, Apr. 2002a. ISSN 0145-479X.

Y. Nakashima, K. Shinzawa-Itoh, K. Watanabe, K. Naoki, N. Hano, and S. Yoshikawa. Steady-state kinetics of NADH:coenzyme Q oxidoreductase isolated from bovine heart mitochondria. *J Bioenerg Biomembr*, 34(1):11–9, Feb. 2002b. ISSN 0145-479X.

J. Napiwotzki and B. Kadenbach. Extramitochondrial ATP/ADP-ratios regulate cytochrome c oxidase activity via binding to the cytosolic domain of subunit IV. *Biol Chem*, 739(3):335–339, 1998.

C. Nazaret, M. Heiske, K. Thurley, and J.-P. Mazat. Mitochondrial energetic metabolism: a simplified model of TCA cycle with ATP production. *J Theor Biol*, 258(3):455–64, June 2009. ISSN 1095-8541. doi: 10.1016/j.jtbi.2008.09.037.

J. Neumann and A. T. Jagendorf. Light induced pH changes related phosphorylation by chloroplasts. *Arch Biochem Biophys. 1964*, 107:109–119, 1964.

D. G. Nicholls. Mitochondria and calcium signaling. *Cell calcium*, 38(3-4):311–7, 2005. ISSN 0143-4160. doi: 10.1016/j.ceca.2005.06.011.

S. Ono, N. Sone, M. Yoshida, and T. Suzuki. ATP synthase that lacks F0a-subunit: isolation, properties, and indication of F0b2-subunits as an anchor rail of a rotating c-ring. *J Biol Chem*, 279(32):33409–12, Aug. 2004. ISSN 0021-9258. doi: 10.1074/jbc.M404993200.

P. S. O'Shea, G. Petrone, R. P. Casey, and A. Azzi. The current-voltage relationships of liposomes and mitochondria. *The Biochemical journal*, 219(3):719–26, May 1984. ISSN 0264-6021.

S. Ouchane, I. Agalidis, and C. Astier. Natural Resistance to Inhibitors of the Ubiquinol Cytochrome c Oxidoreductase of Rubrivivax gelatinosus : Sequence and Functional Analysis of the Cytochrome bc 1 Complex. *J Bacteriol*, 184(14):3815–3822, 2002. doi: 10.1128/JB.184.14.3815.

K. S. Oyedotun and B. D. Lemire. The quaterny structure of the saccharomyces cerevisiae succinate dehydrogenase. *J Biol Chem*, 279(10):9424–9431, 2004. doi: 10.1074/jbc.M311876200.

S. O. Pember, L. C. Fleck, W. K. Moberg, and M. P. Walker. Mechanistic differences in inhibition of ubiquinol cytochrome c reductase by the proximal Qo-site inhibitors famoxadone and methoxyacrylate stilbene. *Arch Biochem Biophys*, 435(2):280–90, Mar. 2005. ISSN 0003-9861. doi: 10.1016/j.abb.2004.12.013.

J. Petersen, K. Förster, P. Turina, and P. Gräber. Comparison of the H+/ATP ratios of the H+-ATP synthases from yeast and from chloroplast. *Proceedings of the National Academy of Sciences of the United States of America*, 109(28):11150–5, July 2012. ISSN 1091-6490. doi: 10.1073/pnas.1202799109.

D. Pietrobon. A non-linear kinetic model of chemiosmotic energy coupling. *Bioelectrochem Bioenerg*, 15:193–209, 1986.

D. Pietrobon and S. R. Caplan. Flow-Force Relationships for a Six-State Proton Pump Model: Intrinsic Uncoupling, Kinetic Equivalence of Input and Output Forces, and Domain of Approximate Linearity. *Biochemistry*, 24:5764–5776, 1985.

D. Pietrobon, M. Zoratti, G. F. Azzone, J. W. Stucki, and D. Walz. Non-equilibrium thermodynamic assessment of redox-driven H+ pumps in mitochondria. *Eur J Biochem*, 127(3):483–94, Oct. 1982. ISSN 0014-2956.

D. Pogoryelov, J. Yu, T. Meier, J. Vonck, P. Dimroth, and D. J. Muller. The c15 ring of the Spirulina platensis F-ATP synthase: F1/F0 symmetry mismatch is not obligatory. *EMBO reports*, 6(11):1040–4, Nov. 2005. ISSN 1469-221X. doi: 10.1038/sj.embor.7400517.

L. Qin, M. Sharpe, R. Garavito, and S. Ferguson-Miller. Conserved lipid-binding sites in membrane proteins: a focus on cytochrome c oxidase. *Curr Opin Struct Biol*, 17 (4):444–450, 2007.

L. Qin, J. Liu, D. Mills, D. Proshlyakov, C. Hiser, and S. Ferguson-Miller. Redox dependent conformational changes in cytochrome c oxidase suggest a gating mechanism for proton uptake. *Biochemistry*, 48(23):5121–5130, 2009. doi: 10.1021/bi9001387.Redox.

G. Quarato, C. Piccoli, R. Scrima, and N. Capitanio. Variation of flux control coefficient of cytochrome c oxidase and of the other respiratory chain complexes at different values of protonmotive force occurs by a threshold mechanism. *Biochim Biophys Acta*, 1807 (9):1114–1124, May 2011. ISSN 0006-3002. doi: 10.1016/j.bbabio.2011.04.001.

S. J. Ralph, R. Moreno-Sánchez, J. Neuzil, and S. Rodríguez-Enríquez. Inhibitors of succinate: quinone reductase/Complex II regulate production of mitochondrial reactive oxygen species and protect normal cells from ischemic damage but induce specific cancer cell death. *Pharmaceutical Research*, 28:2695–2730, 2011. doi: 10.1007/s11095-011-0566-7.

R. Ramakrishna, J. S. Edwards, A. McCulloch, and B. O. Palsson. Flux-balance analysis of mitochondrial energy metabolism: consequences of systemic stoichiometric constraints. *Am J Physiol Regul Integr Comp Physiol*, 280:R695 – R704, 2001.

S. Ransac, N. Parisey, and J.-P. Mazat. The loneliness of the electrons in the bc1 complex. *Biochimica et biophysica acta*, 1777(7-8):1053–9, 2008. ISSN 0006-3002. doi: 10.1016/j.bbabio.2008.05.003.

S. Ransac, C. Arnarez, and J.-P. Mazat. The flitting of electrons in complex I: a stochastic approach. *Biochim Biophys Acta*, 1797(6-7):641–8, 2010. ISSN 0006-3002. doi: 10.1016/j.bbabio.2010.03.011.

S. Ransac, M. Heiske, and J.-P. Mazat. From in silico to in spectro kinetics of respiratory complex I. *Biochim Biophys Acta*, Apr. 2012. ISSN 0006-3002. doi: 10.1016/j.bbabio.2012.03.037.

C. Reder. Metabolic control theory: a structural approach. *J Theor Biol*, 135(2):175–201, 1988.

D. M. Rees, A. G. W. Leslie, and J. E. Walker. The structure of the membrane extrinsic region of bovine ATP synthase. *Proc Natl Acad Sci*, 106(51):21597–601, Dec. 2009. ISSN 1091-6490. doi: 10.1073/pnas.0910365106.

A. Reimann, K. H. Röhm, and B. Kadenbach. Ferricytochrome c induces monophasic kinetics of ferrocytochrome c oxidation in cytochrome c oxidase. *J Bioenerg Biomembr*, 25(4):393–9, Aug. 1993. ISSN 0145-479X.

J. A. Reynolds, E. A. Johnson, and C. Tanford. Incorporation of membrane potential into theoretical analysis of electrogenic ion pumps. *Proc Natl Acad Sci*, 82(20):6869–73, Oct. 1985. ISSN 0027-8424.

A. J. W. Rodgers, S. Wilkens, R. Aggeler, M. B. Morris, S. M. Howitt, and R. A. Capaldi. The Subunit d-Subunit b Domain of the Escherichia coli F1F0 ATPase. *J Biol Chem*, 272(49):31058–31064, 1997.

M. M. Roessler, M. S. King, A. J. Robinson, F. A. Armstrong, J. Harmer, and J. Hirst. Direct assignment of EPR spectra to structurally defined iron-sulfur clusters in complex I by double electron-electron resonance. *Proc Natl Acad Sci*, 107(5):1930–5, Feb. 2010. ISSN 1091-6490. doi: 10.1073/pnas.0908050107.

I. Rose. The state of magnesium in cells as estimated from the adenylate kinase equilibrium. *Proceedings of the National Academy of Sciences*, 61(3):1079–1086, 1968.

R. Rossignol, M. Malgat, J. P. Mazat, and T. Letellier. Threshold effect and tissue specificity. Implication for mitochondrial cytopathies. *J Biol Chem*, 274(47):33426–32, Nov. 1999. ISSN 0021-9258.

H. Rottenberg. Non-equilibrium thermodynamics of energy conversion in bioenergetics. *Biochim Biophys Acta*, 549(3-4):225–253, 1979.

H. Rottenberg and M. Gutman. Control of the rate of reverse electron transport in submitochondrial particles by the free energy. *Biochemistry*, 16(14):3220–7, July 1977. ISSN 0006-2960.

H. Rottenberg, R. Covian, and B. L. Trumpower. Membrane potential greatly enhances superoxide generation by the cytochrome bc1 complex reconstituted into phospholipid vesicles. *The Journal of biological chemistry*, 284(29):19203–10, July 2009. ISSN 0021-9258. doi: 10.1074/jbc.M109.017376.

J. Rutter, D. R. Winge, and J. D. Schiffman. Succinate dehydrogenase - Assembly, regulation and role in human disease. *Mitochondrion*, 10(4):393–401, June 2010. ISSN 1872-8278. doi: 10.1016/j.mito.2010.03.001.

L. Sagan. On the origin of mitosing cells. *J Theor Biol*, 14(3):255–274, 1967.

Y. Sambongi. Mechanical Rotation of the c Subunit Oligomer in ATP Synthase (F0F1): Direct Observation. *Science*, 286(5445):1722–1724, Nov. 1999. ISSN 00368075. doi: 10.1126/science.286.5445.1722.

L. a. Sazanov and P. Hinchliffe. Structure of the hydrophilic domain of respiratory complex I from Thermus thermophilus. *Science (New York, N.Y.)*, 311(5766):1430–6, Mar. 2006. ISSN 1095-9203. doi: 10.1126/science.1123809.

E. Schäfer, H. Seelert, N. H. Reifschneider, F. Krause, N. A. Dencher, and J. Vonck. Architecture of Active Mammalian Respiratory Chain Supercomplexes. *Biol Chem*, 281(22):15370–15375, 2006. doi: 10.1074/jbc.M513525200.

H. Schägger, R. de Coo, M. F. Bauer, S. Hofmann, C. Godinot, and U. Brandt. Significance of respirasomes for the assembly/stability of human respiratory chain complex I. *The Journal of biological chemistry*, 279(35):36349–53, Aug. 2004. ISSN 0021-9258. doi: 10.1074/jbc.M404033200.

A. H. V. Schapira. Mitochondrial diseases. *The Lancet*, 379:1825–1834, 2012. ISSN 0140-6736. doi: 10.1016/S0140-6736(11)61305-6.

B. Schultz and S. Chan. Structures and proton-pumping strategies of mitochondrial respiratory enzymes. *Annu Rev Biophys Biomol Struct*, 30:23–65, 2001.

Scilab Enterprises. *Scilab: free open source software for numerical calculations*. Scilab Enterprises, Orsay, France, 2012. URL `http://www.scilab.org`.

I. H. Segel. *Enzyme Kinetics Behavior and Analysis of Rapid Equilibrium and Steady-State Enzyme Systems*. New York, 1993a. ISBN 978-0-471-30309-1.

I. H. Segel. Rapid equilibrium bireactant systems. In I. H. Segel, editor, *Enzyme Kinetics. Behavior and Analysis of Rapid Equilibrium and Steady-State Enzyme Systems*, chapter chap 6, pages 273–344. John Wiley & Sons, New York, wiley classics library edition, 1993b. ISBN 978-0-471-30309-1.

I. H. Segel. Steady state kinetics of multireactant systems. In I. H. Segel, editor, *Enzyme Kinetics. Behavior and Analysis of Rapid Equilibrium and Steady-State Enzyme Systems*, chapter chap 9, pages 505–845. John Wiley & Sons, New York, wiley classics library edition, 1993c. ISBN 978-0-471-30309-1.

V. A. Selivanov, T. V. Votyakova, V. N. Pivtoraiko, J. Zeak, T. Sukhomlin, M. Trucco, J. Roca, and M. Cascante. Reactive oxygen species production by forward and reverse electron fluxes in the mitochondrial respiratory chain. *PLoS Comput Biol*, 7(3): e1001115, Mar. 2011. ISSN 1553-7358. doi: 10.1371/journal.pcbi.1001115.

S. Sherwood and J. Hirst. Investigation of the mechanism of proton translocation by NADH:ubiquinone oxidoreductase (complex I) from bovine heart mitochondria: does the enzyme operate by a Q-cycle mechanism? *Biochem J*, 400(3):541–50, Dec. 2006. ISSN 1470-8728. doi: 10.1042/BJ20060766.

K. Shinzawa-Itoh, H. Aoyama, K. Muramoto, H. Terada, T. Kurauchi, Y. Tadehara, A. Yamasaki, T. Sugimura, S. Kurono, K. Tsujimoto, T. Mizushima, E. Yamashita, T. Tsukihara, and S. Yoshikawa. Structures and physiological roles of 13 integral lipids of bovine heart cytochrome c oxidase. *EMBO J*, 26(6):1713–25, Mar. 2007. ISSN 0261-4189. doi: 10.1038/sj.emboj.7601618.

S. A. Siletsky and A. A. Konstantinov. Cytochrome c oxidase: charge translocation coupled to single-electron partial steps of the catalytic cycle. *Biochim Biophys Acta*, 1817(4):476–88, Apr. 2012. ISSN 0006-3002. doi: 10.1016/j.bbabio.2011.08.003.

K. M. Sinjorgo, I. Durak, H. L. Dekker, C. M. Edel, T. B. Hakvoort, B. F. van Gelder, and A. O. Muijsers. Bovine cytochrome c oxidases, purfified from heart, skeleton muscle, liver and kidney, differ in the small subunits but show the same reaction kinetics with cytochrome c. *Biochim Biophys Acta*, 893:251–258, 1987.

N. Sone, M. Yoshida, H. Hirata, and Y. Kagawa. Adenosine triphosphate synthesis by electrochemical proton gradient in vesicles reconstituted from purified adenosine triphosphatase and phospholipids of thermophilic bacterium. *J Biol Chem*, 252(9): 2956–60, May 1977. ISSN 0021-9258.

S. H. Speck and E. Margoliash. Characterization of the interaction of cytochrome c and mitochondrial ubiquinol-cytochrome c reductase. *J Biol Chem*, 259(2):1064–72, Jan. 1984. ISSN 0021-9258.

S. Srinivasan and N. G. Avadhani. Cytochrome c oxidase dysfunction in oxidative stress. *Free Radical Biol Med*, 53(6):1252–63, Sept. 2012. ISSN 1873-4596. doi: 10.1016/j.freeradbiomed.2012.07.021.

J. St-Pierre, M. D. Brand, and R. G. Boutilier. Mitochondria as ATP consumers: cellular treason in anoxia. *Proceedings of the National Academy of Sciences of the United States of America*, 97(15):8670–4, July 2000. ISSN 0027-8424. doi: 10.1073/pnas.140093597.

L. Stiburek and J. Zeman. Assembly factors and ATP-dependent proteases in cytochrome c oxidase biogenesis. *Biochim Biophys Acta*, 1797(6-7):1149–58, 2010. ISSN 0006-3002. doi: 10.1016/j.bbabio.2010.04.006.

D. Stock, A. G. W. Leslie, and J. E. Walker. Molecular Architecture of the Rotary Motor in ATP Synthase. *Science*, 286(5445):1700–1705, Nov. 1999. ISSN 00368075. doi: 10.1126/science.286.5445.1700.

A. Stroh, O. Anderka, K. Pfeiffer, T. Yagi, M. Finel, B. Ludwig, and H. Schägger. Assembly of respiratory complexes I, III, and IV into NADH oxidase supercomplex

stabilizes complex I in Paracoccus denitrificans. *J Biol Chem*, 279(6):5000–7, Feb. 2004. ISSN 0021-9258. doi: 10.1074/jbc.M309505200.

J. Stucki. The Thermodynamic-Buffer Enzymes. *Eur J Biochem*, 109:257–267, 1980a.

J. W. Stucki. The optimal efficiency and the economic degrees of coupling of oxidative phosphorylation. *Eur J Biochem*, 109(1):269–83, Aug. 1980b. ISSN 0014-2956.

F. Sun, X. Huo, Y. Zhai, A. Wang, J. Xu, D. Su, M. Bartlam, and Z. Rao. Crystal structure of mitochondrial respiratory membrane protein complex II. *Cell*, 121(7): 1043–57, July 2005. ISSN 0092-8674. doi: 10.1016/j.cell.2005.05.025.

E. B. Tahara, F. D. T. Navarete, and A. J. Kowaltowski. Tissue-, substrate-, and site-specific characteristics of mitochondrial reactive oxygen species generation. *Free Radical Biol Med*, 46(9):1283–97, May 2009. ISSN 1873-4596. doi: 10.1016/j.freeradbiomed.2009.02.008.

J. J. Tomashek and W. S. Brusilow. Stoichiometry of energy coupling by proton-translocating ATPases: a history of variability. *J Bioenerg Biomembr*, 32(5):493–500, Oct. 2000. ISSN 1573-6881.

S. Törnroth-Horsefield and R. Neutze. Opening and closing the metabolite gate. *Proc Natl Acad Sci*, 105(50):19565–6, Dec. 2008. ISSN 1091-6490. doi: 10.1073/pnas.0810654106.

T. Tsukihara, H. Aoyama, E. Yamashita, T. Tomizaki, H. Yamaguchi, K. Shinzawa-Itoh, R. Nakashima, R. Yaono, and S. Yoshikawa. Structures of metal sites of oxidized bovine heart cytochrome c oxidase at 2.8 A. *Science*, 269(5227):1069–74, Aug. 1995. ISSN 0036-8075.

T. Tsukihara, H. Aoyama, E. Yamashita, T. Tomizaki, H. Yamaguchi, K. Shinzawa-Itoh, R. Nakashima, R. Yaono, and S. Yoshikawa. The whole structure of the 13-subunit oxidized cytochrome c oxidase at 2.8 A. *Science*, 272:1136–1144, 1996.

P. Tushurashvili, E. Gavrikova, A. Ledenev, and A. Vinogradov. Studies on the succinate dehydrogenating system. Isolation and properties of the mitochondrial succinate-ubiquinone reductase. *Biochim Biophys Acta*, 809:145–159, 1985.

S. Usui, L. Yu, and C. a. Yu. The small molecular mass ubiquinone-binding protein (QPc-9.5 kDa) in mitochondrial ubiquinol-cytochrome c reductase: isolation, ubiquinone-binding domain, and immunoinhibition. *Biochemistry*, 29(19):4618–26, May 1990. ISSN 0006-2960.

C. Van Der Drift, D. B. Janssen, and P. M. G. F. van Wezenbeek. Hydrolysis and synthesis of ATP by membrane-bound ATPase from a motile streptococcus. *Arch Microbiol*, 119:31–36, 1978.

M. Vendelin, O. Kongas, and V. Saks. Regulation of mitochondrial respiration in heart cells analyzed by reaction-diffusion model of energy transfer. *Am J Physiol Cell Physiol*, 278:C747–C764, 2000.

M. Vendelin, M. Lemba, and V. a. Saks. Analysis of functional coupling: mitochondrial creatine kinase and adenine nucleotide translocase. *Biophys J*, 87:696–713, July 2004. ISSN 0006-3495. doi: 10.1529/biophysj.103.036210.

S. B. Vik and B. J. Antonio. A mechanism of proton translocation by F1F0 ATP synthases suggested by double mutants of the a subunit. *J Biol Chem*, 269(48):30364–9, Dec. 1994. ISSN 0021-9258.

A. D. Vinogradov. Kinetics, control, and mechanism of ubiquinone reduction by the mammalian respiratory chain-linked NADH-ubiquinone reductase. *J Bioenerg Biomembr*, 25(4):367–75, Aug. 1993. ISSN 0145-479X.

A. D. Vinogradov. Steady-state and pre-steady-state kinetics of the mitochondrial F1Fo ATPase: is ATP synthase a reversible molecular machine? *J Exp Biol*, 203(Pt 1): 41–9, Jan. 2000. ISSN 0022-0949.

A. D. Vinogradov. NADH/NAD+ interaction with NADH: ubiquinone oxidoreductase (complex I). *Biochim Biophys Acta*, 1777(7-8):729–34, 2008. ISSN 0006-3002. doi: 10.1016/j.bbabio.2008.04.014.

A. D. Vinogradov, a. B. Kotlyar, V. I. Burov, and Y. O. Belikova. Regulation of succinate dehydrogenase and tautomerization of oxaloacetate. *Advances Enz Regul*, 28(9):271–80, Jan. 1989. ISSN 0065-2571.

T. D. Vo, H. J. Greenberg, and B. O. Palsson. Reconstruction and functional characterization of the human mitochondrial metabolic network based on proteomic and biochemical data. *J Biol Chem*, 279(38):39532–39540, Sept. 2004. ISSN 0021-9258. doi: 10.1074/jbc.M403782200.

D. Voet and J. G. Voet. Elektronentransport und Oxidative Phosphorylierung. In D. Voet and J. G. Voet, editors, *Biochemie*, chapter 20, pages 527–560. VCH, Weinheim, first edit edition, 1994. ISBN 3-527-29249-7.

C. von Ballmoos, A. Wiedenmann, and P. Dimroth. Essentials for ATP synthesis by F1F0 ATP synthases. *Annu Rev Biochem*, 78:649–72, Jan. 2009. ISSN 1545-4509. doi: 10.1146/annurev.biochem.78.081307.104803.

I. N. Watt, M. G. Montgomery, M. J. Runswick, A. G. W. Leslie, and J. E. Walker. Bioenergetic cost of making an adenosine triphosphate molecule in animal mitochondria. *Proc Natl Acad Sci*, 107(39):16823–7, Sept. 2010. ISSN 1091-6490. doi: 10.1073/pnas.1011099107.

A.-C. Wei, M. a. Aon, B. O'Rourke, R. L. Winslow, and S. Cortassa. Mitochondrial energetics, pH regulation, and ion dynamics: a computational-experimental approach.

Biophysical journal, 100:2894–2903, June 2011. ISSN 1542-0086. doi: 10.1016/j.bpj.2011.05.027.

M. Wikström. Two protons are pumped from the mitochondrial matrix per electron transferred between NADH and ubiquinone. *FEBS letters*, 169(2):300–4, Apr. 1984. ISSN 0014-5793.

F. Wu, F. Yang, K. C. Vinnakota, and D. a. Beard. Computer modeling of mitochondrial tricarboxylic acid cycle, oxidative phosphorylation, metabolite transport, and electrophysiology. *J Biol Chem*, 282(34):24525–37, Aug. 2007. ISSN 0021-9258. doi: 10.1074/jbc.M701024200.

Y. Yang, H. Wang, J. Xu, and H. Zhou. Kinetics of modification of the mitochondrial succinate-ubiquinone reductase by 5, 5'-dithiobis-(2-nitro-benzoic acid). *J Prot Chem*, 15(2):169 – 176, 1996.

K. Yugi and M. Tomita. A general computational model of mitochondrial metabolism in a whole organelle scale. *Bioinformatics (Oxford, England)*, 20(11):1795–6, July 2004. ISSN 1367-4803. doi: 10.1093/bioinformatics/bth125.

Z. Zhang, L. Huang, V. M. Shulmeister, Y. I. Chi, K. K. Kim, L.-W. Hung, A. R. Crofts, E. A. Berry, and S.-H. Kim. Electron transfer by domain movement in cytochrome bc1. *Nature*, 392:677–684, 1998.

V. Zickermann, S. Kerscher, K. Zwicker, M. a. Tocilescu, M. Radermacher, and U. Brandt. Architecture of complex I and its implications for electron transfer and proton pumping. *Biochim Biophys Acta*, 1787(6):574–83, June 2009. ISSN 0006-3002. doi: 10.1016/j.bbabio.2009.01.012.

List of Figures

1.1. Oxidative phosphorylation 2
1.2. Mitochondria 3
1.3. Structure of complex I 7
1.4. Structure of complex II 10
1.5. Structure of complex III and Q-cycle mechanism 12
1.6. Structure of complex IV 14
1.7. Structure of ATPsynthase 17

2.1. Aspects of modeling OXPHOS 29
2.2. Comparison of rate equations for the description of OXPHOS complexes . 31
2.3. Spectrum of decylubiquinone at different reduction states 40
2.4. Complex I: Dependence of the activity on the ethanol concentration and of the incubation time at 37°C 42
2.5. Time courses of the non-enzymatic reduction of DCIP by ubiquinol 48
2.6. Initial rate measurements of the chemical reduction of DCIP by ubiquinol 49
2.7. Comparison of the different approaches for the determination of quinols . 50
2.8. Structural formula of coenzyme Q and decylubiquinone 52
2.9. Complex I: Fit to progress curves 55
2.10. Correlation between the specific activity and the Michaelis-Menten constant of quinone 56
2.11. Complex I: Shapes of experimental progress curves 58
2.12. Complex I: rate equations versus experimental data points 62
2.13. Complex I: rate equations versus experimental data points 63
2.14. Complex I: Fit to initial rate measurements with quinone inhibition . . . 67
2.15. Stochastic model: Description of initial rate measurements 71
2.16. Stochastic model with inhibition 73
2.17. Double reciprocal plots of the simulated initial velocities 74
2.18. Complex II: fit to experimental data 76
2.19. Complex III: Fit to initial rate measurements 83
2.20. Complex III: Fit to initial rates assuming inhibition by quinones 86
2.21. Complex IV: Fit to experimental data 90
2.22. Physiological diversity of oxidative phosphorylation 98

3.1. Influence of the electrochemical gradient on the Michaelis-Menten constants 111
3.2. Even repartition of the impact of the electrochemical gradient on the rate constants 113

3.3. Uneven repartition of the impact of the electrochemical gradient on the kinetic constants . . . 115
3.4. The repartition of the proton gradient's influence on the rate constants as a function of the internal energy . . . 117
3.5. Internal energy dependent repartition of the electrochemical gradient on the rate constants . . . 119

4.1. Schematic representation of the OXPOS model . . . 124
4.2. General suitability of the new rate equations . . . 136
4.3. Results of fitting the new model to the Bose data set . . . 137
4.4. Electron entry into the respiratory chain via complex II . . . 140
4.5. Variation of the Michaelis-Menten constants for quinone and quinols at non phosphorylating state . . . 142
4.6. Variation of the Michaelis-Menten constants for quinone and quinols under phosphorylating conditions . . . 143
4.7. Shapes of threshold curves . . . 144
4.8. Simulation of threshold curves at state 3 . . . 145
4.9. Threshold curves at state 4 . . . 146
4.10. Threshold curves of the system CII + CIII + CIV . . . 147
4.11. Threshold curves in absence of the electrochemical gradient . . . 148
4.12. Variation of the proton/ATP ratio of the F_1F_0-ATP-synthase . . . 149
4.13. The electric gradient at state 3 and 4 and the effect of inhibiting complex IV . . . 151
4.14. Time courses: respiration, $\Delta\Psi$ and normalized NADH . . . 153

B.1. Supercomplexes: Shapes of inhibition curves . . . 170
B.2. Scheme of the virtual supercomplexes . . . 171
B.3. Strict channeling model: inhibition curves at state 3 . . . 176
B.4. Strict channeling model: state transition and respiration rate . . . 177
B.5. Partial channeling model: inhibition curves at state 3 respiration . . . 179
B.6. Partial channeling: state transition and respiratory rate . . . 180

List of Tables

2.1. Reduction of DCIP by QH_2 . . . 47
2.2. Complex I: Fit to time course measurements . . . 56
2.3. Complex I: Parameters values for the enzyme mechanism based rate equations . . . 60
2.4. Complex I: Simplified equations . . . 60
2.5. Complex I: Inhibition by quinones . . . 67
2.6. Parameters used in the stochastic model of complex I . . . 69
2.7. Rate constants of substrate and product binding and release used in the stochastic model of complex I . . . 70
2.8. Rate constants of substrate and product binding and release . . . 74
2.9. Complex II: parameter values . . . 78
2.10. Complex III: Parameter values for the different reaction schemes . . . 82
2.11. Complex III: Fit to initial rates assuming inhibition by quinones . . . 85
2.12. Complex IV: Parameter values . . . 89
2.13. Comparison of the kinetic parameters along the respiratory chain . . . 95

3.1. The new rate equations for the proton translocating OXPHOS complexes 120

4.1. Differential equation system of the OXPHOS model . . . 128
4.2. Constraints . . . 129
4.3. Fixed parameters of the models . . . 131
4.4. Weight on each experimental series . . . 133
4.5. Adjustable parameters of the models . . . 134
4.6. Parameters of the new OXPHOS rate equations . . . 138

B.1. Supercomplex distributions used for simulations . . . 169
B.2. Parameters of the strict and partial channeling models . . . 173

Acknowledgments

First of all I want to thank very much my supervisors Edda Klipp and Jean-Pierre Mazat for supporting me during my doctoral thesis, admitting me freedom but being always present if there were questions. And for being patient with concerns on the cotutelle ...

Due to this cooperation I had the great chance to have a good time with nice people of two groups, the 'Mitochondrial Physiopathology' group in Bordeaux and the 'Theoretical Biophysics' group in Berlin, many thanks to all of you for the cordial ambiance and helpful discussions!

I'm especially grateful to Thierry Letellier for scientific advice and great discussions, to Christine Nazaret and Stéphane Ransac for their help with modeling, Amal Arrachiche, Denis Pierron and Nadège Bellance for a warm welcome in Bordeaux, Claire Pertuiset and Elodie Dumont for their assistance in the lab and spreading laughters together with Nicolas Gutierrez and Christophe Rocher.

Special thanks also to François Guillaud, always ready to share science and chocolate, Axel Kowald for scientific advice, Ivo Maintz for saving my computer from time to time and my life on climbing, Friedemann Uschner and Wolfgang Giese for tackling together early morning's Lagrange formalism with Bachelor students and Matteo Barberis, Martina Fröhlich and József Bruck for friendly support.

I'm very grateful to my parents and friends accompanying me in good and hard times during my doctoral thesis.

I acknowledge the Agence Nationale de la Recherche (ANR, France) and the Biotechnology and Biological Sciences Research Council (BBSRC, UK) for funding this work through the project MitoScoP as well as the Bundesministerium für Bildung und Forschung (BMBF, Germany) for support through the GerontoMitoSys project.

Selbständigkeitserklärung

Ich erkläre, dass ich die vorliegende Arbeit selbständig und nur unter Verwendung der angegebenen Literatur und Hilfsmittel angefertigt habe.

Berlin, den 05.11.2012 Margit Heiske